Mathematical models of soft tissue injury repair: towards understanding musculoskeletal disorders

Joanne L. Dunster

Thesis submitted to The University of Nottingham
for the degree of Doctor of Philosophy

July, 2012

Abstract

The process of soft tissue injury repair at the cellular level can be decomposed into three phases: acute inflammation including coagulation, proliferation and remodelling. While the later phases are well understood the early phase is less so. We produce a series of new mathematical models for the early phases coagulation and inflammation. The models produced are relevant not only to soft tissue injury repair but also to the many disease states in which coagulation and inflammation play a role.

The coagulation cascade and the subsequent formation of the enzyme thrombin are central to the creation of blood clots. By focusing on a subset of reactions that occur within the coagulation cascade, we develop a model that exhibits a rich asymptotic structure. Using singular-perturbation theory we produce a sequence of simpler time-dependent models which enable us to elucidate the physical mechanisms that underlie the cascade and the formation of thrombin.

There is considerable interest in identifying new therapeutic targets within the coagulation cascade, as current drugs for treating pathological coagulation (thrombosis) target multiple factors and cause the unwelcome side effect of excessive bleeding. Factor XI is thought to be a potential therapeutic target, as it is implicated in pathological coagulation but not in haemostasis (the stopping of bleeding), but its mechanism of activation is controversial. By extending our previous model of the coagulation cascade to include the whole cascade (albeit in a simplistic way) we use numerical methods to simulate experimental data of the coagulation cascade under normal as well as specific-factor-deficient conditions. We then provide simulations supporting the hypothesis that thrombin activates factor XI.

The interest in inflammation is now increasing due to it being implicated in such diverse conditions as Alzmeimer's disease, cancer and heart disease. Inflammation can either resolve or settle into a self-perpetuating condition which in the context of soft tissue repair is termed chronic inflammation. Inflammation has traditionally been thought gradually to subside but new biological interest centres on the anti-inflammatory processes (relating to macrophages) that are thought to promote resolution and the pro-inflammatory role that neutrophils can provide by causing damage to healthy tissue. We develop a new ordinary differential equation model of the inflammatory process that accounts for populations of neutrophils and macrophages. We use numerical techniques and bifurcation theory to characterise and elucidate the physiological mechanisms that are dominant during the inflammatory phase and the roles they play in the healing process. There is therapeutic interest in modifying the rate of neutrophil apoptosis but

we find that increased apoptosis is dependent on macrophage removal to be anti-inflammatory.

We develop a simplified version of the model of inflammation reducing a system of nine ordinary equations to six while retaining the physical processes of neutrophil apoptosis and macrophage driven anti-inflammatory mechanisms. The simplified model reproduces the key outcomes that we relate to resolution or chronic inflammation. We then present preliminary work on the inclusion of the spatial effects of chemotaxis and diffusion.

Acknowledgements

This thesis would never have been completed without the help of many people. Above all I would like to express my thanks and gratitude to my mathematical supervisors John King and Helen Byrne for their encouragement, help and patience over the course of this project. I would also like to thank Susan Franks, from the Health and Safety Laboratory, for discussions and support and would like to convey my thanks to the Health and Safety Labroratory and the EPSRC for funding.

I would like to express my gratitude to Helen Cunliffe, Dave Parkin, Andrea Blackbourn and Hilary Lonsdale, support staff at the School of Mathematical Sciences. My thanks also go to Jonas Emsley, from the School of Pharmacy at Nottingham, for discussions around factor XI activation and the work in Chapter 4.

I dedicate this thesis to my Dad who will never know how much he inspired me.

Contents

CHAPTER 1

Introduction

The overall sequence of events that soft tissue is believed to follow after various types of injury is remarkably preserved. Thus a burn, wound, sprain or even a heart attack elicit the same interrelated phases of events (Gurtner *et al.*, 2008). This thesis is in part sponsored by the Health and Safety Laboratory who are interested in soft tissue injury repair in relationship to work-related musculoskeletal disorders (WRMSDs). Musculoskeletal disorders encompass a wide range of conditions from acute onset with short duration to lifelong disorders including such clinical conditions as osteoarthritis, sciatica and epicondylitis, as well as less specific conditions such as low back pain (Punnett & Wegman, 2004). They affect many areas of soft tissue including muscles, tendons, ligaments and cartilage.

WRMSDs are caused mainly by factors associated with the work place such as working too long without breaks, awkward working positions and manual handling and are usually due to the nature of a person's work rather than as a result of some hazard (Pheasant & Haslegrave, 1996). The disorders are often multi-factorial, so that there is not a one-to-one correspondence between specific ergonomic exposures and particular MSDs (Forde *et al.*, 2002) such as there is in occupational disorders (e.g. farmer's lung caused by inhalation of spores from mouldy hay). They can have contributory factors such as pre-existing medical conditions and events such as activities outside of the work place, such as sport. They are "work related", not occupational, i.e. they do not have a single identifiable cause. The factors that give rise to WRMSDs can be found in virtually every workplace and it is estimated that 12.3 million days a year are lost in the UK through WRMSDs (H.S.E., 2003). They are the most common work related ailment affecting the general population in Great Britain and they account for more than half of all self reported occupational ill health (H.S.E., 2002).

1.1 Soft tissue healing

In simplistic terms the response of soft tissue to injury has to resolve three problems: damaged vessels, destroyed tissue and bacterial infection. This is achieved through a series of overlapping events, shown in Figure 1.1, that serve to repair any vascular leakages, remove any bacteria and cellular damage and reconstitute damaged tissue. The fastest acting of these

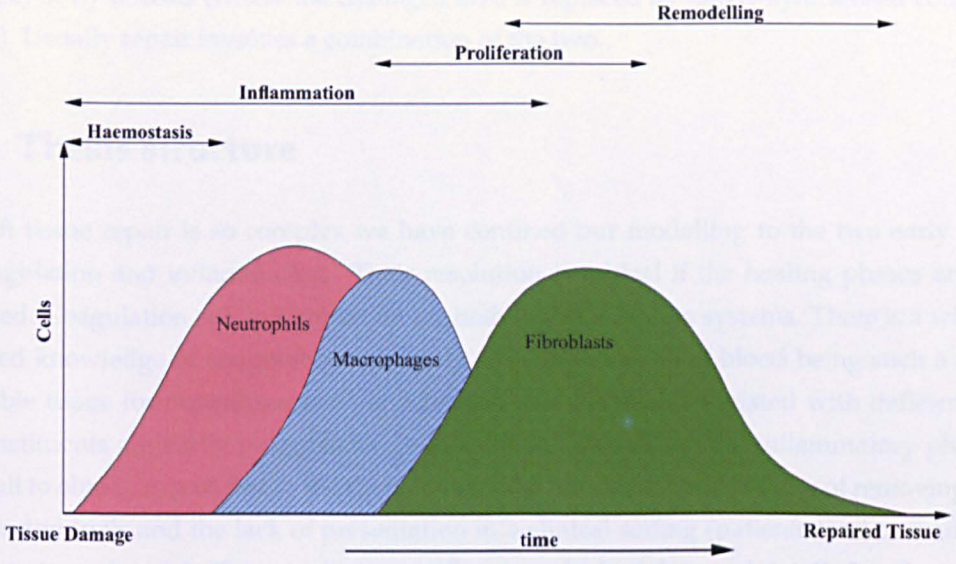

Figure 1.1: Illustrative time-course of regeneration of injured tissue including the major events of haemostasis (coagulation), inflammation, proliferation and remodelling, showing their relationships to the cell types typical of each major event. Haemostasis (coagulation) is the fastest acting event, plugging any local vascular leakages and providing a structure for cellular infiltration. Inflammation is where bacteria and damaged tissue are removed. It is characterised by the infiltration of white blood cells (neutrophils and macrophages). Neutrophils arrive first, being smaller and faster acting, and they are followed by the larger macrophages, which help set in motion the subsequent healing phases of proliferation and remodelling in which damaged tissue is replaced. The dominant cells of these later phases are fibroblasts, which produce the collagen required to replace damaged tissue.

events is coagulation (the formation of fibrin blood clots) which plugs local vascular leakages, acts to wall-off the surrounding areas in an attempt to prevent further damage, holds damaged tissue together and provides a provisional matrix for the recruitment of cells into the injured area (Guyton, 1992). The acute inflammatory phase serves to rid the organism of bacteria and cellular damage, it is closely intertwined and stimulates the reparative phases that it stimulates. Inflammation is characterised by an influx of white blood cells that attempt to kill any bacteria and remove any damaged tissue and cells by the process of phagocytosis. Chemicals that trigger the subsequent healing phases are then released. These reparative processes reconstitute the site of damage, either by resolution (where damaged cells are replaced by cells of a similar type) or by fibrosis (where the damaged area is replaced by newly-synthesised connective tissue). Usually repair involves a combination of the two.

1.2 Thesis structure

As soft tissue repair is so complex we have confined our modelling to the two early phases of coagulation and inflammation. Their resolution is critical if the healing phases are to be initiated. Coagulation and inflammation are both highly complex systems. There is a wide and detailed knowledge of coagulation, probably as a consequence of blood being such a readily available tissue for experimentation and because the diseases associated with deficiencies in its constituents are easily recognisable (Mann, 2003). Data about the inflammatory phase are difficult to obtain, in part due to the short duration of the phase, the difficulty of removing tissue from individuals and the lack of presentation in a clinical setting (patients tend to wait for an injury to turn chronic). These features contribute to a lack of data and detailed understanding of the biology in this area, presenting us with different challenges in terms of modelling.

The thesis splits into two parts: part I, which comprises chapters 2, 3 and 4, relates to coagulation while part II comprises chapters 5, 6, and 7 and relates to inflammation. Chapter eight provides a summary of our major acheivements, a discussion of the insights they provide and an outline for future work in this area.

Part I

Coagulation

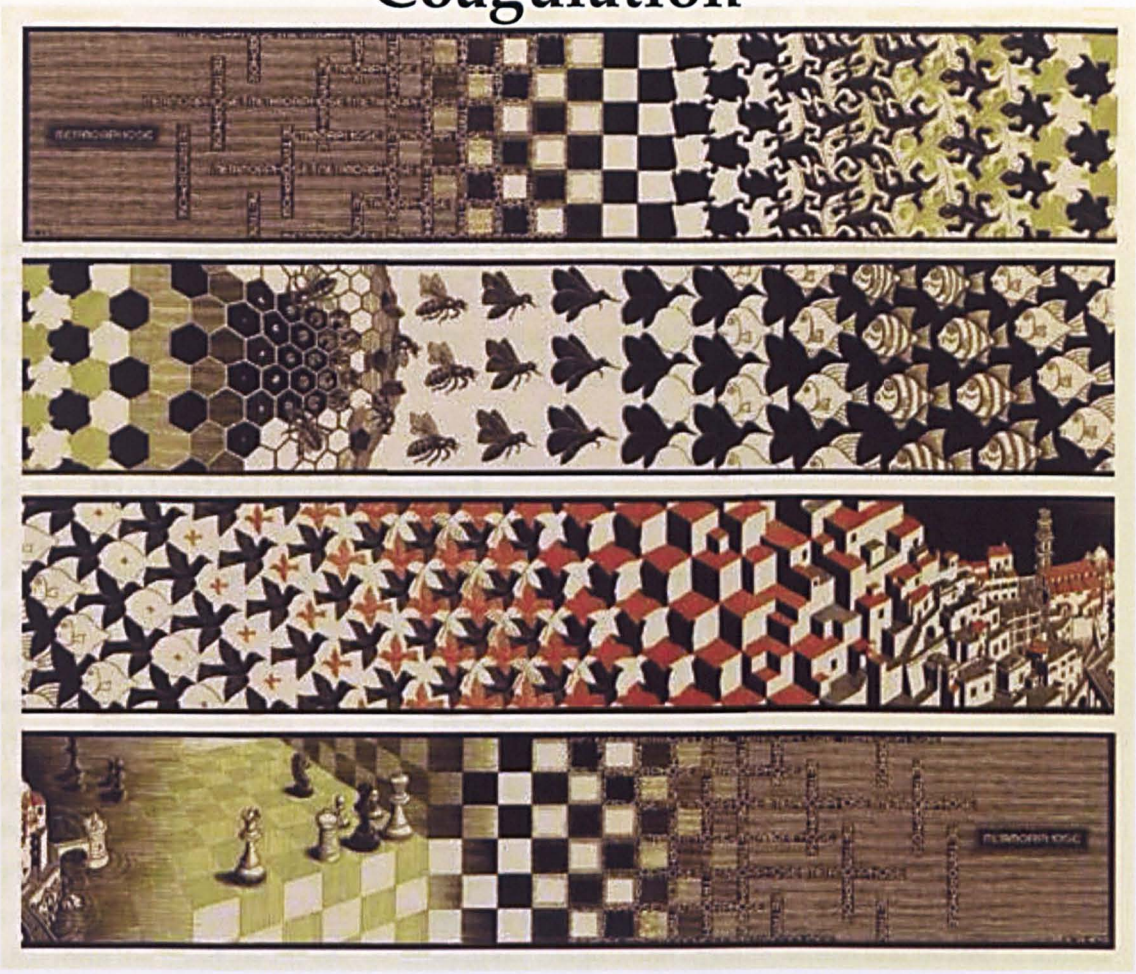

Figure 2.1: M.C. Escher, Metamorphosis. The formation of blood clots (coagulation) occurs over multiple timescales; we can use mathematics to generate a series of simplified models representing the reactions occurring at each timescale. Rather like the picture we move from one scale to the next.

CHAPTER 2

Coagulation Background

This chapter is divided into two main parts. We first present a description of the biological principles of coagulation and follow this, in Section 2.2, with a review of the current mathematical literature relevant to the coagulation cascade and the formation of blood clots. We refer the reader to Colman *et al.* (2000) for a more detailed description of the biology of coagulation.

2.1 Biological background

Haemostasis (the halting of bleeding) is nature's fastest reaction to tissue damage. Its function is to maintain blood in a fluid state under normal conditions and to plug any leaks when the vasculature is damaged. This is achieved by coagulation, a process that converts blood to a solid mass (fibrin blood clots) in a localised area while leaving it fluid in surrounding areas (Majno & Joris, 2004). Generating a blood clot in the correct place and at the correct time requires precise coordination: the clots must form quickly, be easily broken down and should not be stimulated inappropriately.
Fibrin blood clots are formed by the aggregation (clumping together) of platelets and the formation of a fibrin mesh which stabilises and provides strength to the clot. The fibrin monomers that form the mesh are the end product of the coagulation cascade, which is activated at almost the same time as platelets are activated (see Figure 2.2). Thrombin, one of the main components of platelet aggregation (Gurbel *et al.*, 2007) is also responsible for the converting of fibrinogen to fibrin: therefore thrombin is a key enzyme in the formation of a fibrin blood clot.

2.1.1 Coagulation cascade

The coagulation cascade is a network of sequentially activated factors (proteins) that coordinate the production of thrombin. The factors within the cascade are numbered from I to XIII, in their order of discovery rather than function; an 'a' suffix is traditionally added to denote an activated factor (Majno & Joris, 2004). Various reactions within the cascade are assembled on specific cell surfaces, referred to as phospholipids. The limitation of such sites, such as to those exposed on the surfaces of activated platelets, helps to prevent the clot spreading throughout

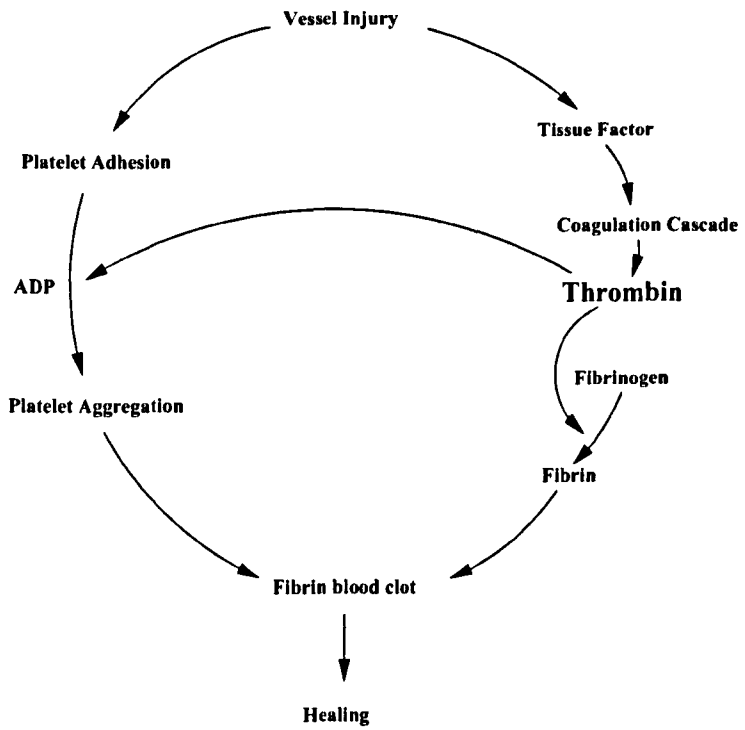

Figure 2.2: Overview of haemostasis. A fibrin blot clot is formed from the dual processes of platelet aggregation and the coagulation cascade. The coagulation cascade produces the fibrin monomers that provide stability to the clot. (Key: ADP, adenosine diphosphate.) Adapted from Colman *et al.* (2000)

the vascular system (Hoffman, 2004). There are also various feedback loops that either inhibit or accelerate the reaction (Majno & Joris, 2004), with thrombin enhancing its own formation by activating factors V, VIII and XI. Anticoagulants which act to contain the clot include the protein C/protein S inhibitory system, antithrombin III (whose speed of action is greatly enhanced by heparin (Porth, 2005)) and tissue factor inhibitor.

Figure 2.3 shows the dynamics of the various factors within the coagulation cascade. It has been traditional to divide it into an extrinsic (that begins with tissue damage) and intrinsic (that begins in the blood) pathway. These pathways converge at the level of factor X activation into a common set of reactions (named the common pathway).

2.1.1.1 Extrinsic pathway

Under normal circumstances (haemostasis) the coagulation cascade is thought to be initiated through the extrinsic pathway and the expression of tissue factor (TF) on the surface of damaged cells (Colman *et al.*, 2000). TF is a receptor normally absent from all cells in direct contact with blood, but is present on damaged cells or on a variety of cells outside the vasculature. When TF does come into contact with blood it binds to plasma factors VII and VIIa (trace levels are present in plasma), TF:VII is subsequently activated by TF:VIIa (autoactivation). The TF:VIIa complex is termed the extrinsic tenase and subsequently activates factor X (Tucker *et al.*, 2009; Colman *et al.*, 2000), a factor common to both pathways.

In a clinical setting, tests for coagulating potential are used when someone has unexplained bleeding or bruising and before surgery. Plasma is drawn from the patient and mixed with activators of the relevant pathway in the presence of high levels of calcium and phospholipids and clot formation time is recorded. The prothrombin time (PT) assay (activated by tissue factor) is such a test that detects deficiencies in factors within the extrinsic pathway.

2.1.1.2 Intrinsic pathway

When blood is brought into contact with negatively charged surfaces (including non-physiological substances such as glass) it results in activation of factor XII, prekallikrein, high molecular weight kininogen and, subsequently, factor XI. This is known as contact activation (its position in the coagulation cascade is shown in Figure 2.3). The lack of abnormal bleeding associated with congenital factor XII deficiency indicates that it may not be important for coagulation *in vivo* (Renné *et al.*, 2006; Gailani & Renne, 2007*a*). Factor XIa converts factor IX to IXa which complexes with factor VIIa to form the intrinsic tenase (a factor X activator). The clinical test for the intrinsic pathway is the activated partial thromboplastin time (aPTT) in which plasma is activated via a material such as silica and the time until a clot is formed is measured. In such tests, plasma that is deficient in a factor of the intrinsic pathway (such as the congenital deficiencies of hemophilia A (clotting factor VIII deficiency) and hemophilia B (clotting factor IX deficiency)) clots slowly (Gailani & Renne, 2007*a*).

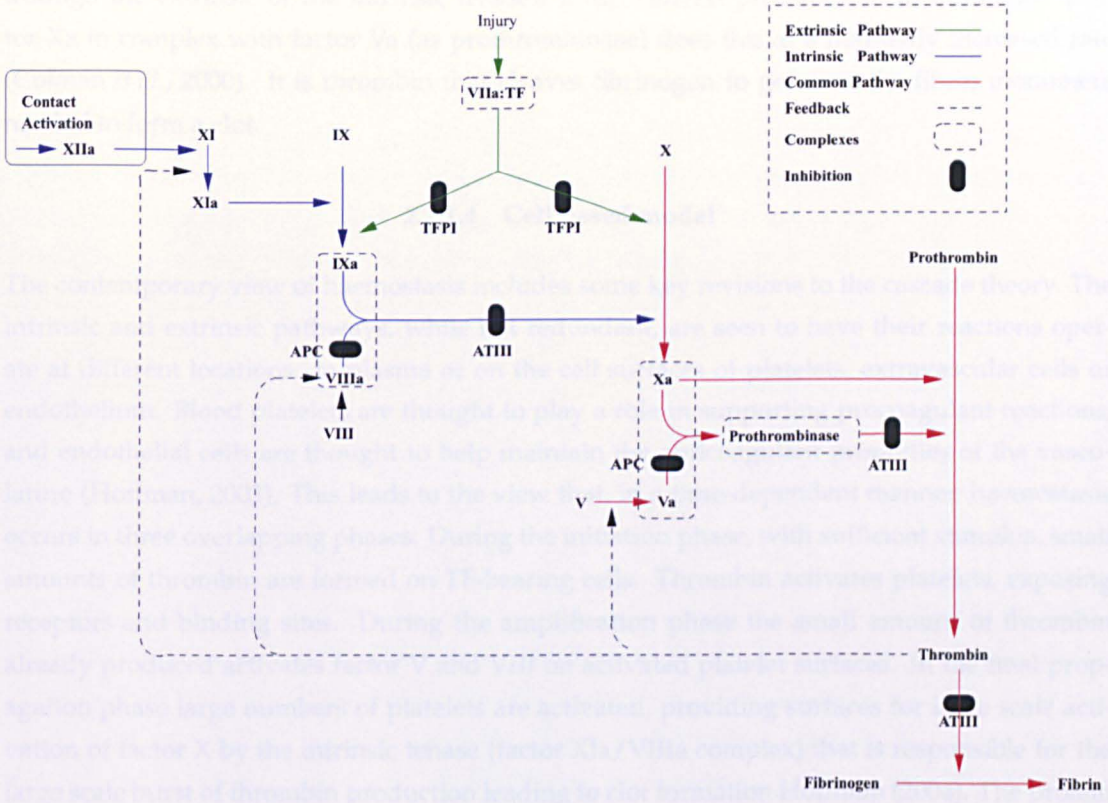

Figure 2.3: Diagram showing the major reactions involved in the coagulation cascade. Under normal conditions initiation of the cascade is considered to involve tissue factor (a receptor on damaged cell surfaces) which acts with factor VIIa (found in blood) to convert factor IX to factor IXa and factor X to factor Xa (the extrinsic pathway, shown by green arrows). The intrinsic pathway (blue arrows) includes contact activation through factor XIIa which activates factor XIa. Factor XIa converts factor IX to IXa. Factor IXa forms a complex with factor VIIa that converts factor X to factor Xa. Factor Xa onwards is sometimes referred to as the common pathway (red arrows). Factor Xa can convert prothrombin to thrombin but, as prothrombinase in complex with factor Va, does this at a markedly increased rate. Thrombin feeds back (interrupted lines) to activate factors V and VIII, which accelerates its own formation and is also thought to trigger the intrinsic pathway by activating factor XI. Thrombin dampens its own activity by activating protein C (not shown) which degrades factors Va and VIIIa. Natural inhibitors retard clotting: tissue factor pathway inhibitor (TFPI) blocks factor VIIa/TF and antithrombin III (ATIII) blocks factors IXa, Xa and thrombin. (*Arrow*, activated factors; *filled rectangles*, sites of inhibitor action; *dashed lines*, feedback reactions; *dashed rectangles*, complex assembled on a cell surface). Adapted from Colman *et al.* (2000).

2.1.1.3 Common pathway

The two pathways converge at factor X and, regardless of how factor Xa is formed (either through the extrinsic or the intrinsic tenase), it can convert prothrombin to thrombin. Factor Xa in complex with factor Va (as prothrombinase) does this at a markedly increased rate (Colman *et al.*, 2000). It is thrombin that cleaves fibrinogen to generate the fibrin monomers needed to form a clot.

2.1.1.4 Cell based model

The contemporary view of haemostasis includes some key revisions to the cascade theory. The intrinsic and extrinsic pathways, while not redundant, are seen to have their reactions operate at different locations: in plasma or on the cell surfaces of platelets, extravascular cells or endothelium. Blood platelets are thought to play a role in supporting procoagulant reactions, and endothelial cells are thought to help maintain the anticoagulant properties of the vasculature (Hoffman, 2003). This leads to the view that, in a time-dependent manner, haemostasis occurs in three overlapping phases. During the initiation phase, with sufficient stimulus, small amounts of thrombin are formed on TF-bearing cells. Thrombin activates platelets, exposing receptors and binding sites. During the amplification phase the small amount of thrombin already produced activates factor V and VIII on activated platelet surfaces. In the final propagation phase large numbers of platelets are activated, providing surfaces for large scale activation of factor X by the intrinsic tenase (factor XIa/VIIIa complex) that is responsible for the large scale burst of thrombin production leading to clot formation Hoffman (2004). The protein C system is thought to localise the generation of thrombin close to the injury by being much more efficient at inactivating factor Va on the surface of endothelial cells than on the surface of platelets, thereby preventing the generation of thrombin on nearby healthy cells (Hoffman, 2003).

2.1.1.5 Inhibition

Inhibition within the coagulation cascade is acheived through antithrombin III (ATIII), the protein C subsystem and tissue factor pathway inhibitor (TFPI).

Antithrombin III inhibits thrombin directly by forming an irreversible compound, and indirectly by inhibiting other factors within the coagulation cascade such as factor XIa and factor IXa. It is present at high concentrations, over twice that of any procoagulant concentration (Mann *et al.*, 2003; Colman *et al.*, 2000).

Thrombin participates in its own inhibition by activating protein C which, as part of the thrombomodulin/protein C/protein S system, regulates the activity of factor VIIIa and Va, cleaving them into inactive fragments, thereby dampening the activity of prothrombinase (Xa:Va) and the tenase complexes (VIIIa:IXa and VIIa:TF) (Dahlbäck & Villoutreix, 2005; Colman *et al.*, 2000).

TFPI is the principal inhibitor of the extrinsic pathway, directly inhibiting factor Xa by the

formation of the Xa:TFPI complex. It also indirectly inhibits the extrinsic tenase (VIIa:TF) by the formation of the Xa:TFPI:VIIa:TF whereby TFPI forms part of a negative feedback loop with factor X, participating in its own inhibition (Broze, 1995).

2.1.2 Therapeutic interventions

Disruption in thrombin generation can have adverse effects on the host. For example, insufficient levels of thrombin lead to excessive bleeding (as observed in congenital deficiencies such as haemophilia) while excessive clotting, or clots in the wrong place, can cause a number of conditions including thrombosis (obstructive clot formation), which is the primary cause of heart attacks and stroke. Therapeutic drugs in common use for thrombosis, including warfarin and heparin, target many factors within the coagulation cascade based on the assumption that thrombosis and normal blood clotting occur by the same pathway (Colman, 2006). Figure 2.4 shows the many factors which these drugs target. Consequently, although effective at limiting thrombus growth, these drugs cause the unwelcome side effect of excessive bleeding (Gailani & Renne, 2007*b*). There is interest in identifying new therapeutic targets which are less blunt, preventing thrombosis formation without promoting bleeding.

Deficiency of either factor IX or its cofactor VIII is associated with severe bleeding disorders (hemophilia A and B respectively). This is in contrast to deficiencies of factor XI and factor XII. Factor XI deficiency is a much milder disorder (hemophilia C), even though it has a prolonged aPTT assay (see Section 2.1.1.2), and factor XII has no bleeding disorder associated with it. Several studies suggest that factor XII is required for thrombosis but not for normal clotting (Colman, 2006). These differences in bleeding tendencies and knowledge of factor XII have stimulated interest in factor XI and factor XII as therapeutic targets (Gailani & Renne, 2007*a*).

2.1.3 Clinical tests and the thrombin generation curve

Clinical tests routinely used for the evaluation of human coagulation include the PT and aPTT (described in Sections 2.1.1.1, 2.1.1.2 respectively). However, though widely used, these tests are non-physical (being activated at much higher levels of TF than occurs phycically, in the case of the PT test, or via the nonphysiological contact pathway for the aPTT test) and, as such, are insensitive to mild bleeding disorders and new therapeutic drugs (van Veen *et al.*, 2008). They ignore the whole of thrombin generation, being based on the time blood takes to clot. In-vitro blood clots, and fibrin formation, occur when thrombin concentration reaches five percent of its peak concentration. In-vivo clotting and fibrin formation occurs later in thrombins formation, this is thought to be due to thrombin diffusing, or being washed away, from the site of injury. Laboratory tests on plasma describing the complete thrombin generation curve have been possible but have been too laborious to use in a clinical setting (Baglin, 2005). New techniques are resulting in a more effective thrombin generation assay (TG) that may be more ameneable to clinical use. The assay produces a thrombin generation curve (see Figure 2.5) that shows thrombin generation lag time, maximum thrombin concentration and the time required to acheive maximum thrombin concentration.The TG assay, unlike the PT and aPTT assay, can

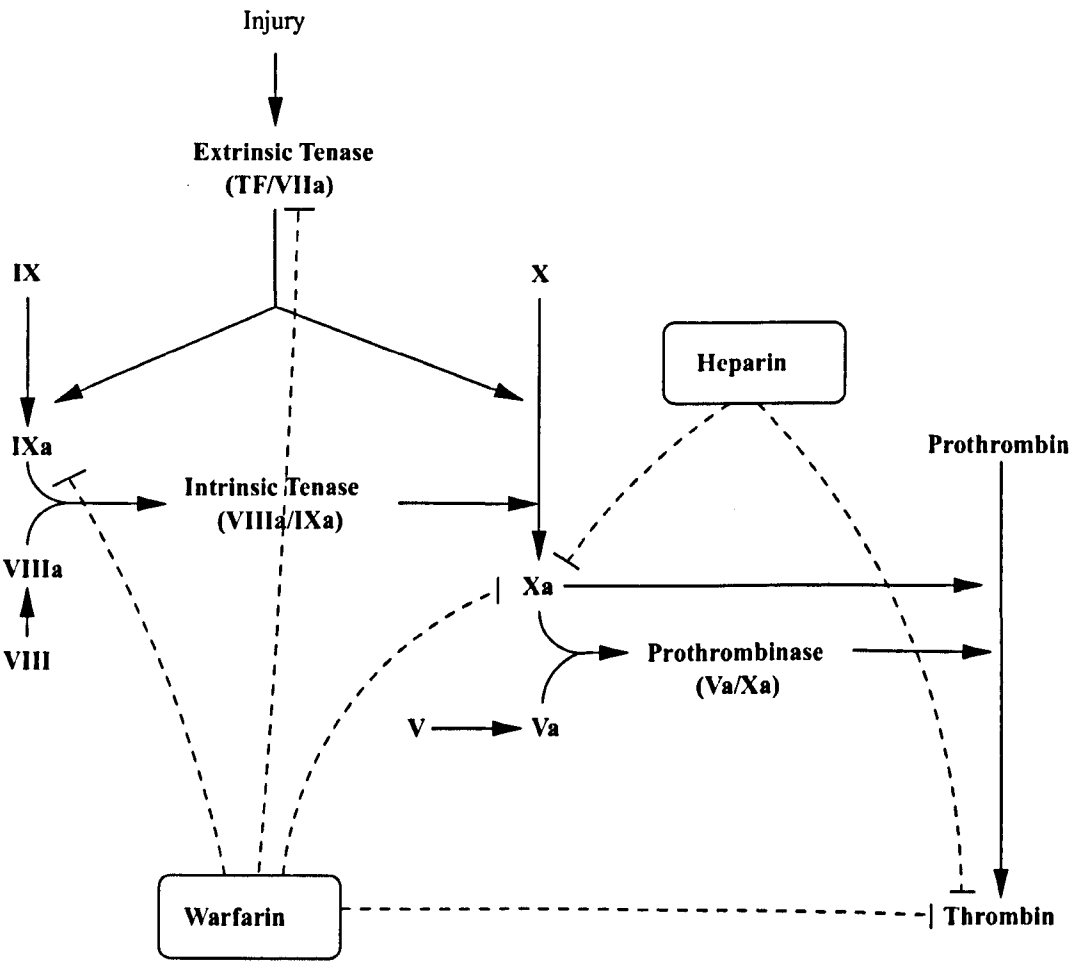

Figure 2.4: The multiple sites within the coagulation cascade that are currently targets for anticoagulant drugs. The dampening of many factors within the cascade effectively blocks thrombus formation but may also cause excessive bleeding. Anticoagulant drugs (warfarin and heparin) are shown and their targeted coagulation factors (dashed blocking arrows). Heparin binds to antithrombin III, increasing its ability to inactivate thrombin and other clotting factors; warfarin decreases prothrombin and other coagulation factors. Adapted from Mackman (2008).

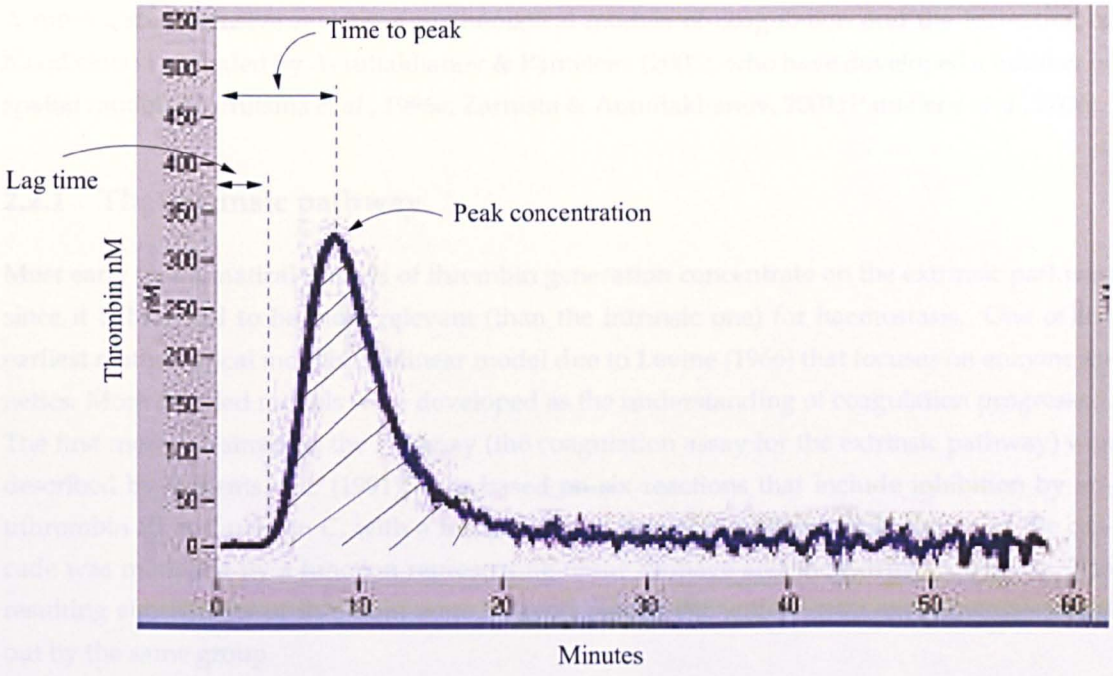

Figure 2.5: Thrombin generation curve produced in a thrombin generation assay. Used by permission from Thrombinoscope BV

detect deficiencies in both the intrinsic and extrinsic pathway (van Veen *et al.*, 2008). Initiation is at physiological levels of tissue factor (much lower than the aPTT is initiated with) making it sensitive to deficiencies in either the intrinsic or extrinsic pathway and therefore correlate more closely with hyper and hypo-coagulable phenotypes than traditional tests (van Veen *et al.*, 2008). This is providing new insights on the function of pro and anti-coagulant proteins present in plasma (Salvagno *et al.*, 2009).

2.2 Mathematical background

A complete model of coagulation would combine the biochemical reactions of the coagulation cascade (including its various inhibitory systems and its interaction with platelets), platelet aggregation, perhaps shear flow (that activates platelets) and the process of a clot breaking down (fibrinolysis). Mathematical models in this area have evolved from simple biochemical reaction models, through more comprehensive reaction pathways, to large detailed models that include blood flow, spatial effects and cell interactions such as the availability of cell surfaces (binding sites) for the formation of complexes. In this review we focus on mathematical models which are relevant to those developed in this thesis. We start by describing models of the coagulation cascade that are based on activation by the extrinsic pathway. In the following section we describe models that concentrate on the intrinsic pathway, with particular focus placed upon factor XI activation.

A more comprehensive review of mathematical models of coagulation and the formation of blood clots is provided by Ataullakhanov & Panteleev (2005), who have developed a number of spatial models (Zarnitsina *et al.*, 1996*a*; Zarnista & Ataullakhanov, 2001; Panteleev *et al.*, 2006).

2.2.1 The extrinsic pathway

Most early mathematical models of thrombin generation concentrate on the extrinsic pathway since it is believed to be more relevant (than the intrinsic one) for haemostasis. One of the earliest mathematical models is a linear model due to Levine (1966) that focuses on enzyme kinetics. More detailed models were developed as the understanding of coagulation progressed. The first model to simulate the PT assay (the coagulation assay for the extrinsic pathway) was described by Willems *et al.* (1991). It is based on six reactions that include inhibition by antithrombin III and protein C, with a feedback from thrombin to factor V. Initiation of the cascade was modelled by a function representing tissue damage and the extrinsic pathway. The resulting simulations of thrombin were in good agreement with *in-vitro* experiments carried out by the same group.

Mann and coworkers have produced a number of models in this area. Nesheim *et al.* (1984) investigated an individual reaction within the coagulation cascade, namely the formation of the complex prothrombinase which is responsible for activating thrombin, discussing it and other cell surface dependent complexes. In two further papers, the same group (Jones & Mann, 1994; Lawson *et al.*, 1994) developed a model of thrombin generation in response to extrinsic pathway activation formulated as a system of eighteen ODEs which accounts for activation of factors IX, X, V, VIII, II and the assembly of the complexes VIIIa:IXa and Va:Xa on cell surfaces. They find that the level of the activator (the extrinsic tenase) affects the time lag between initiation of the system and thrombin generation more significantly than the maximum level of thrombin generated. The model was later extended (Hockin *et al.*, 2002) to incorporate the inhibitory action of TFPI and antithrombin III. The resulting model comprised thirty four ODEs and was successfully compared to laboratory experiments (van't Veer & Mann, 1997) of clot formation in plasma in the presence and absence of inhibitors.

Khanin *et al.* produced two models that concentrate on the extrinsic pathway, the first being a nonlinear model with a positive feedback loop to account for thrombin activation of factor V (Khanin & Semenov, 1989). This model was then extended to describe the PT assay (Khanin *et al.*, 1998) by incorporating three positive feedback loops (one for each of factor V and factor VIII activation by thrombin and for activation of TF-VII complex by factor Xa) and accounts for inhibitors antithrombin III and tissue factor pathway inhibitor (TFPI). A sensitivity analysis of the second model revealed that only severe coagulation disorders associated with large reductions in the concentrations of coagulation factors could be identified using the model.

Other models have focused on other aspects of the coagulation cascade. Beltrami & Jesty (1995) and Jesty *et al.* (2005) considered different long range positive feedback mechanisms within the cascade (such as the activation of factor VIII by thrombin) and showed how these affect the

peak concentration of thrombin produced. Fogelson & Kuharsky (1998) investigated the effect of the density of membrane binding sites on activation thresholds in enzyme reactions, both in a general setting and specifically within the coagulation cascade. Lu *et al.* (2004) studied the membrane dependent reaction for the formation of factors IXa and Xa in the presence of tissue factor pathway inhibitors and antithrombin III.

Further models of coagulation that attempt to incorporate larger macroscopic effects have also been proposed. Alber *et al.* produced a number of multiscale models (Xu *et al.*, 2008, 2009, 2010) of thrombus development in blood, incorporating the microscale interactions of platelets through a discrete cellular Potts model and the macroscale interaction with blood flow through the Navier Stokes equations. The effects of platelets on blood coagulation and thrombus formation have been studied by Fogelson *et al.* in a series of models for biochemical interactions of platelets and plasma (Kuharsky & Fogelson, 2001), continuum models of platelet aggregation (Fogelson, 1992; Fogelson & Guy, 2004) and thrombus formation under blood flow (Fogelson & Guy, 2004; Guy *et al.*, 2007). Anand *et al.* incorporated the mechanical effect of shear stress activation of platelets, biochemical factors and blood flow in a series of models for the growth and lysis of clots (Anand *et al.*, 2003, 2005, 2008).

2.2.2 The intrinsic pathway and factor XI activation.

Less work has been devoted to the intrinsic pathway and, although mathematical models exist for most parts of the pathway, few models account for thrombin activation of factor XI and its potential role as a therapeutic target (see Section 2.1.2). We start by describing models that include all, or part of, the intrinsic pathway but do not include thrombin's activation of factor XI. We then describe, in more detail, those models that account for factor XI activation by thrombin.

2.2.2.1 The intrinsic pathway.

The intrinsic pathway can be studied *in vitro* via the aPTT assay (see Section 2.1.1.2). Kogan *et al.* (2001) developed a model to investigate the sensitivity of this screening test to its activation by factor XII. The impact of the extrinsic pathway and of thrombin activation of factor XI are neglected in the model. The authors concluded that trace amounts of activated factor XII (normally present in plasma) are sufficient to autoactivate factor XII. Prior to this (and in addition to their work on the extrinsic pathway) Khanin *et al.* (1991) studied how platelet activation (providing surfaces for reactions to occur on) affects thrombin generation through the intrinsic pathway. They concluded that the secretion of factor V by platelets is necessary for activation of the system only at low levels of stimulation.

Materials placed in contact with blood are thought to induce coagulation through factor XII and contact activation of the intrinsic pathway (see Figure 2.3). This is of considerable interest since it is often necessary to place materials in contact with blood *in vivo* (such as stents) without inducing pathological coagulation (Zhuo *et al.*, 2005). Guo *et al.* (2006) developed a model to investigate material-induced coagulation through factor XII activation. In their model they

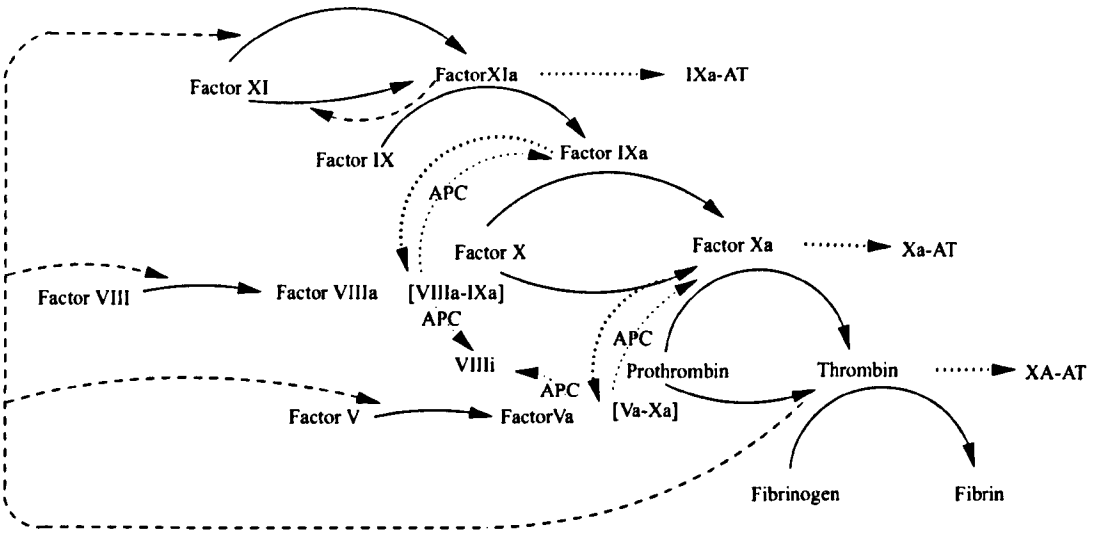

Figure 2.6: The intrinsic pathway of blood coagulation as used by Zarnitsina *et al.* (1996*a*,*b*) in their spatial models of the intrinsic pathway. Only factors of the intrinsic and common pathway are included in their models reflecting the aPTT assay. Activation is via the contact pathway using the initial concentration of factor XIa as an indicator of the level of activation. [Solid arrows, sequential activation; dotted arrows complex formations; dashed arrows, feedback activations.]

reduce the coagulation cascade to two ODEs, representing factor XII activation by a biomaterial and single enzyme/substrate representing the rest of the intrinsic pathway. They concluded that, in material-induced coagulation, the primary mechanism for activation of coagulation involves autoactivation of factor XII mediated by the inducing material.

2.2.2.2 Factor XI activation.

Ataullakhanov *et al.* presented one of the earliest models of the intrinsic pathway (Zarnitsina *et al.*, 1996*a*) and extended this to include factor XI activation by thrombin (Zarnitsina *et al.*, 1996*b*) (see Figure 2.6). A one-dimensional spatial model for the evolution of factors IX, VIII, V, X, II and I and the complexes prothrombinase (VaXa) and the intrinsic tenase (VIIIaIXa) was presented by Zarnitsina *et al.* (1996*a*). There are positive feedbacks from thrombin to factors V and VIII and inhibition via antithrombin III, and the protein C system is also included. Activation is via the intrinsic pathway. Parameter values are taken from the literature and diffusion is incorporated for all factors at the same rate. In the latter paper they solve the model numerically and demonstrate threshold behaviour for different initial conditions of factor XIa, with above-threshold levels producing explosive thrombus growth before decreasing. The model is then modified to incorporate thrombin activation of factor XI. They investigated varying the levels of thrombin activation in the range $0 - 10^{-2}$ min^{-1}, finding that levels greater than 10^{-6} min^{-1} dramatically change the spatial pattern of clot growth with the clot now becoming infinite in size. Ataullakhanov *et al.* have developed further models, including

a mathematical model of factor X activation by the intrinsic tenase (the complex of factors IXa and factor VIIa) (Panteleev *et al.*, 2004) which was incorporated into a spatial model of both the intrinsic and extrinsic pathways (Panteleev *et al.*, 2006), demonstrating that the intrinsic tenase is important in clot propagation far from the activated site. Although these models assume that factor XI is activated via thrombin, this is not discussed further.

Anand *et al.* have proposed several models that incorporate the intrinsic and extrinsic pathway and factor XI activation by thrombin. A detailed discussion of the requirements for a whole clot model was given by Anand *et al.* (2003, 2005), alongside an initial attempt at this in which the biochemical reactions presented in Zarnitsina *et al.* (1996*a*,*b*) were extended to include the extrinsic pathway, blood flow and activated and resting platelets as sources of membrane binding sites for the assembly of prothrombinase and the intrinsic tenase. A model for the growth and lysis of clots in static plasma was given by Anand *et al.* (2008), who again incorporated the extrinsic and intrinsic pathway and factor XI activation by thrombin. They were able to corroborate existing experimental data (Butenas *et al.*, 1999) and discussed two anti-coagulant states antithrombin III and protein C deficiency, but not the implications of thrombins activation of factor XI.

Kramoroff & Nigretto (2001) developed the only model which specifically addresses the activation of factor XI. The model only includes the factors of the intrinsic and common pathway; being designed to simulate the aPTT screening test; activation of factor XI by thrombin is included (see Figure 2.7 for a network diagram of these reactions). Guided by model simulations, they concluded that factor XI autoactivation is more important than thrombin-mediated activation for the formation of thrombin. The model was evaluated by comparing model predictions with laboratory measurements conducted on normal plasma and plasma deficient in one of factors VIII, IX, XI and XIII.

In avascular environments, such as synovial fluid and ovarian follicular fluid, protein components are similar to blood, but there are no platelets. Therefore, complexes form on phospholipid surfaces such as those provided by activated or ruptured endothelial cells. Bungay *et al.* (2003) presented a model of thrombin generation within such environments . The resulting system of seventy-three ODEs (see Figure 2.8 for a simplified network diagram of the reactions included) includes thrombin activation of factor XI, thrombin inhibition through protein C and antithrombin III and cell surfaces on which complexes may form. Activation is through the extrinsic pathway and the VIIa:TF complex. Numerical solutions of the model obtained by using parameter estimates from the literature were shown to be in good qualitative agreement with experiments reported by Butenas *et al.* (1999). By varying the availability of surfaces on which reactions could occur, they concluded that the availability of such surfaces regulates the time and peak level of thrombin generation.

A modification of the above model (Bungay *et al.*, 2006) was used to study thrombin generation in human ovarian follicular fluid, where an absence of feedback mechanisms is thought to account for the low amounts of thrombin produced. The original model was also used to investigate the effects of varying the initial values of the factors VIII, IX and XI (corresponding to haemophilia A, B and C respectively) and shown to yield results that were qualitatively similar

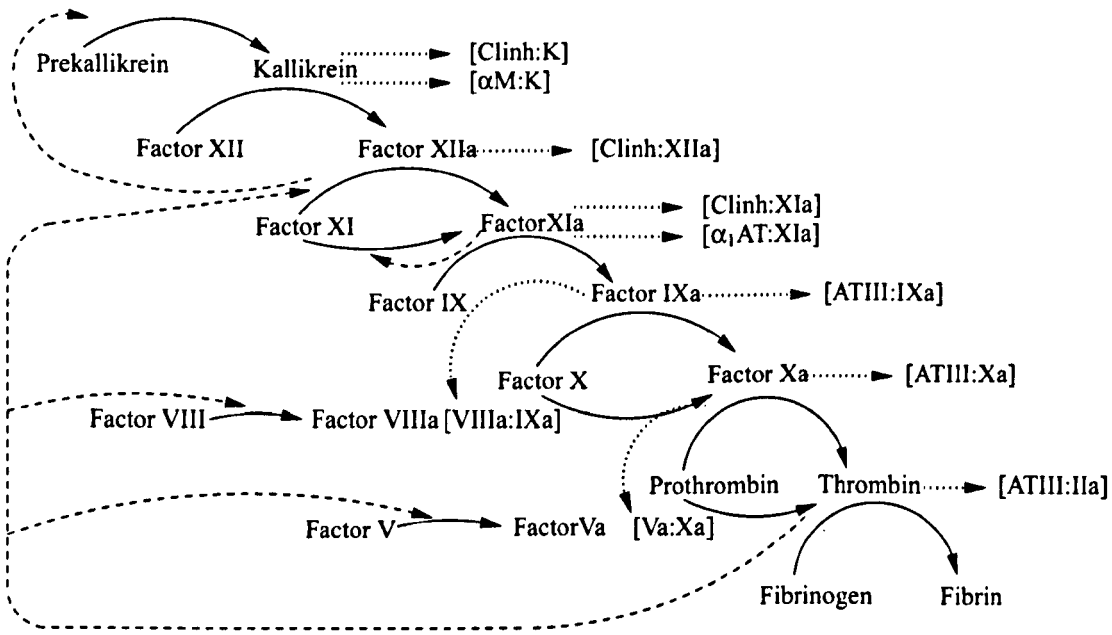

Figure 2.7: Intrinsic pathway of blood coagulation as used by Kramoroff & Nigretto (2001) in their model of the intrinsic pathway. Only factors of the intrinsic and common pathway are included and the system (reflecting the aPTT assay) is activated through initial conditions of activated factor XII. [Solid arrows, sequential activation; dotted arrows complex formations; dashed arrows, feedback activations.]

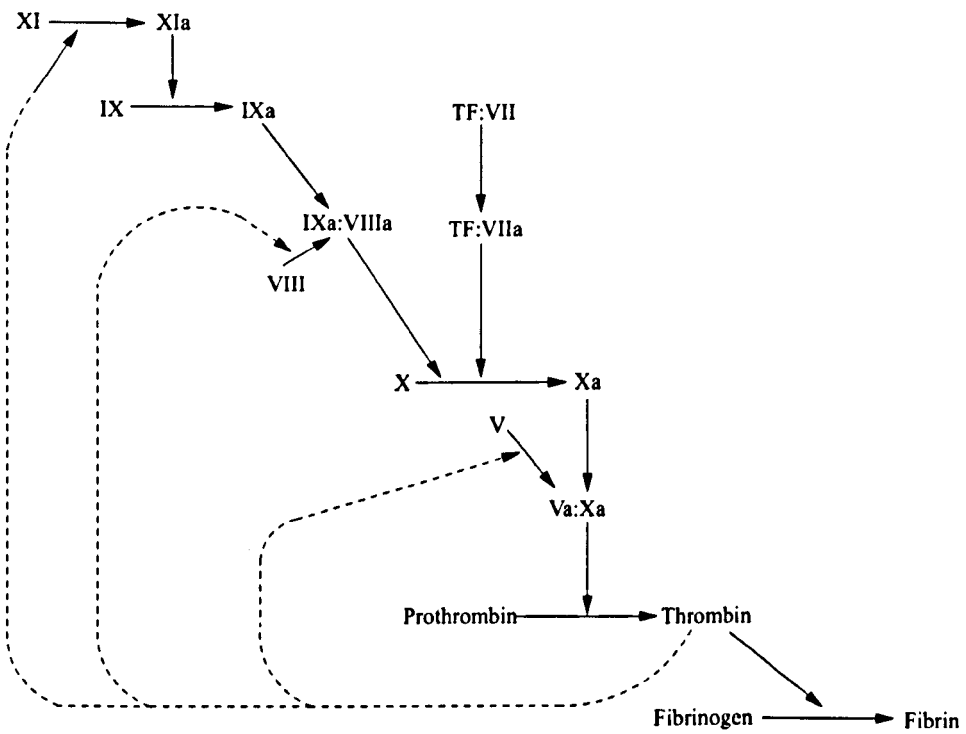

Figure 2.8: A simplified schematic of the reactions included in the pathway of blood coagulation used by Bungay *et al.* (2003); Bungay (2008). Factors of the extrinsic, intrinsic and common pathways are included with variables for their occurrence in fluid and as lipid bound factors. Activation is via VIIa:TF and the extrinsic pathway. [Positive feedback, dashed lines; PL, assembly dependent on phospholipid surfaces.]

to what would be expected (Bungay, 2008).

2.3 Discussion

In this chapter we have provided a biological introduction to coagulation focussing on aspects that will be relevant to our mathematical models. We also reviewed existing relevant mathematical models. Due to the incredible biochemical complexity of the coagulation cascade we start our modelling (chapter 3) with a reduced set of reactions that have previously been shown to produce the characteristic thrombin generation curve (Figure 2.5) and we aim to understand some of the underlying mechanisms of its production. In chapter 4 we extend this model to include the biochemical reactions of the extrinsic and intrinsic pathways and produce simulations discussing, in particular, the activation of factor XI that is thought to be of interest for therapeutic intervention.

CHAPTER 3

An asymptotic analysis of thrombin generation

3.1 Introduction

There are numerous mathematical models of coagulation and the formation of blood clots, including many that concentrate on thrombin generation; a review of these is given in the previous chapter. The coagulation cascade is traditionally thought of as being split into two pathways, the slower (intrinsic) one beginning in the blood and the faster (extrinsic) one being initiated by tissue trauma. The two converge into a common pathway at the formation of factor X (Porth, 2005). This pathway results in the generation of thrombin, which induces the conversion of fibrinogen to fibrin monomers. The contemporary view of haemostasis includes some key revisions: the intrinsic and extrinsic pathways are seen to occur at different locations and the two pathways are linked through such mechanisms as extrinsic tenase activation of factor X (Hoffman, 2004). Models exist for both the intrinsic (Bungay *et al.*, 2003; Guo *et al.*, 2006) and the extrinsic (Kuharsky & Fogelson, 2001; Lawson *et al.*, 1994; Jones & Mann, 1994; Khanin & Semenov, 1989) pathways, with the number of reactions included ranging from small subsets (Jones & Mann, 1994; Khanin & Semenov, 1989; Qiao *et al.*, 2004; Jesty *et al.*, 2005) to more comprehensive models (Hockin *et al.*, 2002; Anand *et al.*, 2008), reflecting how the underlying biology has increasingly succumbed to investigation.

We base our model on a set of reactants from within the common pathway of the cascade activated via the extrinsic pathway and ending with the enzyme thrombin. These reactions have previously been shown to be able to simulate the observed rise and fall of thrombin levels. Willems *et al.* (1991) fully describe the reactions but not the equations derived from them. While we acknowledge that these reactions represent only a vastly reduced subset of what is an extremely complicated network, we contend that they capture many of its characteristic mechanisms, notably participation of thrombin in its own generation (through its activation of factor V) and two important anticoagulant pathways (protein C and antithrombin III inhibition). We analyse the step-by-step processes involved in the generation of thrombin through a process of

time-dependent asymptotic analysis (aided considerably by the availability from the literature of the required parameter values), which enables us to demonstrate the importance of various reactions for thrombin generation and to identify which components of the cascade are active on each timescale. We determine how the resultant series of simplified models over seven timescales corresponds physiologically to various interactions within the cascade, illustrating the usefulness of this technique when applied to such complex systems.

3.2 Mathematical model

3.2.1 Formulation

The reactions and the kinetics used, from (Willems *et al.*, 1991), are listed in Table 3.1 and illustrated in Figure 3.1. We give details of these six reactions below. While Willems *et al.* (1991) describe these reactions and show simulations produced from a mathematical model derived from them they do not describe the mathematical equations. The reactants (factors) within the coagulation cascade are numbered from one to thirteen using Roman numerals, the addition of 'a' denoting (as is traditional) an activated factor; moreover, we use an 'i' for inactivated downstream factors in their various forms. We note that the numerical value does not refer to the reactant's position within the cascade but rather to the historical sequence of discovery. We formulate a system of coupled ordinary differential equations (3.2.1a)-(3.2.3b) based on these reactions; see Tables 3.2 and 3.3 for definitions of the variables and parameters and Table 3.1 for the reactions that we now describe.

Reaction 1. Generation and inactivation of factor Xa. Injury to tissue leads to the activation of factor X through the recruitment of factor VII (found in blood) by tissue factor (TF), a cell-surface receptor, exposed on damaged cells normally found outside the vasculature, (Hoffman, 2004; Crawley *et al.*, 2007). Recruitment of factor VII and factor VIIa by TF leads to the assembly of the TF:VIIa complex, which in turn is responsible for the activation of factor X (Riewald & Ruf, 2003; Crawley *et al.*, 2007). We follow Willems *et al.* (1991) and describe this activation of factor X by the VIIa:TF complex (extrinsic tenase) by the function $H(t) = k_{1a}\gamma_{1a}e^{-\gamma_{1a}t}$ representing the variable production of factor Xa, where k_{1a} is the total amount of factor Xa (concentration f_x^a) produced (while $k_{1a}\gamma_{1a}$ is in effect a measure of the severity of the injury), the rate constant γ_{1a} is associated with the loss of the stimulant by its degradation and sequestration into an inactive form and t is the time after injury; see (3.2.2a). We note that the exponential dependance is for definiteness, the precise functional form being of limited significance; it assumes in particular that the timescale over which Xa is produced by the trauma is much shorter than the timescale for its degradation (the activation of X ceases rapidly following injury due to TFPI inhibition). Antithrombin III inhibits factor Xa by forming an irreversible complex (concentration f_x^i) with rate k_{1b} see (3.2.2a, 3.2.3a).

Reaction 2. Generation and inactivation of factor Va. The conversion of factor V (f_v) into

Reaction	Generation		Inactivation	
	No.	Description	No.	Description
Generation and inactivation of factor Xa	1*a*	$\xrightarrow{H(t)}$ Xa	1*b*	Xa+ATIII $\rightarrow$ Xa:ATIII
Generation and inactivation of factor Va	2*a*	V $\xrightarrow{\text{IIa}}$ Va	2*c*	Va $\xrightarrow{\text{APC}}$ InactiveV
	2*b*	V $\xrightarrow{\text{Xa}}$ Va		
Formation and inactivation of prothrombinase	3*a*	Va+Xa $\rightarrow$ Va:Xa	3*b*	Va:Xa+ATIII $\rightarrow$ Va+Xa:ATIII
			3*c*	Va:Xa $\xrightarrow{\text{APC}}$ InactiveV+Xa
Generation and inactivation of thrombin	4*a*	II $\xrightarrow{\text{Xa}}$ IIa	4*c*	IIa+ATIII $\rightarrow$ IIa:ATIII
	4*b*	II $\xrightarrow{\text{Va:Xa}}$ IIa		
Protein C inhibition	5*a*	C $\xrightarrow{\text{IIa}}$ APC	5*b*	APC $\rightarrow$ InactiveC
Fibrinogen to fibrin	6	Fibrinogen $\xrightarrow{\text{IIa}}$ Fibrin		

Table 3.1: The set of reactions for a reduced model of thrombin generation (Willems *et al.*, 1991). Michaelis-Menten kinetics are adopted for enzymatic reactions 2*a*, 2*b*, 2*c*, 3*c*, 4*a*, 4*b*, while mass-action kinetics are adopted for the remainder, with 1*b*, 3*b*, 4*c*, 5*a*, 5*b* and 6 being of first-order (due to the abundance of ATIII, its concentration is assumed to be constant) and 3*a* (the binding of two proteins) of second order. Reactants (factors) within the cascade are normally denoted by Roman numerals (with the addition of 'a' indicating an activated factor); other terms used are prothrombinase for the complex formed from factor Xa and factor Va, prothrombin (factor II), thrombin (factor IIa), fibrinogen (factor I), fibrin (factor Ia), the inhibitors being protein C (APC in its activated form) and ATIII (antithrombin III). These reactions are shown graphically in Figure 3.1.

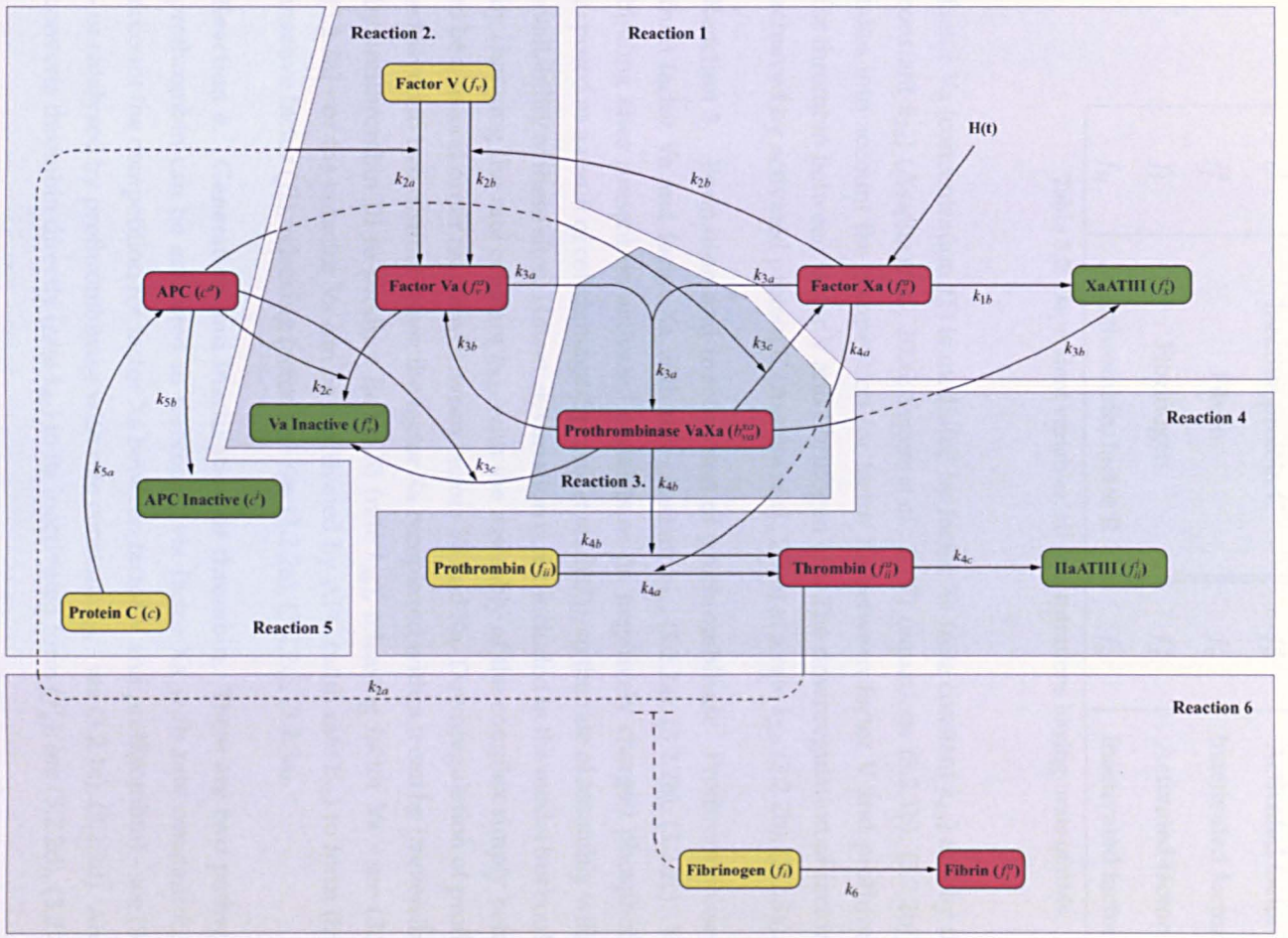

Figure 3.1: A schematic representing the model of thrombin generation based on the reactions shown in Table 3.1. The boxes correspond to the coagulation factors, with the lower case letters in brackets being used in the mathematical model to designate the concentrations. Red boxes (with superscript a) denote the active factors, yellow the procoagulants and green (with superscript i) the inactivated factors. Arrows pointing into boxes represent conversion from one species to another, while those directed at other lines correspond to catalysis.

Variable	Description	Variable	Description
b_{va}^{xa}	Prothrombinase (VaXa)	f_{ii}^{a}	Thrombin, factor IIa
c	Protein C	f_{ii}^{i}	Inactivated thrombin
c^a	Activated protein C (APC)	f_v	Factor V
c^i	Inactive protein C	f_v^a	Activated factor V
f_i^a	Fibrin	f_v^i	Inactivated factor V
f_i	Fibrinogen	f_x^a	Activated factor X
f_{ii}	Prothrombin, factor II	f_x^i	Inactivated factor X

Table 3.2: Dependent variables; all concentrations having units of nMs.

factor Va (concentration f_v^a) is mediated by factor Xa (rate constant k_{2b}) and by thrombin (rate constant k_{2a}) (Asselta *et al.*, 2006; Segers *et al.*, 2007) (equations (3.2.1b), (3.2.2b)). The model takes into account the competition for factor Xa between factor V and prothrombin (f_{ii}) and for thrombin between factor V and fibrinogen (f_i). The downregulation of factor Va activity is achieved by activated protein C (Asselta *et al.*, 2006) at a rate k_{2c}, (3.2.2b), (3.2.3a).

Reaction 3. Formation and inactivation of prothrombinase. Prothrombinase is assembled from factor Va and factor Xa with rate constant k_{3a}, (3.2.2a), (3.2.2b), (3.2.2c). This occurs on binding sites present on activated platelets or on negatively charged phospholipids that are exposed as a result of cell damage (Spronk *et al.*, 2003), so the rate of assembly will vary with the availability of these sites. However, variation is not included in the model but could be explored by changing the rate constant k_{3a}, with the assembly of the complex simply being considered to be a second order reaction between factors Va and Xa. Downregulation of prothrombinase is achieved in two distinct ways: the factor Xa complexed within it can be irreversibly inactivated by antithrombin III to produce factor Xi (rate k_{3b}), releasing factor Va - see (3.2.2b), (3.2.2c), (3.2.3a) - or the cofactor Va can be inactivated by APC (with rate k_{3c}) to form (irreversibly) an inactive factor (f_v^i), releasing factor Xa - see (3.2.2a), (3.2.2c), (3.2.3a).

Reaction 4. Generation and inactivation of thrombin. There are two pathways by which prothrombin can be activated to thrombin, via factor Xa with rate constant k_{4a} (taking into account the competition for factor Xa between factor V and prothrombin) - see (3.2.1c), (3.2.2d) - or catalysed by prothrombinase with rate constant k_{4b} - see (3.2.1c), (3.2.2d). Antithrombin III converts thrombin directly (rate k_{4c}) to its inactivated form (f_{ii}^i); see (3.2.2d), (3.2.3b).

Reaction 5. Protein C system. The inhibitory protein C pathway is modelled as a first-order reaction with activation at rate k_{5a} - see (3.2.1d), (3.2.2e) - and conversion to its inactivated form (c_i) at rate k_{5b} - see (3.2.2e), (3.2.3b).

Reaction 6. Conversion of fibrinogen to fibrin. The conversion of fibrinogen (f_i) to fibrin (f_i^a) (rate constant k_6) is included to account for the reduction in the activation rate of fac-

Parameter	Value	Parameter	Value
k_{1a}	20000 nM	k_{3c}	24 min^{-1}
γ_{1a}	1 min^{-1}	k_{3cm}	20 nM
k_{1b}	0.25 min^{-1}	k_{4a}	2.3 min^{-1}
k_{2a}	14 min^{-1}	k_{4am}	58 nM
k_{2am}	72 nM	k_{4b}	2000 min^{-1}
k_{2b}	2.6 min^{-1}	k_{4bm}	210 nM
k_{2bm}	10 nM	k_{4c}	1.3 min^{-1}
k_{2c}	24 min^{-1}	k_{5a}	0.0014 min^{-1}
k_{2cm}	20 nM	k_{5b}	0.35 min^{-1}
k_{3a}	10 $nM^{-1}min^{-1}$	k_6	2×10^3 min^{-1}
k_{3b}	0.05 min^{-1}	k_{6m}	2000 nM

Table 3.3: Dimensional parameter values, based on values from Willems *et al.* (1991), where a similar parameter set is used for the simulations - Willems *et al.* (1991) adopts a lower value for the initial stimulus ($k_{1a} = 20$). The reasons for adjusting the parameter k_{1a} are given in Section 3.2.3. The value of k_6 is not listed by Willems *et al.* (1991) and we use a value of 2×10^3 min^{-1} taken from Kogan *et al.* (2001); Higgins *et al.* (1983).

tor V caused by the competition for thrombin between fibrinogen and factor V: (3.2.1b), (3.2.2b).

The equations representing the procoagulants are thus:

$$\frac{df_i}{dt} = -k_6 f_i, \tag{3.2.1a}$$

$$\frac{df_v}{dt} = -\frac{k_{2a} f_{ii}^a f_v}{f_v + k_{2am}(1 + \frac{f_i}{k_{6m}})} - \frac{k_{2b} f_x^a f_v}{f_v + k_{2bm}(1 + \frac{f_{ii}}{k_{4am}})}, \tag{3.2.1b}$$

$$\frac{df_{ii}}{dt} = -\frac{k_{4a} f_x^a f_{ii}}{f_{ii} + k_{4am}(1 + \frac{f_v}{k_{2bm}})} - \frac{k_{4b} b_{va}^{xa} f_{ii}}{f_{ii} + k_{4bm}}, \tag{3.2.1c}$$

$$\frac{dc}{dt} = -k_{5a} c, \tag{3.2.1d}$$

with those for the activated factors being

$$\frac{df_x^a}{dt} = H(t) + \frac{k_{3c} c^a b_{va}^{xa}}{b_{va}^{xa} + k_{3cm}} - k_{1b} f_x^a - k_{3a} f_x^a f_v^a, \tag{3.2.2a}$$

$$\frac{df_v^a}{dt} = \frac{k_{2a} f_{ii}^a f_v}{f_v + k_{2am}(1 + \frac{f_i}{k_{6m}})} + \frac{k_{2b} f_x^a f_v}{f_v + k_{2bm}(1 + \frac{f_{ii}}{k_{4am}})} + k_{3b} b_{va}^{xa} - \frac{k_{2c} c^a f_v^a}{f_v^a + k_{2cm}} - k_{3a} f_x^a f_v^a, \tag{3.2.2b}$$

$$\frac{db_{va}^{xa}}{dt} = k_{3a}f_x^a f_v^a - k_{3b}b_{va}^{xa} - \frac{k_{3c}c^a b_{va}^{xa}}{b_{va}^{xa} + k_{3cm}}, \tag{3.2.2c}$$

$$\frac{df_{ii}^a}{dt} = \frac{k_{4a}f_x^a f_{ii}}{f_{ii} + k_{4am}(1 + \frac{f_v}{k_{2bm}})} + \frac{k_{4b}b_{va}^{xa} f_{ii}}{f_{ii} + k_{4bm}} - k_{4c}f_{ii}^a, \tag{3.2.2d}$$

$$\frac{dc^a}{dt} = k_{5a}c - k_{5b}c^a, \tag{3.2.2e}$$

where $H(t) = k_{1a}\gamma_{1a}e^{-\gamma_{1a}t}$ represents the activation of factor X through tissue injury and the extrinsic pathway, k_{1a} reflecting the severity of the injury with $\int_0^\infty H(t')dt' = k_{1a}$ and γ_{1a} being a representative timescale for the extrinsic pathway. Finally, the equations for the downstream inactivated factors and fibrin are

$$\frac{df_x^i}{dt} = k_{1b}f_x^a + k_{3b}b_{va}^{xa}, \quad \frac{df_v^i}{dt} = \frac{k_{2c}c^a f_v^a}{f_v^a + k_{2cm}} + \frac{k_{3c}c^a b_{va}^{xa}}{b_{va}^{xa} + k_{3cm}}, \tag{3.2.3a}$$

$$\frac{df_{ii}^i}{dt} = k_{4c}f_{ii}^a, \quad \frac{dc^i}{dt} = k_{5b}c^a, \quad \frac{df_i^a}{dt} = k_6 f_i. \tag{3.2.3b}$$

Initial conditions are taken from Willems *et al.* (1991), and describe the initial concentrations for procoagulants and regulatory proteins in plasma, it being assumed that no activated or inactivated factors are present at $t = 0$ with the levels of the procoagulants taken to be $f_{ii_0} = 1000$nM for prothrombin, $f_{v_0} = 30$nM for factor V, $c_0 = 100$nM for protein C, and $f_{i_0} = 10000$nM for fibrinogen, i.e. we set

$$\text{at} \quad t = 0, \quad f_i = f_{i0}, \quad f_v = f_{v0}, \quad f_{ii} = f_{ii0}, \quad c = c_0, \quad f_x^a = 0, \quad f_v^a = 0,$$
$$b_{va}^{xa} = 0, \quad f_{ii}^a = 0, \quad c^a = 0, \quad f_x^i = 0, \quad f_v^i = 0, \quad f_{ii}^i = 0, \quad c^i = 0, \quad f_i^a = 0.$$

We note that in this system we have conservation (in their various forms) of fibrinogen, prothrombinase, protein C, factor V and factor X as expressed by

$$f_i^a + f_i = f_{i0}, \quad f_{ii} + f_{ii}^a + f_{ii}^i = f_{ii0}, \quad c + c^a + c^i = c_0,$$
$$f_v + f_v^a + f_v^i + b_{va}^{xa} = f_{v0} + b_{va0}^{xa}, \quad f_x^a + f_x^i + b_{va}^{xa} = \int_0^t H(t')dt' + b_{va0}^{xa}, \tag{3.2.4}$$

which follow from (3.2.1)-(3.2.3).

3.2.2 Nondimensionalisation

We nondimensionalise the model, comprised of equations (3.2.1a)-(3.2.3b), with time scaled such that $\tilde{t} = k_{4c}t$ denotes nondimensional time, $\tilde{t}$ =O(1) being an intermediate timescale that corresponds to the inactivation of thrombin by antithrombin III. The remaining variables are scaled to simplify the corresponding equations as much as possible and are

$$f_x^a = \frac{k_{4c}\tilde{f}_x^a}{k_{3a}}, \qquad f_x^i = \frac{k_{4c}\tilde{f}_x^i}{k_{3a}}, \qquad f_v = k_{2bm}\tilde{f}_v, \qquad f_v^a = k_{2cm}\tilde{f}_v^a, \tag{3.2.5}$$

$$f_v^i = k_{2cm}\tilde{f}_v^i, \qquad b_{va}^{xa} = k_{3cm}\tilde{b}_{va}^{xa}, \qquad f_{ii} = k_{4am}\tilde{f}_{ii}, \qquad f_{ii}^a = \frac{k_{2cm}k_{4c}\tilde{f}_{ii}^a}{k_{2a}}, \tag{3.2.6}$$

$$f_{ii}^i = \frac{k_{2cm}k_{4c}\tilde{f}_{ii}^i}{k_{2am}}, \qquad c = \frac{k_{2cm}k_{4c}\tilde{c}}{k_{2c}}, \qquad c^a = \frac{k_{2cm}k_{4c}\tilde{c}_a}{k_{2c}}, \qquad c^i = \frac{k_{2cm}k_{4c}\tilde{c}_i}{k_{2c}}, \tag{3.2.7}$$

$$f_i = k_{6m}\tilde{f}_i, \qquad f_i^a = k_{6m}\tilde{f}_i^a, \tag{3.2.8}$$

Procoagulant	Dimensional value	Nondim. value
Fibrinogen (f_{i0})	$10\ \mu M$	$\tilde{f}_{i0} = 5$
Factor V (f_{v0})	$30\ nM$	$\tilde{f}_{v0} = 3$
Prothrombin (f_{ii0})	$1\ \mu M$	$\tilde{f}_{ii0} = 17$
Protein C (c_0)	$100\ nM$	$\tilde{c}_0 = 92$

Table 3.4: Initial concentrations of the procoagulants in plasma, taken from Willems *et al.* (1991). It is assumed that no other factors are present at the start.

where tildes denote the nondimensionless variables. The resulting dimensionless parameters are

$$\tilde{k}_{1a} = \frac{k_{1a}k_{3a}}{k_{4c}}, \quad \tilde{\gamma}_{1a} = \frac{\gamma_{1a}}{k_{4c}}, \quad \tilde{k}_{1b} = \frac{k_{1b}}{k_{4c}}, \quad \tilde{k}_{2a} = \frac{k_{2cm}}{k_{2bm}},$$
$$\tilde{k}_{2am} = \frac{k_{2am}}{k_{2bm}}, \quad \tilde{k}_{2b} = \frac{k_{2b}}{k_{3a}k_{2cm}}, \quad \tilde{k}_{3a} = \frac{k_{3a}k_{2cm}}{k_{4c}}, \quad \tilde{q}_{3a} = \frac{k_{2cm}}{k_{3cm}},$$
$$\tilde{k}_{3b} = \frac{k_{3b}}{k_{4c}}, \quad \tilde{k}_{3c} = \frac{k_{3c}}{k_{2c}}, \quad \tilde{k}_{4a} = \frac{k_{4a}k_{2a}}{k_{2cm}k_{3a}k_{4c}}, \quad \tilde{q}_{4a} = \frac{k_{4a}}{k_{4am}k_{3a}},$$
$$\tilde{k}_{4b} = \frac{k_{4b}k_{3cm}}{k_{4am}k_{4c}}, \quad \tilde{k}_{4bm} = \frac{k_{4bm}}{k_{4am}}, \quad \tilde{k}_{5a} = \frac{k_{5a}}{k_{4c}}, \quad \tilde{k}_{5b} = \frac{k_{5b}}{k_{4c}},$$

$$\tilde{k}_6 = \frac{k_6}{k_{4c}}.$$

The dimensionless initial conditions are

$$\tilde{f}_{ii0} = \frac{f_{ii0}}{k_{4am}}, \quad \tilde{c}_0 = \frac{k_{2c}c_0}{k_{2cm}k_{4c}}, \quad \tilde{f}_{i0} = \frac{f_{i0}}{k_{6m}} \quad \text{and} \quad \tilde{f}_{v0} = \frac{f_{v0}}{k_{2bm}} \tag{3.2.9}$$

(numerical values listed in Table 3.4), all other initial conditions being set to zero.

Equations (3.2.1a)-(3.2.3b) transform to give a dimensionless system of fourteen ordinary differential equations, which can be subdivided as follows (henceforth dropping the ˜s). The equations for fibrinogen and fibrin,

$$\frac{df_i}{dt} = -k_6 f_i, \quad \frac{df_i^a}{dt} = k_6 f_i, \tag{3.2.10}$$

are independent and are easily solved in the form

$$f_i = f_{i0}e^{-k_6 t}, \quad f_i^a = f_{i0}\left(1 - e^{-k_6 t}\right). \tag{3.2.11}$$

The equations for protein C in all its forms also decouple

$$\frac{dc}{dt} = -k_{5a}c, \quad \frac{dc^a}{dt} = k_{5a}c - k_{5b}c^a, \quad \frac{dc^i}{dt} = k_{5b}c^a, \tag{3.2.12}$$

and can be solved to give

$$c = c_0 e^{-k_{5a}t}, \quad c^a = \frac{c_0 k_{5a}}{k_{5b} - k_{5a}}\left(e^{-k_{5a}t} - e^{-k_{5b}t}\right),$$
$$c^i = \frac{c_0}{k_{5b} - k_{5a}}\left(k_{5b} - k_{5a} + k_{5a}e^{-k_{5b}t} - k_{5b}e^{-k_{5a}t}\right). \tag{3.2.13}$$

The other dependent variables satisfy the coupled system

$$\frac{df_x^a}{dt} = k_{1a}\gamma_{1a}e^{-\gamma_{1a}t} + \frac{k_{3c}k_{3a}c^a b_{va}^{xa}}{b_{va}^{xa}+1} - k_{1b}f_x^a - k_{3a}f_x^a f_v^a, \tag{3.2.14}$$

$$\frac{df_v^a}{dt} = \frac{f_{ii}^a f_v}{f_v + k_{2am}(1+f_i)} + \frac{k_{2b}f_x^a f_v}{f_v+1+f_{ii}} + \frac{k_{3b}}{q_{3a}}b_{va}^{xa} - \frac{c^a f_v^a}{f_v^a+1} - f_x^a f_v^a, \tag{3.2.15}$$

$$\frac{db_{va}^{xa}}{dt} = q_{3a}f_x^a f_v^a - k_{3b}b_{va}^{xa} - \frac{k_{3c}q_{3a}c^a b_{va}^{xa}}{b_{va}^{xa}+1}, \tag{3.2.16}$$

$$\frac{df_{ii}^a}{dt} = \frac{k_{4a}f_x^a f_{ii}}{f_v+1+f_{ii}} + \frac{k_{4a}k_{4b}f_{ii}b_{va}^{xa}}{q_{4a}(f_{ii}+k_{4bm})} - f_{ii}^a, \tag{3.2.17}$$

$$\frac{df_v}{dt} = -\frac{k_{2a}f_{ii}^a f_v}{f_v + k_{2am}(1+f_i)} - \frac{k_{2a}k_{2b}f_x^a f_v}{f_v+1+f_{ii}}, \tag{3.2.18}$$

$$\frac{df_{ii}}{dt} = -\frac{q_{4a}f_x^a f_{ii}}{f_v+1+f_{ii}} - \frac{k_{4b}f_{ii}b_{va}^{xa}}{f_{ii}+k_{4bm}}, \tag{3.2.19}$$

with the following equations, for downstream inactivated factors, decoupling

$$\frac{df_x^i}{dt} = k_{1b}f_x^a + \frac{k_{3a}k_{3b}}{q_{3a}}b_{va}^{xa}, \quad \frac{df_v^i}{dt} = \frac{c^a f_v^a}{f_v^a+1} + \frac{k_{3c}c^a b_{va}^{xa}}{b_{va}^{xa}+1}, \quad \frac{df_{ii}^i}{dt} = f_{ii}^a. \tag{3.2.20}$$

3.2.3 Parameter Values

Willems *et al.* (1991) take a parameter set from literature and then vary parameters to fit their simulated thrombin generation curve to experimental data from Pieters *et al.* (1988). Taking their initial parameter set (Table 3.3 except $k_{1a} = 20$) and adjusting k_{1a} (representing the total amount of tissue factor expressed) up ($k_{1a} = 20000$) we find that numerical simulations of our model produce a maximum peak thrombin concenration of approximately six hundred nM after one minute, the same as data from Pieters *et al.* (1988).

3.3 Numerical illustration

We solve the full (dimensional) system (3.2.10)-(3.2.20) numerically using a Matlab ODE solver (ode15s) with the initial conditions given in Table 3.4 and the parameter values in Table 3.3. Such results (Figure 3.2) and the range of orders of magnitude of the dimensional parameters (Table 3.5) suggest that reactions occur on many different timescales. To understand these simulations more fully we next use a systematic asymptotic approach to separate the dynamics into a sequence of timescales to elucidate the underlying physical mechanisms. This results in a sequence of seven timescales in which initially only the fastest reactions feature, namely the conversion of fibrinogen to fibrin, with the slower reactions, such as the depletion of activated protein C, contributing on the longer timescales. In Section 3.7 we provide a discussion of all of these timescales and identify the relevant components within the cascade. The scalings required for each variable on each timescale, in terms of the dimensionless variables defined in (3.2.5)-(3.2.8), are given in Table 3.6 and at the start of each subsection they are given relative to those on the previous timescale. If no scaling is given then the variable in question does not require rescaling on that particular timescale. On each timescale we in particular analyse the large-time behaviour of the reduced problem to ascertain the scalings for the next timescale.

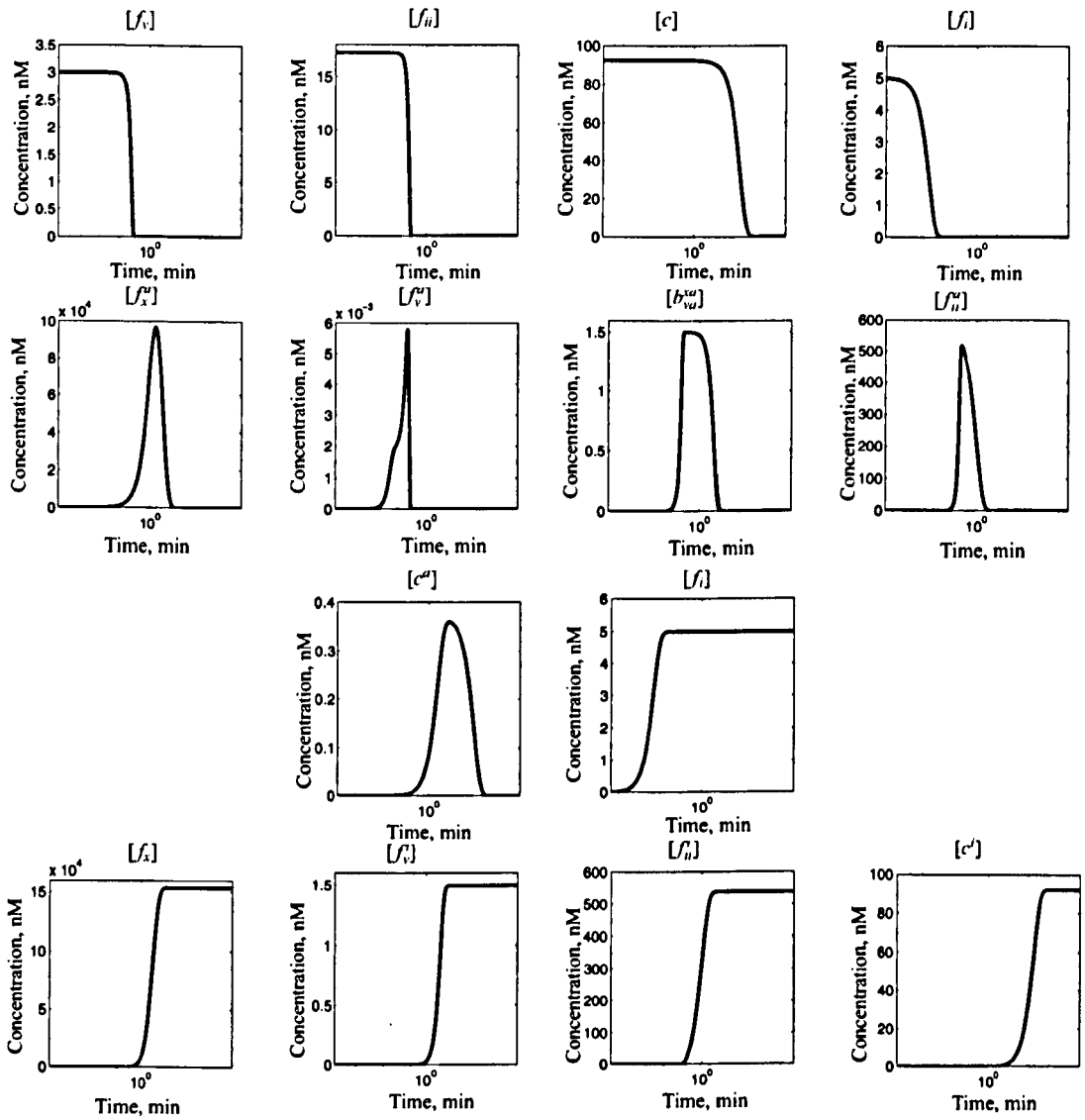

Figure 3.2: Numerical simulations of the dimensional model for (from top to bottom) procoagulants, activated factors and downstream factors. The dynamics of thrombin (fourth plot from left on second row) exhibit its characteristic time lag, explosive growth and decay. Parameters are taken from Table 3.3 and initial conditions for the procoagulants from Table 3.4. Time is shown on a log scale to highlight the multiple timescales involved in the formation of thrombin.

Nondim. param.	Nondim. value	Scaled nondim. param.	Nondim. param.	Nondim. value	Scaled nondim. param.
$\tilde{k}_{1a}$	1.5×10^5	$\bar{k}_{1a} = \epsilon\tilde{k}_{1a} = 166$	$\tilde{k}_{3c}$	1.0	$\bar{k}_{3c} = \epsilon^0\tilde{k}_{3c} = 1.0$
$\tilde{\gamma}_{1a}$	0.77	$\bar{\gamma}_{1a} = \epsilon^0\tilde{\gamma}_{1a} = 0.77$	$\tilde{k}_{4a}$	0.12	$\bar{k}_{4a} = \epsilon^{-1}\tilde{k}_{4a} = 115$
$\tilde{k}_{1b}$	0.19	$\bar{k}_{1b} = \epsilon^{-1}\tilde{k}_{1b} = 180$	$\tilde{q}_{4a}$	0.0040	$\bar{q}_{4a} = \epsilon^{-1}\tilde{q}_{4a} = 3.7$
$\tilde{k}_{2a}$	2.0	$\bar{k}_{2a} = \epsilon^0\tilde{k}_{2a} = 2.0$	$\tilde{k}_{4b}$	5.3×10^2	$\bar{k}_{4b} = \epsilon\tilde{k}_{4b} = 0.57$
$\tilde{k}_{2am}$	7.2	$\bar{k}_{2am} = \epsilon^0\tilde{k}_{2am} = 7.2$	$\tilde{k}_{4bm}$	3.6	$\bar{k}_{4bm} = \epsilon^0\tilde{k}_{4bm} = 3.6$
$\tilde{k}_{2b}$	0.013	$\bar{k}_{2b} = \epsilon^{-1}\tilde{k}_{2b} = 12$	$\tilde{k}_{5a}$	0.0011	$\bar{k}_{5a} = \epsilon^{-1}\tilde{k}_{5a} = 1.0$
$\tilde{k}_{3a}$	1.5×10^2	$\bar{k}_{3a} = \epsilon\tilde{k}_{3a} = 0.17$	$\tilde{k}_{5b}$	0.27	$\bar{k}_{5b} = \epsilon^0\tilde{k}_{5b} = 0.27$
$\tilde{q}_{3a}$	1.0	$\bar{q}_{3a} = \epsilon^0\tilde{q}_{3a} = 1.0$	$\tilde{k}_6$	1.5×10^3	$\bar{k}_6 = \epsilon\tilde{k}_6 = 1.7$
$\tilde{k}_{3b}$	0.038	$\bar{k}_{3b} = \epsilon^{-1}\tilde{k}_{3b} = 35$			

Table 3.5: Nondimensional parameters, the rescaled ones in the third and sixth columns being based on $\epsilon = \tilde{k}_{5a} = 1.1 \times 10^{-3}$; the choice of how certain parameters are scaled with ϵ is, as usual, somewhat arbitary. The nondimensional group $\tilde{k}_{5a}$ measures the ratio of protein C activation to antithrombin III inhibition of thrombin. ATIII attenuates thrombin activity quickly with protein C activating on a longer timescale after thrombin is generated (Mann *et al.*, 2003), we would therefore expect $\tilde{k}_{5a}$ to be a small parameter.

Time-scale	Variable					
	t	f_x^a	f_v^a	b_{va}^{xa}	f_{ii}^a	c^a
1	ϵT	-	$\epsilon^2 F_v^a$	$\epsilon^3 B_{va}^{xa}$	$\epsilon^2 F_{ii}^a$	$\epsilon^2 C^a$
2	$\epsilon^{2/3}\hat{T}$	$\epsilon^{-1/3}\hat{F}_x^a$	$\epsilon^{4/3}\hat{F}_v^a$	$\epsilon^{5/3}\hat{B}_{va}^{xa}$	$\epsilon^{4/3}\hat{F}_{ii}^a$	$\epsilon^{5/3}\hat{C}^a$
3	$\epsilon^{1/2}\check{T}$	$\epsilon^{-1/2}\check{F}_x^a$	$\epsilon\check{F}_v^a$	$\epsilon\check{B}_{va}^{xa}$	$\epsilon^{1/2}\check{F}_{ii}^a$	$\epsilon^{3/2}\check{C}^a$
4	$t_s+\epsilon^{1/2}\check{T}$	$\epsilon^{-1/2}\ln\left(\frac{1}{\epsilon}\right)\check{F}_x^a$	$\epsilon^{1/2}\left(\ln\left(\frac{1}{\epsilon}\right)\right)^{-1}\check{F}_v^a$	$\epsilon^{1/2}\check{B}_{va}^{xa}$	-	$\epsilon^{3/2}\ln\left(\frac{1}{\epsilon}\right)\check{C}^a$
5	$t_s+\epsilon^{1/2}\ln\left(\frac{1}{\epsilon}\right)T^\dagger$	$\epsilon^{-1/2}\ln\left(\frac{1}{\epsilon}\right)\check{F}_x^a$	$\epsilon^{1/2}\left(\ln\left(\frac{1}{\epsilon}\right)\right)^{-1}\check{F}_v^a$	$\epsilon^{1/2}\ln\left(\frac{1}{\epsilon}\right)B_{va}^{xa\dagger}$	-	$\epsilon^{3/2}\ln\left(\frac{1}{\epsilon}\right)\check{C}^a$
6	$T^\ddagger$	$\epsilon^{-1}F_x^{a\ddagger}$	$\epsilon F_v^{a\ddagger}$	-	-	$\epsilon C_a^\ddagger$
7	$\epsilon^{-1}T^\diamond$	$\epsilon^{-1}F_x^{a\ddagger}$	$\epsilon F_{va}^{a\ddagger}$	-	-	$\epsilon C_a^\ddagger$

Table 3.6: Summary of the scalings required on each of the timescales, '-' meaning that the variable does not require scaling. λ, β, γ and the timeshift T_s will be determined in Sections 3.5.3 and 3.5.4. $t_s = \epsilon^{1/2}\ln(1/\epsilon)\,T_s$ is the timeshift in terms of original scaling.

3.4 Dimensionless problem restatement

We introduce $\epsilon = \tilde{k}_{5a} = k_{5a}/k_{4c} = 1.1 \times 10^{-3}$; this small nondimensional parameter expresses the ratio of the rate of activation of the slowly acting protein C inhibitory system to the fast acting rate at which antithrombin III inhibits thrombin. We rescale the dimensionless parameters as indicated in Table 3.5. With the new scalings (Table 3.5), where the constants with bars are taken to be O(1) and the initial values are given in Table 3.4 (from here on we drop the $^-$'s) we have

$$f_i = f_{i0}e^{-k_6 t/\epsilon}, \quad c = c_0 e^{-\epsilon k_{5a} t}, \quad c^a = \frac{\epsilon k_{5a} c_0}{k_{5b} - \epsilon k_{5a}} \left(e^{-\epsilon k_{5a} t} - e^{-k_{5b} t}\right). \tag{3.4.1}$$

These expressions imply that there are at least three timescales (and there turn out to be four more). On the first of these, $t = O(\epsilon)$, the procoagulant fibrinogen (f_i) decays and is exponentially small on all subsequent timescales. On the second, $t = O(1)$, APC (c^a) increases. The last timescale in (3.4.1) has $t = O(1/\epsilon)$, over which both protein C (c) and APC decay, converting to inactivated protein C (c_i). The system (3.2.14)-(3.2.19) takes the rescaled form

$$\epsilon \frac{df_x^a}{dt} = k_{1a}\gamma_{1a} e^{-\gamma_{1a} t} + \frac{k_{3c} k_{3a} c^a b_{va}^{xa}}{b_{va}^{xa} + 1} - \epsilon^2 k_{1b} f_x^a - k_{3a} f_x^a f_v^a, \tag{3.4.2a}$$

$$\frac{df_v^a}{dt} = \frac{b_a f_v}{f_v + k_{2am}(1 + f_i)} + \frac{\epsilon k_{2b} f_x^a f_v}{f_v + 1 + f_{ii}} + \epsilon \frac{k_{3b}}{q_{3a}} b_{va}^{xa} - \frac{c^a f_v^a}{f_v^a + 1} - f_x^a f_v^a, \tag{3.4.2b}$$

$$\frac{db_{va}^{xa}}{dt} = q_{3a} f_x^a f_v^a - \epsilon k_{3b} b_{va}^{xa} - \frac{k_{3c} q_{3a} c^a b_{va}^{xa}}{b_{va}^{xa} + 1}, \tag{3.4.2c}$$

$$\epsilon \frac{df_{ii}^a}{dt} = \frac{\epsilon^2 k_{4a} f_x^a f_{ii}}{f_{ii} + 1 + f_v} + \frac{k_{4a} k_{4b} f_{ii} b_{va}^{xa}}{q_{4a}(f_{ii} + k_{4bm})} - \epsilon f_{ii}^a, \tag{3.4.2d}$$

for the activated factors and

$$\frac{df_v}{dt} = -\frac{k_{2a} f_{ii}^a f_v}{f_v + k_{2am}(1 + f_i)} - \frac{\epsilon k_{2a} k_{2b} f_x^a f_v}{f_v + 1 + f_{ii}}, \tag{3.4.2e}$$

$$\epsilon \frac{df_{ii}}{dt} = -\frac{\epsilon^2 q_{4a} f_x^a f_{ii}}{f_v + 1 + f_{ii}} - \frac{k_{4b} f_{ii} b_{va}^{xa}}{f_{ii} + k_{4bm}}. \tag{3.4.2f}$$

for the procoagulants. This is the system that we analyse, with f_i and c^a given by (3.4.1).

To help guide the asymptotic analysis we first solve the nondimensional system (equations (3.2.10)-(3.2.20)) with the nondimensional parameters set to unity to ensure no complications arise associated with small or large parameters that are nominally of O(1). For example the rescaled parameter $\bar{k}_{4c} = 115$ is large but not as large as ϵ^{-1}, so for the initial validation we set it to unity and, as we see, the asymptotic approximation continues to give viable insight even for the original parameter set. We use this parameter set (unity) for all simulations in the asymptotic analysis (Section 3.5) and provide a comparison to the original parameter set in Section 3.6. Figure 3.3 shows plots for succesively smaller ϵ to helps us tease out the asymptotic structure.

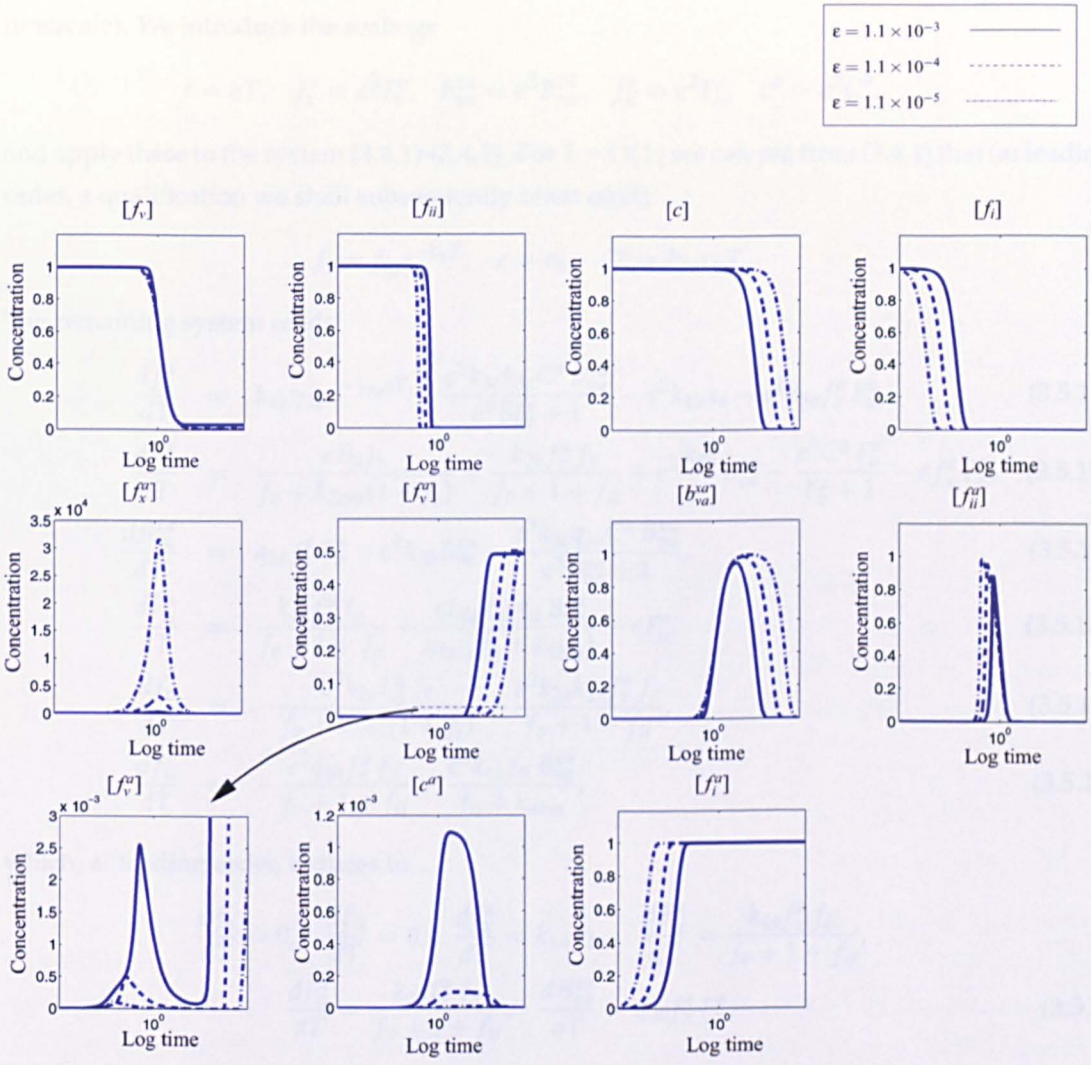

Figure 3.3: Numerical simulations of the nondimensional model (3.4.1),(3.4.2) with parameter values set to one and variable epsilon. The first plot on the bottom row is a blown up region of f_v^a showing the initial peak in factor Va concentration. A decrease in ϵ produces a substantial increase in peak factor Xa concentration, a decrease in APC and a decrease in the initial peak of factor Va concentration.

3.5 Asymptotic analysis

3.5.1 The first timescale, t =O(ϵ)

Initially we look at the short timescale that we obtain from equation (3.4.1), where fibrinogen decays (it turns out that this is the only variable showing non-trivial behaviour on this timescale). We introduce the scalings

$$t = \epsilon T, \quad f_v^a = \epsilon^2 F_v^a, \quad b_{va}^{xa} = \epsilon^3 B_{va}^{xa}, \quad f_{ii}^a = \epsilon^2 F_{ii}^a, \quad c^a = \epsilon^2 C^a,$$

and apply these to the system (3.4.1)-(3.4.2). For T =O(1) we can see from (3.4.1) that (at leading order, a qualification we shall subsequently often omit)

$$f_i = f_{i0} e^{-k_6 T}, \quad c = c_0, \quad C^a = k_{5a} c_0 T.$$

The remaining system reads

$$\frac{df_x^a}{dT} = k_{1a}\gamma_{1a} e^{-\gamma_{1a}\epsilon T} + \frac{\epsilon^5 k_{3c} k_{3a} C^a B_{va}^{xa}}{\epsilon^3 B_{va}^{xa} + 1} - \epsilon^2 k_{1b} x_a - \epsilon^2 k_{3a} f_x^a F_v^a, \tag{3.5.1a}$$

$$\frac{dF_v^a}{dT} = \frac{\epsilon B_a f_v}{f_v + k_{2am}(1+f_i)} + \frac{k_{2b} f_x^a f_v}{f_v + 1 + f_{ii}} + \epsilon^3 \frac{k_{3b}}{q_{3a}} B_{va}^{xa} - \frac{\epsilon^3 C^a F_v^a}{F_v^a + 1} - \epsilon f_x^a F_v^a, \tag{3.5.1b}$$

$$\frac{dB_{va}^{xa}}{dT} = q_{3a} f_x^a F_v^a - \epsilon^2 k_{3b} B_{va}^{xa} - \frac{\epsilon^3 k_{3c} q_{3a} C^a B_{va}^{xa}}{\epsilon^3 B_{va}^{xa} + 1}, \tag{3.5.1c}$$

$$\frac{dF_{ii}^a}{dT} = \frac{k_{4a} f_x^a f_{ii}}{f_v + 1 + f_{ii}} + \frac{\epsilon k_{4a} k_{4b} f_{ii} B_{va}^{xa}}{q_{4a}(f_{ii} + k_{4bm})} - \epsilon F_{ii}^a, \tag{3.5.1d}$$

$$\frac{df_v}{dT} = -\frac{\epsilon^3 k_{2a} F_{ii}^a f_v}{f_v + k_{2am}(1+f_i)} - \frac{\epsilon^2 k_{2a} k_{2b} f_x^a f_v}{f_v + 1 + f_{ii}}, \tag{3.5.1e}$$

$$\frac{df_{ii}}{dT} = -\frac{\epsilon^2 q_{4a} f_x^a f_{ii}}{f_v + 1 + f_{ii}} - \frac{\epsilon^3 k_{4b} f_{ii} B_{va}^{xa}}{f_{ii} + k_{4bm}}, \tag{3.5.1f}$$

which, at leading order, reduces to

$$\frac{df_v}{dT} = 0, \quad \frac{df_{ii}}{dT} = 0, \quad \frac{df_x^a}{dT} = k_{1a}\gamma_{1a}, \quad \frac{dF_{ii}^a}{dT} = \frac{k_{4a} f_x^a f_{ii}}{f_v + 1 + f_{ii}},$$
$$\frac{dF_v^a}{dT} = \frac{k_{2b} f_x^a f_v}{f_v + 1 + f_{ii}}, \quad \frac{dB_{va}^{xa}}{dT} = q_{3a} f_x^a F_v^a. \tag{3.5.2}$$

Solving this system sequentially gives

$$f_v = f_{v0}, \quad f_{ii} = f_{ii0}, \quad f_x^a = k_{1a}\gamma_{1a} T, \quad F_{ii}^a = \frac{k_{4a} k_{1a} \gamma_{1a} f_{ii0}}{2(f_{v0} + 1 + f_{ii0})} T^2,$$
$$F_v^a = \frac{k_{2b} k_{1a} \gamma_{1a} f_{v0}}{2(f_{v0} + 1 + f_{ii0})} T^2, \quad B_{va}^{xa} = \frac{q_{3a} k_{2b} k_{1a}^2 \gamma_{1a}^2 f_{v0}}{8(f_{v0} + 1 + f_{ii0})} T^4. \tag{3.5.3}$$

Fibrinogen (f_i), the precursor of fibrin monomers, is included in the model as it competes with factor V for thrombin (3.5.1b, 3.5.1e) but, from the reduced aymptotic approximation (3.5.2), we can see that fibrinogen in fact plays no role on this timescale (or in the remaining timescales that follow). Its conversion into fibrin is of significance for downstream process that we are not concerned with here; on subsequent timescales it is exponentially small and henceforth we can therefore legitimately simply set it to zero.

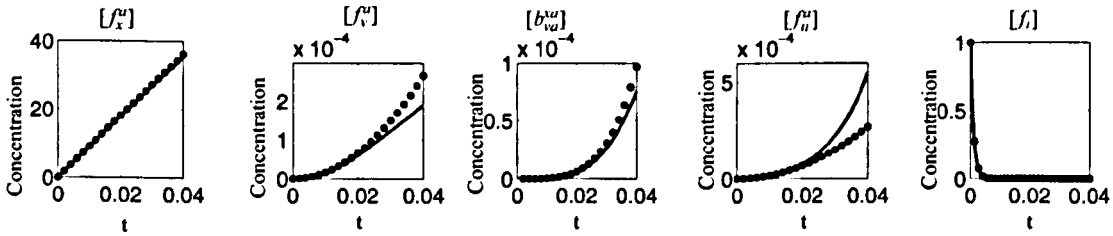

Figure 3.4: A comparison of the asymptotic approximation (3.5.3) (dotted line) and the numerical solutions of equations (3.2.10)-(3.2.20) (solid line) for those factors dominant on the initial timescale t =O(ϵ) with all nondimensional and rescaled nondimensional parameters set to unity ($\epsilon = 1.1 \times 10^{-3}$). Factors Xa, Va, thrombin and the complex prothrombinase increase. Fibrinogen, the precursor of fibrin decays.

On all of the timescales we will relate the results back to the original network diagram and describe the relevant terms and their physiological implications. The network diagram in Figure 3.5 shows in red the reactions that occur at this initial timescale, with all other reactions in blue. It can be seen that activation of factor X is reliant on its initial stimulus and is itself responsible for the subsequent activation of factor V (f_v) and for the conversion of prothrombin (f_{ii}) to thrombin (f_{ii}^a).

Figure 3.4 is a comparison of the full numerical and the asymptotic solutions for those factors that exhibit non-trivial behaviour on this timescale. All nondimensional, rescaled nondimensional parameters and procoagulant initial conditions are set to one: this allows us to assess the validity of asymptotic approximation on this timescale and we will use this parameter set for all simulations in this section (3.5) unless otherwise stated.

3.5.2 The second timescale, t =O($\epsilon^{2/3}$)

We obtain the scalings relevant to this timescale from the large time behaviour of the previous timescale (3.5.3). For example, since F_{ii}^a is growing like T^2 we infer that, with the next reaction entering being the second term in equation (3.5.1d) (whereby the complex prothrombinase catalyses prothrombin to thrombin), $F_{ii}^a = \epsilon^{-2/3}\hat{f}_{ii}^a$. This procedure is followed in the following timescales. The scalings for this timescale are given by

$$T = \epsilon^{-1/3}\hat{T}, \quad F_x^a = \epsilon^{-1/3}\hat{f}_x^a, \quad F_v^a = \epsilon^{-2/3}\hat{f}_v^a, \quad B_{va}^{xa} = \epsilon^{-4/3}\hat{B}_{va}^{xa}, \quad F_{ii}^a = \epsilon^{-2/3}\hat{f}_{ii}^a, \quad C^a = \epsilon^{-1/3}\hat{C}^a.$$

Under this rescaling equations (3.5.1) become (with f_i, as already noted, henceforth set to zero)

$$\frac{d\hat{f}_x^a}{d\hat{T}} = k_{1a}\gamma_{1a}e^{-\gamma_{1a}\epsilon^{2/3}\hat{T}} + \frac{\epsilon^{10/3}k_{3c}k_{3a}\hat{C}^a\hat{B}_{va}^{xa}}{\epsilon^{5/3}\hat{B}_{va}^{xa}+1} - \epsilon^{5/3}k_{1b}\hat{f}_x^a - \epsilon k_{3a}\hat{f}_x^a\hat{f}_v^a, \tag{3.5.4a}$$

$$\frac{d\hat{f}_v^a}{d\hat{T}} = \frac{\epsilon^{2/3}\hat{f}_{ii}^a f_v}{f_v + k_{2am}} + \frac{k_{2b}\hat{f}_x^a f_v}{f_v+1+f_{ii}} + \epsilon^2\frac{k_{3b}}{q_{3a}}\hat{B}_{va}^{xa} - \frac{\epsilon^{7/3}\hat{C}^a\hat{f}_v^a}{\hat{f}_v^a+1} - \epsilon^{\frac{1}{3}}\hat{f}_x^a\hat{f}_v^a, \tag{3.5.4b}$$

$$\frac{d\hat{B}_{va}^{xa}}{d\hat{T}} = q_{3a}\hat{f}_x^a\hat{f}_v^a - \epsilon^{5/3}k_{3b}\hat{B}_{va}^{xa} - \frac{\epsilon^{\frac{7}{3}}k_{3c}q_{3a}\hat{C}^a\hat{B}_{va}^{xa}}{\epsilon^{5/3}\hat{B}_{va}^{xa}+1}, \tag{3.5.4c}$$

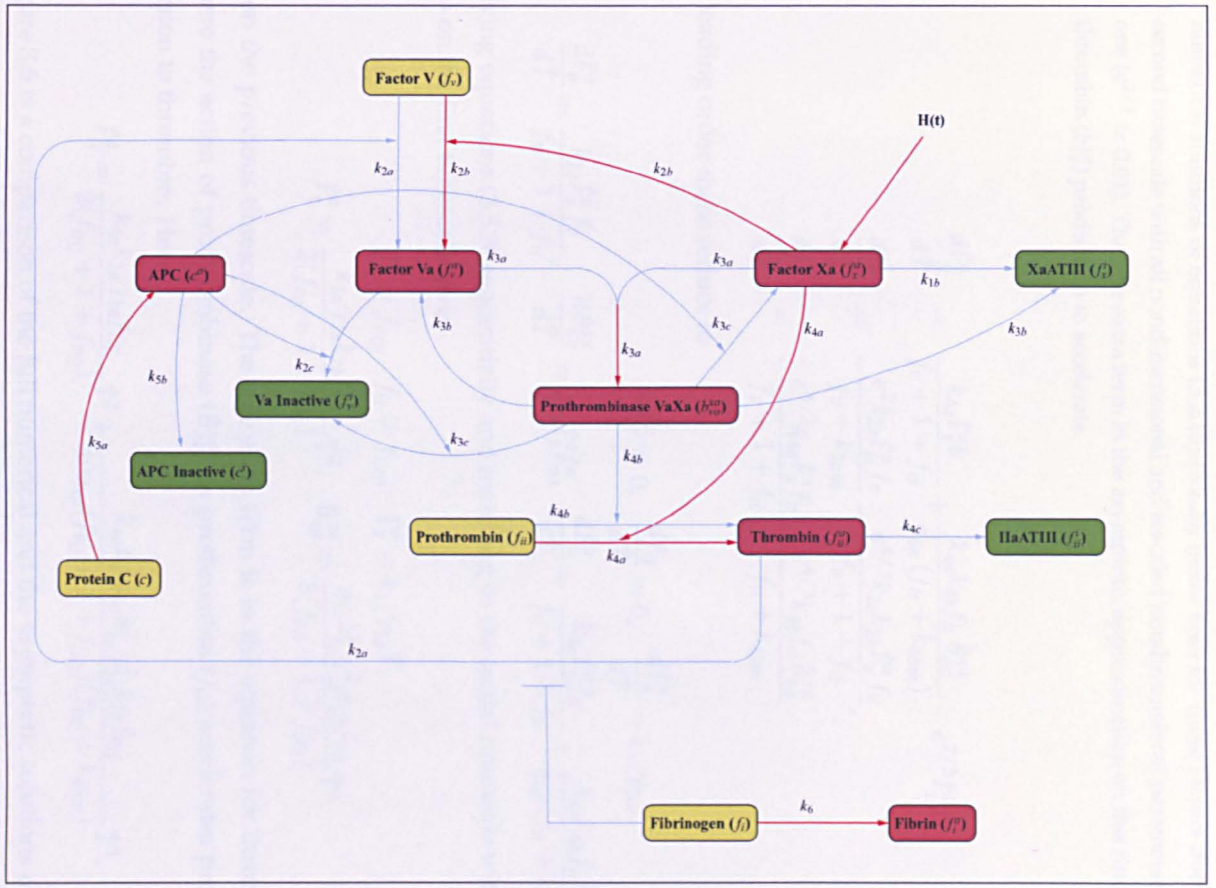

Figure 3.5: Reactions dominant on the initial timescale. Reactions in red are those relevant to the timescale shown with all other reactions in blue. Protein C is activated but has yet to play a role in the remaining network. Factor X is activated by the initial stimulus and it, in turn, activates factor V and prothrombin. The thrombin subsequently formed catalyses the conversion of fibrinogen to fibrin. The conversion of fibrinogen to fibrin is a downstream reaction that is included in the model to account for its competition for thrombin with factor V.

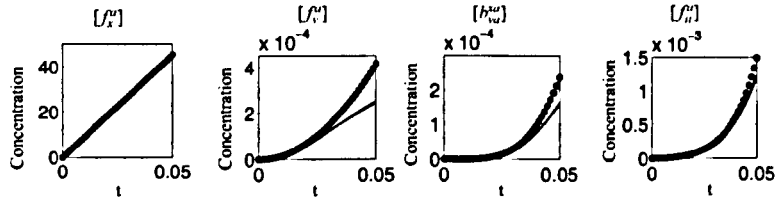

Figure 3.6: A comparison of the asymptotic approximation (3.5.6, 3.5.7) (dotted line) and the numerical solutions of equations (3.2.10)-(3.2.20) (solid line) for those factors dominant on the second timescale with all nondimensional and rescaled nondimensional parameters again set to one ($\epsilon^{2/3} \approx 0.01$). The sole extra term in the asymptotic approximation on this timescale causes thrombin (b_{va}^{xa}) production to accelerate.

$$\frac{d\hat{f}_{ii}^a}{d\hat{T}} = \frac{k_{4a}\hat{f}_x^a b}{f_v+1+f_{ii}} + \frac{k_{4a}k_{4b}f_{ii}\hat{B}_{va}^{xa}}{q_{4a}(f_{ii}+k_{4bm})} - \epsilon^{2/3}\hat{f}_{ii}^a, \tag{3.5.4d}$$

$$\frac{df_v}{d\hat{T}} = -\frac{\epsilon^2 k_{2a}\hat{f}_{ii}^a f_v}{f_v+k_{2am}} - \frac{\epsilon^{4/3}k_{2a}k_{2b}\hat{f}_x^a f_v}{f_v+1+f_{ii}}, \tag{3.5.4e}$$

$$\frac{df_{ii}}{d\hat{T}} = -\frac{\epsilon^{4/3}q_{4a}\hat{f}_x^a f_{ii}}{f_v+1+f_{ii}} - \frac{\epsilon^{4/3}k_{4b}f_{ii}\hat{B}_{va}^{xa}}{f_{ii}+k_{4bm}}. \tag{3.5.4f}$$

At leading order these reduce to

$$\frac{df_v}{d\hat{T}} = 0, \quad \frac{df_{ii}}{d\hat{T}} = 0, \quad \frac{d\hat{f}_x^a}{d\hat{T}} = k_{1a}\gamma_{1a},$$
$$\frac{d\hat{f}_v^a}{d\hat{T}} = \frac{k_{2b}\hat{f}_x^a f_v}{f_v+1+f_{ii}}, \quad \frac{d\hat{B}_{va}^{xa}}{d\hat{T}} = q_{3a}\hat{f}_x^a\hat{f}_v^a, \quad \frac{d\hat{f}_{ii}^a}{d\hat{T}} = \frac{k_{4a}\hat{f}_x^a f_{ii}}{f_v+1+f_{ii}} + \frac{k_{4a}k_{4b}f_{ii}\hat{B}_{va}^{xa}}{q_{4a}(f_{ii}+k_{4bm})}. \tag{3.5.5}$$

Solving equations (3.5.5) sequentially and matching to the initial timescale with the limit $T \to +\infty$ on the first timescale gives

$$f_v = f_{v0}, \quad f_{ii} = f_{ii0}, \quad \hat{f}_x^a = k_{1a}\gamma_{1a}\hat{T},$$
$$\hat{f}_v^a = \frac{k_{1a}\gamma_{1a}k_{2b}f_{v0}}{2(f_{v0}+1+f_{ii0})}\hat{T}^2, \quad \hat{B}_{va}^{xa} = \frac{q_{3a}k_{1a}^2\gamma_{1a}^2k_{2b}f_{v0}}{8(f_{v0}+1+f_{ii0})}\hat{T}^4, \tag{3.5.6}$$

as on the previous timescale. The sole extra term is in the equation for thrombin generation where the action of prothrombinase ($\hat{B}_{va}^{xa}$) on prothrombin (f_{ii}) accelerates prothrombins conversion to thrombin. Here

$$\hat{f}_{ii}^a = \frac{k_{4a}k_{1a}\gamma_{1a}f_{ii0}}{2(f_{ii0}+1+f_{v0})}\hat{T}^2 + \frac{k_{4a}k_{4b}q_{3a}k_{1a}^2\gamma_{1a}^2k_{2b}f_{v0}}{40q_{4a}(f_{v0}+1+f_{ii0})(f_{ii0}+k_{4bm})}\hat{T}^5. \tag{3.5.7}$$

Figure 3.6 is a comparison of the full numerical and the asymptotic solutions on this timescale. As stated above, we set all dimensional and rescaled nondimensional parameters to one. The reactions that are functioning on this timescale are shown in Figure 3.7.

3.5.3 The third timescale, $t = O(\epsilon^{1/2})$

From the $\hat{T} \to +\infty$ behaviour of (3.5.4) it follows that the next terms to come into play are the second and fifth ones of equation (3.5.4b), whereby factor Xa catalyses the activation of factor

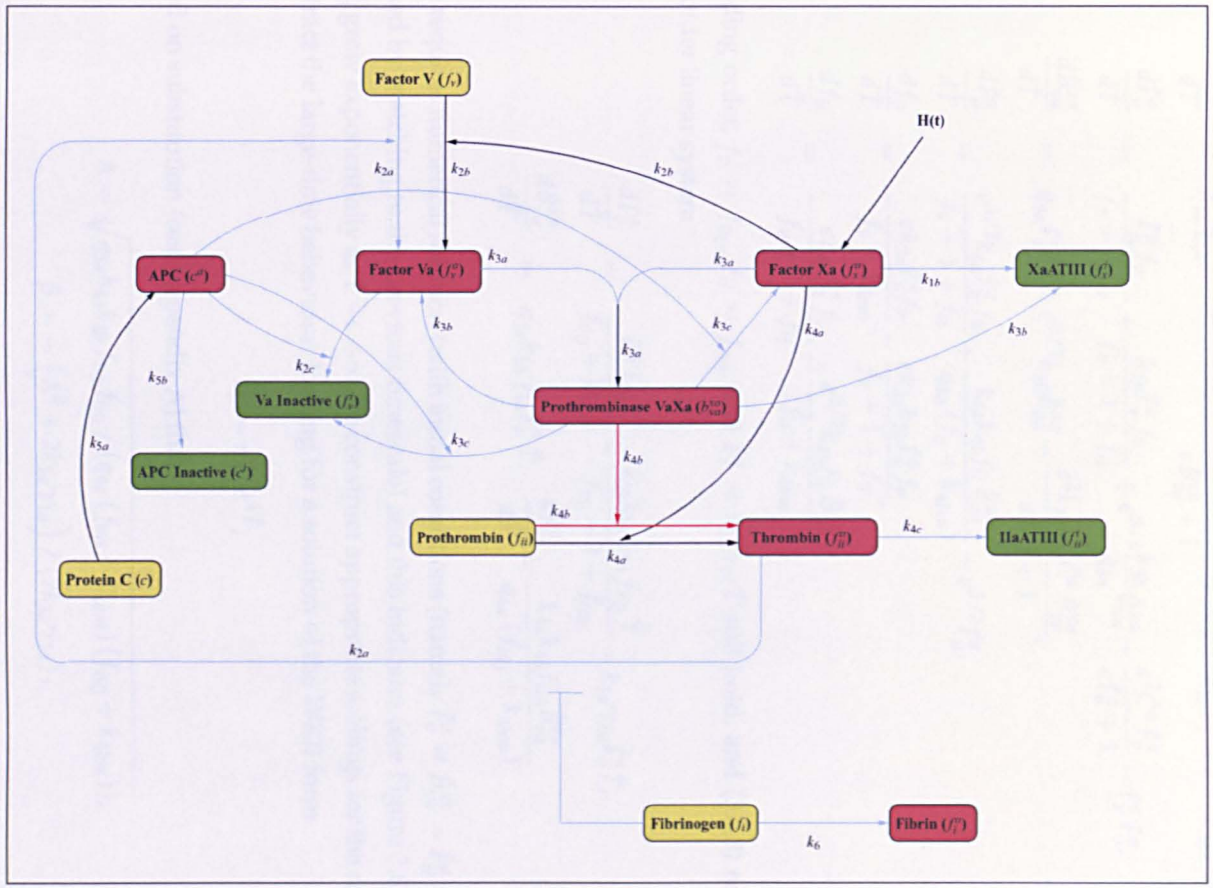

Figure 3.7: Reactions governing the second timescale. Reactions in red and black are those relevant to this timescale (red arrows representing newly featured reactions) with all other reactions in blue. The sole new term represents prothrombinase activation of prothrombin, accelerating thrombin formation.

V and factor Va is assembled into the complex prothrombinase. We thus obtain the scalings relevant to this timescale as

$$\hat{T} = \epsilon^{-1/6}\check{T}, \quad \hat{F}_x^a = \epsilon^{-1/6}\check{F}_x^a, \quad \hat{F}_v^a = \epsilon^{-1/3}\check{F}_v^a, \quad \hat{B}_{va}^{xa} = \epsilon^{-2/3}\check{B}_{va}^{xa}, \quad \hat{F}_{ii}^a = \epsilon^{-5/6}\check{F}_{ii}^a, \quad \hat{C}^a = \epsilon^{-1/6}\check{C}^a,$$

which, when applied to the equations (3.5.4), give the system

$$\frac{d\check{F}_x^a}{d\check{T}} = k_{1a}\gamma_{1a}e^{-\gamma_{1a}\epsilon^{1/2}\check{T}} + \frac{\epsilon^{5/2}k_{3a}k_{3c}\check{C}^a\check{B}_{va}^{xa}}{\epsilon\check{B}_{va}^{xa}+1} - \epsilon^{3/2}k_{1b}\check{F}_x^a - \epsilon^{1/2}k_{3a}\check{F}_x^a\check{F}_v^a, \tag{3.5.8a}$$

$$\frac{d\check{F}_v^a}{d\check{T}} = \frac{\check{F}_{ii}^a f_v}{f_v + k_{2am}} + \frac{k_{2b}\check{F}_x^a f_v}{f_v + 1 + f_{ii}} + \epsilon^{3/2}\frac{k_{3b}}{q_{3a}}\check{B}_{va}^{xa} - \frac{\epsilon^2\check{C}^a\check{F}_v^a}{\epsilon\check{F}_v^a + 1} - \check{F}_x^a\check{F}_v^a, \tag{3.5.8b}$$

$$\frac{d\check{B}_{va}^{xa}}{d\check{T}} = q_{3a}\check{F}_x^a\check{F}_v^a - \epsilon^{3/2}k_{3b}\check{B}_{va}^{xa} - \frac{\epsilon^2 k_{3c}q_{3a}\check{C}^a\check{B}_{va}^{xa}}{\epsilon\check{B}_{va}^{xa}+1}, \tag{3.5.8c}$$

$$\frac{d\check{F}_{ii}^a}{d\check{T}} = \frac{\epsilon^{1/2}k_{4a}\check{F}_x^a f_{ii}}{f_v + 1 + f_{ii}} + \frac{k_{4a}k_{4b}f_{ii}\check{B}_{va}^{xa}}{q_{4a}(f_{ii} + k_{4bm})} - \epsilon^{1/2}\check{F}_{ii}^a, \tag{3.5.8d}$$

$$\frac{df_v}{d\check{T}} = -\frac{\epsilon k_{2a}\check{F}_{ii}^a f_v}{f_v + k_{2am}} - \frac{\epsilon k_{2a}k_{2b}\check{F}_x^a f_v}{f_v + 1 + f_{ii}}, \tag{3.5.8e}$$

$$\frac{df_{ii}}{d\check{T}} = -\frac{\epsilon q_{4a}\check{F}_x^a f_{ii}}{f_v + 1 + f_{ii}} - \frac{\epsilon^{1/2}k_{4b}f_{ii}\check{B}_{va}^{xa}}{f_{ii} + k_{4bm}}. \tag{3.5.8f}$$

At leading order, $f_v = f_{v0}$, $f_{ii} = f_{ii0}$, and $\check{F}_x^a = k_{1a}\gamma_{1a}\check{T}$ still hold, and (3.5.8) reduces to the third-order linear system

$$\frac{d\check{F}_v^a}{d\check{T}} = \frac{\check{F}_{ii}^a f_{v0}}{f_{v0} + k_{2am}} + \frac{k_{2b}k_{1a}\gamma_{1a}f_{v0}\check{T}}{f_{v0} + 1 + f_{ii0}} - k_{1a}\gamma_{1a}\check{F}_v^a\check{T}, \tag{3.5.9a}$$

$$\frac{d\check{B}_{va}^{xa}}{d\check{T}} = q_{3a}k_{1a}\gamma_{1a}\check{F}_v^a\check{T}, \quad \frac{d\check{F}_{ii}^a}{d\check{T}} = \frac{k_{4a}k_{4b}f_{ii0}\check{B}_{va}^{xa}}{q_{4a}(f_{ii0} + k_{4bm})}, \tag{3.5.9b}$$

which requires numerical solution (with initial conditions (namely $\check{F}_v^a = \check{B}_{va}^{xa} = \check{F}_{ii}^a = 0$ at $\check{T} = 0$) obtained by matching to the previous timescale) and this indicates (see Figure 3.8) that $\check{F}_v^a$, $\check{B}_{va}^{xa}$ and $\check{F}_{ii}^a$ grow exponentially as $\check{T} \to +\infty$. To construct appropriate scalings for the next timescale we extract the large-time behaviour: looking for a solution of the WKB form

$$\check{F}_v^a \sim \eta\check{T}^\beta e^{\lambda\check{T}}, \tag{3.5.10}$$

we find on substitution (see Appendix A) that

$$\lambda = \sqrt{q_{3a}k_{4a}k_{4b}f_{v0}f_{ii0} \,/\, (q_{4a}(f_{v0} + k_{2am})(f_{ii0} + k_{4bm}))}, \tag{3.5.11}$$

$$\beta = -\left(\lambda^2 + 2k_{1a}\gamma_{1a}\right) / (2k_{1a}\gamma_{1a}), \tag{3.5.12}$$

the value of the constant η depending on the evaluation over $\check{T} \to +\infty$, moreover

$$\check{B}_{va}^{xa} \sim \frac{\eta\, q_{3a}\, k_{1a}\, \gamma_{1a}}{\lambda}\check{T}^{\beta+1}e^{\lambda\check{T}}, \tag{3.5.13}$$

$$\check{F}_{ii}^a \sim \frac{\eta\, k_{4a}\, k_{4b}\, q_{3a}\, k_{1a}\, \gamma_{1a} f_{ii0}}{q_{4a}(f_{ii0} + k_{4bm})\lambda^2}\check{T}^{\beta+1}e^{\lambda\check{T}} \quad \text{as} \quad \check{T} \to +\infty. \tag{3.5.14}$$

Figure 3.9 compares the numerical solutions to the full governing equations with the numerical solution of the reduced system (3.5.9). Figure 3.10 compares numerical solutions of the reduced

system (3.5.9) with the asymptotic approximations (3.5.10, 3.5.13, 3.5.14). η is obtained to fit the curve - see Figure 3.11 ($\lambda \approx 2.08, \beta \approx -1.02$ holds for the parameters given in Table 3.5 and $\lambda \approx 0.50, \beta \approx -1.13$ holds for parameters set to unity.).

It is on this timescale that we move from the initiation phase to the propagation phase, in which thrombin levels have their characteristic explosive growth. Physiologically we can deduce from the system (3.5.9) that thrombin's dominant activation mechanism is through prothrombinase, factor Xa now having little effect. Factor Va is activated both by factor Xa, as at the previous timescales, and by the inclusion of the positive feedback of thrombin. This feedback loop from thrombin accelerates thrombin's own generation through the assembly of prothrombinase (see Figure 3.12). There is also a conversion term that is dominant for the assembly of factor Va into the cofactor VaXa. These reactions and others dominant on this timescale are shown in Figure 3.13.

3.5.4 The next two timescales: the reduced δ model

Considering the large time behaviour of the previous timescale, whereby $\check{F}_v^a \sim \eta \check{T}^\beta e^{\lambda \check{T}}$, we can infer that the next timescale can be expected to be of the form

$$\check{T} = \frac{\gamma}{\lambda} \ln(1/\epsilon) - \frac{\phi}{\lambda} \ln\ln(1/\epsilon) + \bar{T} \tag{3.5.15}$$

which when substituted into the large scale behaviour of the previous timescale brings it algebraic. The constants ϕ and γ are yet to be calculated. Using this timeshift and the large time behaviour of the variables from the previous timescale we can see that the appropriate matching conditions take the form that

$$\check{F}_x^a \sim k_{1a}\gamma_{1a}\frac{\gamma}{\lambda}\ln(1/\epsilon), \qquad \check{F}_v^a \sim \epsilon^{-\gamma}\left(\frac{\gamma}{\lambda}\right)^\beta (\ln(1/\epsilon))^{\beta-\phi}\eta e^{\lambda\bar{T}}, \tag{3.5.16}$$

$$\check{B}_{va}^{xa} \sim \epsilon^{-\gamma}\left(\frac{\gamma}{\lambda}\right)^{\beta+1} (\ln(1/\epsilon))^{\beta+1-\phi}\frac{\eta\, q_{3a} k_{1a}\gamma_{1a}}{\lambda} e^{\lambda\bar{T}}, \tag{3.5.17}$$

$$\check{F}_{ii}^a \sim \epsilon^{-\gamma}\left(\frac{\gamma}{\lambda}\right)^{\beta+1} (\ln(1/\epsilon))^{\beta+1-\phi}\frac{\eta k_{4a} k_{4b} q_{3a} k_{1a}\gamma_{1a} b_0}{q_{4a}(b_0 + k_{4bm})\lambda^2} e^{\lambda\bar{T}}, \tag{3.5.18}$$

and we have

$$\check{C}^a \sim k_{5a}\frac{\gamma}{\lambda}\ln(1/\epsilon). \tag{3.5.19}$$

We now introduce the notation

$$\delta = \frac{1}{\ln(1/\epsilon)},$$

whereby $0 < \epsilon << \delta << 1$ (in practice, and as usual in such problems, δ is not particularly small; in fact $\delta \approx 0.15$ for $\epsilon = 1.1 \times 10^{-3}$), and this implies the scalings

$$\check{F}_x^a = \left(\frac{1}{\delta}\right)\bar{F}_x^a, \quad \check{F}_v^a = \epsilon^{-\gamma}\left(\frac{1}{\delta}\right)^{\beta-\phi}\bar{F}_v^a,$$

$$\check{B}_{va}^{xa} = \epsilon^{-\gamma}\left(\frac{1}{\delta}\right)^{\beta+1-\phi}\bar{B}_{va}^{xa}, \quad \check{F}_{ii}^a = \epsilon^{-\gamma}\left(\frac{1}{\delta}\right)^{\beta+1-\phi}\bar{F}_{ii}^a, \quad \check{C}^a = \left(\frac{1}{\delta}\right)\bar{C}^a$$

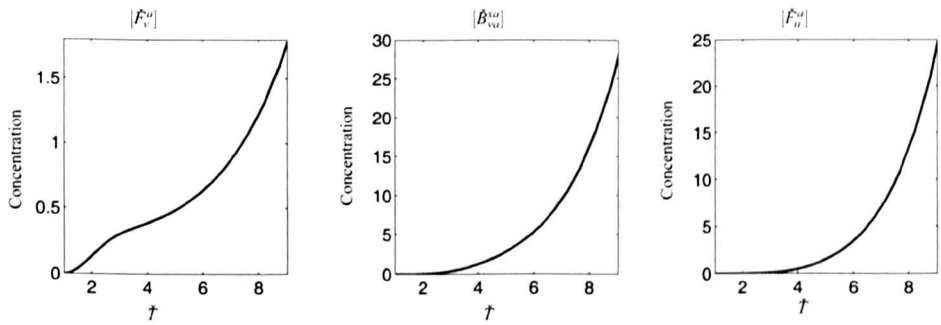

Figure 3.8: Numerical solutions for the system (3.5.9) showing the unbounded growth of factor Va, prothrombinase and thrombin as $\hat{t} \to +\infty$. Parameter values set to unity.

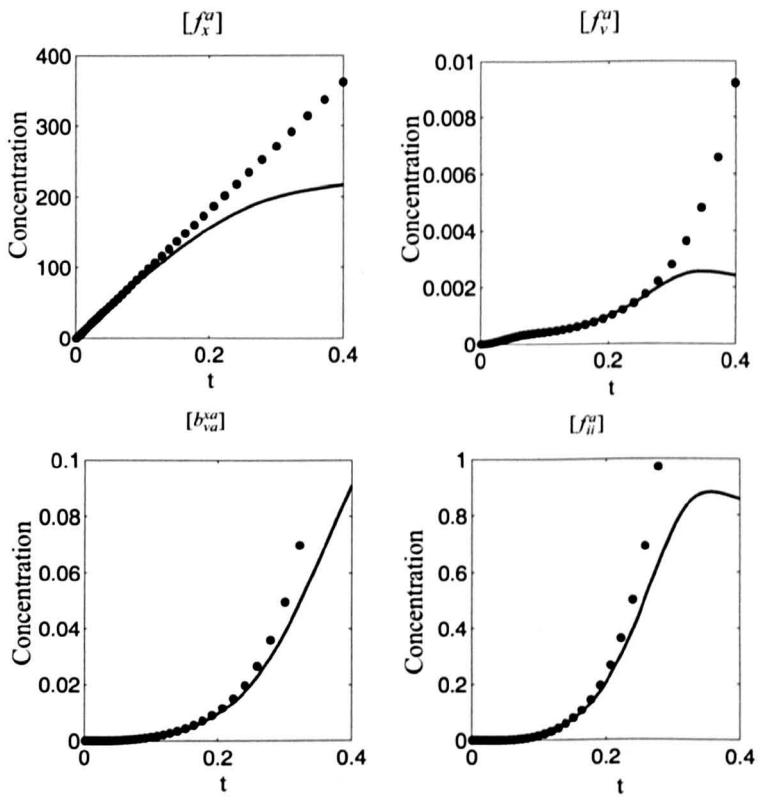

Figure 3.9: Solutions for the system (3.5.9) (dotted line) and the numerical solutions of equations (3.2.10)-(3.2.20) (solid line) for those factors that play a dominant role on the third timescale $t = O(\epsilon^{1/2})$ with parameter values set to unity ($\epsilon^{1/2} \approx 0.03$).

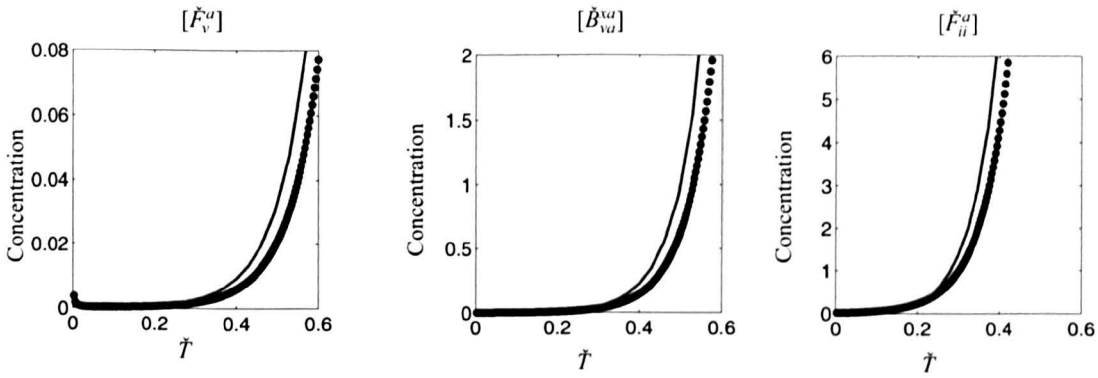

Figure 3.10: Solutions for the asymptotic approximation (3.5.10)-(3.5.14) (dotted line) and the system (3.5.9) (solid line) for those factors that play a dominant role on the third timescale $t = O(\epsilon^{1/2})$ with parameter values set to unity.

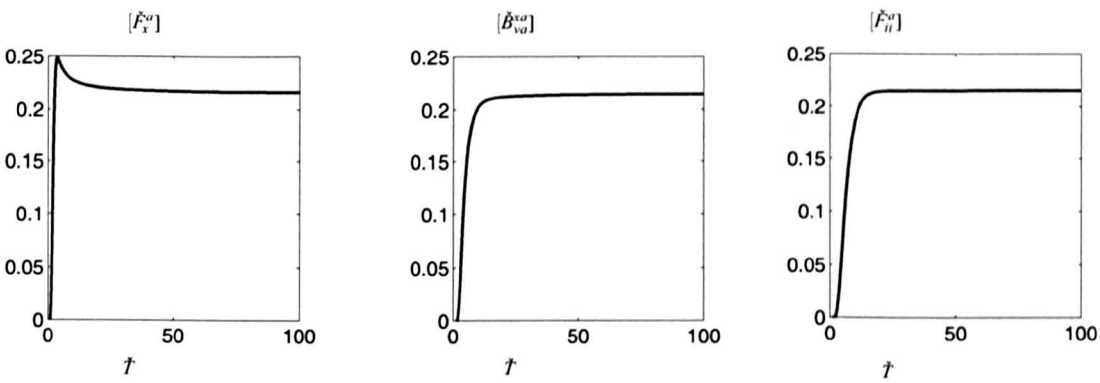

Figure 3.11: Calculation of η, which we henceforth set to 0.22. Numerical solution of (3.5.9) divided by (3.5.10), (3.5.14) as a function of time. Parameter values set to unity.

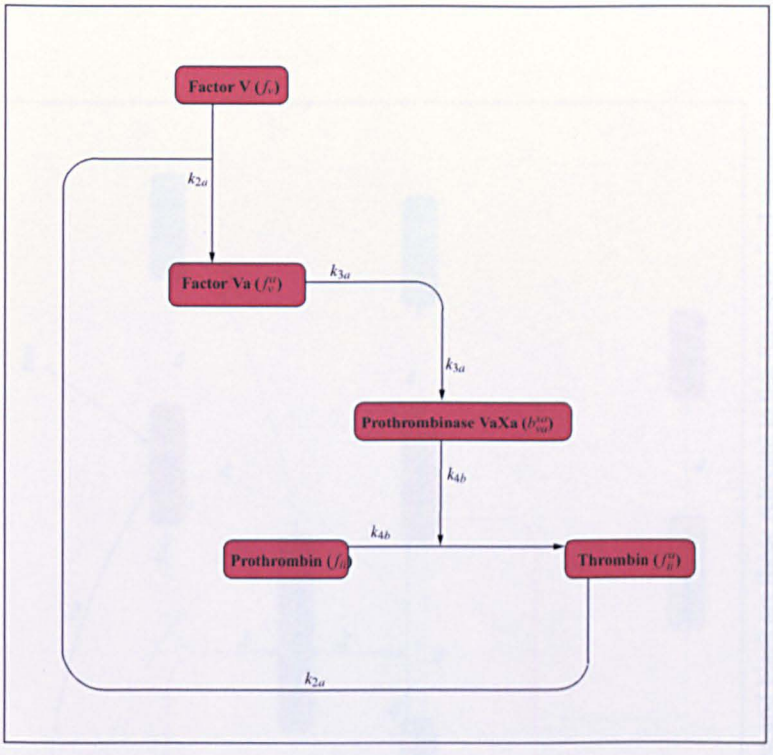

Figure 3.12: Reactions dominant on the third timescale. A closed loop has formed through factor Va, the formation of prothrombinase, the activation of prothrombin and a feedback to factor Va.

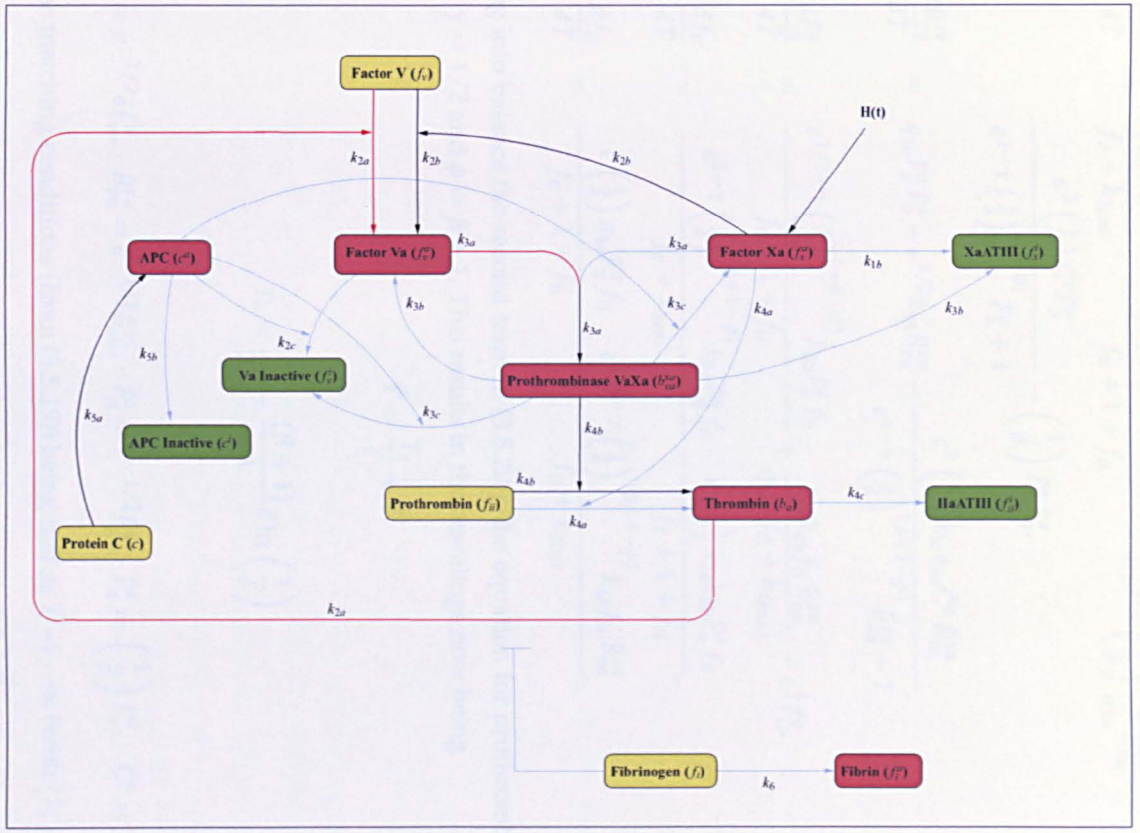

Figure 3.13: Reactions dominant on the third timescale. Reactions in red and black are those relevant to this timescale (red arrows representing newly featured reactions) with all other reactions in blue. We can see that factor Xa no longer has a dominant effect on the activation of prothrombinase to thrombin, it being soley reliant on the effect of prothrombinase. The closed feedback loop is shown in Figure 3.12.

under which equations (3.5.8a) give

$$\frac{d\check{F}_x^a}{d\check{T}} = \delta k_{1a}\gamma_{1a}e^{-\alpha\epsilon^{1/2}\left(\frac{\gamma}{\lambda}\ln(1/\epsilon)-\frac{\phi}{\lambda}\ln\ln(1/\epsilon)+\check{T}\right)} + \frac{\epsilon^{5/2-\gamma}\left(\frac{1}{\delta}\right)^{(\beta+1-\phi)}k_{3c}k_{3a}\check{C}^a\check{B}_{va}^{xa}}{\epsilon^{1-\gamma}\left(\frac{1}{\delta}\right)^{(\beta+1-\phi)}\check{B}_{va}^{xa}+1}$$

$$-\epsilon^{3/2}k_{1b}\check{F}_x^a - \epsilon^{1/2-\gamma}\left(\frac{1}{\delta}\right)^{(\beta-\phi)}k_{3a}\check{F}_x^a\check{F}_v^a, \tag{3.5.20a}$$

$$\frac{d\check{F}_v^a}{d\check{T}} = \frac{\left(\frac{1}{\delta}\right)\check{F}_{ii}^a f_v}{f_v+k_{2am}} + \frac{\epsilon^{\gamma}\left(\frac{1}{\delta}\right)^{(1-\beta+\phi)}k_{2b}\check{F}_x^a f_v}{f_v+1+f_{ii}} + \epsilon^{3/2}\left(\frac{1}{\delta}\right)\frac{k_{3b}}{q_{3a}}\check{B}_{va}^{xa} -$$

$$\frac{\epsilon^2\left(\frac{1}{\delta}\right)\check{C}^a\check{F}_v^a}{\epsilon^{1-\gamma}\left(\frac{1}{\delta}\right)^{(\beta-\phi)}\check{F}_v^a+1} - \left(\frac{1}{\delta}\right)\check{F}_x^a\check{F}_v^a, \tag{3.5.20b}$$

$$\frac{d\check{B}_{va}^{xa}}{d\check{T}} = q_{3a}\check{F}_x^a\check{F}_v^a - \epsilon^{3/2}k_{3b}\check{B}_{va}^{xa} - \frac{\epsilon^2\left(\frac{1}{\delta}\right)k_{3c}q_{3a}\check{C}^a\check{B}_{va}^{xa}}{\epsilon^{1-\gamma}\left(\frac{1}{\delta}\right)^{(\beta+1-\phi)}\check{B}_{va}^{xa}+1}, \tag{3.5.20c}$$

$$\frac{d\check{F}_{ii}^a}{d\check{T}} = \frac{\epsilon^{1/2+\gamma}\left(\frac{1}{\delta}\right)^{(-\beta+\phi)}k_{4a}\check{F}_x^a f_{ii}}{f_v+1+f_{ii}} + \frac{k_{4a}k_{4b}f_{ii}\check{B}_{va}^{xa}}{q_{4a}(f_{ii}+k_{4bm})} - \epsilon^{\frac{1}{2}}\check{F}_{ii}^a, \tag{3.5.20d}$$

$$\frac{df_v}{d\check{T}} = -\frac{\epsilon^{1-\gamma}\left(\frac{1}{\delta}\right)^{(\beta+1-\phi)}k_{2a}\check{F}_{ii}^a f_v}{f_v+k_{2am}} - \frac{\epsilon\left(\frac{1}{\delta}\right)k_{2a}k_{2b}\check{F}_x^a f_v}{f_v+1+f_{ii}}, \tag{3.5.20e}$$

$$\frac{df_{ii}}{d\check{T}} = -\frac{\epsilon\left(\frac{1}{\delta}\right)q_{4a}\check{F}_x^a f_{ii}}{f_v+1+f_{ii}} - \frac{\epsilon^{1/2-\gamma}\left(\frac{1}{\delta}\right)^{(\beta+1-\phi)}k_{4b}f_{ii}\check{B}_{va}^{xa}}{f_{ii}+k_{4bm}}. \tag{3.5.20f}$$

To bring into balance the second term in (3.5.20f), the equation for prothrombin (f_{ii}), we need to take $\gamma = 1/2$ and $\phi = \beta + 1$. This results in the rescalings now being

$$\check{T} = \frac{T_s}{\delta} + \check{T}$$

where

$$T_s = \frac{1}{2\lambda} - \frac{(\beta+1)}{\lambda}\delta\ln\left(\frac{1}{\delta}\right) \tag{3.5.21}$$

and

$$\check{F}_v^a = \epsilon^{-1/2}\delta\check{F}_v^a, \quad \check{B}_{va}^{xa} = \epsilon^{-1/2}\check{B}_{va}^{xa}, \quad \check{F}_{ii}^a = \epsilon^{-1/2}\check{F}_{ii}^a, \quad \check{F}_x^a = \left(\frac{1}{\delta}\right)\check{F}_x^a, \quad \check{C}^a = \left(\frac{1}{\delta}\right)\check{C}^a, \tag{3.5.22}$$

with the matching conditions (from (3.5.19)) being that as $\check{T} \to -\infty$ (with $|\check{T}| \ll \delta^{-1}$)

$$\check{F}_x^a \sim k_{1a}\gamma_{1a}T_s + \delta k_{1a}\gamma_{1a}\check{T}, \quad \check{F}_v^a \sim \left(\frac{1}{2\lambda}\right)^{\beta}\eta e^{\lambda\check{T}}, \tag{3.5.23a}$$

$$\check{B}_{va}^{xa} \sim \frac{\eta\, q_{3a}\,k_{1a}\,\gamma_{1a}}{\lambda}\left(\frac{1}{2\lambda}\right)^{\beta+1}e^{\lambda\check{T}}, \quad \check{F}_{ii}^a \sim \frac{\eta\, k_{4a}\,k_{4b}\,q_{3a}\,k_{1a}\,\gamma_{1a}\,f_{ii0}}{q_{4a}(f_{ii0}+k_{4bm})\lambda^2}\left(\frac{1}{2\lambda}\right)^{\beta+1}e^{\lambda\check{T}}, \quad f_{ii} \to f_{ii0}, \tag{3.5.23b}$$

we impose these conditions numerically at $\check{T} = -5$ with T_s taken from (3.5.21). $T_s \approx 1$ (with parameters set to unity), so that (note that $\delta \approx 0.15$, so in the first of (3.5.23a) the first term on the right hand side dominates the second)

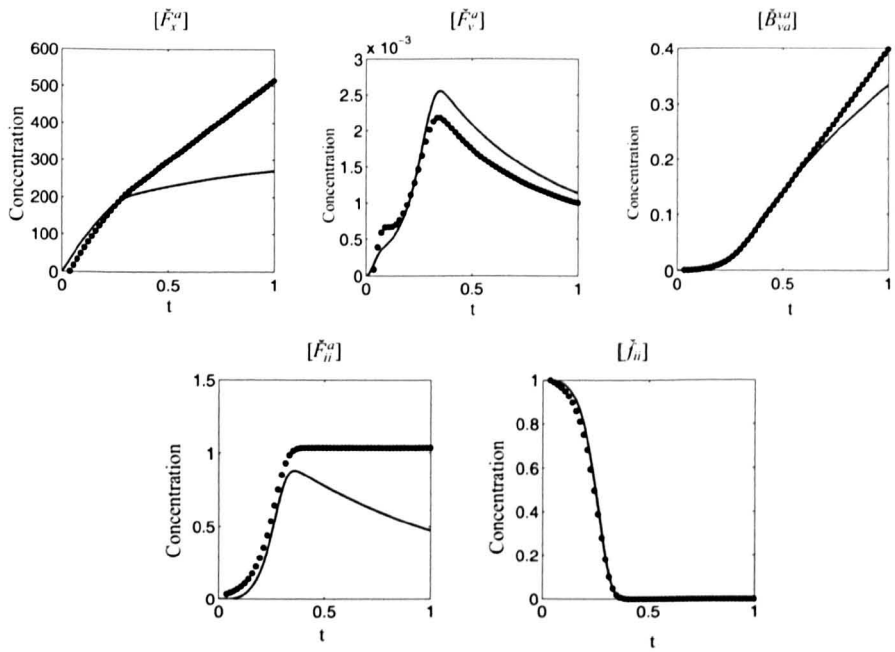

Figure 3.14: A comparison of the reduced δ model (3.5.24) (dotted line) and the numerical solutions of equations (3.2.10)-(3.2.20) (solid line) for those factors dominant on the reduced delta model with parameters values set to unity. $T_s \approx 1$ which applies over $\approx O(\epsilon^{1/2})$ of that value with $\epsilon^{1/2} \approx 0.03$.

Ignoring terms that are algebraically smaller in ϵ (but retaining all the δ terms) we obtain

$$\frac{df_v}{d\check{T}} = 0, \quad \frac{d\check{F}_x^a}{d\check{T}} = \delta\left(k_{1a}\gamma_{1a} - k_{3a}\check{F}_x^a\check{F}_v^a\right), \quad \delta\frac{d\check{F}_v^a}{d\check{T}} = \frac{\check{F}_{ii}^a f_v}{f_v + k_{2am}} - \check{F}_x^a\check{F}_v^a, \tag{3.5.24a}$$

$$\frac{d\check{B}_{va}^{xa}}{d\check{T}} = q_{3a}\check{F}_x^a\check{F}_v^a, \quad \frac{d\check{F}_{ii}^a}{d\check{T}} = \frac{k_{4a}k_{4b}f_{ii}\,\check{B}_{va}^{xa}}{q_{4a}\left(f_{ii} + k_{4bm}\right)}, \quad \frac{df_{ii}}{d\check{T}} = -\frac{k_{4b}f_{ii}\check{B}_{va}^{xa}}{f_{ii} + k_{4bm}}. \tag{3.5.24b}$$

which we term the reduced δ model. This reduced model is represented physiologically in the network diagram shown in Figure 3.15. This system is valid to all logarithmic orders in ϵ (i.e. algebraic orders in δ) and is therefore a useful simplification in its own right, Figure 3.14 shows the reactions dominant in this model against the full governing equations. Nevertheless, we can simplify it further by taking the limit $\delta \to 0$ and this subsidiary asymptotic limit itself involves consideration of two distinct timescales. The following expressions are exact for (3.5.24):

$$f_v = f_{v0}, \quad q_{3a}\check{F}_x^a + \delta k_{3a}\check{B}_{va}^{xa} = k_{1a}\gamma_{1a}q_{3a}\left(T_s + \delta\check{T}\right), \quad \check{F}_{ii}^a + \frac{k_{4a}}{q_{4a}}f_{ii} = \frac{k_{4a}k_{4b}}{q_{4a}}f_{ii0}. \tag{3.5.25}$$

3.5.4.1 The fourth timescale, $t - \epsilon^{1/2}\ln 1/\epsilon T_s = O(\epsilon^{1/2})$

Using the reduced δ model (3.5.24), we obtain at leading order in δ (using the matching conditions (3.5.23))

$$\check{F}_x^a = \frac{k_{1a}\gamma_{1a}}{2\lambda}, \quad \check{F}_v^a = \frac{f_{v0}}{\left(f_{v0} + k_{2am}\right)}\frac{\check{F}_{ii}^a}{\check{F}_x^a}, \tag{3.5.26}$$

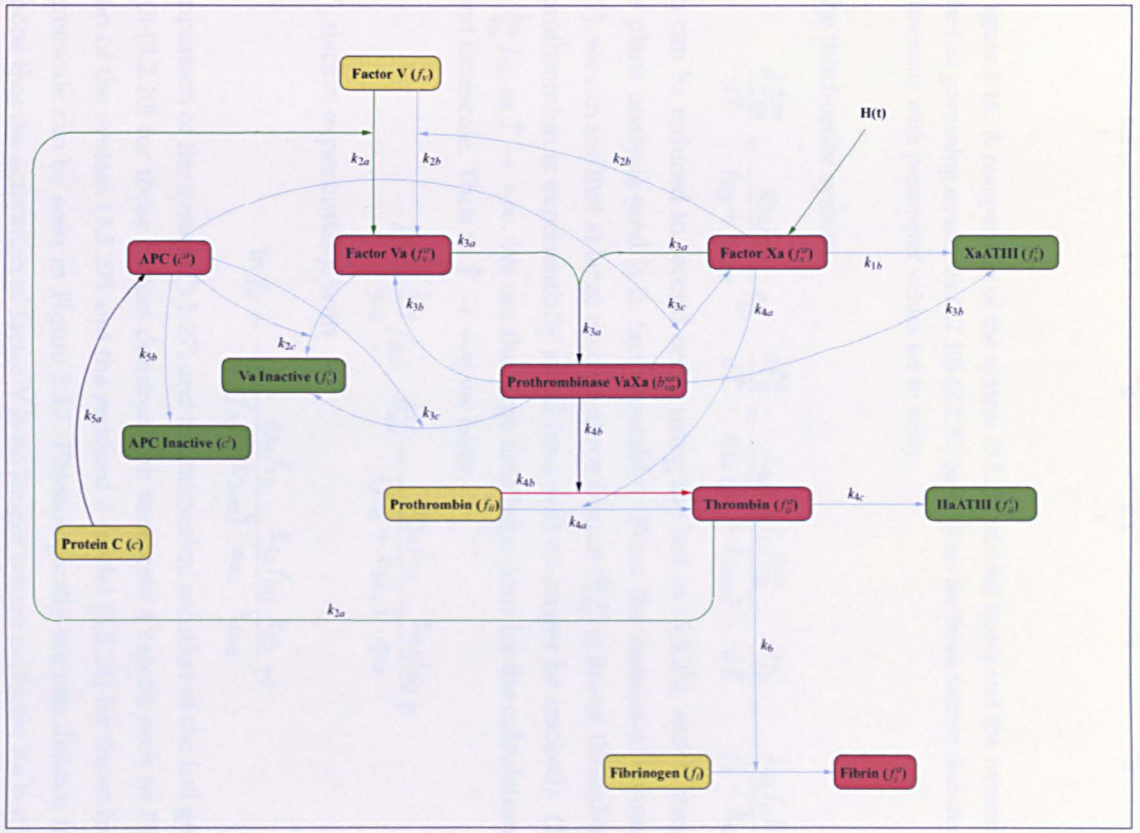

Figure 3.15: Reactions relevant to the reduced δ model. Reactions in red, black and green are those relevant to this timescale (red arrows representing newly featured reactions and green representing reactions in equilibrium) with all other reactions in blue. The reaction k_{4b} (prothrombinase to thrombin) is shown in red to emphasise that prothrombinase is now being depleted through this route, on the previous timescale the term was dominant only for thrombin activation. Factor Xa is constant on the fourth timescale and starts evolving on the fifth.

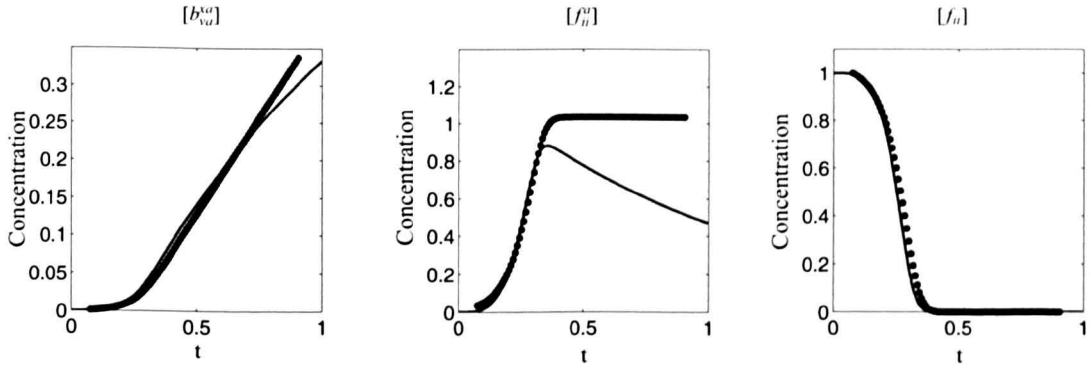

Figure 3.16: A comparison of the system (3.5.27) (dotted lines) and the numerical solutions of the full governing equations (3.2.10)-(3.2.20) (solid line) for those factors dominant on the fourth timescale with parameter values set to unity.

and the third-order system

$$\frac{d\check{B}_{va}^{xa}}{d\check{T}} = \frac{q_{3a}f_{v0}}{f_{v0}+k_{2am}}\check{F}_{ii}^{a}, \quad \frac{d\check{F}_{ii}^{a}}{d\check{T}} = \frac{k_{4a}k_{4b}f_{ii}\check{B}_{va}^{xa}}{q_{4a}\left(f_{ii}+k_{4bm}\right)}, \quad \frac{df_{ii}}{d\check{T}} = -\frac{k_{4b}f_{ii}\check{B}_{va}^{xa}}{f_{ii}+k_{4bm}}, \tag{3.5.27}$$

which can be reduced to second order using the last of (3.5.25), and is therefore amenable to phase plane analysis (and is in fact separable). From the numerical solution (Figure 3.16) of (3.5.27), we can see that at large time prothrombinase ($\check{B}_{va}^{xa}$) is linear, thrombin tends to constant and prothrombin is exponentially small (and will no longer be tracked). (3.5.25) implies that $\check{F}_{ii}^{a} \to \frac{k_{4a}}{q_{4a}}f_{ii0}$ as $\check{T} \to +\infty$. We use the large time behaviour for the calculation of the scalings for the next timescale. Thus as $\check{T} \to +\infty$ we have

$$\check{F}_{ii}^{a} \sim \frac{k_{4a}}{q_{4a}}f_{ii0}, \quad \check{B}_{va}^{xa} \sim \frac{q_{3a}f_{v0}}{\left(f_{v0}+k_{2am}\right)}\frac{k_{4a}f_{ii0}}{q_{4a}}\check{T} \tag{3.5.28}$$

and f_{ii} decays exponentially, with

$$\ln f_{ii} \sim -\frac{1}{2}\frac{q_{3a}f_{v0}}{\left(f_{v0}+k_{2am}\right)}\frac{k_{4a}f_{ii0}}{q_{4a}}\frac{k_{4b}}{k_{4bm}}\check{T}^{2} \tag{3.5.29}$$

A comparison of the system (3.5.27) and the numerical solution of the full governing equations (3.2.10)-(3.2.20) for those factors dominant on timescale 4 can be seen in Figure 3.16. A comparison of the system (3.5.27) and the reduced δ model (3.5.24) for those factors dominant on this timescale can be seen in Figure 3.17. Physiologically we can deduce from this system of equations that the activation of factor V is no longer reliant on factor Xa but is totally reliant on the positive feedback loop from thrombin, and this can be seen in Figure 3.15 (a schematic of the reactions dominant for the reduced delta model and for timescale 4).

3.5.4.2 The fifth timescale, $t - \epsilon^{1/2}\ln 1/\epsilon T_s = \mathbf{O}\left(\epsilon^{1/2}\ln\left(\frac{1}{\epsilon}\right)\right)$

At this timescale we are still able to use the reduced δ model (3.5.24); on the basis of (3.5.28) we obtain a new balance in the equations for factor Xa and factor Va by rescaling $\check{T} = \left(\frac{1}{\delta}\right)T^{\dagger}$ and

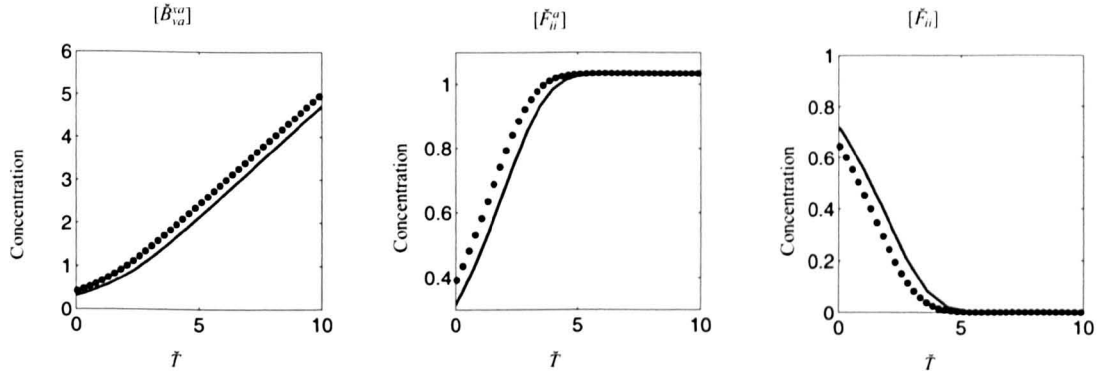

Figure 3.17: A comparison of the system (3.5.27) (dotted lines) and the reduced δ model (solid lines) solved numerically for those factors dominant on the fourth timescale $t - T_s = \mathrm{O}\left(\epsilon^{\frac{1}{2}}\right)$ with all nondimensional and rescaled non-dimensional parameters set to one.

$\check{B}^{xa}_{va} = \left(\frac{1}{\delta}\right) B^{\dagger xa}_{va}$, under which (3.5.24) gives

$$\frac{d\check{F}^a_x}{dT^\dagger} = k_{1a}\gamma_{1a} - k_{3a}\check{F}^a_x\check{F}^a_v, \qquad \delta^2\frac{d\check{F}^a_v}{dT^\dagger} = \frac{\check{F}^a_{ii}f_{v0}}{f_{v0}+k_{2am}} - \check{F}^a_x\check{F}^a_v, \tag{3.5.30a}$$

$$\frac{d\check{B}^{xa}_{va}}{dT^\dagger} = q_{3a}\check{F}^a_x\check{F}^a_v, \qquad \delta^2\frac{d\check{F}^a_{ii}}{dT^\dagger} = \frac{k_{4a}k_{4b}f_{ii}\check{B}^{xa}_{va}}{q_{4a}(f_{ii}+k_{4bm})}, \qquad \delta^2\frac{df_{ii}}{dT^\dagger} = -\frac{k_{4b}f_{ii}\check{B}^{xa}_{va}}{f_{ii}+k_{4bm}}. \tag{3.5.30b}$$

At leading order in δ, with f_{ii} exponentially small, we thus have

$$\frac{d\check{F}^a_x}{dT^\dagger} = k_{1a}\gamma_{1a} - k_{3a}\check{F}^a_x\check{F}^a_v, \quad 0 = \frac{\check{F}^a_{ii}f_{v0}}{f_{v0}+k_{2am}} - \check{F}^a_x\check{F}^a_v, \quad \frac{dB^{xa\dagger}_{va}}{dT^\dagger} = q_{3a}\check{F}^a_x\check{F}^a_v \quad , \frac{d\check{F}^a_{ii}}{dT^\dagger} = 0 \tag{3.5.31}$$

Matching to the previous timescale at $T^\dagger = 0$ gives

$$\check{F}^a_v = \frac{f_{v0}\check{F}^a_{ii0}}{(f_{v0}+k_{2am})\check{F}^a_x}, \qquad \check{F}^a_x = \left(k_{1a}\gamma_{1a} - k_{3a}\frac{f_{v0}\check{F}^a_{ii0}}{f_{v0}+k_{2am}}\right)T^\dagger + \frac{k_{1a}\gamma_{1a}}{2\lambda}, \tag{3.5.32a}$$

$$B^{xa\dagger}_{va} = \left(\frac{q_{3a}f_{v0}\check{F}^a_{ii0}}{f_{v0}+k_{2am}}\right)T^\dagger. \tag{3.5.32b}$$

For the original parameter set and with rescaled nondimensional parameters set to unity we have $k_{1a}\,\gamma_{1a} > k_{3a}\frac{f_{v0}\check{F}^a_{ii0}}{f_{v0}+k_{2am}}$ (i.e. $1 > 0.5$). This inequality corresponds to two classes of behaviour within the asymptotic analysis and with an alternate parameter set factor Xa (in particular) can in consequence display qualitatively different behaviour. Willems *et al.* (1991) used parameter values similar to ours except k_{1a} was three orders of magnitude lower so that $k_{1a}\,\gamma_{1a} < k_{3a}\frac{f_{v0}\check{F}^a_{ii0}}{f_{v0}+k_{2am}}$. Figure 3.18 shows a comparison of simulations of the numerical solutions of equations (3.2.10)-(3.2.20), with the rescaled nondimensional parameters set to unity (full line), and with the rescaled nondimensional parameters set to unity except for $k_{1a} = 0.001$ (a reduction in three orders of magnitude). With the parameter value adjusted Factor Xa displays two peaks in its concentration. However, the time to reach peak concentration and the peak concentration in thrombin concentration is similar in the two simulations. We will not pursue the asymptotics of this second regime here.

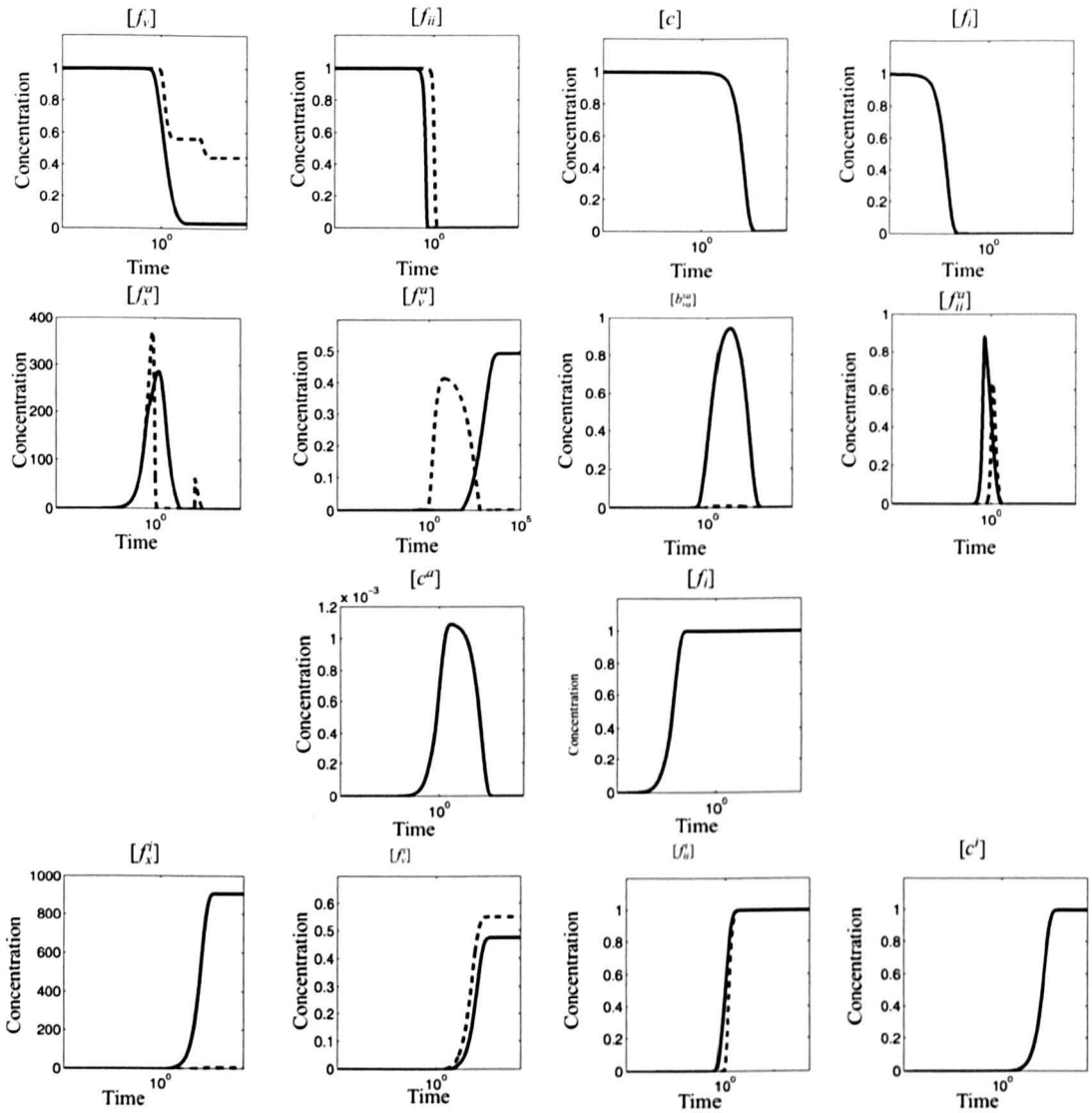

Figure 3.18: Numerical solutions for the full nondimensional system (equations (3.2.10)-(3.2.20)) showing a comparison between simulations with all nondimensional rescaled parameters set to unity (solid line) and simulations with all nondimensional rescaled parameters set to unity except $k_{1a} = 0.001$ (broken line). With the parameter k_{1a} adjusted down Factor Xa displays two peaks in its concentration. Factor Va displays a solitary peak in concentration and prothrombinase formation is substantially reduced. However, the time to reach peak concentration and the peak concentration in thrombin concentration is similar in the two simulations.

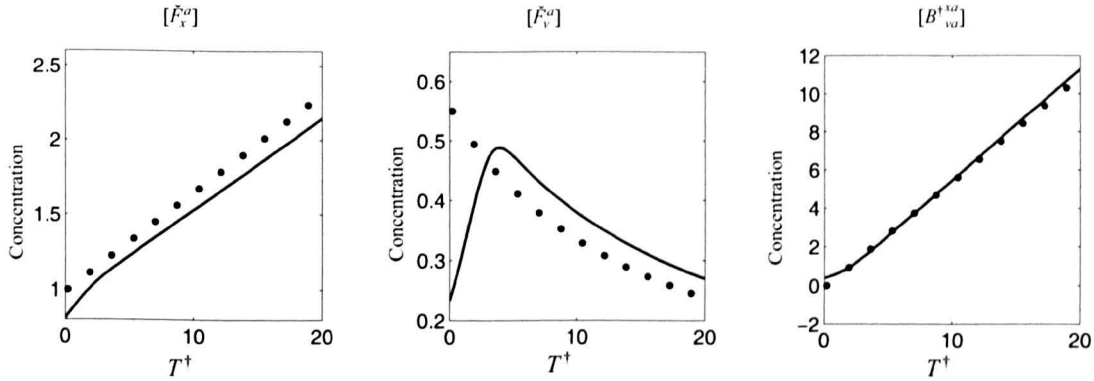

Figure 3.19: A comparison of the asymptotic approximations (3.5.32) (dotted lines) and the reduced delta model (3.5.24) (solid lines) solved numerically for those factors dominant on the fifth timescale $t - T_S = \mathrm{O}\left(\epsilon^{\frac{1}{2}}\right)$ with all rescaled and non-dimensional parameters set to unity.

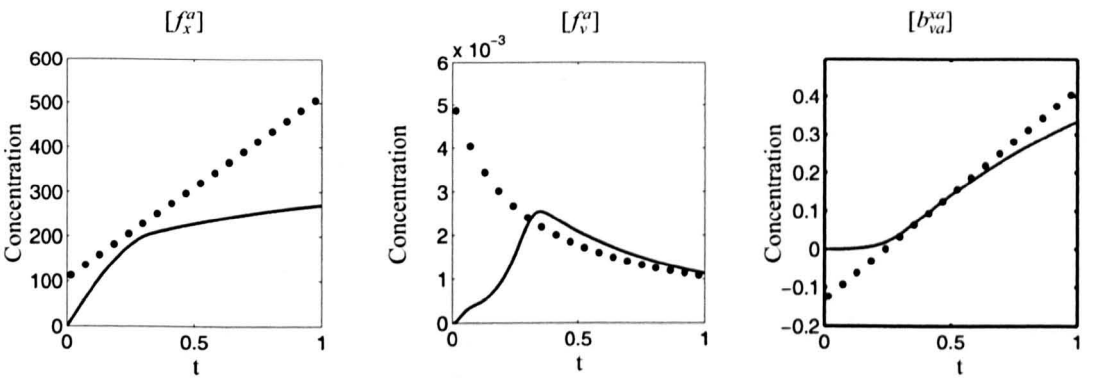

Figure 3.20: A comparison of the asymptotic approximations (3.5.32) (dotted lines) and the numerical solutions of equations (3.2.10)-(3.2.20) (solid line) for those factors dominant on the fifth timescale with all nondimensional and rescaled non-dimensional parameters set to one.

Physiologically, at this timescale, we can see that the assembly of factor Xa into the cofactor prothrombinase now becomes a dominant reaction. This, and the other reactions dominant on this timescale, are shown in Figure 3.21. A comparison of the asymptotic approximation (3.5.32) at this timescale and the reduced delta model (3.5.24) are shown in Figure 3.19. A comparison of the asymptotic approximations (3.5.32) and the numerical solutions of the full nondimensional model (3.2.10)-(3.2.20) for those factors dominant on the fifth timescale is shown in Figure 3.20.

3.5.5 The sixth timescale, $t = \mathrm{O}(1)$

We now return to the original ϵ model (3.5.20) with the rescalings for the fifth timescale applied. As $t = \mathrm{O}(1)$ applies on the current tomescale, we now include the equations for APC (c^a) and protein C (c). Considering the large time behaviour of timescale five bringing into balance the terms for the depletion of factor V we deduce the new scalings for this timescale. While we introduce $T^\ddagger$ here for consitency $T^\ddagger = t$ in fact applies in what follows:

$$T^\dagger = \delta\epsilon^{-1/2}T^\ddagger, \quad \check{F}_x^a = \delta\epsilon^{-1/2}F_x^{a\ddagger}, \quad \check{F}_V^a = \delta^{-1}\epsilon^{1/2}F_v^{a\ddagger}, \quad B_{va}^{xa\dagger} = \delta\epsilon^{-1/2}B_{va}^{xa\ddagger}, \quad \check{C}^a = \delta\epsilon^{-1/2}C^{a\ddagger}.$$

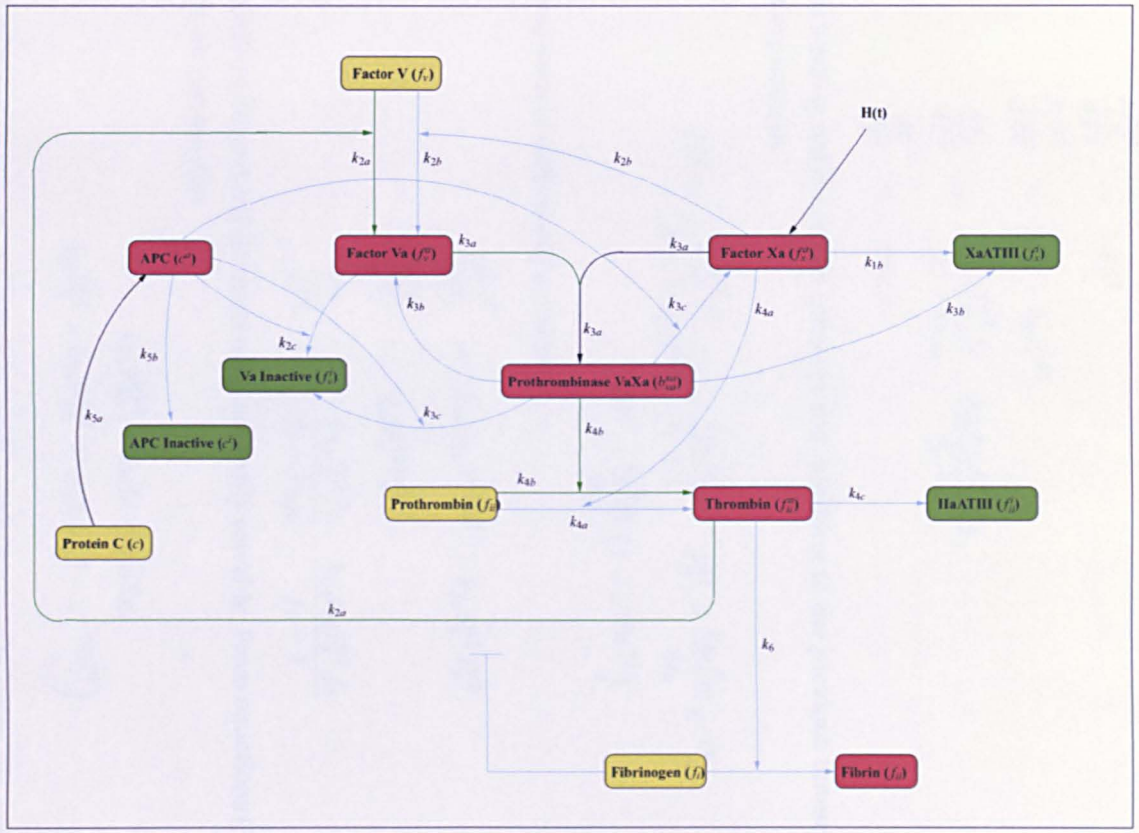

Figure 3.21: Reactions dominant on the fifth timescale. Reactions in red, green and black are those relevant to this timescale (red arrows representing newly featured reactions and green representing reactions in equilibrium) with all other reactions in blue. The feedback mechanism and factor Va's participation in prothrombinase formation is still in equilibrium. Thrombin formation from prothrombin is no longer dominant but factor Xa evolves.

Applying these scalings results in the system

$$\frac{dF_x^{a\ddagger}}{dT^\ddagger} = k_{1a}\gamma_{1a}e^{-\gamma_{1a}T^\ddagger} + \frac{\epsilon k_{3c}k_{3a}C^{a\ddagger}B_{va}^{xa\ddagger}}{B_{va}^{xa\ddagger}+1} - \epsilon k_{1b}F_x^{a\ddagger} - k_{3a}F_x^{a\ddagger}F_v^{a\ddagger}, \tag{3.5.33a}$$

$$\epsilon\frac{dF_v^{a\ddagger}}{dT^\ddagger} = \frac{F_{ii}^{a\ddagger}f_v}{f_v+k_{2am}} + \frac{k_{2b}F_x^{a\ddagger}f_v}{f_v+1} + \epsilon\frac{k_{3b}}{q_{3a}}B_{va}^{xa\ddagger} - \frac{\epsilon C_a{}^\ddagger F_v^{a\ddagger}}{F_v^{a\ddagger}+1} - F_x^{a\ddagger}F_v^{a\ddagger}, \tag{3.5.33b}$$

$$\frac{dB_{va}^{xa\ddagger}}{dT^\ddagger} = q_{3a}F_x^{a\ddagger}F_v^{a\ddagger} - \epsilon k_{3b}B_{va}^{xa\ddagger} - \frac{\epsilon q_{3a}k_{3c}C_a{}^\ddagger B_{va}^{xa\ddagger}}{B_{va}^{xa\ddagger}+1}, \tag{3.5.33c}$$

$$\frac{dF_{ii}^{a\ddagger}}{dT^\ddagger} = -F_{ii}^{a\ddagger}, \tag{3.5.33d}$$

$$\frac{dC^{a\ddagger}}{dT^\ddagger} = k_{5a}c - k_{5b}C^{a\ddagger}, \tag{3.5.33e}$$

$$\frac{df_v}{dT^\ddagger} = -\frac{k_{2a}F_{ii}^{a\ddagger}f_v}{f_v+k_{2am}} - \frac{k_{2a}k_{2b}F_x^{a\ddagger}f_v}{f_v+1}, \tag{3.5.33f}$$

$$\frac{dc}{dT^\ddagger} = -\epsilon k_{5a}c. \tag{3.5.33g}$$

Thus, at leading order c is still constant and matching to the previous timescale results in the explicit expressions

$$F_v^{a\ddagger} = \frac{F_{ii}^{a\ddagger}f_v}{(f_v+k_{2am})F_x^{a\ddagger}} + \frac{k_{2b}f_v}{f_v+1}, \qquad F_{ii}^{a\ddagger} = \frac{k_{4a}f_{ii0}}{q_{4a}}e^{-T^\ddagger}, \tag{3.5.34a}$$

$$C^{a\ddagger} = \frac{c_0k_{5a}}{k_{5b}}\left(1-e^{-k_{5b}T^\ddagger}\right) \tag{3.5.34b}$$

and the system of differential equations

$$\frac{dF_x^{a\ddagger}}{dT^\ddagger} = k_{1a}\gamma_{1a}e^{-\gamma_{1a}T^\ddagger} - k_{3a}F_x^{a\ddagger}F_v^{a\ddagger}, \tag{3.5.35a}$$

$$\frac{dB_{va}^{xa\ddagger}}{dT^\ddagger} = q_{3a}F_x^{a\ddagger}F_v^{a\ddagger}, \tag{3.5.35b}$$

$$\frac{df_v}{dT^\ddagger} = -\frac{k_{2a}F_{ii}^{a\ddagger}f_v}{f_v+k_{2am}} - \frac{k_{2a}k_{2b}F_x^{a\ddagger}f_v}{f_v+1}. \tag{3.5.35c}$$

This system of differentiable equations is not easily solvable. From equations (3.5.34a), (3.5.35a), (3.5.35b) we can see that

$$k_{2a}B_{va}^{xa\ddagger} + q_{3a}f_v = q_{3a}f_{v0}, \tag{3.5.36a}$$

$$q_{3a}F_x^{a\ddagger} + k_{3a}B_{va}^{xa\ddagger} = q_{3a}k_{1a}\left(1-e^{-\gamma_{1a}T^\ddagger}\right). \tag{3.5.36b}$$

From equation (3.5.36) we can see that, with parameters set to unity, we are on a bifurcation point that depends on the initial concentration of the procoagulant factor V (f_{v0}). Figure 3.22 illustrates the effect of varying the initial concentration of the procoagulant factor V by comparing simulations of the full nondimensional model with all parameters and initial conditions of the procoagulants set to unity except factor V, which is varied. With $f_v = 0.5$ factor V settles to a positive constant and, when compared to setting $f_v = 1$, the peak concentration of factor Xa is reduced. On the other side of the bifurcation with $f_v = 2$ factor V decays to zero but factor Xa peak concentration increases.

Figure 3.23 shows a comparison of the full nondimensional system (equations (3.2.10)-(3.2.20)) and the asymptotic approximations (equations (3.5.34), (3.5.35)) for those factors dominant on the sixth timescale. Three sets of simulations are shown. The top set (Figure 3.23 A) with initial concentration of the procoagulant factor V set to one where we the concentrations of factor Xa ($F_x^{a\ddagger}$) and factor V (f_v) decay. With a lower initial concentration of the procoagulant factor V ($f_v = 0.5$), factor V now decays exponentially but factor Xa settles to a positive constant (Figure 3.23 B). The final set of simulations (Figure 3.23 C) has the initial concentration of factor V set to 2, we are the other side of the bifurcation point and factor Xa decays exponentially but factor V settles to a positive constant. The asymptotic approximations show good agreement for all three sets of simulations.

From Figure 3.23 we can see that as $T^\ddagger \to +\infty$ thrombin ($F_{ii}^{a\ddagger}$) decays exponentially and will henceforth no longer be tracked, and so within these six timescales we have now captured the complete evolution of thrombin formation. The remaining factors are still evolving but their evolution over the remaining timescales is difficult to capture due to the delicate balance between factor Xa and factor Va. From the numerical solutions in Figure 3.23 we can see that prothrombinase ($B_{va}^{xa\ddagger}$) and APC ($C^{a\ddagger}$) tend to constants but the evolution of factor Xa and factor Va depends on the initial concentration of factor V. We attempt to follow the asymptotic analysis assuming factor Xa is not depleted and settles to a positive constant. The border line case with factor Xa and factor Va depleting will be very delicate and so will not be followed. From 3.5.33b we observe that Factor Va will increase again as APC and factor Xa decay but the timescale over which this occurs will depend on the decay rates and will not be discussed here where we assume factor Va is small and set to zero. The dominant reactions relevant at this timescale are shown in Figure 3.24.

3.5.6 The seventh timescale, $t = O(\epsilon^{-1})$

Considering the large time behaviour of the previous timescale we find that to move from the sixth to the final timescale requires only $T^\ddagger$ to be rescaled ($T^\ddagger = \epsilon^{-1}T^\circ$) since all other variables are henceforth negligble or are constant for large $T^\ddagger$ giving

$$\epsilon\frac{dF_x^{a\ddagger}}{dT^\circ} = k_{1a}\gamma_{1a}e^{\epsilon^{-1}T^\circ} + \frac{\epsilon k_{3a}k_{3c}C^{a\ddagger}B_{va}^{xa\ddagger}}{B_{va}^{xa\ddagger}+1} - \epsilon k_{1b}F_x^{a\ddagger}, \tag{3.5.37a}$$

$$\frac{dB_{va}^{xa\ddagger}}{dT^\circ} = -k_{3b}B_{va}^{xa\ddagger} - \frac{q_{3a}k_{3c}C^{a\ddagger}B_{va}^{xa\ddagger}}{B_{va}^{xa\ddagger}+1}, \tag{3.5.37b}$$

$$\epsilon\frac{dC^{a\ddagger}}{dT^\circ} = k_{5a}c - k_{5b}C^{a\ddagger}, \tag{3.5.37c}$$

$$\frac{dc}{dT^\circ} = -k_{5a}c. \tag{3.5.37d}$$

To leading order, matched to the previous timescale and solving sequentially where possible we obtain

$$c = c_0e^{-k_{5a}T^\circ}. \qquad C^{a\ddagger} = \frac{k_{5a}}{k_{5b}}c_0e^{-k_{5a}T^\circ} \tag{3.5.38a}$$

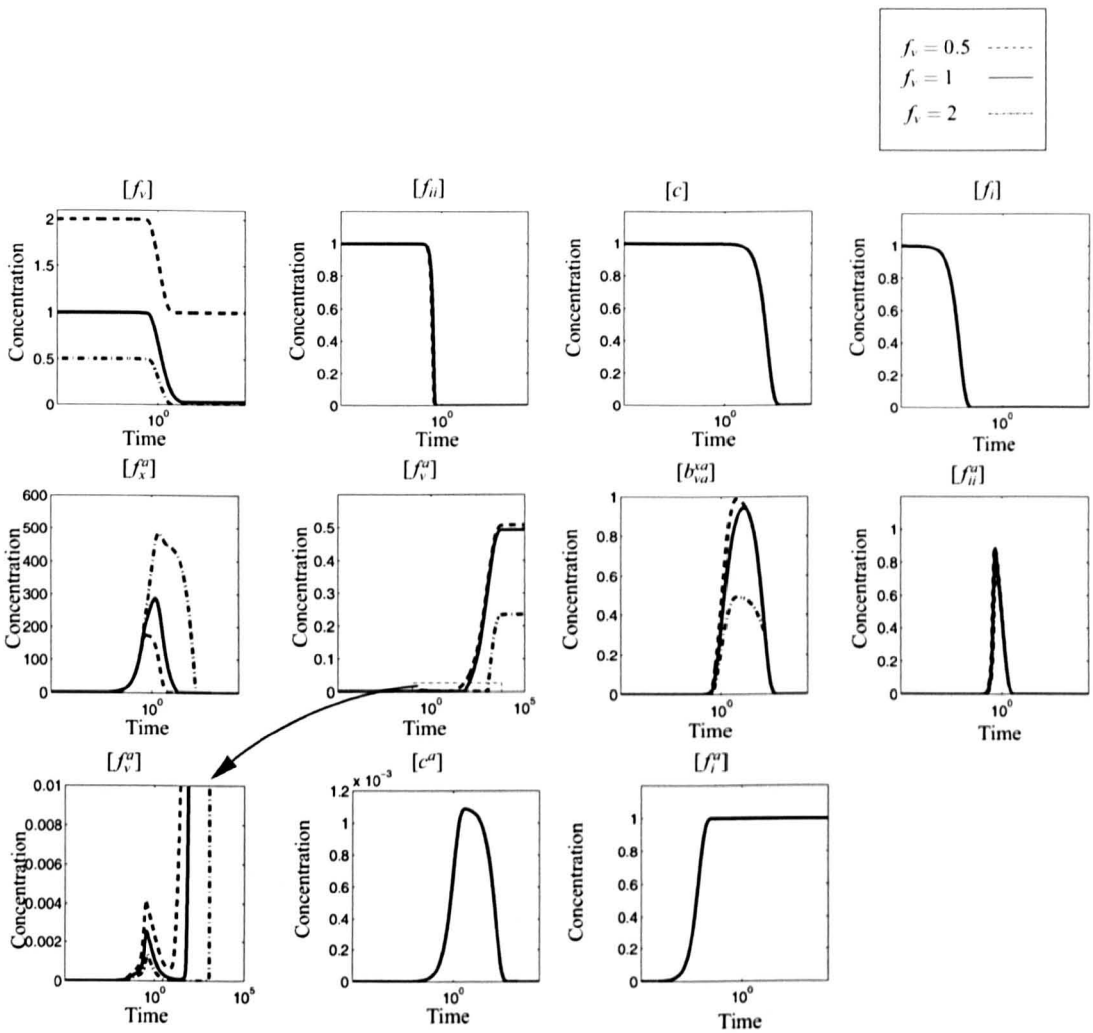

Figure 3.22: Numerical solutions for the full nondimensional system (equations (3.2.10)-(3.2.20)) showing how all factors evolve when the initial concentration of the procoagulant factor V is varied. All other initial concentrations of the procoagulants and the rescaled nondimensional parameters are set to one. Significant differences are seen in the evolution of factor V, factor Xa, factor Va and prothrombinase but not in thrombin concentration.

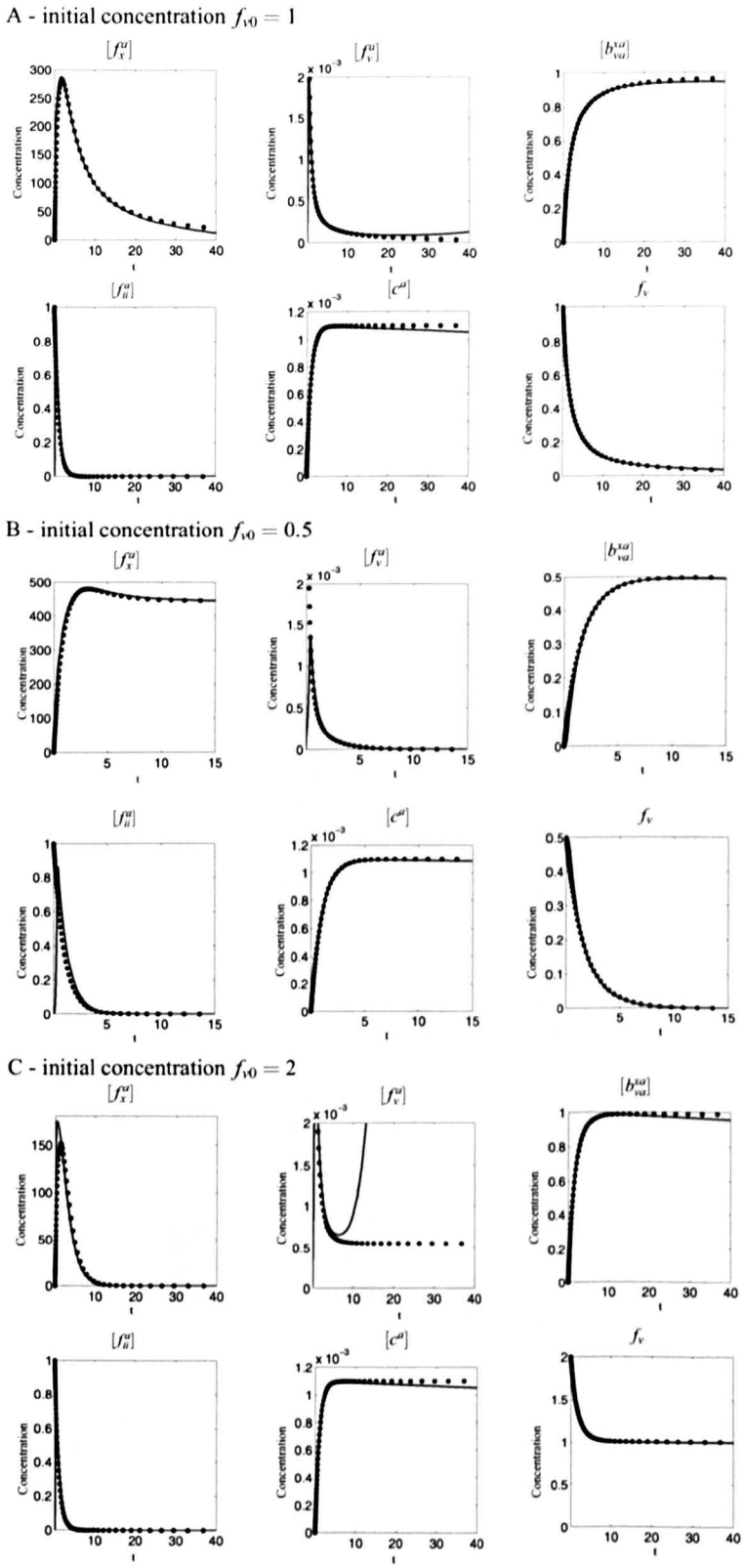

Figure 3.23: A comparison of the numerical solutions for the asymptotic approximations (equations (3.5.34), (3.5.35)) and the numerical solutions of the full nondimensional system (equations (3.2.10)-(3.2.20)) (solid line) for those factors dominant on the sixth timescale with all nondimensional and rescaled non-dimensional parameters set to one except the initial concentration of factor V which is varied. A - $f_{v0} = 1$, B - $f_{v0} = 0.5$, C - $f_{v0} = 2$.

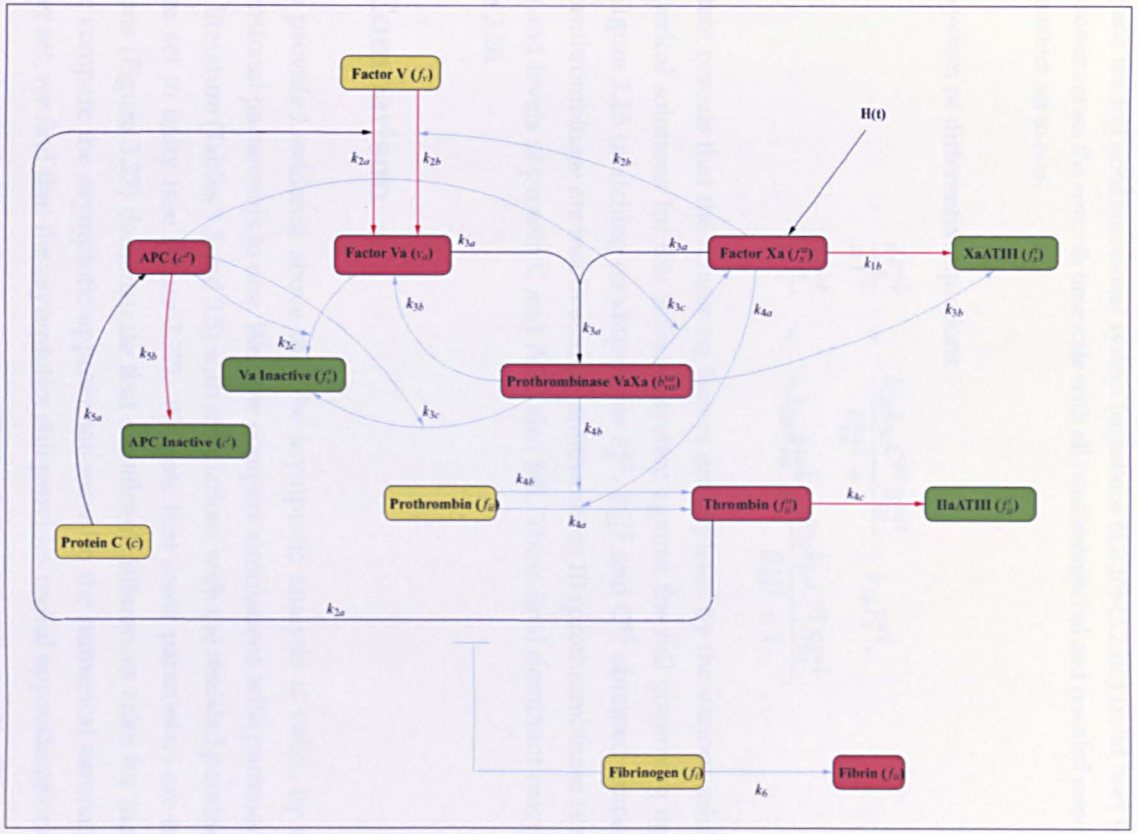

Figure 3.24: Reactions dominant on the sixth timescale. Reactions in red and black are those relevant to this timescale (red arrows representing newly featured reactions) with all other reactions in blue.

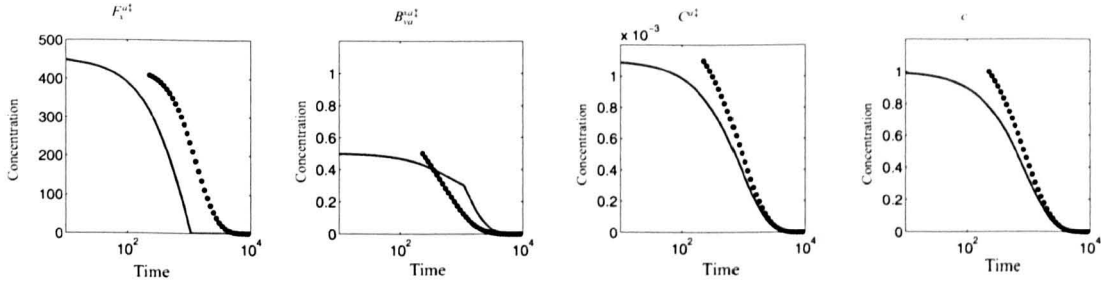

Figure 3.25: A comparison of the numerical solutions for the system (equations (3.5.39)) (dotted line) and the full nondimensional system (equations (3.2.10)-(3.2.20)) (solid line) for those factors dominant on the seventh timescale with all nondimensional and rescaled non-dimensional parameters set to one.

and the system of differential equations

$$\frac{dF_x^{a\ddagger}}{dT^{\diamond}} = \frac{k_{3a}k_{3c}C^{a\ddagger}B_{va}^{xa\ddagger}}{B_{va}^{xa\ddagger}+1} - k_{1b}F_x^{a\ddagger}, \tag{3.5.39a}$$

$$\frac{dB_{va}^{xa\ddagger}}{dT^{\diamond}} = -k_{3b}B_{va}^{xa\ddagger} - \frac{q_{3a}k_{3c}C^{a\ddagger}B_{va}^{xa\ddagger}}{B_{va}^{xa\ddagger}+1}. \tag{3.5.39b}$$

This system reveals that the remaining factors are depleted by the various inhibitory systems. The numerical solutions for this reduced system against the full governing equations can be seen in Figure 3.25 (matching conditions for $F_x^{a\ddagger}$, $B_{va}^{xa\ddagger}$ and $C^{a\ddagger}$ obtained numerically). Factor Xa and prothrombinase are inactivated by antithrombin III (prothrombinase is also inactivated by APC) and levels of protein C and APC also fall. These final dominant reactions are shown in Figure 3.26.

3.6 Comparison

We have provided evidence above that the asymptotic analysis is valid, by setting most of the dimensional parameters to one. We now compare simulations with parameter values taken from the literature (Tables 3.3 and 3.5) with simulations with the rescaled parameters and initial conditions set to unity (see Figure 3.27). We note that some parameters are not O(1). These simulations (Figure 3.27) demonstrate that significant differences arise for many factors but, when we compare the asymptotic approximations with the numerical simulations of the full parameter set, we find that the asymptotics still provides useful approximations and insight.

With parameter values from the literature (Tables 3.3 and 3.5) factor Xa (Figure 3.27 first plot, second row) displays a greater peak concentration (the level of stimulus of factor Xa is now $\bar{k}_{1a} = 166$) than when the nondimensional parameters where set to unity. Prothrombinase, assembled from factor Xa and Va, displays earlier and greater peak concentration and this is reflected in the increase in peak thrombin concentration. Activated protein C shows a marked increase in peak concentration attributable to the factor C initial concentration ($c_0 = 92$) not being O(1). Factor Va has a single rise and fall in concentration, settling to a negligible value whereas with parameter values set to unity a second peak concentration occurs with factor Va

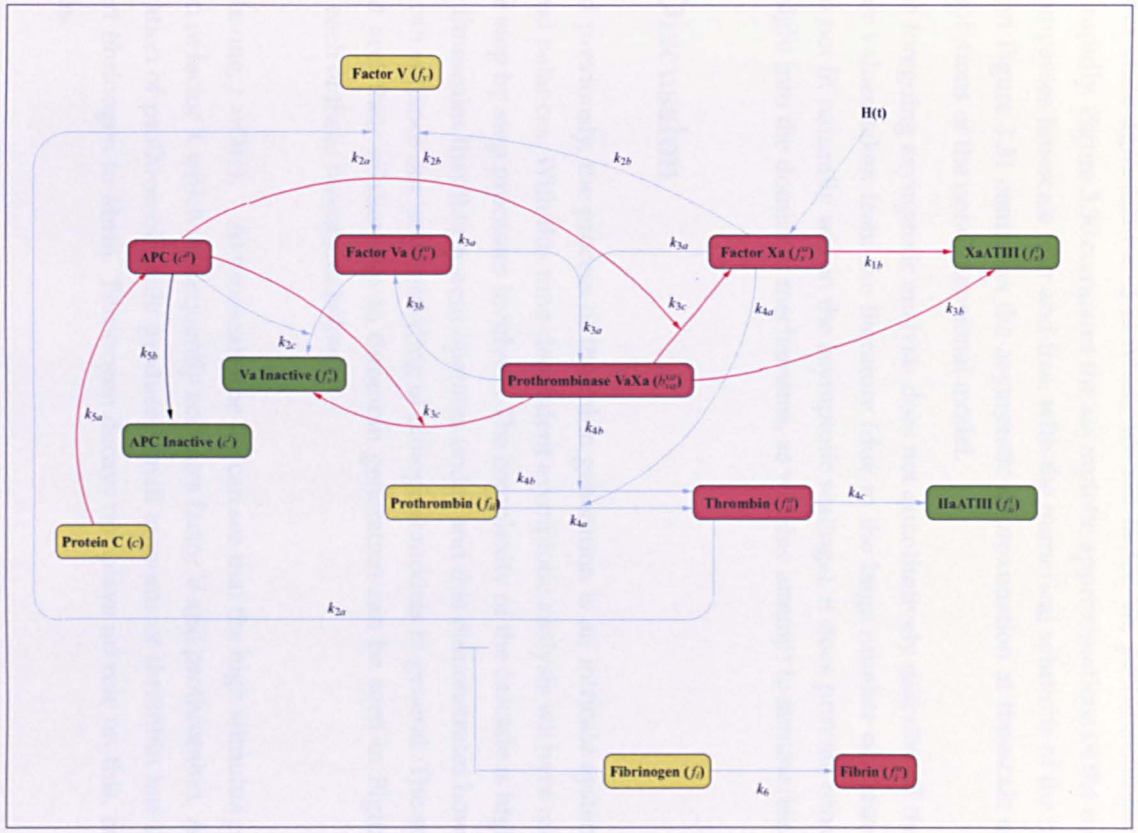

Figure 3.26: Reactions dominant on the seventh timescale. Reactions in red and black are those relevant to this timescale (red arrows representing newly featured reactions) with all other reactions in blue.

settling to this value. This can be attributed to prothrombinase production which now occurs earlier. Factor Va released from the prothrombinase complex, when factor Xa is inactivated, can be effectively inactivated by activated protein C, now produced at a greater concentration.

We now compare the asymptotic approximations at each timescale to the full nondimensional model. Figure 3.28 compares the asymptotic approximations at timescale one and two with the numerical solutions of the nondimensional model. Figure 3.29 compares the asymptotic approximations at timescale three with the numerical solutions of the nondimensional model. This shows close agreement and is where we see factor Va, prothrombinase and thrombin growing rapidly. Figure 3.30 compares the asymptotic approximations of the reduced δ model, that encompasses timescale four and five, with the numerical solutions of the nondimensional model and Figure 3.31 compares the asymptotic approximation at timescale six with the numerical solutions of the nondimensional model.

While the foregoing asymptotic analysis does not quantitatively describe all the behaviour for parameter values taken from the literature (due to the large number of parameters, some of which do not fit naturally within the asymptotic scalings), it does provide considerably qualitative insight into the dominant mechanisms, as we now attempt to summarise.

3.7 Discussion

As stated previously, the process of thrombin generation is an intricate system of fine tuned checks and balances. With this time-dependent asymptotic analysis we have aimed to demonstrate the step by step processes involved. The complexity of the cascade is highlighted by the multiple timescales that this system operates under and this demonstrates how an asymptotic analysis can enhance our understanding of biological models in general. The seven timescales discussed and their relationship to thrombin generation can be seen in Figure 3.32 and we describe each of these timescales below.

Timescale one, $t = O(\epsilon)$. At timescale one we can see that the high stimulus produces robust activation of factor X which subsequently activates factor V and prothrombin. At this timescale the activation of prothrombin only produces small amounts of thrombin but this is sufficient to convert fibrinogen to fibrin. Fibrinogen decays but plays no role on this, and subsequent, timescales.

Timescale two, $t = O(\epsilon^{2/3})$. The asymptotic approximation for timescale two resembles that for timescale one. The sole additional term is prothrombinase activation of prothrombin, this accelerates thrombin's formation. Timescale two encompass all the reactions of timescale one except fibrinogen decay, but fibrinogen plays no role in the previous timescale and so timescale one can be neglected.

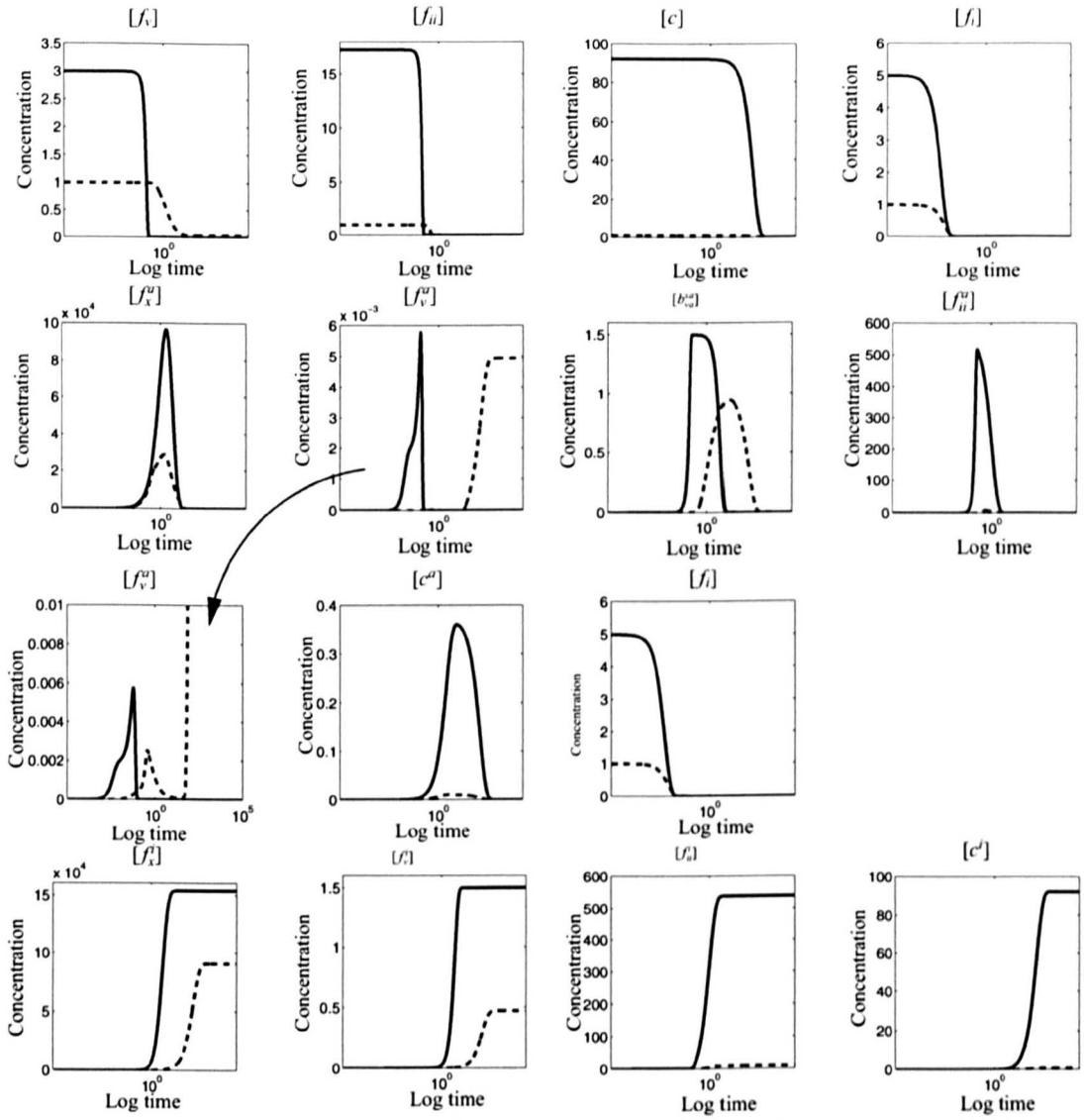

Figure 3.27: A comparison of the numerical solutions of the full nondimensional system (equations (3.2.10)-(3.2.20)) with the original parameter set (solid line) (Table 3.3 and 3.5) and with the rescaled nondimensional parameters and the initial concentrations set to unity (broken line).

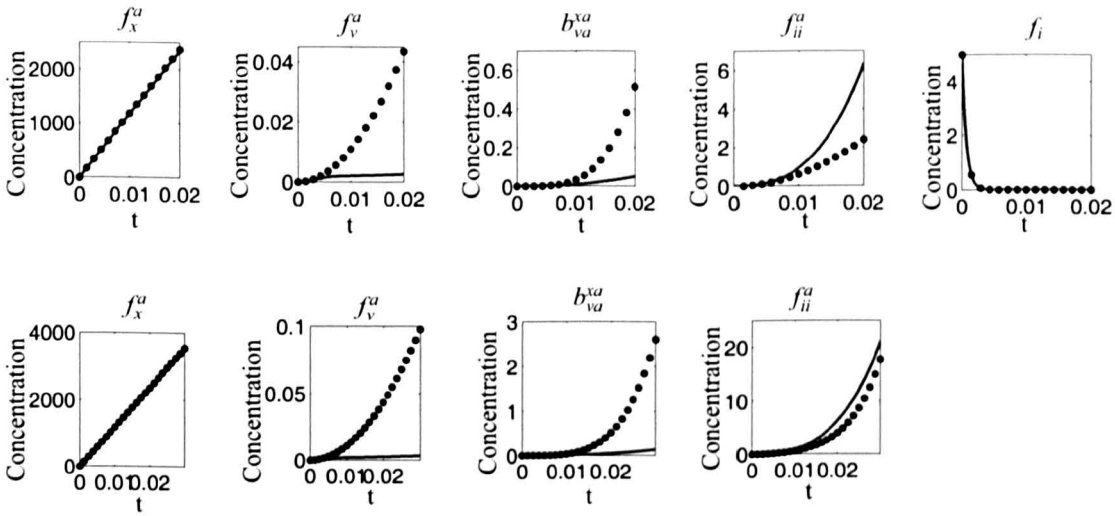

Figure 3.28: A comparison of the asymptotic approximations for timescale one ((3.5.3), top row, dotted line) and two ((3.5.6)-(3.5.7), bottom row, dotted line) and the numerical solutions of equations (3.2.10)-(3.2.20) (solid line) for those factors dominant on the first timescale t =O(ϵ) (with $\epsilon = 1.1 \times 10^{-3}$).

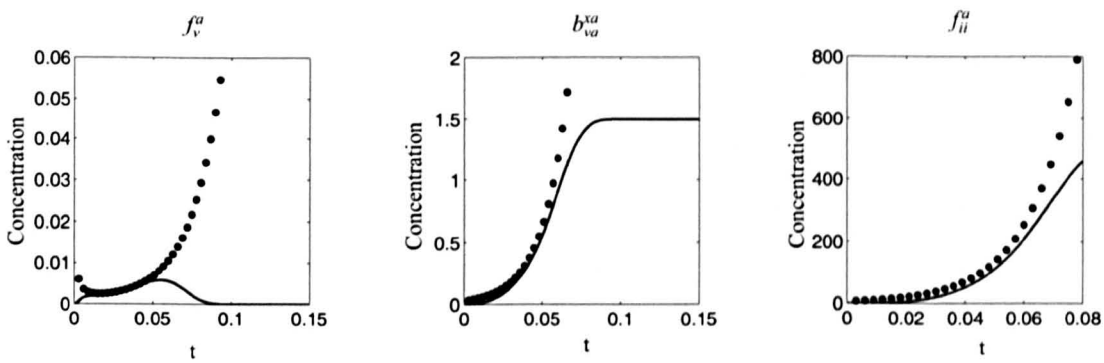

Figure 3.29: Solutions for the asymptotic approximation (3.5.10, 3.5.14) (dotted line) and the numerical solutions of equations (3.2.10)-(3.2.20) (solid line) for those factors that play a dominant role on the third timescale t =O($\epsilon^{1/2}$).

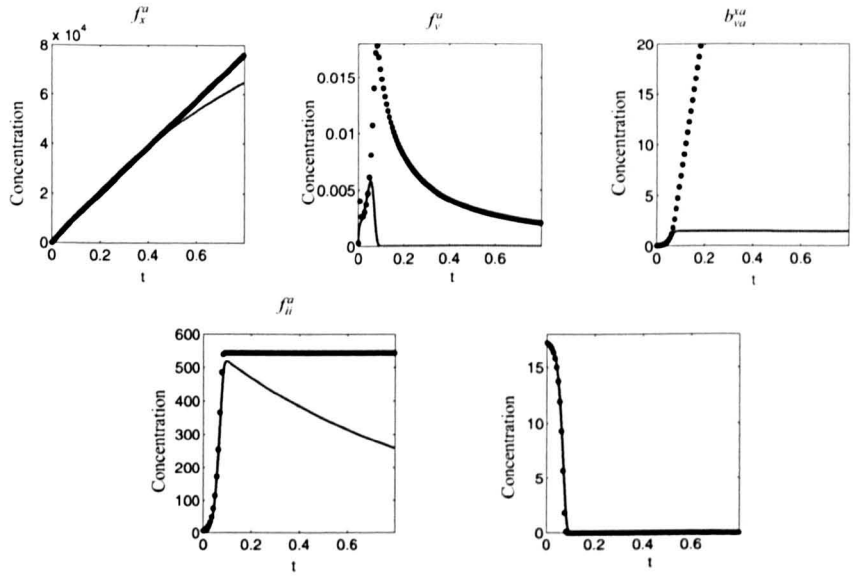

Figure 3.30: A comparison of the numerical solutions of the system (3.5.24) (dotted lines) and the numerical solutions of equations (3.2.10)-(3.2.20) (solid line) for those factors dominant in the reduced delta model ($\delta = 0.15$). Matching conditions now imposed at T= -0.6.

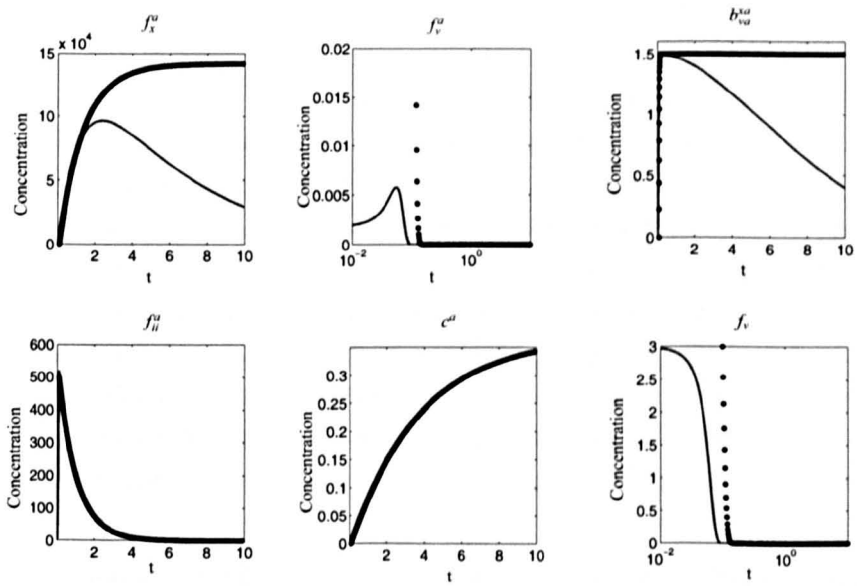

Figure 3.31: A comparison of the numerical solutions for the asymptotic approximations (equations (3.5.34), (3.5.35)) and the full nondimensional system (equations (3.2.10)-(3.2.20)) for those factors dominant on the sixth timescale t =O(1).

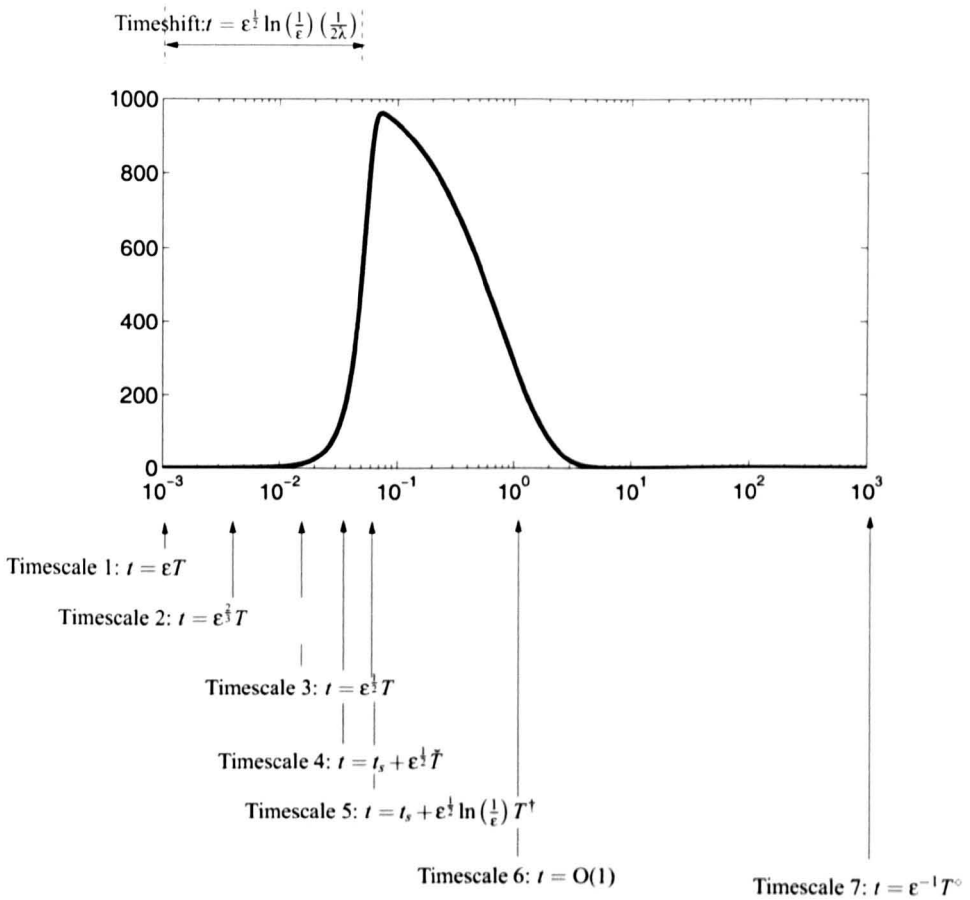

Figure 3.32: Timeline of asymptotic timescales shown against the simulation of thrombin.

Timescale three, t =O($\epsilon^{1/2}$). It is at timescale three that thrombin displays its characteristic explosive growth. At this timescale it is the action of the complex prothrombinase which solely activates prothrombin to thrombin. The large growth in thrombin generation can be accounted for by the inclusion of the positive feedback from thrombin to the activation of factor V; factor Va subsequently being assembled with factor Xa into the complex prothrombinase. A closed loop is formed (see Figure 3.12) and thus thrombin enhances its own activation. In dimensional form $\lambda = \sqrt{k_{4b} k_{2a} f_{v0} f_{ii0} / \left(k_{4c}^2 \left(f_{v0} + k_{2am}/k_{2bm}\right)\left(f_{ii0} + k_{4bm}/k_{4am}\right)\right)}$ and suggests that thrombins explosive growth is dependent on the initial concentrations of factor V and prothrombin as well as the rate that prothrombinase catalyses prothrombin to thrombin, the rate that thrombin activates factor V and the rate that ATIII inactivates thrombin.

The reduced δ model: timescale four and five. With a timestep of approximately $t_s \approx \epsilon^{1/2} \ln(1/\epsilon) \frac{1}{2\lambda}$ we capture the peak in factor Va and thrombin concentration. Thrombin generation settles to a constant and factor Va concentration starts to fall. Prothrombin, the procoagulant of thrombin declines to zero and prothrombinase and factor Xa continue to rise. The timeshift at the reduced delta model can be seen as an approximation of the time lag to where the large bolus of thrombin concentration is achieved.

Timescale six, t =O(1). It is at this timescale that thrombin is inactivated by the action of antithrombin III and we see a decline in thrombin levels. Protein C has yet to play a role.

Timescale seven, t =O(ϵ^{-1}). The remaining inhibitory processes take their effect. Activated protein C inactivates factor Va complexed within prothrombinase releasing factor Xa. ATIII acts on factor Xa, both within the prothrombinase complex and with out to sequester it to its inactive form. The procoagulant protein C decays.

Timescale six (where we see thrombin decay) and timescale three (where the thrombin concentration increases rapidly) capture the majority of reactions for the formation and inhibition of thrombin.

Within this chapter we have formulated a model that encompass a reduced subset of reactions of the coagulation cascade. We have, using singular-perturbation theory, produced a series of reduced models in time that provide insight into the underlying mechanisms responsible for thrombin's characteristic time lag, explosive growth and decay.

CHAPTER 4

The thrombin generation assay.

4.1 Introduction

Clinical testing of the bloods potential to clot requires, at present, two distinct tests that, while widely performed, are blunt and unreliable at detecting new anticoagulant therapies. A new clinical test is required and it is thought that the thrombin generation assay (TG) may fulfill this role. These experiments allow assessment of the entire coagulation system in plasma. The more traditional PT and aPTT assays (described in Sections 2.1.1.1 and 2.1.1.2) terminate with the formation of a clot, which occurs when only five percent of thrombin is generated. While these are useful in identifying congenital abnormalities, the newer thrombin generation assay provides a more accurate description of thrombin generation showing its complete evolution, which is relevant for the formation of a blood clot in-vivo, its lag-time and peak concentration (Mann *et al.*, 2003). It is possible to watch the concentration of thrombin as it develops in clotting (platelet-rich) plasma and activation is achieved via the more physiologically relevant TF rather than via contact activation.

There is great interest in finding new therapeutic means to disrupt the pathological formation of blood clots (thrombosis), as existing drugs target multiple factors within the coagulation cascade and, as a result, have the unwelcome side effect of excessive bleeding. There is particular interest in factors XI and XII as therapeutic targets since they are thought to play key roles in thrombosis but lesser ones in haemostasis. This makes them ideal candidates for limiting thrombus growth, without producing the side effect of excessive bleeding (Gailani & Renne, 2007*a*). Factor XI appears to lower the incidence of ischaemic stroke in humans and reduce thrombus formation in mice (Renne *et al.*, 2006) and, while it seems to play a supportive role in haemostasis, a severe factor XI deficiency does not generally produce bleeding tendency (Gailani & Renne, 2007*a*).

There has been some controversy surrounding the activation mechanism of factor XI. While it is known that factor XI is activated by factor XIIa, as reflected in the intrinsic pathway and the aPPT assay, it is thought that there is an alternative method of activation (Gailani & Renne, 2007*a*) with congenital deficiencies of factor XII (normal bleeding and a prolonged aPTT) and of factor XI (a mild bleeding disorder) being consistent with the existence of an alternative

pathway to factor XI activation (Kravtsov *et al.*, 2009). Candidates for activating factor XI include thrombin and factor XIa auto-activation (Naito & Fujikawa, 1991; Gailani & Broze, 1991). While recent studies (Kravtsov *et al.*, 2009; Wielders *et al.*, 2004; Keularts *et al.*, 2001; Oliver *et al.*, 1999) suggest that the alternative pathway may involve a feedback loop from thrombin, this result is at variance with other studies (Pedicord *et al.*, 2007) including the theoretical work of Kramoroff & Nigretto (2001). Both of these papers suggest that factor XI is auto-activated.

In this chapter we formulate and analyse a mathematical model that mimics the thrombin generation assay and use this for investigating the contribution of the intrinsic pathway and factor XI to thrombin generation. We extend our previous model of the common pathway of the coagulation cascade by incorporating the intrinsic and extrinsic pathways and factor XI activation via thrombin. This allows us to use the resulting system of twenty-nine ordinary differential equations to produce simulations that we can compare to the experimental work on factor XI activation in tissue factor stimulated plasma in the absence of factor XII (Kravtsov *et al.*, 2009). The results of Kravtsov *et al.* are consistent with the existence of a feedback loop that links thrombin to factor XI and contributes to coagulation in the absence of factor XII. Previous mathematical models that include an explicit feedback mechanism from thrombin to factor XI (Zarnitsina *et al.*, 1996*b*; Kramoroff & Nigretto, 2001) are formulated so that they are comparable to experimental data based on the aPTT assay. Such models do not account for the whole coagulation system and are activated via the contact system.

This chapter is organised as follows. In the next section we develop our model; we describe in detail the reactions included in the model and the roles they play within the coagulation cascade, we discuss the assumptions which we have made and present the model in full. In Section 4.3 we numerically solve subsystems of our model, evaluating the contributions they make to thrombin generation in terms of peak thrombin production and time to reach this peak. Parameter values are restricted to those found in literature (Table 4.4) and we set initial conditions to the levels typical of human plasma (Table 4.3). Model simulations are compared to the experimental work of Kravtsov *et al.* (2009) and are able to detect the contribution to thrombin generation of thrombin activation of factor XI. We discuss these results, and further modifications that could be made to the model, in Section 4.4. A detailed review of the relevant biology and previous mathematical models was presented in Chapter 2.

4.2 Mathematical model

4.2.1 Formulation

In this section we construct a new kinetic model of the coagulation cascade which can be used to simulate experiments (Kravtsov *et al.*, 2009) conducted with a Thrombinoscope®. The model consists of a system of ordinary differential equations which describe the changes in concentration of factors within the coagulation cascade. We extend the model of thrombin formation presented in Chapter 3 to include those factors of the extrinsic and intrinsic pathways. The model excludes factors of contact activation so as to mimic experiments carried out in plasma

deficient in factor XII. We include three feedback loops from thrombin: to factor V, to factor VIII and, controversially to factor XI. To facilitate a step-by-step description of the model we have decomposed the cascade into eleven reactions summarised in Table 4.1, in which we also distinguish those present in the previous model. We describe the reactions in more detail in Table 4.2. The factors included in our model are shown diagrammatically in Figure 4.1 while Figure 4.2 shows the position of each subset of reactions (those of the previous model, the extrinsic pathway, the intrinsic pathway and factor XI activation) within the full cascade.

Factors within the coagulation cascade are numbered 1–13, as indicated by their roman numerals. We introduce the variables listed in Table 4.3 where f denotes a factor, with its relevant roman numeral as a subscript, and a superscript indicating activation ('a') or inactivation ('i'). Complexes are denoted by b being formed by the binding of the two factors indicated in its subscript and superscript. The inhibitory factors TFPI and protein C are denoted by p and c respectively, while intrinsic tenase is denoted by n. According to the reaction scheme in Table 4.1, the rate of change in each variable of the common pathway is given by

$$\frac{df_x}{dt} = -k_{1f} - k_{1c} - k_{1d}, \tag{4.2.1a}$$

$$\frac{df_x^a}{dt} = k_{1f} + k_{1c} + k_{1d} + k_{3c} - [k_{1b}] - [k_{3a}] - k_{1e}, \tag{4.2.1b}$$

$$\frac{df_x^i}{dt} = [k_{1b}] + [k_{3b}], \tag{4.2.1c}$$

$$\frac{df_v}{dt} = -[k_{2a}] - [k_{2b}], \tag{4.2.1d}$$

$$\frac{df_v^a}{dt} = [k_{2a}] + [k_{2b}] + [k_{3b}] - [k_{2c}] - [k_{3a}], \tag{4.2.1e}$$

$$\frac{df_v^i}{dt} = [k_{2c}] + [k_{3c}], \tag{4.2.1f}$$

$$\frac{db_{v_a}^{x_a}}{dt} = [k_{3a}] - [k_{3b}] - [k_{3c}], \tag{4.2.1g}$$

$$\frac{df_{ii}}{dt} = -[k_{4a}] - [k_{4b}], \tag{4.2.1h}$$

$$\frac{df_{ii}^a}{dt} = [k_{4a}] + [k_{4b}] - [k_{4c}], \tag{4.2.1i}$$

$$\frac{df_{ii}^i}{dt} = [k_{4c}], \tag{4.2.1j}$$

$$\frac{df_i}{dt} = -[k_6], \tag{4.2.1k}$$

$$\frac{df_i^a}{dt} = [k_6], \tag{4.2.1l}$$

and the variables of the protein C subsystem evolve in the following way

$$\frac{dc}{dt} = -[k_{5a}], \tag{4.2.1m}$$

$$\frac{dc^a}{dt} = [k_{5a}] - [k_{5b}], \tag{4.2.1n}$$

$$\frac{dc^i}{dt} = [k_{5b}]. \tag{4.2.1o}$$

Reaction	Generation		Inactivation	
	No.	Description	No.	Description
Generation and inactivation of factor Xa	$1f$	$X \xrightarrow{VIIa:TF} Xa$	$1b*$	Xa+ATIII $\rightarrow$ Xa:ATIII
	$1c*$	$X \xrightarrow{IXa} Xa$	$1e$	Xa+TFPI $\rightarrow$ Xa:TFPI
	$1d$	$X \xrightarrow{VIIIa:IXa} Xa$		
Generation and inactivation of factor Va	$2a*$	$V \xrightarrow{IIa} Va$	$2c*$	$Va \xrightarrow{APC}$ Va:Inactive
	$2b*$	$V \xrightarrow{Xa} Va$		
Formation of prothrombinase	$3a*$	Va+Xa $\leftrightarrow$ Va:Xa	$3b*$	Va:Xa+ATIII $\rightarrow$ Va+Xa:ATIII
			$3c*$	$Va:Xa \xrightarrow{APC}$ Va:Inactive+Xa
Generation and inactivation of thrombin	$4a*$	$II \xrightarrow{Xa} IIa$	$4c*$	IIa+ATIII $\rightarrow$ IIa:ATIII
	$4b*$	$II \xrightarrow{Va:Xa} IIa$		
Protein C	$5a*$	$C \xrightarrow{IIa} APC$	$5b*$	APC $\rightarrow$ APC:Inactive
Fibrinogen to fibrin	$6*$	Fibrinogen $\xrightarrow{IIa}$ Fibrin		
Generation and inactivation of factor XIa	$7a$	$XI \xrightarrow{IIa} XIa$	$7b$	XIa+ATIII $\rightarrow$ XIa:ATIII
Generation and inactivation of factor IXa	$8a$	$IX \xrightarrow{XIa} IXa$	$8b$	IXa+ATIII $\rightarrow$ IXa:ATIII
	$8c$	$IX \xrightarrow{TF:VIIa} IXa$		
Generation and inactivation of factor VIIIa	$9a$	$VIII \xrightarrow{IIa} VIIIa$	$9b$	$VIIIa \xrightarrow{APC}$ VIIIa:Inactive
Formation of intrinsic tenase	$10a$	VIIIa+IXa $\leftrightarrow$ VIIIa:IXa	$10b$	$VIIIa:IXa \xrightarrow{APC}$ VIIIa:Inactive+IXa
			$10c$	VIIIa:IXa+ATIII $\rightarrow$ VIIIa+IXa:ATIII
Activation and inactivation of the extrinsic tenase	11_a	$f(t) \leftrightarrow$ VIIa:TF	11_b	VIIa:TF+Xa:TFPI $\rightarrow$ VIIa:TF:Xa:TFPI

Table 4.1: Summary of reactions (detailed in Table 4.2) included in our model (equations (4.2.5, 4.2.6, 4.2.7)) of the coagulation cascade. Enzymatic reactions ($1c$, $1d$, $1f$,$2a$, $2b$, $2c$, $3c$, $4a$, $4b$, $7a$, $8a$, $8c$, $9a$, $9b$, $10b$) are represented by Michaelis-Menten kinetics, while mass-action kinetics are adopted for other reactions, with $1b$, $3b$, $4c$, $5a$, $5b$, 6, $7b$, $8b$ and $10c$ being of first-order and $1e$, $3a$, $10a$ and $11b$ (complex formation) of second order. Due to the abundance of ATIII, its concentration is assumed to be constant. Reactants (factors) within the cascade are normally denoted by Roman numerals (with 'a' indicating an activated factor); prothrombinase is the complex formed from factors Xa and Va; intrinsic tenase for the complex formed from factor IXa and factor VIIIa, extrinsic tenase for the complex formed from factor VIIa and TF, prothrombin (factor II), thrombin (factor IIa), fibrinogen (factor I), fibrin (factor Ia), the inhibitors being protein C (APC in its activated form), TFPI (tissue factor pathway inhibitor) and ATIII (antithrombin III). Reactions marked with a $*$ are included in the model from Chapter 3. These reactions are also depicted graphically in Figure 4.1.

Reaction 1. Generation and inactivation of factor Xa.
Factor X marks the start of the common pathway. In our previous model of thrombin generation (Chapter 3) factor Xa production was assumed to depend on tissue damage and the extrinsic pathway (via the function $H(t)$). In this model we include extrinsic tenase (n) and the intrinsic pathway and so factor Xa is activated by the extrinsic pathway (through tissue factor and extrinsic tenase VIIa:TF) at rate k_{1f} and the intrinsic pathway (through factor IXa) at rate k_{1c} and the intrinsic tenase VIIIa:IXa at rate k_{1d} - see equations (4.2.5a), (4.2.6b). Competition for extrinsic tenase between factor X and factor IX is also included. Factor X is inactivated by antithrombin III which forms an irreversible complex (concentration x_i) at rate k_{1b} (see (4.2.6b), (4.2.7c)). With the inclusion of TFPI (p) in this model we can now include TFPI inactivation of factor Xa by the formation of the complex Xa:TFPI ($b^p_{x_a}$) with rate k_{1e} (see equations (4.2.5i), (4.2.6b), (4.2.7a)).
Reaction 2. Generation and inactivation of factor Va.
The activation of factor V (f_v) is mediated by factor Xa (rate constant k_{2b}) and by thrombin (rate constant k_{2a}) (Asselta *et al.*, 2006; Segers *et al.*, 2007) (equations (4.2.5b), (4.2.6c)). The model accounts for competition between factor V and prothrombin (b) for factor Xa and between factor V, fibrinogen (f_i), factor VIII (f_{viii}) and factor XI (f_{xi}) for thrombin. The down-regulation of factor Va activity is achieved by activated protein C (Asselta *et al.*, 2006) at rate k_{2c} (see equations (4.2.6c), (4.2.7d)).
Reaction 3. Formation of prothrombinase.
Prothrombinase is assembled from factor Va and factor Xa at rate constant k_{3a} (see equations (4.2.6b), (4.2.6c), (4.2.6d)). Down-regulation of prothrombinase is achieved in two ways: the factor Xa complexed within it can be inactivated by antithrombin III (rate k_{3b}), releasing factor Va (see (4.2.6c), (4.2.6d), (4.2.7c)). Alternatively cofactor Va can be inactivated by binding irreversibly to APC (with rate constant k_{3c}) forming inactive factor V (v_i) and releasing factor Xa (see (4.2.6b), (4.2.6d), (4.2.7d)).
Reaction 4. Generation and inactivation of thrombin.
There are two pathways by which prothrombin can be activated to thrombin: via factor Xa with rate constant k_{4a} (taking into account competition for factor Xa between factor V and prothrombin) - see (4.2.5c), (4.2.6e) - and catalysed by prothrombinase, with rate constant k_{4b} - see (4.2.5c, 4.2.6e). Antithrombin III directly converts thrombin (rate k_{4c}) to its inactivated form (x_i); see (4.2.6e, 4.2.7e).
Reaction 5. Protein C system.
The inhibitory protein C pathway is modelled as a first order reaction, with activation at rate k_{5a} - see (4.2.5h), (4.2.6j) - and conversion to its inactivated form (c_i) occurs at rate k_{5b}; see (4.2.6j, 4.2.7j).
Continued on next page

Table 4.2: Detailed description of each reaction listed in Table 4.1.

Reaction 6. Conversion of fibrinogen to fibrin.
The conversion of fibrinogen (g) to fibrin (f) (rate constant k_6) is included to account for the reduction in the activation rate of factor V caused by the competition for thrombin of fibrinogen and factor V (4.2.5d, 4.2.7f).
Reaction 7. Generation and inactivation of factor XIa.
Factor XI is activated by thrombin with rate constant k_{7a} (equations (4.2.5e), (4.2.6f)). Factor XI competes for thrombin with factor V, fibrinogen (g) and factor VIII ($viii$). Antithrombin III inactivates factor XIa (rate k_{7b}) by binding irreversibly to it (concentration xi_i) with rate k_{7b} (see equations (4.2.6f), (4.2.7h)).
Reaction 8. Generation and inactivation of factor IXa.
Factor IX is activated by factor XIa with rate constant k_{8a} (see equations (4.2.5f), (4.2.6g)). Antithrombin III binds irreversibly with factor XIa at rate k_{8b} to form a complex with concentration xi_i (see equations (4.2.6g), (4.2.7g)).
Reaction 9. Generation and inactivation of factor VIIIa.
Factor VIII is activated by thrombin with rate constant k_{9a} (see equations (4.2.5g), (4.2.6h)). It competes for thrombin with factor V, fibrinogen (g) and factor XI (xi). Protein C inactivates factor VIII at rate k_{9b} (see (4.2.6h), (4.2.7i)).
Reaction 10. Formation of intrinsic tenase.
Intrinsic tenase (q) is assembled from factor VIIIa and factor IXa with rate constant k_{10a} (see equations (4.2.6g), (4.2.6h), (4.2.6i)). Down-regulation of intrinsic tenase occurs when antithrombin III binds to factor IXa (rate k_{10c}) releasing factor VIIIa (see (4.2.6i), (4.2.6h), (4.2.7g)). Alternatively cofactor VIIIa can bind irreversibly to APC (with rate k_{10b}) forming an inactive factor ($viii_i$) and releasing factor IXa (see (4.2.6i), (4.2.6g), (4.2.7i)).
Reaction 11. Formation of the extrinsic tenase.
In the absence of suitable data, we assume that the extrinsic pathway is initiated at the level of the extrinsic tenase and model its formation by a function $G(t) = k_{11a}e^{-k_{11ax}t}$ representing the variable production of extrinsic tenase, where k_{11a} is the total amount of extrinsic tenase (concentration n) produced, the rate constant k_{11ax} is associated with the loss of the stimulant by its degradation. $G(t)$ is modified (via parameters k_{11a}, k_{11ax}) so that the simulation of the TF:VIIa complex approximates data from Orfeo *et al.* (2005) of extrinsic tenase concentrations over time in response to tissue factor activation of plasma (see Figure 4.3). Extrinsic tenase is inhibited by binding to the complex Xa:TFPI at rate k_{11b} (4.2.6a, 4.2.7b).

Table 4.2: Detailed description of each reaction listed in Table 4.1.

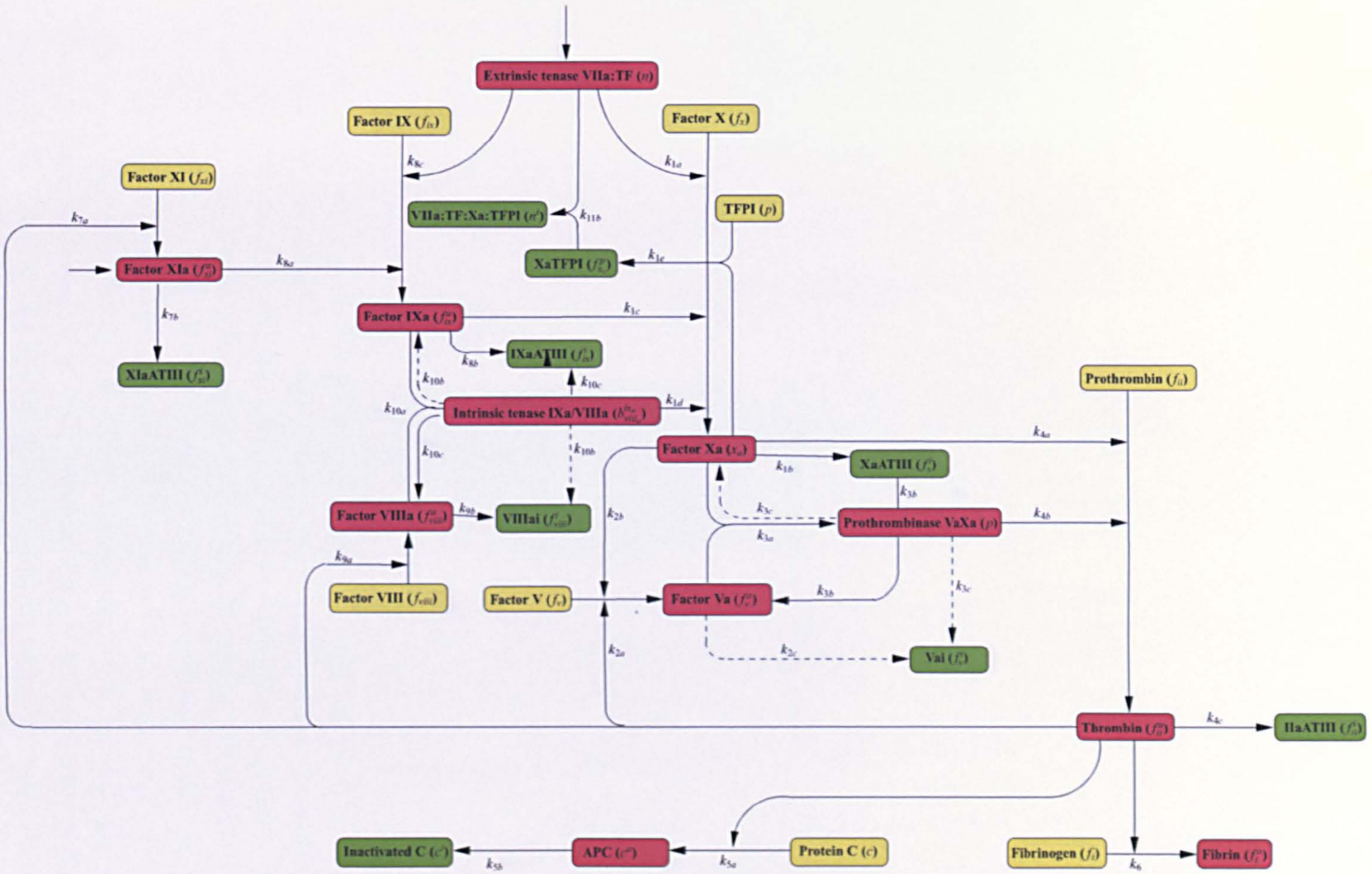

Figure 4.1: A schema of our model of the coagulation cascade based on the reactions shown in Table 4.1. The boxes correspond to coagulation factors and lower case letters denote concentrations. Red boxes (with superscript a) denote active factors, yellow procoagulants and green (with superscript *i*) inactivated factors. Arrows pointing into boxes represent conversion from one species to another while those directed at other lines correspond to catalysis. Rate parameters are shown above their respective reactions. Dashed lines show protein C inhibition. There is no variable for antithrombin III as it occurs at such high levels that it is not considered rate limiting.

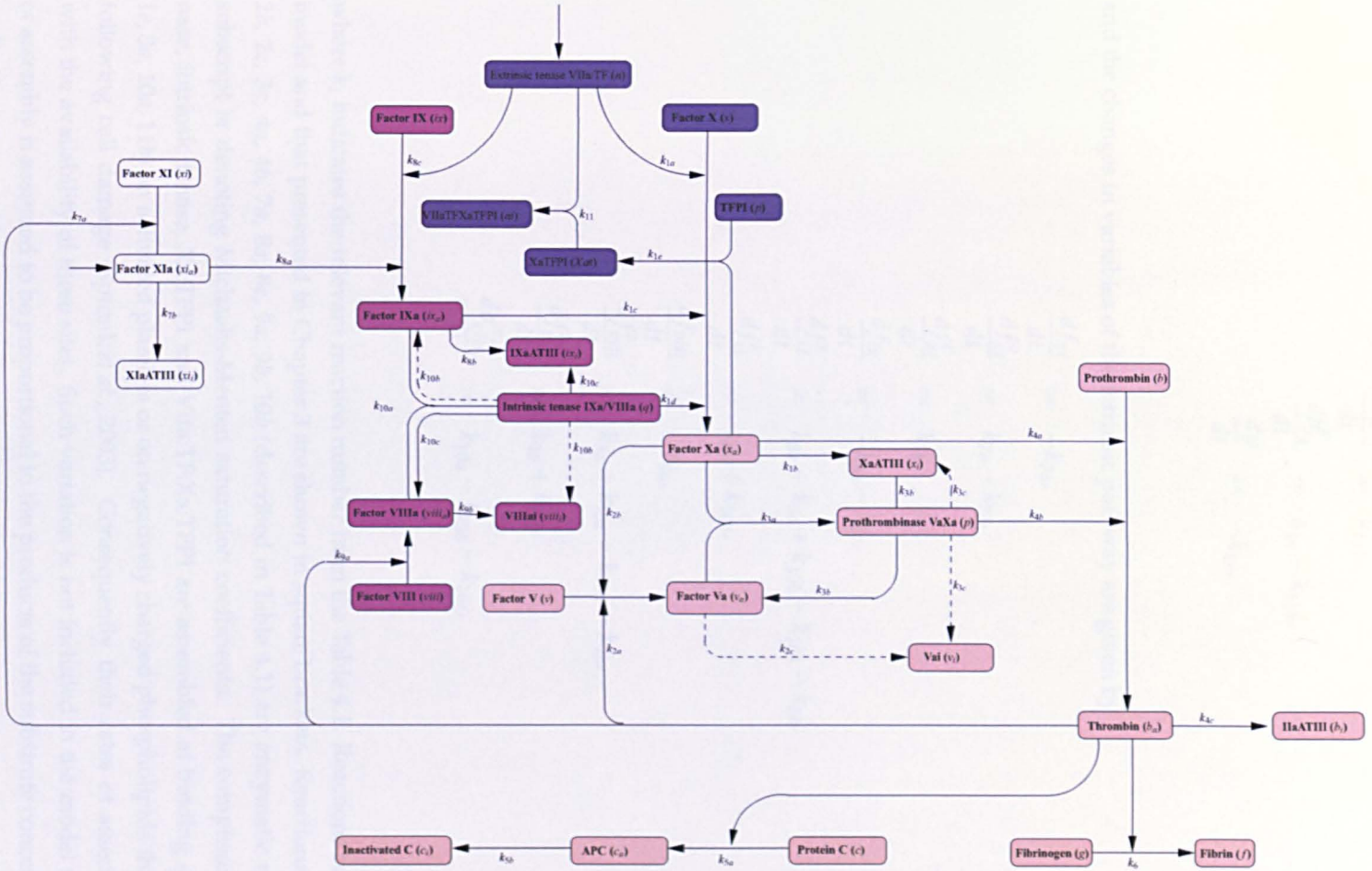

Figure 4.2: A schema of the coagulation cascade based on the reactions shown in Table 4.1. Boxes correspond to coagulation factors, with the lower case letters in brackets being used in the mathematical model to designate concentrations. Boxes denote factors included in the model presented in Chapter 3 (pink), factors of the extrinsic pathway (blue), factors of the intrinsic pathway (magenta) and factors relevant to thrombin activation of factor XI (white). Arrows pointing into boxes represent conversion from one species to another while those directed at other lines correspond to catalysis. Rate parameters are shown above their respective reactions. Dashed lines show protein C inhibition.

The changes in variables of the extrinsic pathway are

$$\frac{dn}{dt} = G(t) - k_{11b} \tag{4.2.2a}$$

$$\frac{db_n^{x_a p}}{dt} = k_{11b}, \tag{4.2.2b}$$

$$\frac{db_{x_a}^{p}}{dt} = k_{1e} - k_{11b}, \tag{4.2.2c}$$

$$\frac{dp}{dt} = -k_{1e}, \tag{4.2.2d}$$

and the changes in variables of the intrinsic pathway are given by

$$\frac{df_{xi}}{dt} = -k_{7a}, \tag{4.2.3a}$$

$$\frac{df_{xi}^{a}}{dt} = k_{7a} - k_{7b}, \tag{4.2.3b}$$

$$\frac{df_{xi}^{i}}{dt} = k_{7b}, \tag{4.2.3c}$$

$$\frac{df_{ix}}{dt} = -k_{8a} - k_{8c}, \tag{4.2.3d}$$

$$\frac{df_{ix}^{a}}{dt} = k_{8a} + k_{8c} + k_{10b} - k_{10a} - k_{8b}, \tag{4.2.3e}$$

$$\frac{df_{ix}^{i}}{dt} = k_{8b} + k_{10c}, \tag{4.2.3f}$$

$$\frac{df_{viii}}{dt} = -k_{9a}, \tag{4.2.3g}$$

$$\frac{df_{viii}^{a}}{dt} = k_{9a} + k_{10c} - k_{10a} - k_{9b}, \tag{4.2.3h}$$

$$\frac{df_{viii}^{i}}{dt} = k_{9b} + k_{10b}. \tag{4.2.3i}$$

$$\frac{db_{viii_a}^{ix_a}}{dt} = k_{10a} - k_{10b} - k_{10c}, \tag{4.2.3j}$$

where k_i indicates the relevant reaction number from the Table 4.1. Reactions common to this model and that presented in Chapter 3 are shown in square brackets. Reactions 1*c*, 1*d*, 1*f*, 2*a*, 2*b*, 2*c*, 3*c*, 4*a*, 4*b*, 7*a*, 8*a*, 8*c*, 9*a*, 9*b*, 10*b* (described in Table 4.1) are enzymatic reactions, with subscript m denoting Michaelis-Menten saturation coefficients. The complexes prothrombinase, intrinsic tenase, Xa:TFPI and VIIa:TF:Xa:TFPI are assembled at binding sites (reactions 1*e*, 3*a*, 10*a*, 11*b*) on activated platelets or on negatively charged phospholipids that are exposed following cell damage (Spronk *et al.*, 2003). Consequently their rates of assembly will vary with the availability of these sites. Such variation is not included in the model where the rate of assembly is assumed to be proportional to the products of the substrate concentrations. Due to the abundance of ATIII, its concentration is assumed to be constant and reactions 1*b*, 3*b*, 4*c*, 7*b* 8*b* and 10*c* are effectively first order. As in chapter 3 we follow Willems *et al.* (1991) and treat the protein C system and the conversion of fibrinogen to fibrin as first-order reactions (5*a*, 5*b*, 6).

Variable	Description	Initial condition	
		Dim.	Nondim.
$b_{v_a}^{x_a}$ *	Prothrombinase (VaXa)		
$b_{viii_a}^{ix_a}$	Intrinsic tenase		
$b_{x_a}^{p}$	Inactivated factor X		
c *	protein C	60 nM	1.68
c^a *	activated protein C		
c^i *	inactivated protein C		
f_i *	Fibrinogen	8300 nM	2.22
f_i^a *	Fibrin		
f_{ii} *	Prothrombin, factor II	1400 nM	24.14
f_{ii}^a *	Thrombin, factor IIa		
f_{ii}^i *	Thrombin, inactivated		
f_v *	Factor V	21 nM	1.92
f_v^a *	Activated factor V		
f_v^i *	Inactivated factor V		
f_{viii}	Factor VIII	0.7 nM	6.25×10^{-6}
f_{viii}^a	Activated factor VIII		
f_{viii}^i	Inactivated factor VIII		
f_{ix}	Factor IX	90 nM	3.75
f_{ix}^a	Activated factor IX		
f_{ix}^i	Inactivated factor IX		
f_x	Factor X	133 nM	0.71
f_x^a *	Activated factor X		
f_x^i *	Inactivated factor X		
f_{xi}	Factor XI	25 nM	0.60
f_{xi}^a	Activated factor XI		
f_{xi}^i	Inactivated factor XI		
n	Extrinsic tenase		
n^i	Inactivated extrinsic tenase		
p	TFPI	2.5 nM	1.68

Table 4.3: Summary of dependent variables; concentrations, where indicated, are typical factor levels for human plasma (taken from Butenas *et al.* (1999)). * indicates variables common to this model and the model presented in Chapter 3. The nondimensional variables are described in equations (4.2.8) and (4.2.9).

We note that with this extended system we have conservation (in their various forms) of fibrinogen, prothrombinase, protein C, factor V, factor X, factor XI, factor IX, factor VIII, TFPI, complexes Xa:TFPI, VIIa:TF:Xa:TFPI and intrinsic tenase in the form

$$f_i + f_i^a = f_{i0}, \qquad f_{ii} + f_{ii}^a + f_{ii}^i = f_{ii0}, \qquad c + c^a + c^i = c_0,$$
$$f_v + f_v^a + f_v^i + b_{v_a}^{x_a} = f_{v0} + b_{v_a 0}^{x_a}, \qquad f_{viii} + f_{viii}^a + f_{viii}^i + b_{viii_a}^{ix_a} = f_{viii0} + b_{viii_{a0}}^{ix_a},$$
$$f_{ix} + f_{ix}^a + f_{ix}^i + b_{viii_a}^{xi_a} = f_{ix0} + b_{viii_{a0}}^{ix_a}, \qquad f_x + f_x^a + f_x^i + b_{v_a}^{x_a} = f_{x0} + b_{v_a 0}^{x_a},$$
$$f_{xi} + f_{xi}^a + f_{xi}^i = f_{xi0}, \qquad n + n^i = \int_0^t G(t')dt' + n_0. \tag{4.2.4}$$

For each reactant we substitute in (4.2.1) - (4.2.3) the functional forms for the reactions listed in Table 4.3 formulating an ordinary differential equation. The equations for the procoagulants can be written as follows:

$$\frac{df_x}{dt} = -\frac{k_{1f}\, n\, f_x}{f_x + k_{1fm}(1 + \frac{f_{ix}}{k_{8cm}})} - \frac{k_{1c}\, f_{ix}^a\, f_x}{f_x + k_{1cm}} - \frac{k_{1d}\, b_{viii_a}^{ix_a} f_x}{f_x + k_{1dm}}, \tag{4.2.5a}$$

$$\frac{df_v}{dt} = -\frac{k_{2a} f_{ii}^a f_v}{f_v + k_{2am}(1 + \frac{f_i}{k_{6m}} + \frac{f_{xi}}{k_{7am}} + \frac{f_{viii}}{k_{9am}})} - \frac{k_{2b}\, x_a\, f_v}{f_v + k_{2bm}(1 + \frac{f_{ii}}{k_{4am}})}, \tag{4.2.5b}$$

$$\frac{df_{ii}}{dt} = -\frac{k_{4a}\, f_x^a\, f_{ii}}{f_{ii} + k_{4am}(1 + \frac{f_v}{k_{2bm}})} - \frac{k_{4b}\, b_{x_a}^{vii_a} f_{ii}}{f_{ii} + k_{4bm}}, \tag{4.2.5c}$$

$$\frac{df_i}{dt} = -k_6\, f_i, \tag{4.2.5d}$$

$$\frac{df_{xi}}{dt} = -\frac{k_{7a}\, f_{ii}^a\, f_{xi}}{f_{xi} + k_{7am}(1 + \frac{f_i}{k_{6m}} + \frac{f_v}{k_{2am}} + \frac{f_{viii}}{k_{9am}})}, \tag{4.2.5e}$$

$$\frac{df_{ix}}{dt} = -\frac{k_{8a}\, f_{xi}^a\, f_{ix}}{f_{ix} + k_{8am}} - \frac{k_{8c}\, n\, f_{ix}}{f_{ix} + k_{8cm}(1 + \frac{f_x}{k_{1fm}})}, \tag{4.2.5f}$$

$$\frac{df_{viii}}{dt} = -\frac{k_{9a}\, f_{ii}^a\, f_{viii}}{f_{viii} + k_{9am}(1 + \frac{f_i}{k_{6m}} + \frac{f_v}{k_{2am}} + \frac{f_{xi}}{k_{7am}})}, \tag{4.2.5g}$$

$$\frac{dc}{dt} = -k_{5a}\, c, \tag{4.2.5h}$$

$$\frac{dp}{dt} = -k_{1e}\, p\, f_x^a. \tag{4.2.5i}$$

The evolution for the activated factors is described by the following system of ODEs

$$\frac{dn}{dt} = G(t) - k_{11b}\, b_{x_a}^{n}\, n \tag{4.2.6a}$$

$$\frac{df_{x_a}}{dt} = \frac{k_{1f}\, n\, f_x}{f_x + k_{1fm}(1 + \frac{f_{ix}}{k_{8cm}})} + \frac{k_{1c}\, f_{ix}^a\, f_x}{f_x + k_{1cm}} + \frac{k_{1d}\, b_{viii_a}^{ix_a} f_x}{f_x + k_{1dm}} + \frac{k_{3c}\, c^a\, b_{v_a}^{x_a}}{b_{v_a}^{x_a} + k_{3cm}}$$
$$-k_{1b}\, f_x^a - k_{3a}\, f_x^a\, f_v^a - k_{1e}\, p\, f_x^a, \tag{4.2.6b}$$

$$\frac{df_v^a}{dt} = \frac{k_{2a}\, f_{ii}^a\, f_v}{f_v + k_{2am}(1 + \frac{f_i}{k_{6m}} + \frac{f_{xi}}{k_{7am}} + \frac{f_{viii}}{k_{9am}})} + \frac{k_{2b}\, f_x^a\, f_v}{f_v + k_{2bm}(1 + \frac{f_{ii}}{k_{4am}})} + k_{3b}\, b_{v_a}^{x_a}$$
$$-\frac{k_{2c}\, c^a\, f_v^a}{f_v^a + k_{2cm}} - k_{3a}\, f_x^a\, f_v^a, \tag{4.2.6c}$$

$$\frac{db_{v_a}^{x_a}}{dt} = k_{3a} f_x^a f_v^a - k_{3b} b_{v_a}^{x_a} - \frac{k_{3c} c^a b_{v_a}^{x_a}}{b_{v_a}^{x_a} + k_{3cm}}, \tag{4.2.6d}$$

$$\frac{df_{ii}^a}{dt} = \frac{k_{4a} f_x^a f_{ii}^a}{f_{ii}^a + k_{4am}(1 + \frac{f_v}{k_{2bm}})} + \frac{k_{4b} b_{v_a}^{x_a} f_{ii}}{f_{ii} + k_{4bm}} - k_{4c} f_{ii}^a, \tag{4.2.6e}$$

$$\frac{df_{xi}^a}{dt} = \frac{k_{7a} f_{ii}^a f_{xi}}{f_{xi} + k_{7am}(1 + \frac{f_i}{k_{6m}} + \frac{f_v}{k_{2am}} + \frac{f_{viii}}{k_{9am}})} - k_{7b} f_{xi}^a, \tag{4.2.6f}$$

$$\frac{df_{ix}^a}{dt} = \frac{k_{8a} f_{xi}^a f_{ix}}{f_{ix} + k_{8am}} + \frac{k_{8c} n f_{ix}}{f_{ix} + k_{8cm}(1 + \frac{f_x}{k_{1fm}})} + \frac{k_{10b} c^a b_{viii_a}^{ix_a}}{b_{viii_a}^{ix_a} + k_{10bm}} - k_{10a} f_{ix}^a f_{viii}^a$$
$$-k_{8b} f_{ix}^a, \tag{4.2.6g}$$

$$\frac{df_{viii}^a}{dt} = \frac{k_{9a} f_{ii}^a f_{viii}}{f_{viii} + k_{9am}(1 + \frac{f_i}{k_{6m}} + \frac{f_{xi}}{k_{7am}} + \frac{f_v}{k_{2am}})} + k_{10c} b_{viii_a}^{ix_a} - k_{10a} f_{ix}^a f_{viii}^a$$
$$-\frac{k_{9b} c^a f_{viii}^a}{f_{viii}^a + k_{9bm}}, \tag{4.2.6h}$$

$$\frac{db_{viii_a}^{ix_a}}{dt} = k_{10a} f_{ix}^a f_{viii}^a - \frac{k_{10b} c^a b_{viii_a}^{ix_a}}{b_{viii_a}^{ix_a} + k_{10bm}} - k_{10c} b_{viii_a}^{ix_a}, \tag{4.2.6i}$$

$$\frac{dc^a}{dt} = k_{5a} c - k_{5b} c^a. \tag{4.2.6j}$$

In 4.2.6a $G(t) = k_{11a} e^{-k_{11ax} t}$ represents the variable production of extrinsic tenase (this is discussed further in Section 4.2.3). The evolution of the complex Xa:TFPI, which, though an inactivated factor, participates in the above equations by forming a complex with the extrinsic tenase (n), is given by

$$\frac{db_{x_a}^p}{dt} = k_{1e} p f_x^a - k_{11b} b_{x_a}^p n. \tag{4.2.7a}$$

Finally, the downstream, inactivated factors and fibrin are goverened by the following ODEs:

$$\frac{db_n^{x_a p}}{dt} = k_{11b} b_{x_a}^p n, \tag{4.2.7b}$$

$$\frac{df_x^i}{dt} = k_{1b} f_x^a + k_{3b} b_{v_a}^{x_a}, \tag{4.2.7c}$$

$$\frac{df_v^i}{dt} = \frac{k_{2c} c^a f_v^a}{f_v^a + k_{2cm}} + \frac{k_{3c} c^a b_{v_a}^{x_a}}{b_{v_a}^{x_a} + k_{3cm}}, \tag{4.2.7d}$$

$$\frac{df_{ii}^i}{dt} = k_{4c} f_{ii}^a, \tag{4.2.7e}$$

$$\frac{df_i^a}{dt} = k_6 f_i, \tag{4.2.7f}$$

$$\frac{df_{ix}^i}{dt} = k_{8b} f_{ix}^a + k_{10c} b_{viii_a}^{ix_a}, \tag{4.2.7g}$$

$$\frac{df_{xi}^i}{dt} = k_{7b} f_{xi}^a, \tag{4.2.7h}$$

$$\frac{df_{viii}^i}{dt} = \frac{k_{9b} c^a f_{viii}^a}{f_{viii}^a + k_{9bm}} + \frac{k_{10b} c^a b_{viii_a}^{ix_a}}{b_{viii_a}^{ix_a} + k_{10bm}}, \tag{4.2.7i}$$

$$\frac{dc^i}{dt} = k_{5b} c^a. \tag{4.2.7j}$$

Estimates for the values for the dimensional parameters are taken from literature where possible (Table 4.4). The kinetic parameters for coagulation are generally well established, blood being a relatively easy biological system to test *in vitro*. While estimates are available for the majority of the parameters required, those involving the binding of the complex intrinsic tenase and the activity of protein C are less well defined and established estimates have been used.

Initial conditions are typical factor levels for human plasma (taken from Butenas *et al.* (1999)), it being assumed that no activated or inactivated factors are present at $t = 0$ with the levels of the procoagulants taken to be $f_{i0} = 8300$nM for fibrinogen, $f_{ii0} = 1400$nM for prothrombin, $f_{v0} = 21$nM for factor V, $f_{viii0} = 0.7$nM for factor VIII, $f_{ix0} = 90$nM for factor IX, $f_{x0} = 133$nM for factor X, $f_{xi0} = 25$nM for factor XI, $c_0 = 60$nM for protein C, and $p_0 = 2.5$nM for TFPI, i.e. we set

$$\begin{aligned}\text{at } t=0,\ & f_i = f_{i0},\ f_{ii} = f_{ii0},\ f_v = f_{v0},\ f_{viii} = f_{viii0},\ f_{ix} = f_{ix0},\ f_x = f_{x0},\ f_{xi} = f_{xi0},\\ & c = c_0,\ p = p_0,\ f_i^a = 0,\ f_{ii}^a = 0,\ f_{ii}^i = 0,\ f_v^a = 0,\ f_v^i = 0,\ f_{viii}^a = 0,\ f_{viii}^i = 0,\\ & f_{ix}^a = 0,\ f_{ix}^i = 0,\ f_x^a = 0,\ f_x^i = 0,\ f_{xi}^a = 0,\ f_{xi}^i = 0,\ b_{va}^{xa} = 0,\ b_{viiia}^{ixa} = 0,\ b_{xa}^{p} = 0,\\ & b_n^{x_a p} = 0,\ n_0 = 0,\ c^a = 0,\ c^i = 0.\end{aligned}$$

4.2.2 Nondimensionalisation

We nondimensionalise equations (4.2.5), (4.2.6), (4.2.7) in a manner similar to that in which we rescaled the model of thrombin generation in Chapter 3. Time is scaled in the same manner as in Chapter 3, with k_{4c}^{-1} so that $\tilde{t} = k_{4c}t$ denotes nondimensional time, (k_{4c}^{-1} is an intermediate timescale, representing the rate at which antithrombin III inhibits thrombin). The variables common to both models (see equations (4.2.6b), (4.2.7c), (4.2.5b), (4.2.6c), (4.2.7d), (4.2.6d), (4.2.5c), (4.2.6e), (4.2.7e), (4.2.5h), (4.2.6j), (4.2.7j), (4.2.5d), (4.2.7f)) are scaled as in Chapter 3 so that

$$f_x^a = \frac{k_{4c}}{k_{3a}}\tilde{f}_x^a, \qquad f_x^i = \frac{k_{4c}}{k_{3a}}\tilde{f}_x^i, \qquad f_v = k_{2bm}\tilde{f}_v, \qquad f_v^a = k_{2cm}\tilde{f}_v^a, \tag{4.2.8a}$$

$$f_v^i = k_{2cm}\tilde{f}_v^i, \qquad b_{v_a}^{x_a} = k_{3cm}\tilde{b}_{v_a}^{x_a}, \qquad f_{ii} = k_{4am}\tilde{f}_{ii}, \qquad f_{ii}^a = \frac{k_{2cm}k_{4c}}{k_{2a}}\tilde{f}_{ii}^a, \tag{4.2.8b}$$

$$f_{ii}^i = \frac{k_{2cm}k_{4c}}{k_{2am}}\tilde{f}_{ii}^i, \qquad c = \frac{k_{2cm}k_{4c}}{k_{2c}}\tilde{c}, \qquad c^a = \frac{k_{2cm}k_{4c}}{k_{2c}}\tilde{c}^a, \qquad c^i = \frac{k_{2cm}k_{4c}}{k_{2c}}\tilde{c}^i, \tag{4.2.8c}$$

$$f_i = k_{6m}\tilde{f}_i, \qquad f_i^a = k_{6m}\tilde{f}_i^a. \tag{4.2.8d}$$

The remaining variables (see equations (4.2.5f), (4.2.6g), (4.2.7g), (4.2.5g), (4.2.6h), (4.2.7i), (4.2.5e), (4.2.6f), (4.2.7h), (4.2.6a), (4.2.7a), (4.2.6i), (4.2.5i), (4.2.5a), (4.2.7b)) are scaled as follows to minimise the number of parameters in the dimensionless equations:

$$f_{ix} = k_{8cm}\tilde{f}_{ix}, \qquad f_{ix}^a = \frac{k_{8c}k_{1fm}}{k_{1f}}\tilde{f}_{ix}^a, \qquad f_{ix}^i = \frac{k_{8c}k_{1fm}}{k_{1f}}\tilde{f}_{ix}^i, \tag{4.2.9a}$$

$$f_{viii} = k_{9am}\tilde{f}_{viii}, \qquad f_{viii}^a = k_{9bm}\tilde{f}_{viii}^a, \qquad f_{viii}^i = k_{9bm}\tilde{f}_{viii}^i, \tag{4.2.9b}$$

$$f_{xi} = k_{7am}\tilde{f}_{xi}, \qquad f^a_{xi} = \frac{k_{7a}k_{2cm}}{k_{2a}}\tilde{f}^a_{xi}, \qquad f^i_{xi} = \frac{k_{7a}k_{2cm}}{k_{2a}}\tilde{f}^i_{xi}, \tag{4.2.9c}$$

$$n = \frac{k_{1fm}k_{4c}}{k_{1f}}\tilde{n}, \qquad b^n_{x_ap} = \frac{k_{1fm}k_{4c}}{k_{1f}}\tilde{b}^n_{x_ap}, \qquad b^{ix_a}_{viii_a} = k_{10bm}\tilde{b}^{ix_a}_{viii_a}, \tag{4.2.9d}$$

$$p = \frac{k_{4c}}{k_{1e}}\tilde{p}, \qquad f_x = k_{1fm}\tilde{f}_x, \qquad b^p_{x_a} = k_{1fm}\tilde{b}^p_{x_a}, \tag{4.2.9e}$$

where tildes denote dimensionless variables. The dimensionless parameter groupings common to the present model and that from Chapter 3 are:

$$\tilde{k}_{1b} = \frac{k_{1b}}{k_{4c}}, \qquad \tilde{k}_{2a} = \frac{k_{2cm}}{k_{2bm}}, \qquad \tilde{k}_{2am} = \frac{k_{2am}}{k_{2bm}}, \qquad \tilde{k}_{2b} = \frac{k_{2b}}{k_{3a}k_{2cm}}, \tag{4.2.10a}$$

$$\tilde{k}_{3a} = \frac{k_{3a}k_{2cm}}{k_{4c}}, \qquad \tilde{q}_{3a} = \frac{k_{2cm}}{k_{3cm}}, \qquad \tilde{k}_{3b} = \frac{k_{3b}}{k_{4c}}, \qquad \tilde{k}_{3c} = \frac{k_{3c}}{k_{2c}}, \tag{4.2.10b}$$

$$\tilde{k}_{4a} = \frac{k_{4a}k_{2a}}{k_{2cm}k_{3a}k_{4c}}, \qquad \tilde{q}_{4a} = \frac{k_{4a}}{k_{4am}k_{3a}}, \qquad \tilde{k}_{4b} = \frac{k_{4b}k_{3cm}}{k_{4am}k_{4c}}, \qquad \tilde{k}_{4bm} = \frac{k_{4bm}}{k_{4am}}, \tag{4.2.10c}$$

$$\tilde{k}_{5a} = \frac{k_{5a}}{k_{4c}}, \qquad \tilde{k}_{5b} = \frac{k_{5b}}{k_{4c}}, \qquad \tilde{k}_6 = \frac{k_6}{k_{4c}}. \tag{4.2.10d}$$

The dimensionless parameters introduced in this chapter are

$$\tilde{q}_{1c} = \frac{k_{1c}k_{8c}}{k_{1f}k_{4c}}, \qquad \tilde{k}_{1cm} = \frac{k_{1cm}}{k_{1fm}}, \qquad \tilde{k}_{1d} = \frac{k_{1d}k_{3a}k_{10bm}}{k_{4c}^2}, \qquad \tilde{k}_{1dm} = \frac{k_{1dm}}{k_{1fm}}, \tag{4.2.11a}$$

$$\tilde{k}_{1e} = \frac{k_{1e}}{k_{3a}}, \qquad \tilde{q}_{1e} = \frac{k_{1f}}{k_{4c}}, \qquad \tilde{k}_{1f} = \frac{k_{1fm}k_{3a}}{k_{4c}}, \qquad \tilde{k}_{7a} = \frac{k_{7a}k_{2cm}}{k_{7am}k_{2a}}, \tag{4.2.11b}$$

$$\tilde{k}_{7b} = \frac{k_{7b}}{k_{4c}}, \qquad \tilde{k}_{8a} = \frac{k_{8a}k_{7a}k_{2cm}}{k_{2a}k_{4c}k_{8cm}}, \qquad \tilde{k}_{8am} = \frac{k_{8am}}{k_{8cm}}, \qquad \tilde{k}_{8b} = \frac{k_{8b}}{k_{4c}}, \tag{4.2.11c}$$

$$\tilde{k}_{8c} = \frac{k_{8c}k_{1fm}}{k_{8cm}k_{1f}}, \qquad \tilde{k}_{9a} = \frac{k_{9a}k_{2cm}}{k_{9am}k_{2a}}, \qquad \tilde{q}_{9a} = \frac{k_{9a}k_{2cm}}{k_{9bm}k_{2a}}, \qquad \tilde{k}_{9b} = \frac{k_{9b}k_{2cm}}{k_{9bm}k_{2c}}, \tag{4.2.11d}$$

$$\tilde{k}_{10a} = \frac{k_{10a}k_{9bm}}{k_{4c}}, \qquad \tilde{q}_{10a} = \frac{k_{10a}k_{1fm}k_{8c}}{k_{4c}k_{1f}}, \qquad \tilde{k}_{10b} = \frac{k_{10b}k_{1f}k_{2cm}}{k_{1fm}k_{2c}k_{8c}}, \qquad \tilde{q}_{10b} = \frac{k_{10b}k_{2cm}}{k_{10bm}k_{2c}}, \tag{4.2.11e}$$

$$z_{10b} = \frac{k_{10b}k_{2cm}}{k_{9bm}k_{2c}}, \qquad \tilde{k}_{10c} = \frac{k_{10c}k_{10bm}}{k_{4c}k_{9bm}}, \qquad \tilde{q}_{10c} = \frac{k_{10c}}{k_{4c}}, \qquad z_{10c} = \frac{k_{10bm}k_{1f}}{k_{1fm}k_{8c}}, \tag{4.2.11f}$$

$$\tilde{k}_{11a} = \frac{k_{11a}k_{1f}}{k_{1fm}k_{4c}^2}, \qquad \tilde{k}_{11ax} = \frac{k_{11ax}}{k_{4c}}, \qquad \tilde{k}_{11b} = \frac{k_{11b}k_{1am}}{k_{4c}}. \tag{4.2.11g}$$

The equations representing the procoagulants (4.2.5) transform to give

$$\frac{df_x}{dt} = -\frac{n f_x}{f_x + (1 + f_{ix})} - \frac{q_{1c} f^a_{ix} f_x}{f_x + k_{1cm}} - \frac{k_{1d} b^{ix_a}_{viii_a} f_x}{k_{1f}(f_x + k_{1dm})}, \tag{4.2.12a}$$

$$\frac{df_v}{dt} = -\frac{k_{2a} f^a_{ii} f_v}{f_v + k_{2am}(1 + f_i + f_{xi} + f_{viii})} - \frac{k_{2a}k_{2b} f^a_x f_v}{1 + f_v + f_{ii}}, \tag{4.2.12b}$$

$$\frac{df_{ii}}{dt} = -\frac{q_{4a} f^a_x f_{ii}}{1 + f_v + f_{ii}} - \frac{q_{4b} b^{x_a}_{v_a} f_{ii}}{f_{ii} + k_{4bm}}, \tag{4.2.12c}$$

$$\frac{df_i}{dt} = -k_6 f_i, \tag{4.2.12d}$$

$$\frac{df_{xi}}{dt} = -\frac{k_{7a} f^a_{ii} f_{xi}}{f_{xi} + (1 + f_i + f_v + f_{viii})}, \tag{4.2.12e}$$

(4.2.12f)

Param.	Description	Value	References	Source
k_{1b}	Xa+ATIII $\rightarrow$ Xa:ATIII	0.347 nM^{-1} min^{-1}	Anand *et al.* (2008)	Wiebe *et al.* (2003)
k_{1c}	X $\xrightarrow{IXa}$ Xa	$k_{cat} = 0.04$ min^{-1}, $k_m = 2000$ nM	Kogan *et al.* (2001)	Rawala-Sheikh *et al.* (1990) and Hultin (1982)
k_{1d}	X $\xrightarrow{VIIIa:IXa}$ Xa	$k_{cat} = 2391$ min^{-1}, $k_m = 160$ nM	Anand *et al.* (2008)	Rawala-Sheikh *et al.* (1990)
		$k_{cat} = 1740$ min^{-1}, $k_m = 190$ nM *	Kogan *et al.* (2001)	Rawala-Sheikh *et al.* (1990)
k_{1e}	Xa+TFPI $\rightarrow$ Xa:TFPI	0.48 nM^{-1} min^{-1}	Anand *et al.* (2008)	Huang *et al.* (1993), and Jesty *et al.* (1994)
		1×10^6 nM^{-1} min^{-1}	Khanin *et al.* (1998)	Jesty *et al.* (1994)
k_{1f}	X $\xrightarrow{TF:VIIa}$ Xa	$k_{cat} = 103$ min^{-1}, $k_m = 380$ nM	Khanin *et al.* (1998)	Komiyama *et al.* (1990)
		$k_{cat} = 103$ min^{-1}, $k_m = 240$ nM *	Anand *et al.* (2008)	Komiyama *et al.* (1990)
k_{2a}	V $\xrightarrow{IIa}$ Va	$k_{cat} = 27$ min^{-1}, $k_m = 140.5$ nM *	Anand *et al.* (2008)	Monkovic & Tracy (1990)
		$k_{cat} = 27$ min^{-1}, $k_m = 141$ nM	Khanin *et al.* (1998)	Monkovic & Tracy (1990)
		$k_{cat} = 14$ min^{-1}, $k_m = 72$ nM	Kogan *et al.* (2001)	Monkovic & Tracy (1990)
		$k_{cat} = 14$ min^{-1}, $k_m = 72$ nM	Willems *et al.* (1991)	Monkovic & Tracy (1990)
k_{2b}	V $\xrightarrow{Xa}$ Va	$k_{cat} = 2.6$ min^{-1}, $k_m = 10.4$ nM	Kogan *et al.* (2001), Willems *et al.* (1991)	Monkovic & Tracy (1990)
k_{2c}	Va $\xrightarrow{APC}$ VaInactive	$k_{cat} = 10.2$ min^{-1}, $k_m = 14.6$ nM *	Anand *et al.* (2008)	Solymoss *et al.* (1988)
		$k_{cat} = 24$ min^{-1}, $k_m = 20$ nM	Willems *et al.* (1991)	Solymoss *et al.* (1988)
k_{3a}	Va+Xa $\leftrightarrow$ Va:Xa	0.1 nM^{-1} min^{-1} *	Anand *et al.* (2008)	Mann (1987)
		10 nM^{-1} min^{-1}	Willems *et al.* (1991)	Giesen *et al.* (1991)

Continued on next page

Table 4.4: Summary of parameters and their corresponding reactions, values and sources. Parameter values used in previous mathematical models are indicated (references) with the relevant biological sources (sources). * indicates value used in numerical simulations. Where values are available from multiple sources we have tried to take a consistent approach, following Anand *et al.* (2008). We have not included references to models that use second-order kinetics (such as (Kramoroff & Nigretto, 2001; Bungay *et al.*, 2003)) in place of Michaelis-Menten kinetics for enzyme reactions.

Param.	Description	Value	References	Source
k_{3b}	VaXa+ATIII $\rightarrow$ Va+Xa:ATIII	0.05 min^{-1}	Willems *et al.* (1991)	Schoen *et al.* (1989)
k_{3c}	VaXa $\xrightarrow{APC}$ VaInactive+Xa	$k_{cat} = 24$ min^{-1}, $k_m = 20$ nM	Willems *et al.* (1991)	Solymoss *et al.* (1988)
k_{4a}	II $\xrightarrow{Xa}$ IIa	$k_{cat} = 2.25$ min^{-1}, $k_m = 58$ nM	Kogan *et al.* (2001), Willems *et al.* (1991)	Rosing *et al.* (1980)
k_{4b}	II $\xrightarrow{Va:Xa}$ IIa	$k_{cat} = 1344$ min^{-1}, $k_m = 1060$nM *	Anand *et al.* (2008)	Krishnaswamy *et al.* (1987)
		$k_{cat} = 1700$ min^{-1}, $k_m = 1000$ nM	Khanin *et al.* (1998)	Krishnaswamy *et al.* (1987), and Tracy *et al.* (1985)
		$k_{cat} = 2000$ min^{-1}, $k_m = 210$ nM	Willems *et al.* (1991)	Rosing *et al.* (1980)
k_{4c}	IIa+ATIII $\rightarrow$ IIa:ATIII	1.3 min^{-1}	Willems *et al.* (1991)	
k_{5a}	C $\rightarrow$ APC	0.0014 min^{-1}	Willems *et al.* (1991)	——
k_{5b}	APC $\rightarrow$ APCInactive	0.35 min^{-1}	Willems *et al.* (1991),	——
		0.34 min^{-1}	Qiao *et al.* (2004)	Rezaie & Esmon (1993)
k_6	Fibrinogen $\xrightarrow{IIa}$ Fibrin	$k_{cat} = 3540$ min^{-1}, $k_m = 3160$ nM *	Anand *et al.* (2008)	Tsiang *et al.* (1996)
		$k_{cat} = 5040$ min^{-1}, $k_m = 7200$ 2M	Kogan *et al.* (2001)	Higgins *et al.* (1983)
		k_{cat} not listed, $k_m = 2000$ nM	Willems *et al.* (1991)	Smith (1984)
k_{7a}	XI $\xrightarrow{IIa}$ XIa	$k_{cat} = 0.0078$ min^{-1}, $k_m = 50$ nM	Anand *et al.* (2008)	Gailani & Broze (1991)
k_{7b}	XIa+ATIII $\rightarrow$ XIa:ATIII	1.6×10^{-3} nM^{-1} min^{-1}	Anand *et al.* (2008)	Soons *et al.* (1987)
k_{8a}	IX $\xrightarrow{XIa}$ IXa	$k_{cat} = 11$ min^{-1}, $k_m = 160$ nM *	Anand *et al.* (2008)	Sun & Gailani (1996)
		$k_{cat} = 225$$min^{-1}$, $k_m = 350$ nM	Kogan *et al.* (2001)	Walsh *et al.* (1984),
				Sinha *et al.* (1987),

Continued on next page

Table 4.4: Summary of parameters and their corresponding reactions, values and sources. Parameter values used in previous mathematical models are indicated (references) with the relevant biological sources (sources). * indicates value used in numerical simulations. Where values are available from multiple sources we have tried to take a consistent approach, following Anand *et al.* (2008). We have not included references to models that use second-order kinetics (such as (Kramoroff & Nigretto, 2001; Bungay *et al.*, 2003)) in place of Michaelis-Menten kinetics for enzyme reactions.

Param.	Description	Value	References	Source
				and Warn-Cramer & Bajaj (1986)
k_{8b}	IXa+ATIII $\rightarrow$ IXa:ATIII	0.0162 nM^{-1}	Anand *et al.* (2008)	Wiebe *et al.* (2003)
k_{8c}	IX $\xrightarrow{\text{VIIa:TF}}$ IXa	$k_{cat} = 32.4\ min^{-1}$, $k_m = 24$ nM	Anand *et al.* (2008)	Komiyama *et al.* (1990)
k_{9a}	VIII $\xrightarrow{\text{IIa}}$ VIIIa	$k_{cat} = 194.4\ min^{-1}$, $k_m = 112000$ nM	Anand *et al.* (2008)	De Cristofaro *et al.* (2003)
k_{9b}	VIIIa $\xrightarrow{\text{APC}}$ VIIIaInactive	$k_{cat} = 10.2\ min^{-1}$, $k_m = 14.6$ nM	Anand *et al.* (2008)	Due to lack of data, assumed to be the same as k_{2c}.
k_{10a}	VIIIa+IXa $\leftrightarrow$ VIIIa:IXa	1 $nM^{-1}min^{-1}$ 10 $nM^{-1}min^{-1}$	Khanin *et al.* (1998) Kogan *et al.* (2001)	—— ——
k_{10b}	VIIIa:IXa $\xrightarrow{\text{APC}}$ VIIIaInactive+IXa	$k_{cat} = 10.2\ min^{-1}$, $k_m = 14.6$ nM		Due to lack of data, assumed to be the same as (k_{9b})
k_{10c}	VIIIa:IXa+ATIII $\rightarrow$ VIIIa+IXa:ATIII	0.0162 nM^{-1}		Due to lack of data, assumed to be the same as (k_{8b})
k_{11a}	$f(t) = k11a\, e^{-k11ax\,t}$	3×10^{-5} nM min^{-1}	fitted to experimental data	
k_{11ax}	$f(t) = k11a\, e^{-k11ax\,t}$	0.2	fitted to experimental data	
k_{11b}	VIIa:TF + Xa:TFPI	0.64 nM^{-1} min^{-1}	Khanin *et al.* (1998)	Jesty *et al.* (1994)

Table 4.4: Summary of parameters and their corresponding reactions, values and sources. Parameter values used in previous mathematical models are indicated (references) with the relevant biological sources (sources). * indicates value used in numerical simulations. Where values are available from multiple sources we have tried to take a consistent approach, following Anand *et al.* (2008). We have not included references to models that use second-order kinetics (such as (Kramoroff & Nigretto, 2001; Bungay *et al.*, 2003)) in place of Michaelis-Menten kinetics for enzyme reactions.

$$\frac{df_{ix}}{dt} = -\frac{k_{8a} f_{xi}^a f_{ix}}{f_{ix} + k_{8am}} - \frac{k_{8c} n f_{ix}}{f_{ix} + 1 + f_x}, \tag{4.2.12g}$$

$$\frac{df_{viii}}{dt} = -\frac{k_{9a} f_{ii}^a f_{viii}}{f_{viii} + (1 + f_i + f_v + f_{xi})}, \tag{4.2.12h}$$

$$\frac{dc}{dt} = -k_{5a} c, \tag{4.2.12i}$$

$$\frac{dp}{dt} = -k_{1e} p f_x^a. \tag{4.2.12j}$$

The equations for the activated factors (4.2.6) transforming to give

$$\frac{dn}{dt} = k_{11a} e^{-k_{11ax} t} - k_{11b} b_{x_a p}^n n \tag{4.2.13a}$$

$$\frac{df_x^a}{dt} = \frac{k_{1f} n f_x}{f_x + (1 + f_{ix})} + \frac{q_{1c} k_{1f} f_{ix}^a f_x}{f_x + k_{1cm}} + \frac{k_{1d} b_{viii_a}^{ix_a} f_x}{f_x + k_{1dm}} + \frac{k_{3c} k_{3a} c^a b_{v_a}^{x_a}}{b_{v_a}^{x_a} + 1}$$
$$- k_{1b} f_x^a - k_{3a} f_x^a f_v^a - p f_x^a, \tag{4.2.13b}$$

$$\frac{df_v^a}{dt} = \frac{f_{ii}^a f_v}{f_v + k_{2am}(1 + f_i + f_{xi} + f_{viii})} + \frac{k_{2b} f_{ii}^a f_v}{f_v + 1 + f_{ii}} + \frac{k_{3b}}{q_{3a}} b_{v_a}^{x_a}$$
$$- \frac{c^a f_v^a}{f_v^a + 1} - f_x^a f_v^a, \tag{4.2.13c}$$

$$\frac{db_{v_a}^{x_a}}{dt} = q_{3a} f_x^a f_v^a - q_{3a} k_{3b} b_{v_a}^{x_a} - \frac{k_{3c} q_{3a} c^a b_{v_a}^{x_a}}{b_{v_a}^{x_a} + 1}, \tag{4.2.13d}$$

$$\frac{df_{ii}^a}{dt} = \frac{k_{4a} f_x^a f_{ii}}{f_{ii} + 1 + f_v} + \frac{k_{4a} k_{4b} b_{v_a}^{x_a} f_{ii}}{q_{4a}(f_{ii} + k_{4bm})} - f_{ii}^a, \tag{4.2.13e}$$

$$\frac{df_{xi}^a}{dt} = \frac{f_{ii}^a f_{xi}}{f_{xi} + (1 + f_i + f_v + f_{viii})} - k_{7b} f_{xi}^a, \tag{4.2.13f}$$

$$\frac{df_{ix}^a}{dt} = \frac{k_{8a} f_{xi}^a f_{ix}}{k_{8c}(f_{ix} + k_{8am})} + \frac{n f_{ix}}{f_{ix} + (1 + f_x)} + \frac{k_{10b} c^a b_{viii_a}^{ix_a}}{b_{viii_a}^{ix_a} + 1} - k_{10a} f_{ix}^a f_{viii}^a \tag{4.2.13g}$$
$$- k_{8b} f_{ix}^a, \tag{4.2.13h}$$

$$\frac{df_{viii}^a}{dt} = \frac{q_{9a} f_{ii}^a f_{viii}}{f_{viii} + 1 + f_i + f_{xi} + f_v} + k_{10c} b_{viii_a}^{ix_a} - q_{10a} f_{ix}^a f_{viii}^a$$
$$- \frac{k_{9b} c^a f_{viii}^a}{f_{viii}^a + 1}, \tag{4.2.13i}$$

$$\frac{db_{viii_a}^{ix_a}}{dt} = \frac{k_{10a}}{z_{10c}} f_{ix}^a f_{viii}^a - \frac{q_{10b} c^a b_{viii_a}^{ix_a}}{b_{viii_a}^{ix_a} + 1} - q_{10c} b_{viii_a}^{ix_a}, \tag{4.2.13j}$$

$$\frac{dc^a}{dt} = k_{5a} c - k_{5b} c_a, \tag{4.2.13k}$$

and those equations for the downstream, inactivated factors and fibrin (4.2.7) transform to give

$$\frac{db_{x_a}^p}{dt} = \frac{q_{1e}}{k_{1f}} p f_x^a - \frac{k_{11b}}{q_{1e}} b_{x_a}^p n, \tag{4.2.14a}$$

$$\frac{db_{x_a p}^n}{dt} = k_{11b} b_{x_a}^p n, \tag{4.2.14b}$$

$$\frac{df_x^i}{dt} = k_{1b} f_x^a + \frac{k_{3a} k_{3b}}{q_{3a}} b_{v_a}^{x_a}, \tag{4.2.14c}$$

$$\frac{df_v^i}{dt} = \frac{c^a f_v^a}{f_v^a + 1} + \frac{k_{3c} c^a b_{v_a}^{x_a}}{b_{v_a}^{x_a} + 1}, \tag{4.2.14d}$$

$$\frac{df_{ii}^i}{dt} = f_{ii}^a, \tag{4.2.14e}$$

$$\frac{df_i^a}{dt} = k_6 f_i, \tag{4.2.14f}$$

$$\frac{dc^i}{dt} = k_{5b} c^a. \tag{4.2.14g}$$

$$\frac{df_{ix}^i}{dt} = k_{8b} f_{ix}^a + z_{10c} b_{viii_a}^{ix_a}, \tag{4.2.14h}$$

$$\frac{df_{xi}^i}{dt} = k_{7b} f_{xi}^a, \tag{4.2.14i}$$

$$\frac{df_{viii}^i}{dt} = \frac{k_{9b} c^a f_{viii}^a}{f_{viii}^a + 1} + \frac{z_{10b} c^a b_{viii_a}^{ix_a}}{b_{viii_a}^{ix_a} + 1}. \tag{4.2.14j}$$

The dimensionless initial conditions are listed in Table 4.3. Our model comprises twenty-nine ordinary differential equations and has forty-two nondimensional parameters (see Table ??).

4.2.3 System activation

We assume that the concentrations of the procoagulants and regulatory proteins are initially equal to those in human plasma (Table 4.3). This is a static environment with no replenishment of factors as would occur by convection *in vivo*. The experimental system (Kravtsov *et al.*, 2009) is activated (at $t = 0$) by the addition of TF. Our model does not include a separate species for TF and is instead assumed to be activated by the VIIa:TF complex. Orfeo *et al.* (2005) provide data profiles of VIIa:TF expression in response to TF activation (see Figure 4.3). We mimic this data by adjusting the parameters of the function $G(t) = k_{11a} e^{-k_{11ax} t}$ to provide a similar profile of VIIa:TF expression to that provided by Orfeo *et al.* (2005) (see Figure 1 (B)). Obtaining a profile of extrinsic tenase in response to activation by TF 5 pM requires $k_{11a} = 3 \times 10^{-5}$ nM min^{-1}, $k_{11ax} = 0.2$. This approach to activating the coagulation cascade follows Anand *et al.* (2008) who estimate initial conditions for their model of the formation and lysis of blood clots by matching profiles of VIIa:TF to data provided by Orfeo *et al.* (2005) for the expression of extrinsic tenase.

4.3 Numerical solution

We proceed by first numerically solving two subsystems of the full model: this enables us to investigate the contribution of each pathway to the full model. Subsystem one comprises the extrinsic and common pathway. This subsystem is obtained by assuming that the concentrations of the procoagulants of the intrinsic pathway are initially set to zero ($XI = 0$, $IX = 0$, and $VIII = 0$; see pink and blue boxes in Figure 4.2), so that the effects of reactions associated with the intrinsic pathway can be neglected. We discuss this subsystem in Section 4.3.1 and the second subsystem in Section 4.3.2 . The second subsystem comprises the extrinsic, common

Nondim. param.	Nondim. value	Nondim. param.	Nondim. value
k_{1b}	0.267	k_6	2.723×10^3
q_{1c}	0.010	k_{7a}	8.436×10^{-5}
k_{1cm}	8.333	k_{7b}	0.001
k_{1d}	2.066×10^3	k_{8a}	0.001
k_{1dm}	0.667	k_{8am}	6.667
k_{1e}	4.8	k_{8b}	0.0125
q_{1e}	73.23	k_{8c}	3.146
k_{1f}	18.462	k_{9a}	9.386×10^{-4}
k_{2a}	1.404	q_{9a}	7.2
k_{2am}	13.510	k_{9b}	1.000
k_{2b}	1.781	k_{10a}	11.231
k_{3a}	1.123	q_{10a}	58.073
q_{3a}	0.730	k_{10b}	0.193
k_{3b}	0.053	q_{10b}	1
k_{3c}	2.353	z_{10b}	1.431
k_{4a}	32.007	k_{10c}	0.0125
q_{4a}	0.388	q_{10c}	0.0125
k_{4b}	3.565	z_{10c}	0.193
k_{4bm}	18.276	k_{11a}	7.618×10^{-6}
k_{5a}	0.001	k_{11ax}	0.154
k_{5b}	0.269	k_{11b}	1.182

Table 4.5: Dimensionless parameters and values. The dimensionless groups are described in equations (4.2.10), (4.2.11).

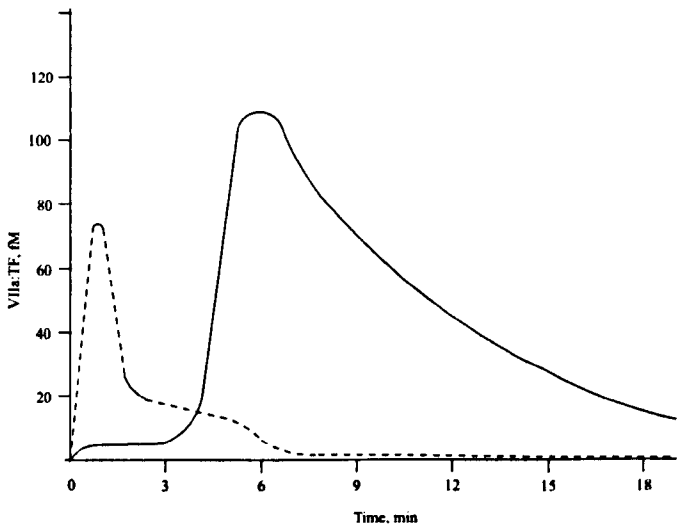

Figure 4.3: The evolution of the concentration of extrinsic tenase (VIIa:TF) in plasma in response to activation by 5 pM TF (VIIa:TF derived from endogenous VIIa (broken line); VIIa:TF derived from VIIa activated during coagulation (solid line)): data from Orfeo *et al.* (2005).

and intrinsic pathway, neglecting thrombin activation of factor XI (see pink, blue and magenta boxes on Figure 4.2). We obtain this subsystem by setting the initial condition of the procoagulant XI to zero. The initial conditions for all other variables are taken from Table 4.3. We solve the full model and discuss the implications of including thrombin activation of factor XI in Section 4.3.3.1. Throughout this chapter, simulations are computed in Matlab using a stiff solver (ode15s) with parameter values that, as described in Table 4.3 occur over many orders of magnitude. Numerical results showed no significant changes to variations in tolerance and step size. Simulation results are obtained by solving the nondimensional model (equations (4.2.12), (4.2.13), (4.2.14)) but presented in dimensional form to facilitate comparison with experimental data. A summary of the figures presented (and the simulations they demonstrate) is provided in Appendix B.

4.3.1 The extrinsic pathway

Simulations of the reactions of the extrinsic and common pathway are obtained (Figure 4.4) by numerically solving equations (4.2.12), (4.2.13), (4.2.14) using parameter values from Table 4.4 and initial conditions from Table 4.3, except for factors XI, IX, and $VIII$ of the intrinsic pathways which we set to zero so that $f_{xi} = f^a_{xi} = f^i_{xi} = f_{ix} = f^a_{ix} = f^i_{ix} = f_{viii} = f^a_{viii} = f^i_{viii} = b^{ix}_{viii} = 0$ for all t. The resulting set of equations is similar to the model presented in Chapter 3. However, it includes the extrinsic tenase, its activation of factor X, and inhibition of factor Xa by TFPI which subsequently inactivates the extrinsic tenase. Early mathematical models (Willems *et al.*, 1991; Khanin & Semenov, 1989)) excluded the intrinsic pathway believing that the extrinsic and intrinsic pathways were not linked and so activation by tissue factor did not involve the reactions of the intrinsic pathway. In seminal work (Osterud & Rapaport, 1977) demonstrated that the two pathways are linked through activation of factor IX via the extrinsic tenase (Colman *et al.*, 2000) and later mathematical models take this into account

(Jones & Mann, 1994; Khanin *et al.*, 1998). We exclude the intrinsic pathway to help us evaluate the contribution of this pathway to coagulation.

In Figure 4.4 (A) we present a time-dependent solution for the concentration of the TF:VIIa complex. The production of factor Xa in response to TF:VIIa activation is shown in Figure 4.4 (C). The second peak in factor Xa production can be explained by the action of protein C on the prothrombinase complex. When protein C interacts with prothrombinase, factor Xa is released from the complex and inactivates factor Va by degradation. Our understanding of this is enhanced by the asymptotic analysis provided in Chapter 3. At timescale 5 we found a bifurcation where with sufficiently low levels of factor Xa activation two peaks in factor Xa concentration occur. ATIII and TFPI form complexes Xa:ATIII and Xa:TFPI respectively (Figure 4.4 (D)) when they come into contact with factor Xa. The binary complexes Xa:TFPI and extrinsic tenase (Figure 4.4 (B)) can combine to form VIIa:TF:Xa:TFPI and, in this form, factor Xa participates in its own inhibition (see Figure 4.5). Factor Va is generated via a feedback loop involving thrombin (see Figure 4.4 (C)) and participates in the formation of prothrombinase (Figure 4.4 (C)). As in Chapter 3, it is the feedback from thrombin to factor V and the subsequent formation complex prothrombinase which is responsible for the burst in thrombin concentration that occurs after approximately 25 minutes (see Figure 4.4 (C)).

The prothrombin time (PT) is traditionally used to assess clinical problems with factors within the extrinsic and common pathways. The test is activated with very high tissue factor concentrations (greater than 200 nM) which subsequently overwhelm the TFPI anticoagulant mechanism and convert all prothrombin to thrombin within 15 seconds (Baglin, 2005). For thrombin generation to be sensitive to all procoagulant concentrations within the extrinsic and intrinsic pathway much lower levels of initiation (at least $4-5$ orders of magnitude) are thought to be needed (Baglin, 2005). The thrombin generation assay that we simulate is activated with low levels of tissue factor, 5 pM or less, a decrease in tissue factor concentration of 6 orders of magnitude. While we cannot exactly replicate activation of the model by 200 nM TF (as we have no data for extrinsic tenase formation in response to this level of activation) we can show that at high levels of activation ($k_{11a} = 300\,\text{nM}^{-1}\,\text{min}^{-1}$) all prothrombin is converted to thrombin in less than 30 seconds (see Figure 4.6 (B)). Panel (A) in Figure 4.6 demonstrates that much lower levels of activation are required for incomplete conversion of the procoagulant prothrombin to thrombin ($k_{11a} < 0.003\,\text{nM}^{-1}\,\text{min}^{-1}$).

4.3.2 The full cascade – without factor XI activation

We now explore the contribution of the intrinsic pathway to thrombin formation. In the full coagulation cascade, factor X activation occurs via two pathways: the extrinsic tenase and the intrinsic tenase. Thus the intrinsic tenase can contribute to a higher level of factor Xa. The intrinsic tenase is composed of factors IXa and VIIIa, factor IX is activated via extrinsic tenase and factor VIII is activated via feedback from thrombin; once both factors have been activated the complex can form. Congenital deficiencies in components of the intrinsic tenase lead to severe bleeding disorders such as haemophilias A (factor VIII deficiency - see Figure 4.10 for

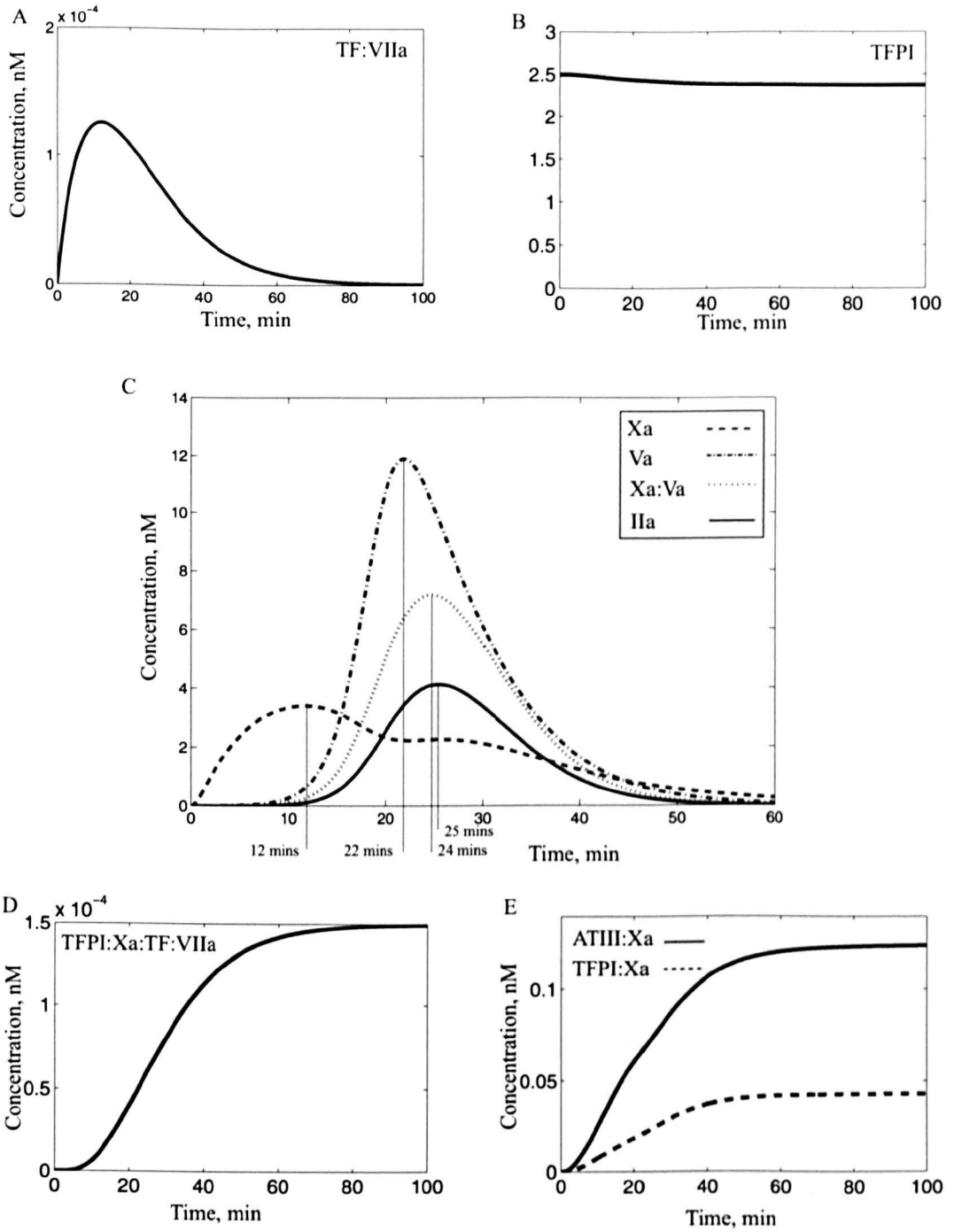

Figure 4.4: Time-dependent solutions of subsystem one obtained by solving equations (4.2.12), (4.2.13), (4.2.14) and neglecting factors associated with the intrinsic pathway. Parameters are taken from Table 4.4 and initial conditions from Table 4.3, except that the initial concentrations of the procoagulants of the intrinsic pathway are set to zero ($XII = 0$, $XI = 0$, and $VIII = 0$). Factor Xa which is activated by the extrinsic tenase (D) reaches its peak concentration after 12 minutes. Factor Xa can activate thrombin which in turn activates factor Va, whose levels then peak after 22 minutes. Factors Va and Xa form prothrombinase (peak formation 24 minutes) which promotes thrombin formation which peaks at a level of 4 nM after 25 minutes. The profiles of Factor Xa and prothrombinase have been multiplied by 10^3.

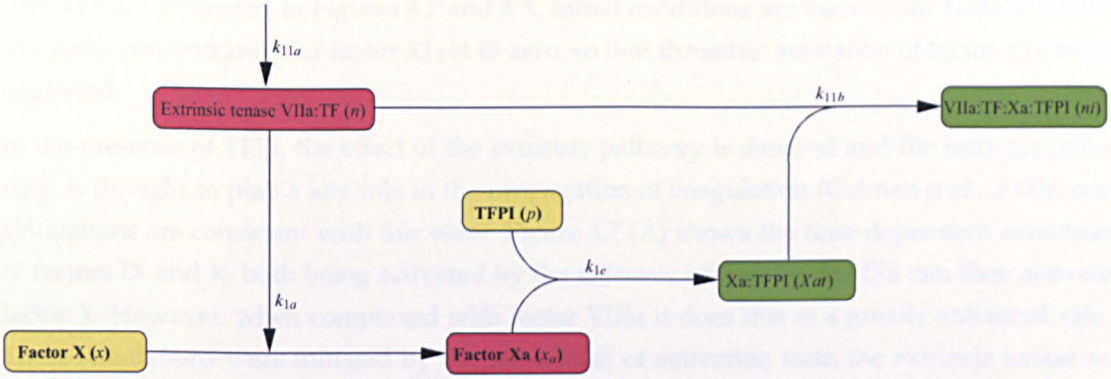

Figure 4.5: Network diagram illustrating how factor Xa participates in its own inhibition by the formation of the inactive complexes Xa:TFPI and VIIa:TF:Xa:TFPI. The complex VIIa:TF:Xa:TFPI sequesters the extrinsic tenase (VIIa:TF) and hence reduces levels of the active form that are available to activate factor X.

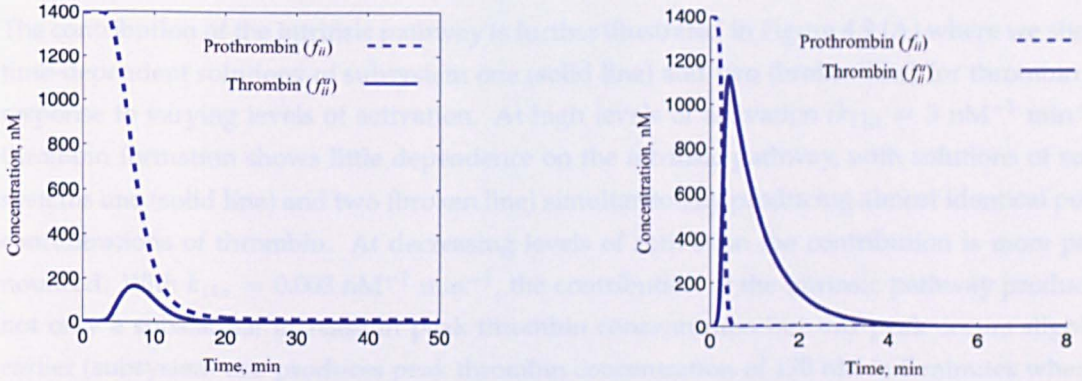

Figure 4.6: Time-dependent solutions of subsystem one demonstrating that high levels of activation result in complete prothrombin conversion to thrombin (B) whereas at lower levels of activation incomplete conversion is acheived (A). Numerical simulations of equations (4.2.12), (4.2.13), (4.2.14) neglecting factors of the intrinsic pathway. Initial conditions from Table 4.3, except that the initial concentrations of the procoagulants of the intrinsic pathway are set to zero ($XII = 0$, $XI = 0$, and $VIII = 0$). Parameters are taken from Table 4.4 except simulations (A) use $k_{11a} = 0.003\ \text{nM}^{-1}\ \text{min}^{-1}$ and (B) $k_{11a} = 300\ \text{nM}^{-1}\ \text{min}^{-1}$.

simulations) and B (factor IX deficiency - see Figure 4.10 for simulations); these results highlight the importance of this complex for generating sufficient levels of coagulation for haemostasis. Typical simulations of the full model (equations (4.2.12), (4.2.13), (4.2.14)) including the intrinsic pathway are presented in Figures 4.7 and 4.8. Initial conditions are taken from Table 4.3, with the initial concentration for factor XI set to zero, so that thrombin activation of factor XI can be neglected.

In the presence of TFPI, the effect of the extrinsic pathway is damped and the intrinsic pathway is thought to play a key role in the propagation of coagulation (Colman *et al.*, 2000): our simulations are consistent with this view. Figure 4.7 (A) shows the time-dependent evolution of factors IX and X, both being activated by the extrinsic tenase. Factor IXa can then activate factor X. However, when complexed with factor VIIIa it does this at a greatly enhanced rate. These simulations were initiated by the same level of activation from the extrinsic tenase as the simulations in the previous section (Figure 4.4) and the marked ten-fold increase which we see in peak factor Xa concentration, when compared to simulations of subsystem one, where factor X was activated solely by extrinsic tenase, can be accounted for by the contribution of the intrinsic tenase to activation of factor X. Simulations of factor Xa are no longer bimodal (as they were in subsystem one) with a higher level of activation being provided via the intrinsic tenase. Factor VIII is activated by thrombin and Figure 4.8 (B) shows the evolution of this and the subsequent formation of the VIIIa:IXa complex (intrinsic tenase). The evolution of factors V and Va and the subsequent formation of prothrombinase (Va:Xa) is shown in Figure 4.8 (A). Figure 4.7 (B) shows the time-dependent evolution of thrombin, which reaches a peak concentration of 520 nM in approximately 24 minutes. We conclude that, at this level of activation, the intrinsic pathway makes a significant contribution to peak thrombin formation.

The contribution of the intrinsic pathway is further illustrated in Figure 4.9 (A) where we show time-dependent solutions of subsystem one (solid line) and two (broken line) for thrombin in response to varying levels of activation. At high levels of activation ($k_{11a} = 3$ nM^{-1} min^{-1}) thrombin formation shows little dependence on the intrinsic pathway, with solutions of subsystems one (solid line) and two (broken line) simultaneously producing almost identical peak concentrations of thrombin. At decreasing levels of activation the contribution is more pronounced. With $k_{11a} = 0.003$ nM^{-1} min^{-1}, the contribution of the intrinsic pathway produces not only a substantial increase in peak thrombin concentration but this peak occurs slightly earlier (subsystem one produces peak thrombin concentration of 170 nM in 7 minutes wheras subsystem two produces 760 nM in 6.5 minutes). In Figure 4.9 we show how peak thrombin concentrations (B) and time to reach peak (C) vary as a function of the level of activation (k_{11a}). Solutions of subsystem one and two make it clear that the take-home message is that at low levels of activation peak thrombin concentration is significantly enhanced by the inclusion of the intrinsic pathway and their the time to reach this peak being reduced slightly.

Investigators report that plasma from individuals with either haemophilia A or B is unable to generate intrinsic tenase and, will lead to a slight prolongation of the time to clot but a major impairment in peak thrombin generation (Mann *et al.*, 2003). Below, we use our model to simulate haemophilia A and B to determine whether our model can reproduce these results.

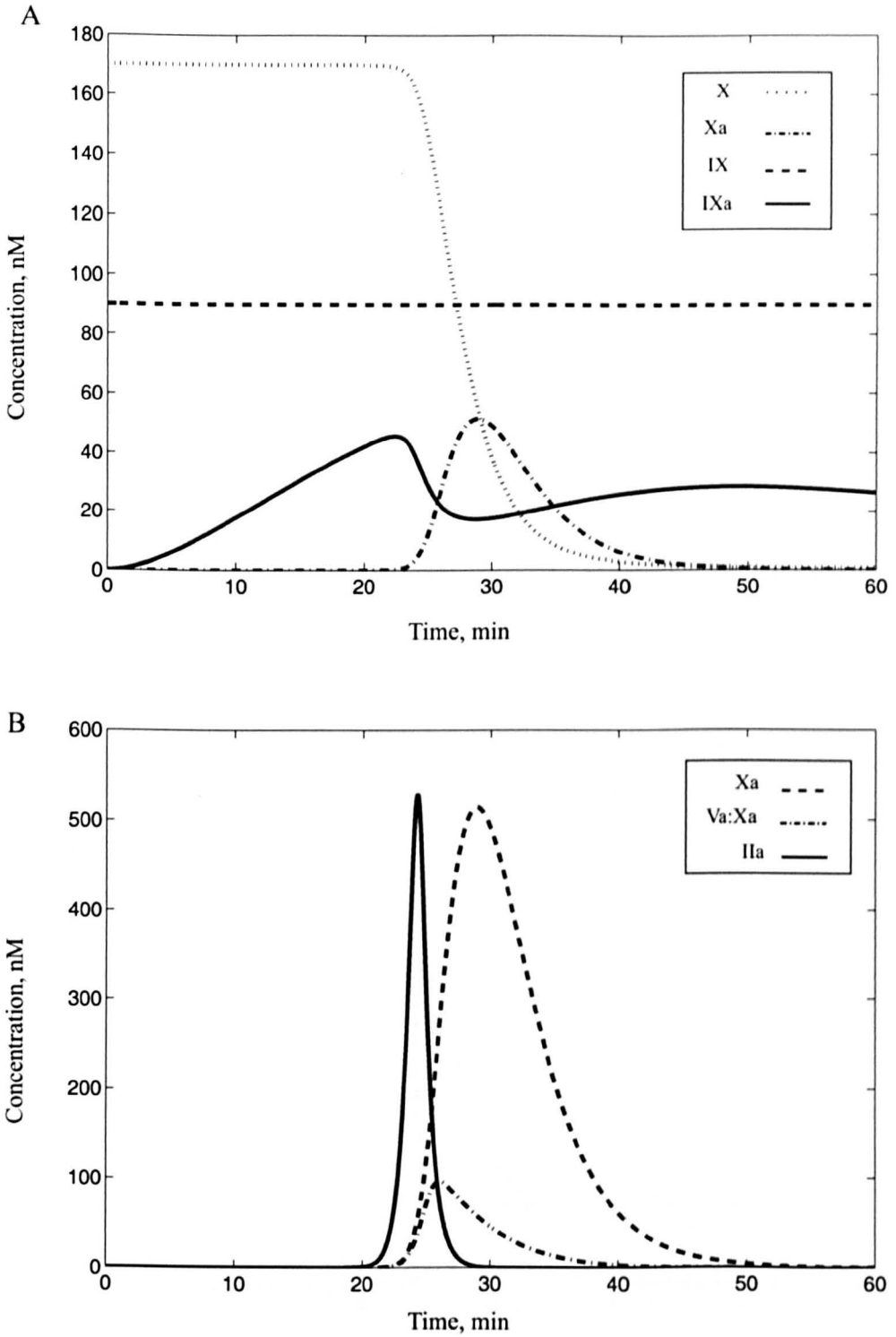

Figure 4.7: Time-dependent solutions of the coagulation cascade (equations (4.2.12), (4.2.13), (4.2.14)) when thrombin activation of factor XI is neglected. Parameters are taken from Table 4.4 and initial conditions from Table 4.3, except that the initial concentration of the procoagulant factor XI is set to zero. (A) shows the evolution of factors X, Xa, IX nd IXa, which are activated via the extrinsic tenase. (B) shows the evolution of factor Xa, the prothrombinase complex and thrombin, the two former activating the later. Same simulations as Figure 4.8 which provides additional variables.

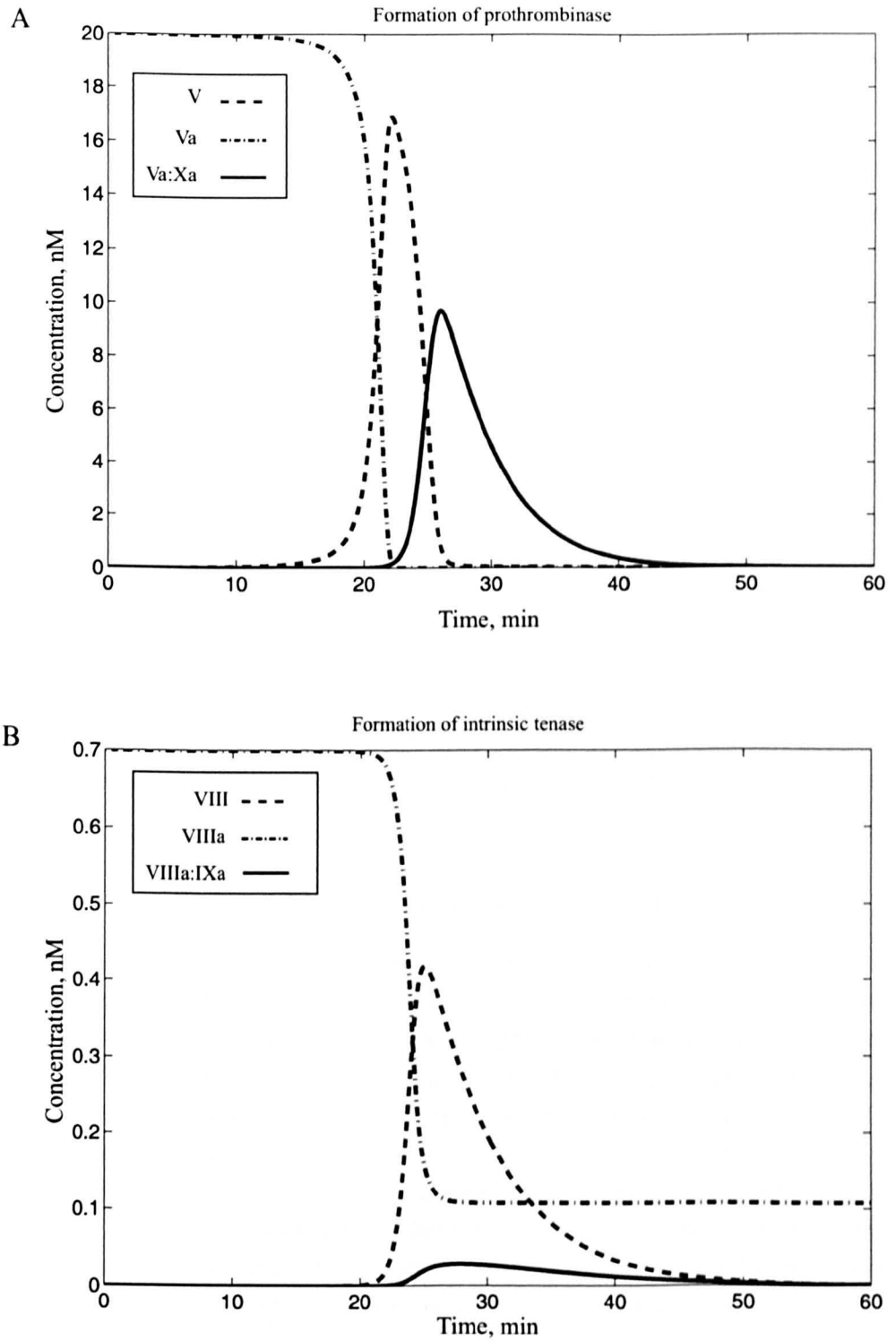

Figure 4.8: Time-dependent solutions of the coagulation cascade (equations (4.2.12), (4.2.13), (4.2.14)) neglecting thrombin activation of factor XI. Parameters are taken from Table 4.4 and initial conditions from Table 4.3, except that the initial concentration of procoagulant factor XI is set to zero. (A) shows the time dependent evolution of factor V and its contribution to the complex prothrombinase. (B) shows the evolution of factor VIII and its contribution to the intrinsic tenase. Same simulations as Figure 4.7 which provides additional variables.

4.3.2.1 Simulations of haemophilia A

Haemophilia A is caused by a congenital deficiency of factor VIII and is the most common form of haemophilia. Figure 4.10 shows the time-dependent profile of thrombin concentration for numerical solutions of subsystem two with initial concentrations taken from Table 4.3 except that the initial concentration of factor VIII is varied (100%, 80%, 60%, 40%, 20%, 10%, 5% in each successive simulation). Parameter values for all simulations are taken from Table 4.4. Our simulations demonstrate that 46 percent of maximum thrombin generation was achieved with only 5 percent of factor VIII (a reduction from 540 nM (100% factor VIII) thrombin to 250 nM (5% factor VIII)). With no factor VIII the peak level of thrombin production was that observed with solutions of subsystem one (4 nM). The greatest increase in peak thrombin formation occurs between 0 and 5 percent (an increase of 246 nM). The time to reach peak thrombin concentration increased from 24 minutes (100% factor VIII) to 38 minutes (5% factor VIII), an increase of 58 percent. The time to reach peak and the peak thrombin concentration reveals the influence of factor VIII on the coagulation cascade. An experimental study of the influence of factor VIII on a thrombin generation assay (Salvagno *et al.*, 2009) uses healthy plasma diluted with factor VIII-depleted plasma to obtain different factor VIII concentrations. Maximum thrombin generation of 362 nM (100% factor VIII) reduced to 160 nM (5% factor VIII), a reduction of 56 percent. The study measured the lag phase (*i.e.* the time to the start of the main bolus of thrombin generation) rather than time to peak thrombin concentration and found this to be increased from 11 minutes to 18 minutes (an increase of 64 percent). The experimentally-observed trends in the time to peak and the reduction in peak thrombin concentration are reproduced by our model.

4.3.2.2 Simulations of haemophilia B

Haemophilia B involves congenital deficiencies in factor IX (which is also known as Christmas factor (Giangrande, 2003)). Figure 4.11 shows time-dependent thrombin concentration for numerical solutions of subsystem two when the initial concentration of factor IX is varied (100%, 80%, 60%, 40%, 20%, 10%, 5% of original plasma concentration in each successive simulation). Our simulations demonstrate that 43 percent of maximum thrombin generation was achieved with only 5 percent of factor IX (a reduction from 540 nM thrombin to 310 nM). When no factor IX was present the peak level of thrombin production was that observed with solutions of subsystem one (4 nM). As levels of factor IX decrease from normal plasma levels, the time to reach the peak thrombin concentration also decreases attaining a minimum value when it is present at 20% of normal levels. For lower values the time to reach peak increases.

The profiles for peak thrombin concentration are similar to those for haemophilia A (Figure 4.10) in that the peak thrombin concentration falls as the concentration of factor IX is reduced. An experimental study using a thrombin generation assay on plasma from patients with haemophilia B revealed a similar correlation between the peak thrombin concentration and the factor IX concentrations but they observed a steady increase in time to reach peak thrombin concentration as levels of factor IX were reduced (Dargaud *et al.*, 2005). The poor agreement for

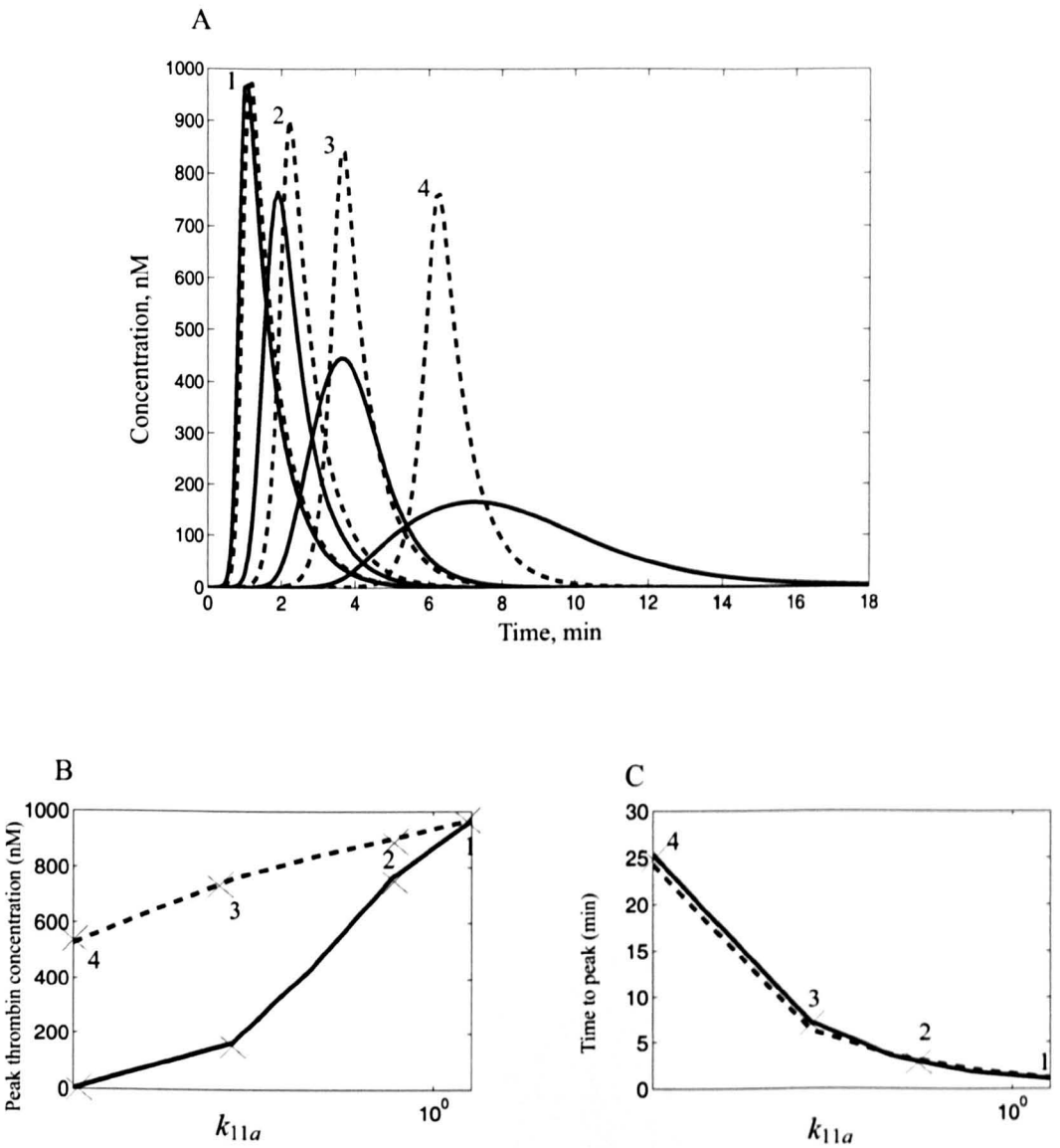

Figure 4.9: Simulations illustrating the contribution of the intrinsic pathway to thrombin generation. (A) The time-dependent evolution of thrombin is presented for solutions of subsystem one (solid line) and subsystem two (broken line) using parameter values taken from Table 4.4, except that each successive pair of simulations has k_{11a} decreased to adjust the level of activation: (1) $k_{11a} = 3$, (2) $k_{11a} = 0.3$, (3) $k_{11a} = 0.03$, (4) $k_{11a} = 0.003$ nM^{-1} min^{-1}. (B) shows peak thrombin concentrations as a function of the level of activation (k_{11a}). Numerical solutions of subsystem two (broken line) show consistently greater peak thrombin concentrations than solutions of subsystem one (solid line) until $k_{11a} = 30$ nM^{-1} min^{-1} when the contribution of the intrinsic pathway to thrombin formation becomes negligible. (C) shows how the time to reach peak thrombin concentration varies with k_{11a} for subsystems one (solid line) and two (broken line). At low levels of activation there is a slight decrease in the time to reach peak thrombin concentration when the inclusion of the intrinsic pathway is active.

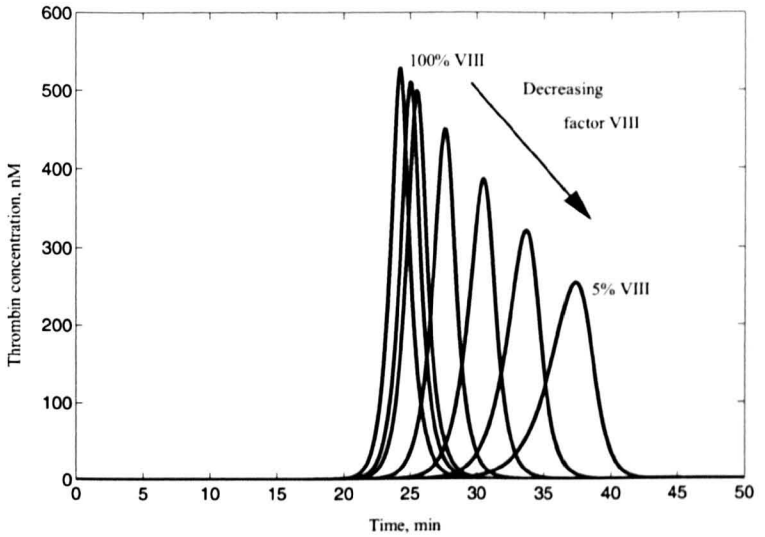

Figure 4.10: Simulations demonstrating the effect of reducing the initial concentration of the procoagulant VIII for subsystem two. The initial conditions are taken from Table 4.3 (except that the initial concentration of factor VIII is varied 100%, 80%, 60%, 40%, 20%, 10%, 5% of the plasma VIII concentration listed in Table 4.3 in each successive simulation). Parameter values are taken from table 4.4.

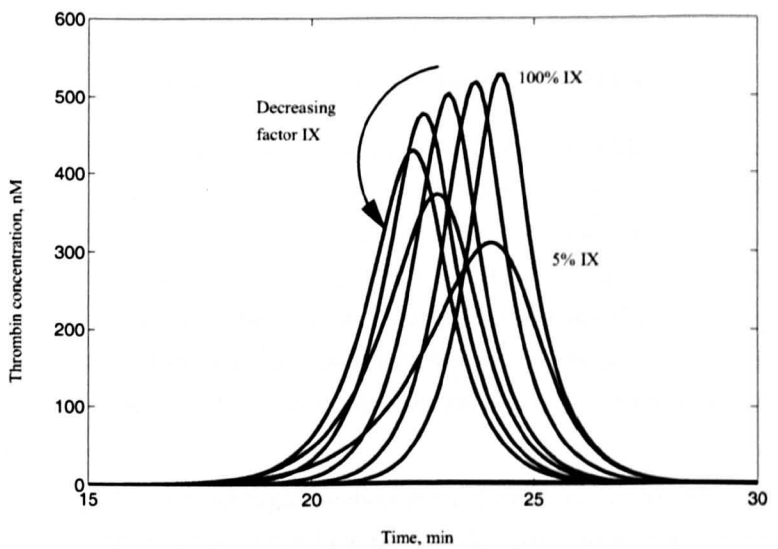

Figure 4.11: Simulations demonstrating the effect of reducing the initial concentration of procoagulant IX. Numerical simulations are of subsystem two with initial conditions from Table 4.3 (except for IX varied to 100%, 80%, 60%, 40%, 20%, 10%, 5% of plasma IX concentration in each successive simulation). Parameter values are from table 4.4. The time to reach peak thrombin concentration shows unusual behaviour with a reduction in time to reach peak for a decrease in factor XI concentration (from 100% to 20%). This is investigated further in Section 4.3.4.

time to reach peak between our model simulations and the experimental results is discussed in Section 4.3.4.

4.3.3 The full cascade

4.3.3.1 Sensitivity of thrombin generation to factor XI

Kravtsov *et al.* (2009) performed experiments to determine how thrombin generation depends on factor XI. Plasma deficient in factor XI was activated by the addition of factor XIa. To replicate these experiments, we numerically solve the full model, with parameter values from Table 4.4 and initial conditions taken from Table 4.3. Additionally, we fix $k_{11a} = 0\ \text{nM}^{-1}\ \text{min}^{-1}$ so that the extrinsic pathway is not activated and we set the initial concentration of factor XI to zero (ensuring that thrombin activation of factor XI does not occur). In separate simulations we set the initial concentration of factor XIa to 300, 30, 3, 0.3 and 0.003 pM, so that the model is activated via the intrinsic pathway. While our numerical solutions (Figure 4.12) are qualitatively similar to experimental results (Kravtsov *et al.* (2009), Figure 2) in that similar profiles are obtained with decreasing peaks, our simulations show greater peak thrombin concentrations for identical levels of activation. Numerical solutions of our model under activation by 300 pM factor XIa show peak thrombin levels of 950 nM after 8 minutes. Experimental results show peak thrombin production of 460 nM in 10 minutes. Activation by 30 and 3 pM of factor XIa lead to reductions in peak thrombin formation and increased times to reach the peak. Experimental data for activation by 0.3 pM factor XIa show no detectable thrombin formation while our simulations show 700 nM being formed after 58 minutes.

4.3.3.2 Thrombin activation of factor XI

The model was built to investigate the effect of factor XI on thrombin generation and this can be seen in Figure 4.13. Numerical simulations of our model are obtained for subsystem two and the full model for decreasing values of extrinsic tenase activation ($k_{11a} = 300$, $k_{11a} = 30$, $k_{11a} = 3$, $k_{11a} = 0.3$ $k_{11a} = 0.03$, $k_{11a} = 0.003$, $k_{11a} = 0.0003\ \text{nM}^{-1}\ \text{min}^{-1}$). These results are similar to those obtained in Figure 4.9 where we discuss the contribution of the intrinsic pathway and find that, at high levels of extrinsic tenase activation, the contribution of the intrinsic pathway is negligible. At lower levels of activation the intrinsic tenase contributes significantly to peak thrombin formation.

Figure 4.13 demonstrates that, at high levels of activation ($k_{11a} = 300\ \text{nM}^{-1}\ \text{min}^{-1}$), the contribution to thrombin activation of factor XI is negligible, with simulations of subsystem two and the full model producing peak thrombin formation of approximately 1150 nM after 1 minutes. At lower levels of activation ($k_{11a} < 0.3$) numerical solutions of the full model, when compared to solutions of subsystem two, show an increase in peak thrombin production and an increase in the time to reach that peak. In the region $0.3 > k_{11a} < 30$ factor XI produces a decline in peak thrombin concentration. While the increase in peak thrombin concentration due to the inclusion of the feedback from thrombin to factor XI at low levels of activation corresponds to

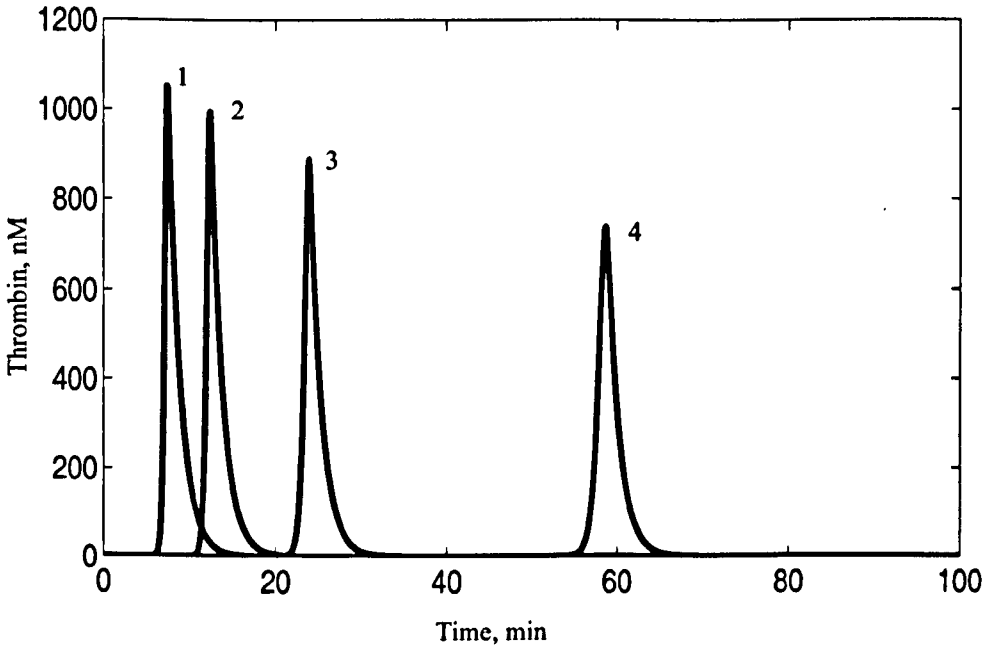

Figure 4.12: Series of profiles obtained from numerical simulation of equations (4.2.12) and (4.2.14) showing how factor XIa influences Thrombin generation in factor XI deficient plasma. Parameters values are taken from Table 4.4 and initial conditions from Table 4.3 except that factor $XI = 0$ and factor XIa varies: (1) 300, (2) 30, (3) 3, (4) 0.3 pM.

experiments results (Kravtsov *et al.* (2009), Figure 1) a decrease in peak thrombin concentration and an increase in the time to reach peak is at variance with the experimental results.

4.3.4 Modifications

Results presented in Sections 4.3.2.2 and 4.3.3.2 are at variance with experimental results. We now present a simplification of the nondimensional system (equations (4.2.12), (4.2.13), (4.2.14)) in which competition for thrombin (between fibrinogen and factors V, VIII and XI) for the intrinsic tenase (between factor IX and X) and for factor Xa (between factor V and prothrombin) is neglected.

The equations for the procoagulants (equations (4.2.12)) simplify to give

$$\frac{df_x}{dt} = -\frac{n f_x}{f_x + 1} - \frac{q_{1c} f_{ix}^a f_x}{f_x + k_{1cm}} - \frac{k_{1d} b_{viii_a}^{ix_a} f_x}{k_{1f}(f_x + k_{1dm})}, \tag{4.3.1a}$$

$$\frac{df_v}{dt} = -\frac{k_{2a} f_{ii}^a f_v}{f_v + k_{2am}} - \frac{k_{2a} k_{2b} f_x^a f_v}{1 + f_v}, \tag{4.3.1b}$$

$$\frac{df_{ii}}{dt} = -\frac{q_{4a} f_x^a f_{ii}}{1 + f_{ii}} - \frac{q_{4b} b_{v_a}^{x_a} f_{ii}}{f_{ii} + k_{4bm}}, \tag{4.3.1c}$$

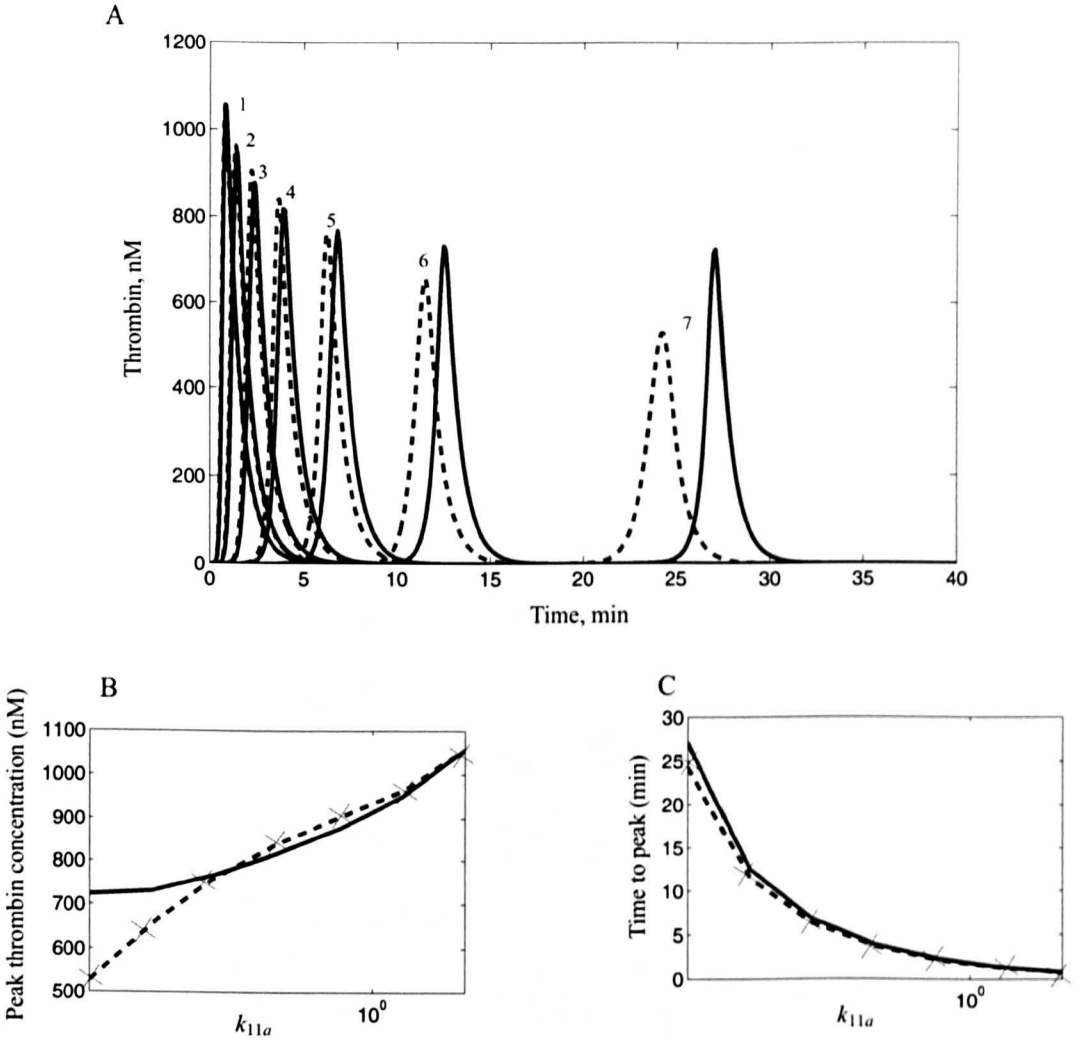

Figure 4.13: Simulations demonstrating the contribution of thrombin activation of factor XI to the generation of thrombin. Initial conditions are taken from Table 4.3 and parameter values from Table 4.4 except that k_{11a} is varied to adjust the level of activation via the extrinsic tenase: (1) $k_{11a} = 300$, (2) $k_{11a} = 30$, (3) $k_{11a} = 3$, (4) $k_{11a} = 0.3$ (5) $k_{11a} = 0.03$,(6) $k_{11a} = 0.003$, (7) $k_{11a} = 0.0003$, nM min^{-1} (simulations in Figures 4.4, 4.7, 4.8 use $k_{11a} = 0.00003$ nM min^{-1}). (A) Simulations of the full model (solid line) and subsystem two (broken line). (B) Peak thrombin concentrations as a function of the level of activation (k_{11a}). (C) The time to reach peak thrombin concentration as a function of the level of activation (k_{11a}). Numerical solutions of the full model (full line) show greater peak thrombin concentrations than solutions of subsystem two with $300 > k_{11a} > 30$ and $k_{11a} < 0.3$. Between this region the contribution of thrombin activation of factor XI produces a decline in peak thrombin concentration.

$$\frac{df_i}{dt} = -k_6 f_i, \tag{4.3.1d}$$

$$\frac{df_{xi}}{dt} = -\frac{k_{7a} f_{ii}^a f_{xi}}{f_{xi}+1}, \tag{4.3.1e}$$

$$\frac{df_{ix}}{dt} = -\frac{k_{8a} f_{xi}^a f_{ix}}{f_{ix}+k_{8am}} - \frac{k_{8c} n f_{ix}}{f_{ix}+1}, \tag{4.3.1f}$$

$$\frac{df_{viii}}{dt} = -\frac{k_{9a} f_{ii}^a f_{viii}}{f_{viii}+1}, \tag{4.3.1g}$$

$$\frac{dc}{dt} = -k_{5a} c, \tag{4.3.1h}$$

$$\frac{dp}{dt} = -k_{1e} p f_x^a. \tag{4.3.1i}$$

The equations for the activated factors (4.2.13) simplify so that

$$\frac{dn}{dt} = k_{11a} e^{-k_{11ax} t} - k_{11b} b_{x_a p}^n n \tag{4.3.2a}$$

$$\frac{df_x^a}{dt} = \frac{k_{1f} n f_x}{f_x+1} + \frac{q_{1c} k_{1f} f_{ix}^a f_x}{f_x + k_{1cm}} + \frac{k_{1d} b_{viii_a}^{ix_a} f_x}{f_x + k_{1dm}} + \frac{k_{3c} k_{3a} c^a b_{v_a}^{x_a}}{b_{v_a}^{x_a}+1}$$
$$- k_{1b} f_x^a - k_{3a} f_x^a f_v^a - p f_x^a, \tag{4.3.2b}$$

$$\frac{df_v^a}{dt} = \frac{f_{ii}^a f_v}{f_v + k_{2am}} + \frac{k_{2b} f_{ii}^a f_v}{f_v + 1 + f_{ii}} + \frac{k_{3b}}{q_{3a}} b_{v_a}^{x_a}$$
$$- \frac{c^a f_v^a}{f_v^a + 1} - f_x^a f_v^a, \tag{4.3.2c}$$

$$\frac{db_{v_a}^{x_a}}{dt} = q_{3a} f_x^a f_v^a - q_{3a} k_{3b} b_{v_a}^{x_a} - \frac{k_{3c} q_{3a} c^a b_{v_a}^{x_a}}{b_{v_a}^{x_a}+1}, \tag{4.3.2d}$$

$$\frac{df_{ii}^a}{dt} = \frac{k_{4a} f_x^a f_{ii}}{f_{ii}+1} + \frac{k_{4a} q_{4b} b_{v_a}^{x_a} f_{ii}}{q_{4a}(f_{ii}+k_{4bm})} - f_{ii}^a, \tag{4.3.2e}$$

$$\frac{df_{xi}^a}{dt} = \frac{f_{ii}^a f_{xi}}{f_{xi}+1} - k_{7b} f_{xi}^a, \tag{4.3.2f}$$

$$\frac{df_{ix}^a}{dt} = \frac{k_{8a} f_{xi}^a f_{ix}}{k_{8c}(f_{ix}+k_{8am})} + \frac{n f_{ix}}{f_{ix}+1} + \frac{k_{10b} c^a b_{viii_a}^{ix_a}}{b_{viii_a}^{ix_a}+1} - k_{10a} f_{ix}^a f_{viii}^a \tag{4.3.2g}$$
$$- k_{8b} f_{ix}^a, \tag{4.3.2h}$$

$$\frac{df_{viii}^a}{dt} = \frac{q_{9a} f_{ii}^a f_{viii}}{f_{viii}+1} + k_{10c} b_{viii_a}^{ix_a} - q_{10a} f_{ix}^a f_{viii}^a$$
$$- \frac{k_{9b} c^a f_{viii}^a}{f_{viii}^a + 1}, \tag{4.3.2i}$$

$$\frac{db_{viii_a}^{ix_a}}{dt} = \frac{k_{10a}}{z_{10c}} f_{ix}^a f_{viii}^a - \frac{q_{10b} c^a b_{viii_a}^{ix_a}}{b_{viii_a}^{ix_a}+1} - q_{10c} b_{viii_a}^{ix_a}, \tag{4.3.2j}$$

$$\frac{dc^a}{dt} = k_{5a} c - k_{5b} c_a, \tag{4.3.2k}$$

and the equations for the downstream inactivated factors and fibrin (4.2.14) simplify to

$$\frac{db^p_{x_a}}{dt} = \frac{q_{1e}}{k_{1f}} p\, f^a_x - \frac{k_{11b}}{q_{1e}} b^p_{x_a}\, n, \tag{4.3.3a}$$

$$\frac{db^n_{x_a p}}{dt} = k_{11b}\, b^p_{x_a}\, n, \tag{4.3.3b}$$

$$\frac{df^i_x}{dt} = k_{1b}\, f^a_x + \frac{k_{3a}k_{3b}}{q_{3a}} b^{x_a}_{v_a}, \tag{4.3.3c}$$

$$\frac{df^i_v}{dt} = \frac{c^a\, f^a_v}{f^a_v + 1} + \frac{k_{3c}\, c^a\, b^{x_a}_{v_a}}{b^{x_a}_{v_a} + 1}, \tag{4.3.3d}$$

$$\frac{df^i_{ii}}{dt} = f^a_{ii}, \tag{4.3.3e}$$

$$\frac{df^a_i}{dt} = k_6\, f_i, \tag{4.3.3f}$$

$$\frac{dc^i}{dt} = k_{5b}\, c^a. \tag{4.3.3g}$$

$$\frac{df^i_{ix}}{dt} = k_{8b}\, f^a_{ix} + z_{10c}\, b^{ix_a}_{viii_a}, \tag{4.3.3h}$$

$$\frac{df^i_{xi}}{dt} = k_{7b}\, f^a_{xi}, \tag{4.3.3i}$$

$$\frac{df^i_{viii}}{dt} = \frac{k_{9b}\, c^a\, f^a_{viii}}{f^a_{viii} + 1} + \frac{z_{10b}\, c^a\, b^{ix_a}_{viii_a}}{b^{ix_a}_{viii_a} + 1}. \tag{4.3.3j}$$

All parameter values, initial conditions and nondimensional groupings are as before.

Simulations of this simplified system, which show how factor XI contributes to thrombin activation of the generation of thrombin, are presented in Figure 4.14. These profiles show a reduction in peak thrombin concentration and an increase in the time to reach peak concentration for simulations of subsystem two relative to the full model. This trend is more consistent with the experimental data.

Our original simulations of haemophilia B also showed a discrepancy with experimental data, in that the time to reach peak reduced with reductions in factor IX concentrations from 100% to 20% (see Figure 4.11). New simulations neglecting competition show better agreement with the experiments with the time to reach peak thrombin concentration increasing as factor IX concentration decreases (see Figure 4.15).

Thrombin activation of factor IX and factor VIII, that forms a complex with factor XI, is poorly understood and therefore competition for thrombin could be more complicated than we originally presumed. The simulations from the reduced model are more consistent with experimental data and provide the better model for the biological information that is available.

4.4 Discussion

Our model of the common pathway from Chapter 3 has been extended to include the extrinsic and intrinsic pathways. The resulting model provides a description of the full coagulation cascade which neglects contact activation and factor XII while including the controversial feedback

from thrombin to factor XI. Our model replicates the thrombin generation assay which, unlike the traditional PT assay which is activated with very high levels of tissue factor, is activated by low concentrations of tissue factors, therby allowing investigation of the whole coagulation cascade. Prior to the development of this assay, analysis of the factors of the intrinsic pathway were always performed using the aPTT assay (which is still in clinical use), where plasma is activated via the contact pathway. Contact activation is not known to be physiologicaly relevant (Renné *et al.*, 2006; Gailani & Renne, 2007*a*) wheras tissue factor activation is thought to be the predominant mechanism for haemostasis (Colman *et al.*, 2000).

The impact of each pathway was investigated by comparing solutions for two subsystems. Subsystem one comprises the extrinsic and common pathway and subsystem two additionally includes the reactions of the common pathway neglecting thrombin activation of factor XI. The effect of neglecting the intrinsic pathway was studied by comparing peak thrombin generation and time to reach peak for the two subsystems. We found that, at low levels of activation, the absence of the intrinsic pathway restricts the amount of thrombin produced and increases the time to reach the peak. At high levels of activation the contribution of the intrinsic pathway has a negligble effect on both the magnitude of peak thrombin generation and the time to reach it. These results are consistent with experiments using the traditional PT assay, which is activated with high levels of tissue factor (2000 nM). With such high levels of activation the contribution of the intrinsic pathway cannot be detected and clinicians have to use the aPTT assay to detect deficiencies in factors of the intrinsic pathway (Baglin, 2005).

By running successive simulations of subsystem two with decreasing initial concentrations of the procoagulants VIII and IX, we were able to compare our model predictions to experimental observations of thrombin formation for plasma deficient in factors VIII and IX which can be related to haemophilia A and B respectively. Simulations of haemophilia A show a close correlation to experimental data with simulations demonstrating that 46 percent of maximum thrombin generation was achieved with only 5 percent of factor VIII. The time to reach peak thrombin concentration increased from 24 minutes (100% factor VIII) to 38 minutes (5% factor VIII), an increase of 58 percent. Experimental data of the influence of factor VIII on a thrombin generation assay (Salvagno *et al.*, 2009) demonstrate a maximum thrombin generation reduction of 56 percent. The time to the start of the main bolus of thrombin generation (rather than time to peak thrombin concentration) increased 64 percent. Simulations of Haemophilia B demonstrated a fall in peak thrombin concentration as the concentration of factor IX was reduced which agreed with an experimental study (Dargaud *et al.*, 2005) but the time to reach peak thrombin concentration as levels of factor IX decreased demonstrated poor agreement.

We then solved the full model and discussed the effect of thrombin activation on factor XI and its contribution to thrombin generation. Simulations of the full model under activation by factor XIa exhibited behaviour qualitatively similar to experiments (Kravtsov *et al.* (2009), Figure 2) designed to assess the sensitivity of thrombin production to factor XIa activation. They do, however, show a marked increase in peak thrombin formation. These discrepancies could be due to a number of factors. For example, we have had to rely on established estimates for the parameters representing the rate of intrinsic tenase formation and the rate that protein C and

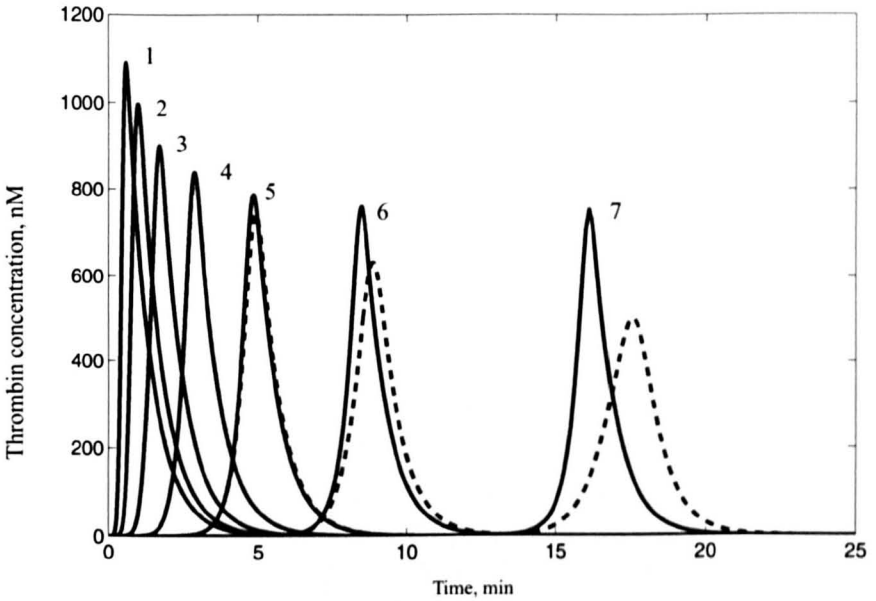

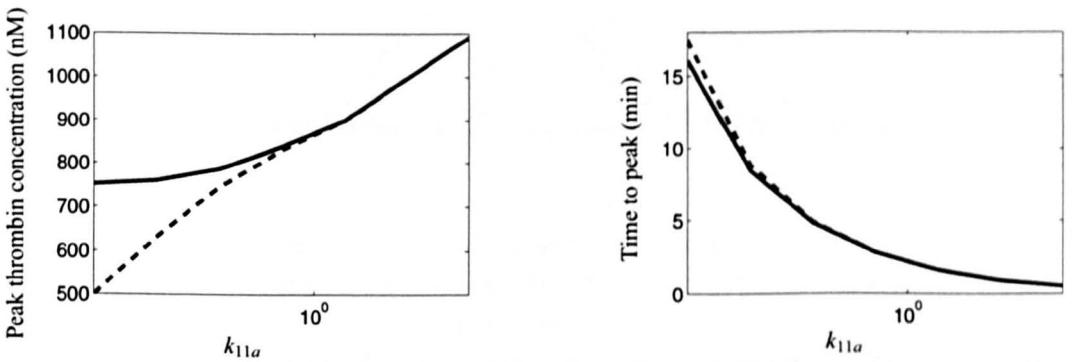

Figure 4.14: Simulations of the simplified system (equations (4.3.1), (4.3.2), (4.3.3)) demonstrating the contribution of thrombin activation of factor XI to the generation of thrombin. These simulations are of equations with competition for thrombin between fibrinogen, factor V and factor VIII removed. Initial conditions are taken from Table 4.3 and parameter values from Table 4.4 except that k_{11a} is varied to adjust the level of activation via the extrinsic tenase: (1) $k_{11a} = 300$, (2) $k_{11a} = 30$, (3) $k_{11a} = 3$, (4) $k_{11a} = 0.3$, (5) $k_{11a} = 0.03$, (6) $k_{11a} = 0.003$, (7) $k_{11a} = 0.0003$ nM min^{-1} (simulations in Figures 4.4, 4.7, 4.8 use $k_{11a} = 0.00003$ nM min^{-1}). (B) shows peak thrombin concentrations as a function of the level of activation (k_{11a}). Numerical solutions of the full model (full line) show consistently greater peak thrombin concentrations than solutions of subsystem two, the extrinsic, intrinsic and common pathway (broken line). (C) compares the time to reach peak thrombin concentration.

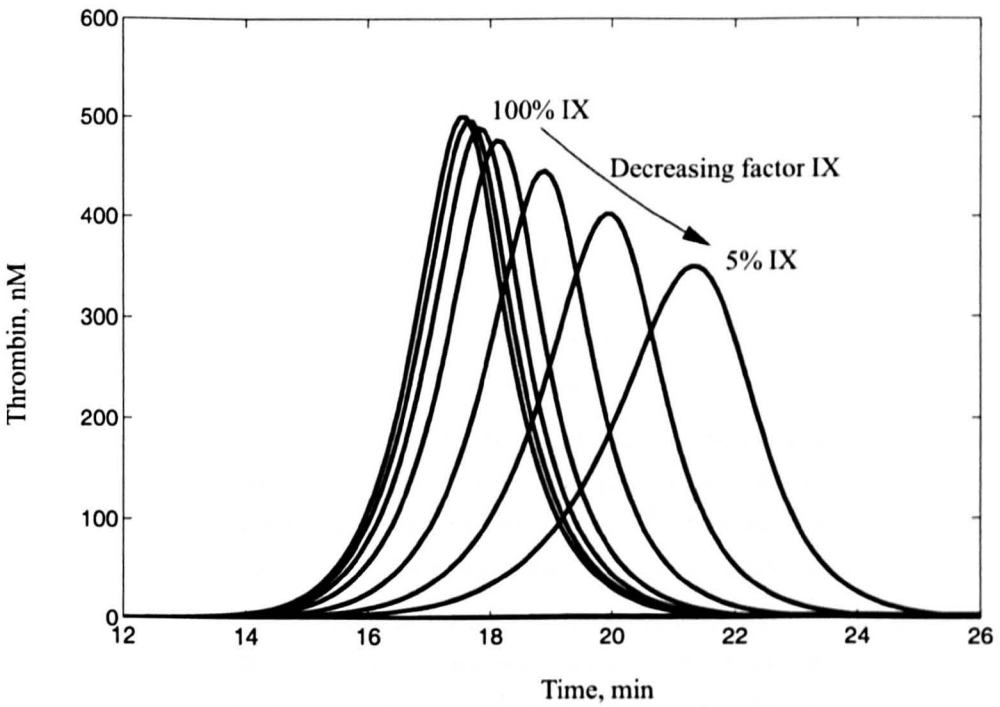

Figure 4.15: Simulations of the simplified system (equations (4.3.1), (4.3.2), (4.3.3)) demonstrating the effect of reducing the initial concentration of the procoagulant IX. Numerical simulations are of subsystem two with initial conditions from Table 4.3 (except for IX varied to 100%, 80%, 60%, 40%, 20%, 10%, 5% of plasma IX concentration in each successive simulation). Parameter values are from table 4.4.

ATIII break it down into its constitutive parts. Our model also neglects other important biological features such as the interaction of cell-surfaces. By extending our model to include these and other processes it should be possible to improve agreement with experimental observations.

The model was designed to replicate experimental conditions in which thrombin generation is measured in plasma stimulated by the addition of TF. While more detailed mathematical models of coagulation exist, our model, which accounts for the biochemistry of the coagulation cascade and limits parameter values to those taken from literature, is able to demonstrate that thrombin activation of factor XI can affect thrombin generation in plasma. This contradicts results from a previous mathematical model (Kramoroff & Nigretto, 2001) that specifically investigated factor XI activation. The model was formulated to reflect the APTT screening assay and hence was based on a subset of reactions of the coagulation cascade that excluded the extrinsic pathway and was activated via high levels of factor XII.

There were discrepancies between simulations of equations (4.2.12), (4.2.13), (4.2.14) and experimental data for haemophilia B and for the contribution that thrombin activation of factor XI makes to peak thrombin concentration. A simple modification to neglect competition between fibrinogen and factors V, VIII and XI for thrombin, between factors IX and X for extrinsic tenase and between factor V and prothrombinase for factor Xa produces simulations that show a stronger correlation to experiments. Our approach of removing competition may be clumsy. Greater knowlwdge of the mechanisms of competition within the cascade and relevant parameter values may enable us to investigate this further.

Our approach may have oversimplified some aspects of the coagulation cascade. Due to the paucity of biological knowledge and kinetic data, we activate our model at the level of the extrinsic tenase. It would, however, be of interest to include the formation of this complex from factor VII and tissue factor, allowing better comparison with experimental data activated by TF.

The effect of cell surfaces has also been neglected. The availability of platelets and cell surfaces are thought to be rate-limiting for the formation of the complexes prothrombinase and extrinsic and intrinsic tenase (Hoffman, 2003). The influence of platelets on factor XI is not considered in our model even though there is evidence that platelets enhance its rate of activation by thrombin (Kravtsov *et al.*, 2009; Baglia & Walsh, 1998). We neglect spatial effects; this is justifiable as we develop the present model to replicate *in-vitro* experimental conditions carried out in well-mixed plasma. However thrombin activation of factor IX is thought to proceed far from the site of injury and it would be interesting to investigate this further. To mimic *in-vivo* conditions the impact of fluid flow would need to be included since this effects the rates of which different factors are delivered to, and from, the site of injury.

While our model is a simplification it has however shown close correlation to experimental data in a number of areas and has shown that a mathematical model of the thrombin generation assay can detect a contribution from thrombin activation of factor XI to thrombin formation.

Part II

Inflammation

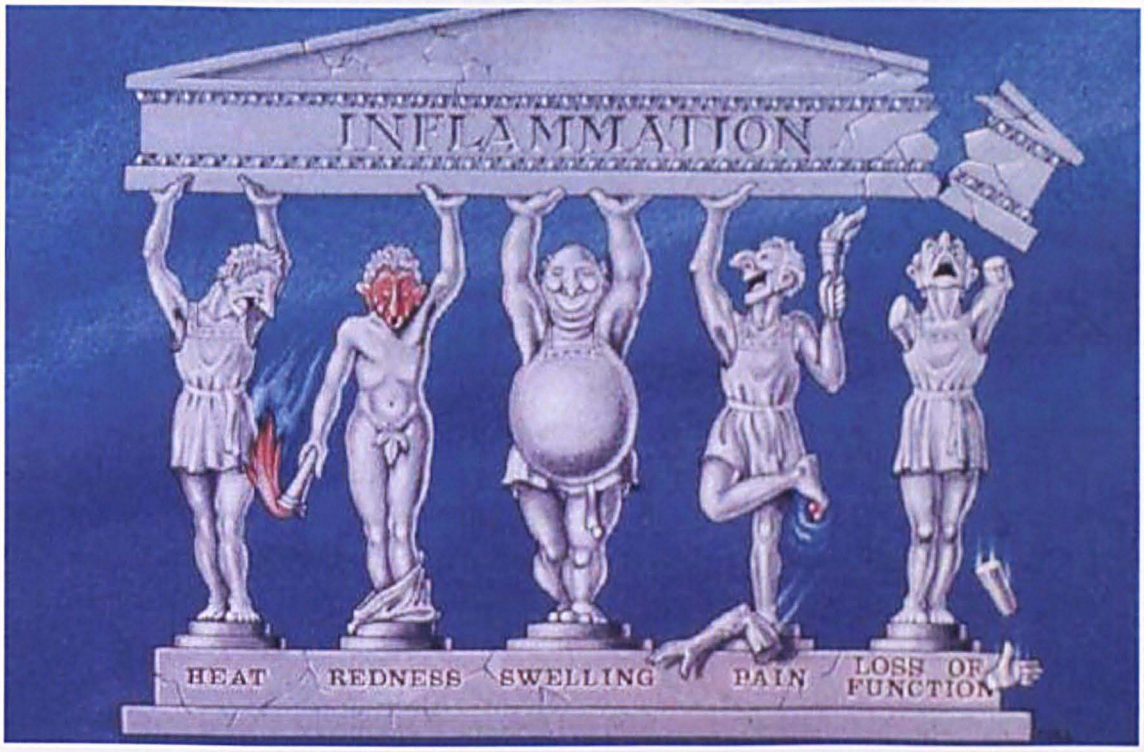

Figure 5.1: The visible signs of inflammation. Courtesy of Molecular Medicine website by Dr. Daniele Focosi, MD at www.myhematologist.net.

CHAPTER 5

Inflammation Background

This chapter is divided into two main parts. We present a description of the biological processes involved in an inflammatory response to tissue damage in Section 5.1 and follow this, in Section 5.2, with a review of the current mathematical literature relevant to soft tissue inflammation.

5.1 Biological background

Inflammation has long been recognised by its clinical symptoms of heat, redness, swelling, pain and loss of function described by Celsus in the first century (see Figure 5.1). It is the body's first line of defence against tissue damage and invading pathogens that attempts to kill the pathogens and remove damaged and dead tissue so healing can proceed. It is a key component in the repair process that soft tissue undergoes and is triggered in response to real or perceived threats: these include the introduction of pathogens and mechanical stress (Butterfield *et al.*, 2006). Inflammation can occur in both sterile and non-sterile conditions, where the body reacts to tissue trauma as if the emergency is infection (Nathan, 2002). Haemorrhage, surgical wounds (Szpaderska & DiPietro, 2005) and muscle loading (Koh & Pizza, 2009) can each trigger an inflammatory response that appears to be independent of infection (Nathan, 2002).

Inflammation is normally a beneficial process, removing dead tissue and killing pathogens before initiating the subsequent healing phases and subsiding, but it can have an alternative fate - instead of subsiding it can progress to a self-perpetuating, chronic inflammatory condition where tissue repair is compromised (Giles & Lawrence, 2008; Serhan *et al.*, 2008). Chronic low grade inflammation has long been know to contribute to many diseases including rheumatoid arthritis, chronic bronchitis and asthma but in recent years it has also been recognised as playing a key role in illnesses such as Alzheimer's disease, cardiovascular disease, Parkinson's disease and cancer (Serhan *et al.*, 2008; Perretti & Flower, 2008). Inflammation has also been shown to have a relationship to obesity, insulin resistance and ageing (Vassileva & Piquette-Miller, 2010), all topics of increasing interest.

The mechanisms involved in the resolution of inflammation are now widely studied. While the signals and mechanisms that promote inflammation have been well studied and are un-

derstood, the events and signals that contribute to its resolution are less so. Until recently resolution was thought to be a passive process which terminates the chemotactic signals and gradients burn out (Majno & Joris, 2004). There is now agreement that it is an active process and that deficiencies within it contribute to many inflammatory diseases (Serhan *et al.*, 2008).

The inflammatory reaction in soft tissue is depicted in Figure 5.2. Endogenous pro-inflammatory chemical mediators such as vasoactive and chemotactic chemicals are released from damaged tissue. These mediators are many and include histamine from damaged mast cells, clotting system products (plasmin, fibronectin and fibrin), lipid-derived inflammatory mediators (such as prostaglandins and leukotrienes), cytokines and chemokines (such as interleukin-1) and oxygen derived radicals (Gilroy *et al.*, 2004). White blood cells (both neutrophils and macrophages) respond to these signals by migrating from the surrounding vasculature into the damaged tissue where they drive the inflammatory response with the further release of pro-inflammatory mediators such as LTB_4 (Serhan, 2007).

Neutrophils are the first white blood cells to arrive, being smaller and faster moving than macrophages (Majno & Joris, 2004). Once within the tissue they become activated and set about digesting (phagocytosing) any foreign material or necrotic debris left over from the original injury. They are essential for the removal of invading micro-organisms but, in attempting to neutralise these micro-organisms they generate substances such as reactive oxygen species (ROS) that can be toxic for healthy tissue (Giles & Lawrence, 2008). Neutrophils have a short lifespan, dying within 6-8 hours by a process called apoptosis (Summers *et al.*, 2010), during which they release signals that are recognised by the later arriving macrophages, which respond by phagocytosing them. Rates of neutrophil apoptosis can be modified, with pro-inflammatory signals and bacterial derived products supporting neutrophil survival, and phagocytosis of neutrophils by macrophages produces growth factors that decrease neutrophil survival inducing their death (Heasman *et al.*, 2003; Kobayashi & DeLeo, 2009). Macrophages are considered to have differentiated from resident monocytes and those that have migrated from the surrounding vasculature (Gordon & Taylor, 2005). Once within inflamed tissue they are activated to release pro-inflammatory mediators and phagocytose necrotic debris and apoptotic neutrophils. It is now thought that macrophages can alter their activation state so that at the point at which they engulf apoptotic neutrophils, they switch to a pro-resolution phenotype producing anti-inflammatory mediators such as transforming growth factor beta (TGF-β) which is associated with resolution and repair (Giles & Lawrence, 2008). The mechanisms responsible for this transition are still unknown but are thought to include macrophage recognition and phagocytosis of apoptotic neutrophils (Porcheray *et al.*, 2005; Sampson, 2000; Gordon & Taylor, 2005; Stout *et al.*, 2005; Arnold *et al.*, 2007).

The removal of apoptotic neutrophils is also thought to be crucial in the resolution process due to the dual role of neutrophils in inflammation (Whyte *et al.*, 2008). Initially, neutrophils provide a beneficial effect by removing debris and killing any perceived local pathogen. However the agents they release to kill the pathogens can, of high enough concentrations, damage healthy tissue, and thereby amplify the inflammatory response (Serhan, 2008). Additionally, damage can occur if the neutrophils undergo necrosis, a process of violent cell death during which the

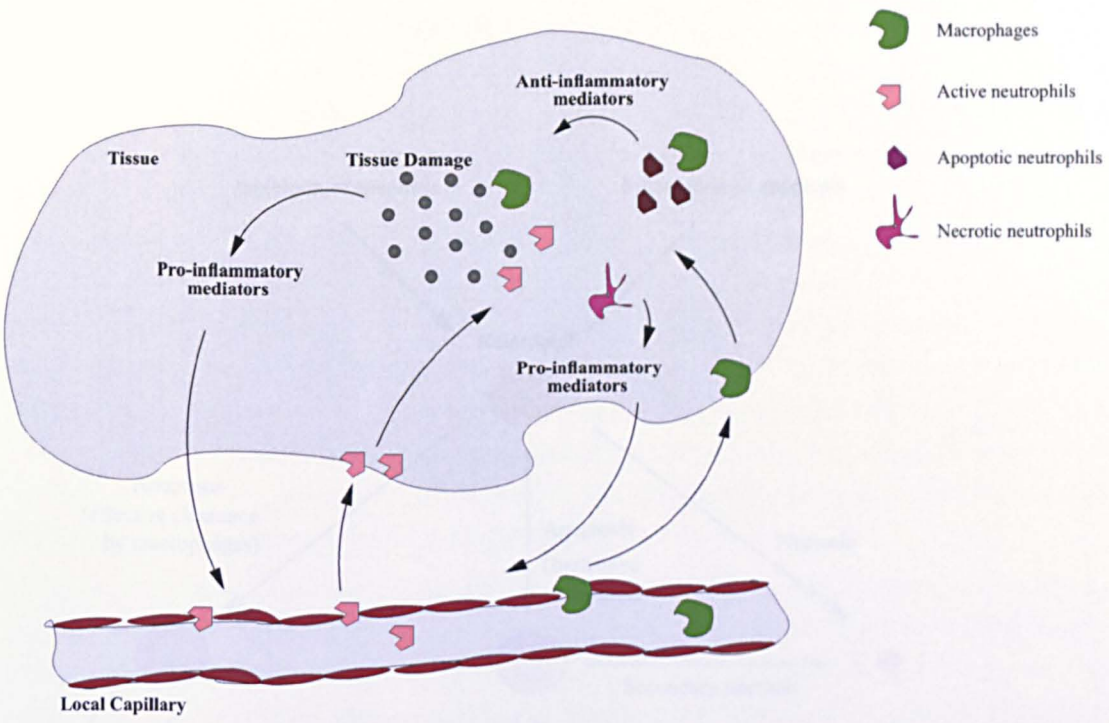

Figure 5.2: Events in acute inflammation. 'Triggers' such as surgical trauma, tissue injury and invading pathogens activate the release of pro-inflammatory mediators. These recruit white blood cells, both neutrophils and macrophages, which can further enhance the process. Neutrophils, through the release of toxic agents to kill invading micro-organisms and through necrosis, can cause ongoing stimulus by damage otherwise healthy tissue. This can be limited by the timely removal of apoptotic neutrophils by macrophages, which promotes a temporal switch to a pro-resolutory signalling network whereby anti-inflammatory mediators bring the inflammatory response under control.

neutrophils lose their membrane integrity and spill their toxic contents into the surrounding tissue. Necrosis can be stimulated by tissue damage. Equally, if there is a delay in the clearance of apoptotic neutrophils, they undergo secondary necrosis, leading to damage and persistent inflammation (Lawrence & Gilroy, 2007; Van Hove *et al.*, 2008; Rossi & Sawatzky, 2008). So, both the behaviour of neutrophils and their apoptotic removal by macrophages are thought to be crucial to the resolution of inflammation (see Figure 5.3). Finally, macrophages leave the site of inflammation and it is thought that they migrate predominantly to the nearest lymph node where they die by apoptosis (Van Hove *et al.*, 2008).

For the inflammatory response to subside the injurious agent must be cleared. It is then that anti-inflammatory signals and events can be set in motion in order to counter the many proinflammatory signals (Serhan, 2007). These regulatory substances reverse vascular changes, inhibit leukocyte migration and activation and promote the safe removal of inflammatory cells, exudate and fibrin, thereby leading to restoration of the inflammed tissue (Gilroy *et al.*, 2004). Anti-inflammatory mediators include cytokines such as Interleukin-10 (IL-10) and transform-

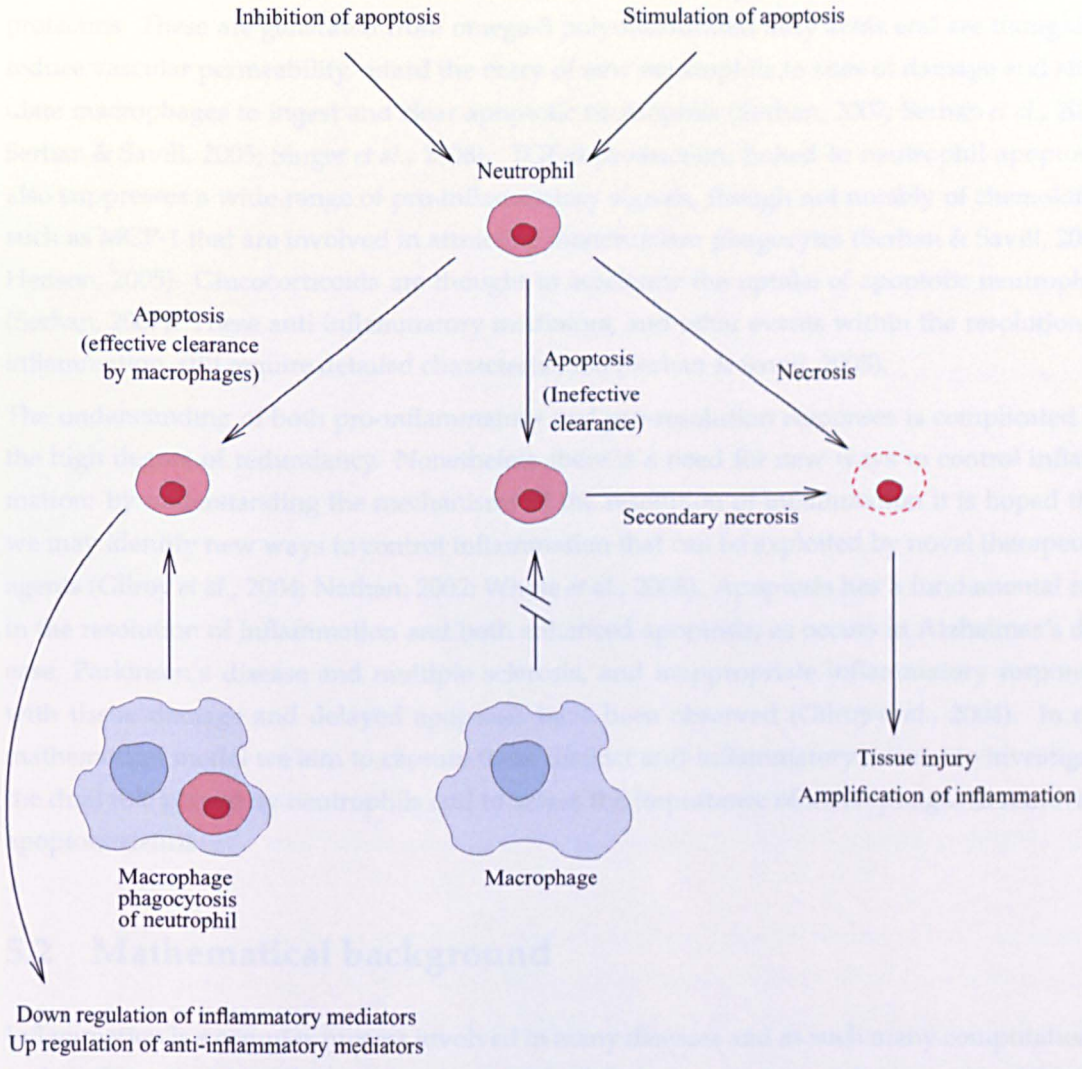

Figure 5.3: A schematic of neutrophil removal and its implications. Their are various factors that influence the apoptotic rate of neutrophils. Once neutrophils have undergone apoptosis they can be phagocytosed by macrophages, further to this there is no release of pro-inflammatory mediators but an up-regulation of anti-inflammatory mediators by macrophages. If the neutrophils become apoptotic but are not removed by macrophages they can undergo 'secondary necrosis'. Neutrophils can also undergo necrosis before phagocytosis. Either form of necrosis has the potential to cause tissue injury and through the release of pro-inflammatory mediators amplify the inflammatory process. Modified from Ward *et al.* (1999).

ing growth factor beta (TGF-β), glucocorticoids, resolvins and protectins (Van Hove *et al.*, 2008). Aspirin is known to be anti-inflammatory, due to its ability to limit the formation of lipid mediators such as thromboxanes and prostraglandins. It is also thought to trigger the production of the newly identified lipid mediators resolvins (resolution phase interaction products) and protectins. These are generated from omega-3 polyunsaturated fatty acids and are thought to reduce vascular permeability, retard the entry of new neutrophils to sites of damage and stimulate macrophages to ingest and clear apoptotic neutrophils (Serhan, 2007; Serhan *et al.*, 2008; Serhan & Savill, 2005; Singer *et al.*, 2008). TGF-β production, linked to neutrophil apoptosis, also suppresses a wide range of pro-inflammatory signals, though not notably of chemokines such as MCP-1 that are involved in attracting mononuclear phagocytes (Serhan & Savill, 2005; Henson, 2005). Glucocorticoids are thought to accelerate the uptake of apoptotic neutrophils (Serhan, 2007). These anti-inflammatory mediators, and other events within the resolution of inflammation, still require detailed characterization (Serhan & Savill, 2005).

The understanding of both pro-inflammatory and pro-resolution responses is complicated by the high degree of redundancy. Nonetheless there is a need for new ways to control inflammation: by understanding the mechanisms of the resolution of inflammation it is hoped that we may identify new ways to control inflammation that can be exploited by novel therapeutic agents (Gilroy *et al.*, 2004; Nathan, 2002; Whyte *et al.*, 2008). Apoptosis has a fundamental role in the resolution of inflammation and both enhanced apoptosis, as occurs in Alzheimer's disease, Parkinson's disease and multiple sclerosis, and inappropriate inflammatory responses with tissue damage and delayed apoptosis have been observed (Gilroy *et al.*, 2004). In our mathematical model we aim to capture these distinct anti-inflammatory events, to investigate the dual role played by neutrophils and to assess the importance of macrophages in removing apoptotic debris.

5.2 Mathematical background

Inflammation is a complex process involved in many diseases and as such many computational and mathematical models exist that describe the inflammatory process downstream of the initial acute inflammatory response or seek to model different disease scenarios (Tran *et al.*, 1995; Gammack *et al.*, 2005; Warrender *et al.*, 2006; Kumar *et al.*, 2008). We limit our review to those mathematical models that are specific to a generic inflammatory response or show significant overlap to the biological mechanisms that we include in our model.

Some of the earliest models of the acute inflammatory response were developed by Lauffenburger and coworkers. For example, Lauffenburger & Keller (1979) produced a model that looks at a bacterial infection in a microscopic area of tissue surrounding a single venule. The model consists of three partial differential equations for bacterial density, leukocyte density and chemoattractant concentration and is used to study the effectiveness of the inflammatory response against bacterial infection and its dependence upon the values of the leukocyte random motility and chemotactic parameters. A later, macroscopic model (Lauffenburger & Kennedy, 1981) also considered an inflammatory response to bacteria and was formulated as a system of

two coupled ordinary equations for bacteria and leukocytes where the dynamics of the leukocyte effectiveness in clearing a bacterial infection are studied. This model was later extended to investigate the influence of spatial effects (Lauffenburger & Kennedy, 1983). By varying the importance of cell motility and chemotaxis the authors showed how cell densities can be highly localised if the bacteria are not eliminated, with the subsequent potential for severe tissue damage. Alt & Lauffenburger extended Lauffenburger & Kennedy's microscopic model by including an additional equation for a chemoattractant (Alt & Lauffenburger, 1985). The resulting model was approximated by a system of two nonlinear ordinary differential equations and used to show that defects in leukocyte chemotaxis correlate with an increase in severity of bacteria infection but not with the concentration of leukocytes.

Kumar *et al.* (2004) presented a simple model to describe an inflammatory response to a pathogen. The model consists of three ordinary differential equations representing a pathogen and two phases of an inflammatory response (early and late). The authors used their model to investigate whether the inflammatory response can clear the invading pathogen or whether it stimulates a sustained inflammatory response. Reynolds *et al.* (2006) presented a reduced ODE model that they used to investigate the resolution of the inflammatory response to a bacterial invasion, building on the previous model of Kumar *et al.* (2004) by adding an anti-inflammatory mediator. The resulting system of four ODEs with dependent variables representing pathogens, activated phagocytes, tissue damage and anti-inflammatory mediators was examined by first considering two subsystems of the model and then combining them to give the complete system. By building up the models to a three and then "complete" four variable system the role and "therapeutic" use of anti-inflammation was analysed. The model of Day *et al.* (2006) replaces the pathogen equation of the previous model with an equation for endotoxin so they can emulate multiple administrations of endotoxin, successfully matched by experimental studies in mice.

Other mathematical models exist that, while not modelling a similar inflammatory response in soft tissue, involve white bloods and we list a few of these, some of which we have used as a source for parameter values. Marée *et al.* (2005); Marée *et al.* (2006, 2008) model macrophage clearance of apoptotic β-cells in mice using two simple ODE models and generate simulations that show a wave of apoptosis in β-cells leading to a chronic condition. Waugh & Sherratt (2006, 2007) discuss macrophage dynamics within the context of wound healing under diabetic conditions. An ODE model, with three variables representing two distinct macrophage phenotypes and TFG-β, is extended to include further mediators and fibroblast and collagen densities. By simulating different treatment protocols, they find that the key mediator for successful healing is hyaluronan and successfully correlate time-to-healing results to clinical trials. Previous mathematical models that investigate macrophage dynamics in the context of mycobacterium tuberculosis include Wigginton & Kirschner (2001), who developed an ODE model for the various macrophage classes, T cells, cytokines and intracellular and extracellular bacteria. Simulations of disease trajectories are obtained and show a dependence on the effective removal of bacterially-infected macrophages. Gammack *et al.* (2004) developed a model consisting of reaction-diffusion-advection PDEs governing macrophages, bacteria and mediators in a tuber-

colosis infected environment. Numerical simulations show two infection outcomes: controlled and uncontrolled formation of granulomas (clumps of macrophages).

5.3 Discussion

In this chapter we have provided a biological introduction to inflammation, focussing on aspects that will be relevant to the mathematical models that are developed in the following chapters. We also reviewed relevant existing mathematical models. Previous models of the inflammatory response have not focused on the processes that limit inflammation, particularly the interactions of white blood cells. In the next chapter (Chapter 6) we produce an ODE model concentrating on these interactions. We then reduce our model, showing that this simplification retains the same outcomes, and extend it to include spatial effects (Chapter 7).

CHAPTER 6

The Resolution of Inflammation

6.1 Introduction

The acute inflammatory response initiated by tissue damage involves a cascade of events that normally resolves within hours (Rossi & Sawatzky, 2008). It has the aim of removing any cellular and tissue debris caused by the initial injury, killing any invading microorganisms and initiating the healing phases during which damaged tissue is replaced (proliferation) and remodelled. In general, inflammation is a self-limiting process but, if it remains unchecked, as it can if the injurious agent persists, it can progress to chronic inflammation, a self-perpetuating process that can last for weeks, months or even years. While knowledge about the mechanisms involved in inducing and perpetuating the inflammatory response are well-characterised, those that limit and down-regulate it are less well understood (Butterfield *et al.*, 2006; Eming *et al.*, 2007). However, there is evidence that apoptosis and the timely removal of neutrophils by macrophages play key roles in the resolution of inflammation (Kobayash *et al.*, 2003; Serhan & Savill, 2005; Rossi & Sawatzky, 2008).

We present, below, a time-dependent model that is formulated as a system of ordinary differential equations and concentrates on neutrophils, macrophages and their interactions. Where possible, parameter values are taken from the literature and otherwise, we make estimates guided by our understanding of the biology. In Section 6.3 we investigate the different qualitative behaviours that our model exhibits and discuss them in terms of the inflammatory response and its possible outcomes. In Section 6.5 we construct bifurcation diagrams in order to study the effects of varying some key control parameters such as the rate of neutrophil apoptosis. We discuss the biological implications of these results, and possible model modifications in Section 6.6.

6.2 Mathematical model

6.2.1 Formulation

The model describes the evolution of nine variables (see Table 6.1) over a time-scale of several days. Unlike previous mathematical models of inflammation that consider only a single population of white blood cells (Lauffenburger & Keller, 1979; Lauffenburger & Kennedy, 1981, 1983; Alt & Lauffenburger, 1985; Reynolds *et al.*, 2006), our model distinguishes between distinct populations of white blood cells by incorporating the following cell types: two distinct macrophage phenotypes, namely the initial inflammatory form (population size $m_1(t)$) and the later anti-inflammatory phenotype ($m_2(t)$) that initiates the subsequent reparative phases, and active and apoptotic neutrophil populations ($n_1(t)$ and $n_2(t)$ respectively). Most previous models (Lauffenburger & Kennedy, 1981, 1983; Alt & Lauffenburger, 1985; Kumar *et al.*, 2004) do not include an anti-inflammatory mediator, concentrating instead on the processes that drive inflammation. Being interested in both pro and anti-inflammatory pathways, we include a generic pro-inflammatory mediator (concentration $c(t)$) that is chemotactic for white blood cells and a generic anti-inflammatory mediator ($g(t)$) that is released from macrophages when they remove apoptotic neutrophils. The reference space for our model is a generic soft tissue. We distinguish between damaged (volume fraction $w(t)$) and healthy ($h(t)$) tissue and, as we are interested in neutrophil death and its implications for the resolution of inflammation, we include, in a single variable ($\sigma(t)$), the concentration of toxic substances released by necrotic neutrophils and by active neutrophils in their attempt to clear pathogens. Since we wish to specialise the model for musculoskeletal disorders, we incorporate an external stimulus ($f(t)$) to represent the effects of damage caused by mechanical stress. Previous models (Lauffenburger & Kennedy, 1981, 1983; Alt & Lauffenburger, 1985; Kumar *et al.*, 2004; Chow *et al.*, 2005; Reynolds *et al.*, 2006) have concentrated on the response from an evolving pathogen and our model could be modified to incorporate this by modifying the functional form of $f(t)$.

In the next section we introduce our model process by process with the aid of increasingly detailed schematics. The schematics enable us gradually to reveal the full model. We then use this network diagram (Figure 6.8) to formulate a system of nine ordinary differential equations (6.2.6). The dimensional model parameters are defined in Table 6.2.

6.2.2 Process 1: Tissue damage

We distinguish between healthy (volume fraction $h(t)$) and damaged (volume fraction $w(t)$) tissue. Healthy tissue can be damaged by an external stimulus ($f(t)$) at rate k_{hl} (equation (6.2.1a)) reflecting an injury such as mechanical trauma. Upon damage, a variety of chemical mediators are released (cell adhesion molecules, cytokines, chemokines *etc.*) from distressed resident cells such as mast cells (Luster *et al.*, 2005). These chemical mediators initiate and augment the inflammatory response and include chemokines such as IL-8 (Adams & Lloyd, 1997). While

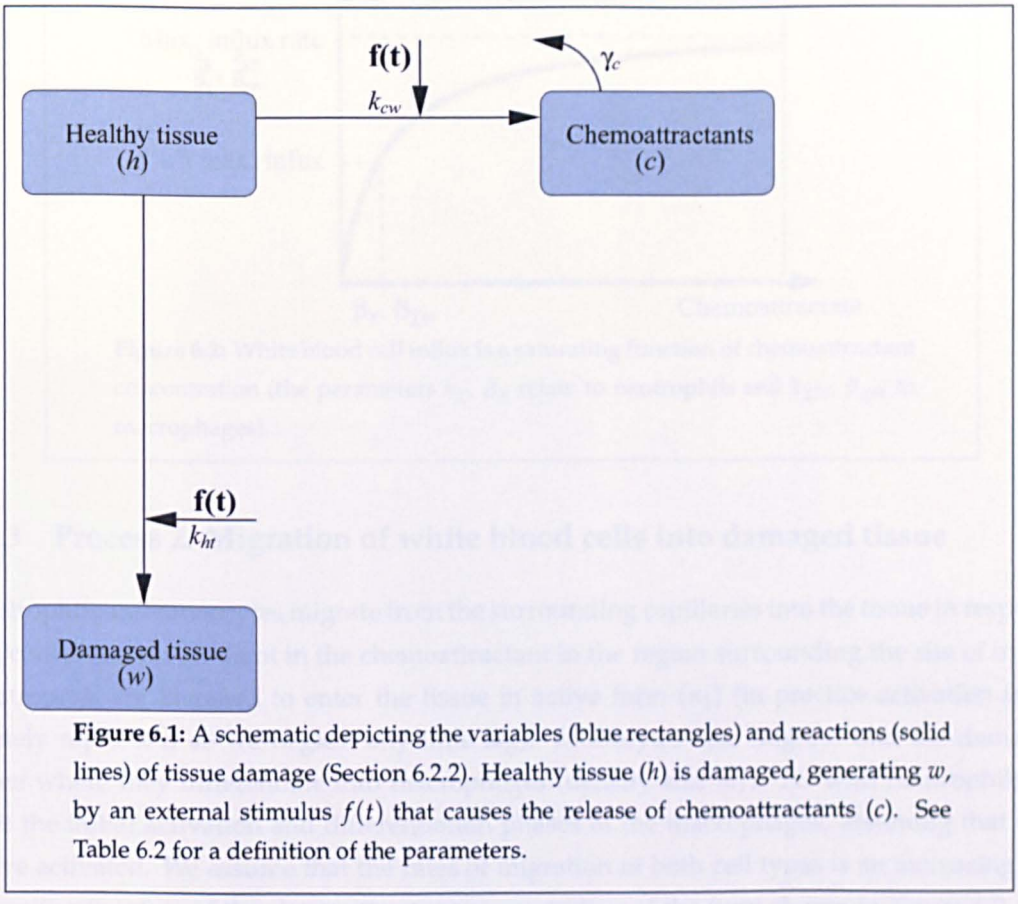

Figure 6.1: A schematic depicting the variables (blue rectangles) and reactions (solid lines) of tissue damage (Section 6.2.2). Healthy tissue (h) is damaged, generating w, by an external stimulus $f(t)$ that causes the release of chemoattractants (c). See Table 6.2 for a definition of the parameters.

more than fifty chemoattractants have been identified for white blood cells (Burke & Lewis, 2002; Reid *et al.*, 2006), we make no distinction between them, instead making the simplifying assumption that there is a single chemical regulator (concentration c) which attracts both neutrophils and macrophages. The regulator is released upon damage to tissue (rate constant k_{cw}) and decays at rate γ_c. These events are depicted in Figure 6.1 and the (incomplete, i.e. including only the terms that have been described thus far) associated equations for healthy and damaged tissue and the chemoattractant can be written as follows:

$$\frac{dh}{dt} = -\underbrace{k_{ht} f(t) h}_{damage}, \tag{6.2.1a}$$

$$\frac{dw}{dt} = \underbrace{k_{ht} f(t) h}_{damage}, \tag{6.2.1b}$$

$$\frac{dc}{dt} = \underbrace{k_{cw} f(t) h}_{release} - \underbrace{\gamma_c c}_{\text{decay}}. \tag{6.2.1c}$$

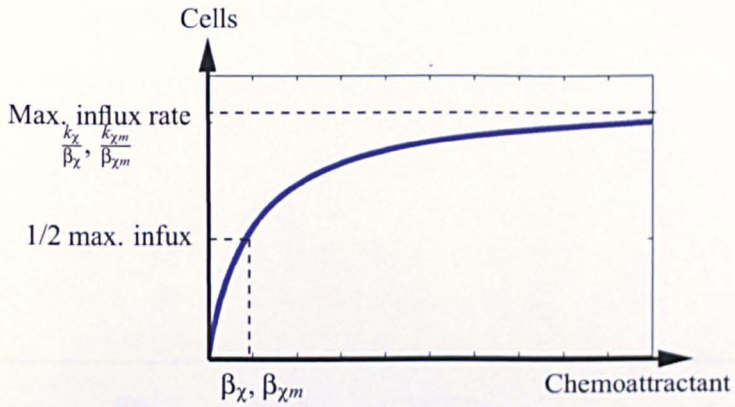

Figure 6.2: White blood cell influx is a saturating function of chemoattractant concentration (the parameters k_χ, β_χ relate to neutrophils and $k_{\chi m}$, $\beta_{\chi m}$ to macrophages).

6.2.3 Process 2: Migration of white blood cells into damaged tissue

Neutrophils and monocytes migrate from the surrounding capillaries into the tissue in response to a concentration gradient in the chemoattractant in the region surrounding the site of injury. Neutrophils are assumed to enter the tissue in active form (n_1) (in practice activation is extremely rapid and so we neglect any time lag). Monocytes also migrate into the damaged tissue where they differentiate into macrophages (density size m_1). As with neutrophils we omit the initial activation and differentiation phases of the macrophages, assuming that they arrive activated. We assume that the rates of migration of both cell types is an increasing and saturating function of the chemoattractant concentration of the form shown in Figure 6.2. The saturating form places a physical limit on the rate at which cells can migrate due to limits on their passage through the tissue. We assume that crowding does not affect this response. We denote by k_χ and $k_{\chi m}$ the maximal rates of neutrophil and macrophage influx, respectively and by β_χ and $\beta_{\chi m}$ the chemoattractant concentration at which these rates are half-maximal (see equations (6.2.2a)). These events are depicted in Figure 6.3 and, with the newly introduced equations for n_1 and m_1 shown in red, the system is now given by:

$$\frac{dn_1}{dt} = \underbrace{\frac{k_\chi c}{\beta_\chi + c}}_{\text{migration}}, \qquad \frac{dm_1}{dt} = \underbrace{\frac{k_{\chi m} c}{\beta_{\chi m} + c}}_{\text{migration}}, \tag{6.2.2a}$$

$$\frac{dh}{dt} = -k_{ht} f(t) h, \qquad \frac{dw}{dt} = k_{ht} f(t) h, \tag{6.2.2b}$$

$$\frac{dc}{dt} = k_{cw} f(t) h - \gamma_c c. \tag{6.2.2c}$$

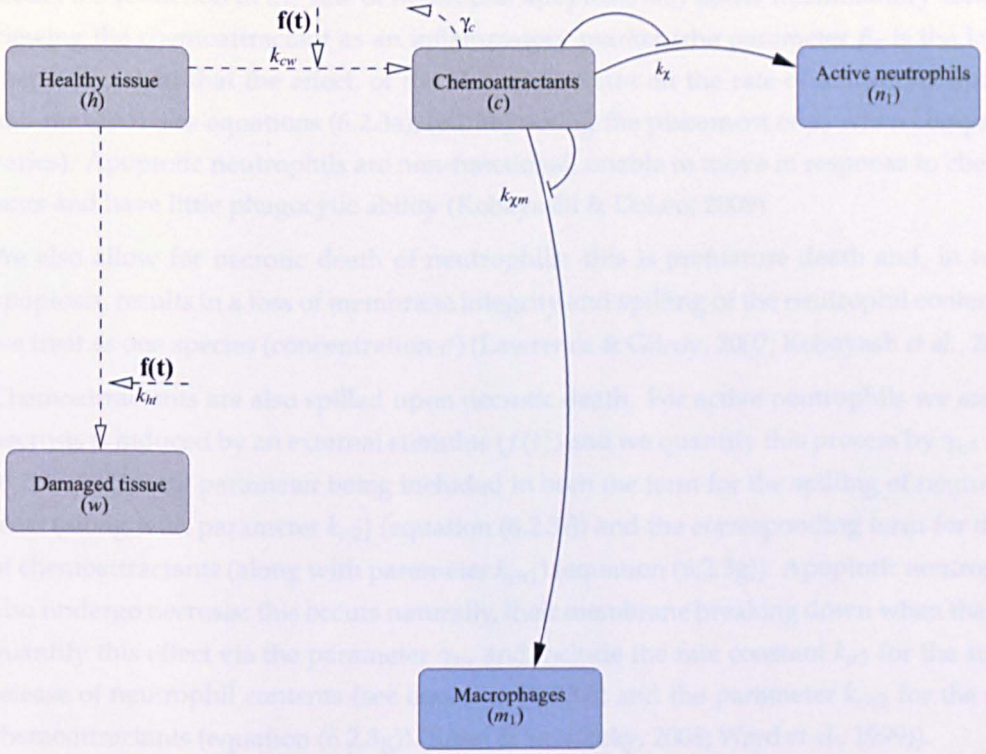

Figure 6.3: A schematic depicting the variables (blue rectangles) and reactions (solid lines) associated with white blood cell migration into damaged tissue (Section 6.2.3). The variables (grey rectangles) and the reactions (dashed lines) introduced in Figure 6.1 are included for clarity. Populations of neutrophils (n_1) and macrophages (m_1) arrive in response to chemoattractants (concentration c) which are released when healthy tissue is damaged. See Table 6.2 for a definition of the parameters.

6.2.4 Process 3: Neutrophil death

We assume that neutrophils can exist in two states, active (density n_1) and apoptotic (density n_2). Neutrophils are activated once in tissue and die by a normal death process called apoptosis. Whilst neutrophils normally have a short lifespan, dying by apoptosis within 6-10 hours, it is well known that the rate at which neutrophils undergo apoptosis can be modified by extra-cellular stimuli (Whyte *et al.*, 2008). For example their lifespan is thought to increase several-fold once they are in inflamed tissue (Akgul *et al.*, 2001) and there is some evidence that this effect is due to pro-inflammatory mediators (Rossi & Sawatzky, 2008; Lee *et al.*, 1993). We model the reduction in the rate of neutrophil apoptosis (k_n) under inflammatory conditions by viewing the chemoattractant as an inflammatory marker (the parameter β_c is the level of the chemoattractant that the effect, of the chemoattractant on the rate of neutrophil apoptosis, is half-maximal: see equations (6.2.3a), (6.2.3b) noting the placement of β_c when compared to β_χ varies). Apoptotic neutrophils are non-functional, unable to move in response to chemoattractants and have little phagocytic ability (Kobayashi & DeLeo, 2009).

We also allow for necrotic death of neutrophils: this is premature death and, in contrast to apoptosis, results in a loss of membrane integrity and spilling of the neutrophil contents, which we treat as one species (concentration σ) (Lawrence & Gilroy, 2007; Kobayash *et al.*, 2003).

Chemoattractants are also spilled upon necrotic death. For active neutrophils we assume that necrosis is induced by an external stimulus ($f(t)$) and we quantify this process by γ_{n1} (equation (6.2.3a)), this rate parameter being included in both the term for the spilling of neutrophil contents (along with parameter $k_{\sigma 2}$) (equation (6.2.3f)) and the corresponding term for the release of chemoattractants (along with parameter k_{cn1}) (equation (6.2.3g)). Apoptotic neutrophils may also undergo necrosis: this occurs naturally, their membrane breaking down when they age. We quantify this effect via the parameter γ_{n_2} and include the rate constant $k_{\sigma 3}$ for the subsequent release of neutrophil contents (see equation (6.2.3f)) and the parameter k_{cn2} for the release of chemoattractants (equation (6.2.3g)) (Rossi & Sawatzky, 2008; Ward *et al.*, 1999)).

Damaged tissue is a broad category which includes necrotic neutrophils (conversion factors k_{w1}, k_{w2}). The events described above are depicted in Figure 6.4 and, with the newly introduced terms and equations (shown in red), the system now reads

$$\frac{dn_1}{dt} = \frac{k_\chi c}{\beta_\chi + c} - \underbrace{\gamma_{n1} f(t) n_1}_{\text{necrotic death}} - \underbrace{\frac{k_n n_1}{\left(1 + \frac{c}{\beta_c}\right)}}_{\text{apoptosis}}, \tag{6.2.3a}$$

$$\frac{dn_2}{dt} = \underbrace{\frac{k_n n_1}{\left(1 + \frac{c}{\beta_c}\right)}}_{\text{apoptotic death}} - \underbrace{\gamma_{n2} n_2}_{\text{secondary necrosis}}, \tag{6.2.3b}$$

$$\frac{dm_1}{dt} = \frac{k_{\chi m} c}{\beta_{\chi m} + c}, \tag{6.2.3c}$$

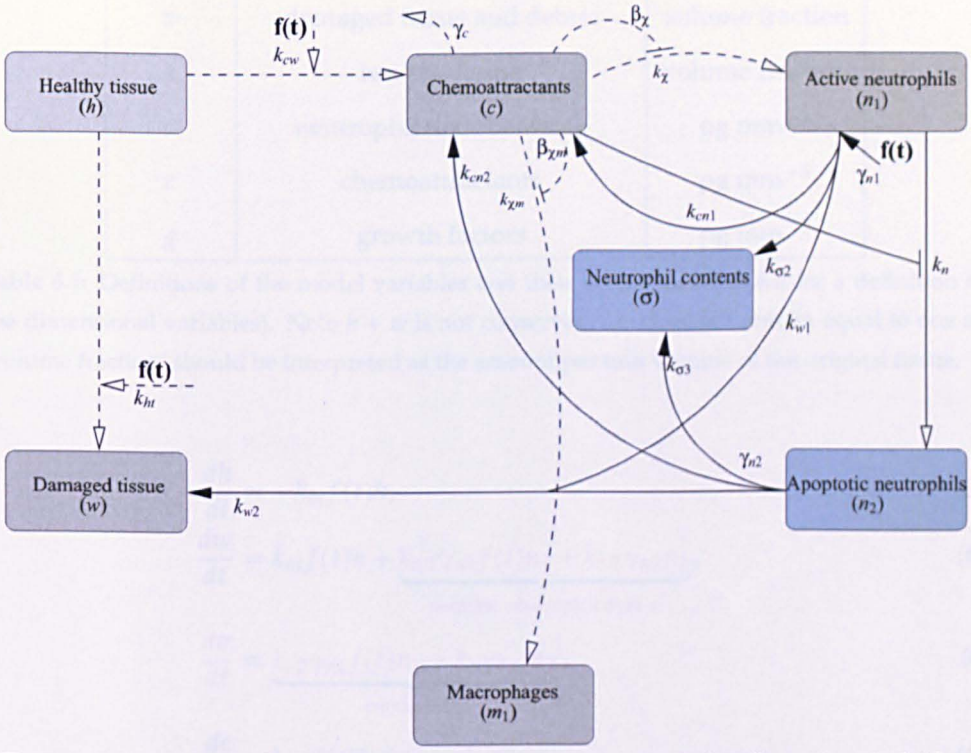

Figure 6.4: A schematic depicting the the variables (blue rectangles) and reactions (solid lines) associated with neutrophil death (Section 6.2.4). Variables (grey rectangles) and reactions (dashed lines) introduced in Figures 6.1 and 6.3 are included for clarity. Active neutrophils (population size n_1) die by first becoming apoptotic (population size n_2), the rate of apoptosis (k_n) being reduced in an inflammatory situation. Both active and apoptotic neutrophils can undergo necrosis. Necrotic neutrophils contribute to damaged tissue (rates k_{w1}, k_{w2}). See Table 6.2 for a definition of the parameters.

Variable	Description	Unit
n_1	active neutrophils	cells mm^{-3}
n_2	apoptotic neutrophils	cells mm^{-3}
m_1	pro-inflammatory macrophages	cells mm^{-3}
m_2	anti-inflammatory macrophages	cells mm^{-3}
w	damaged tissue and debris	volume fraction
h	healthy tissue	volume fraction
σ	neutrophil toxic contents	pg mm^{-3}
c	chemoattractants	pg mm^{-3}
g	growth factors	pg mm^{-3}

Table 6.1: Definitions of the model variables and their units (see Table 6.2 for a definition of the dimensional variables). Note $h + w$ is not conserved, *i.e.* does not remain equal to one so 'volume fraction' should be interpreted as the amount per unit volume of the original tissue.

$$\frac{dh}{dt} = -k_{ht} f(t) h, \tag{6.2.3d}$$

$$\frac{dw}{dt} = k_{ht} f(t) h + \underbrace{k_{w1}\gamma_{n1} f(t) n_1 + k_{w2}\gamma_{n2} n_2}_{\text{necrotic neutrophil debris}}, \tag{6.2.3e}$$

$$\frac{d\sigma}{dt} = \underbrace{k_{\sigma 2}\gamma_{n1} f(t) n_1 + k_{\sigma 3}\gamma_{n2} n_2}_{\text{production}}, \tag{6.2.3f}$$

$$\frac{dc}{dt} = k_{cw} f(t) h + \underbrace{k_{cn1}\gamma_{n1} f(t) n_1 + k_{cn2}\gamma_{n2} n_2}_{\text{production}} - \gamma_c c. \tag{6.2.3g}$$

6.2.5 Process 4: Neutrophil toxicity

Activated neutrophils seem to be programmed to treat an injury as infected, releasing toxic chemicals that they have stored in granules within them in an attempt to counter the infection (Scott *et al.*, 2004; Nathan, 2002). These chemicals, which include reactive oxygen species, are highly toxic and, while effective at killing bacteria, can cause damage to the surrounding tissue if present at high enough concentrations (Haslett, 1999). For simplicity we treat these toxic chemicals as neutrophil contents (concentration σ) and assume that they are released by active neutrophils (rate constant $k_{\sigma 1}$). We assume neutrophil contents cause damage at low levels. However, as these contents accumulate, the damage they cause to healthy tissue increases, saturating at high levels of σ to a maximal value of k_h. They cause the release of chemoattractants in a similar manner to a maximal value of k_{ch}. We use the functional form depicted in Figure

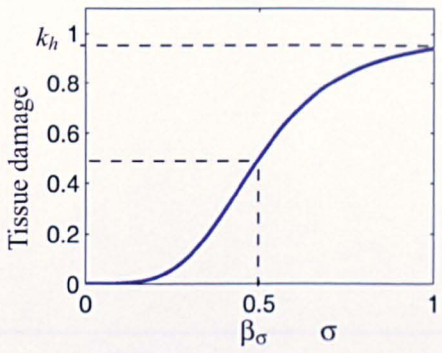

Figure 6.5: Sketch of the Hill function (with Hill coefficient two) used to model the rate of tissue damage caused by neutrophils contents (σ). Maximal damage, at rate k_h occurs when $\sigma \to \infty$, and β_σ is the value of σ at which the rate of damage is half-maximal.

6.2, denoting by β_σ the amount of σ required for half-maximal damage to tissue. We assume that these chemicals undergo linear decay (rate constant γ_σ) and are consumed while damaging healthy tissue (rate $\gamma_{\sigma h}$), producing pro-inflammatory mediators including chemoattractants. These events are depicted in Figure 6.6 and, with the newly introduced terms and equations (depicted in red), our model now reads

$$\frac{dn_1}{dt} = \frac{k_\chi c}{\beta_\chi + c} - \gamma_{n1} f(t) n_1 - \frac{k_n n_1}{\left(1 + \frac{c}{\beta_c}\right)}, \tag{6.2.4a}$$

$$\frac{dn_2}{dt} = \frac{k_n n_1}{\left(1 + \frac{c}{\beta_c}\right)} - \gamma_{n2} n_2, \tag{6.2.4b}$$

$$\frac{dm_1}{dt} = \frac{k_{\chi m} c}{\beta_{\chi m} + c}, \tag{6.2.4c}$$

$$\frac{dh}{dt} = -k_{ht} f(t) h - \underbrace{k_h h \left(\frac{\sigma^2}{\beta_\sigma^2 + \sigma^2}\right)}_{\text{damaged by } \sigma}, \tag{6.2.4d}$$

$$\frac{dw}{dt} = k_{ht} f(t) h + \underbrace{k_h h \left(\frac{\sigma^2}{\beta_\sigma^2 + \sigma^2}\right)}_{\text{damaged by } \sigma} + k_{w1} \gamma_{n1} f(t) n_1 + k_{w2} \gamma_{n2} n_2, \tag{6.2.4e}$$

$$\frac{d\sigma}{dt} = \underbrace{k_{\sigma 1} n_1}_{\text{production}} + k_{\sigma 2} \gamma_{n1} f(t) n_1 + k_{\sigma 3} \gamma_{n2} n_2 - \underbrace{\gamma_{\sigma h} h \left(\frac{\sigma^2}{\beta_\sigma^2 + \sigma^2}\right)}_{\text{uptake}} - \underbrace{\gamma_\sigma \sigma}_{\text{decay}}, \tag{6.2.4f}$$

$$\frac{dc}{dt} = k_{cw} f(t) h + \underbrace{k_{ch} h \left(\frac{\sigma^2}{\beta_\sigma^2 + \sigma^2}\right)}_{\text{colorred damage}} + k_{cn1} \gamma_{n1} f(t) n_1 + k_{cn2} \gamma_{n2} n_2$$
$$- \left(\gamma_{cn} n_1 + \gamma_{cm} m_1\right) c - \gamma_c c. \tag{6.2.4g}$$

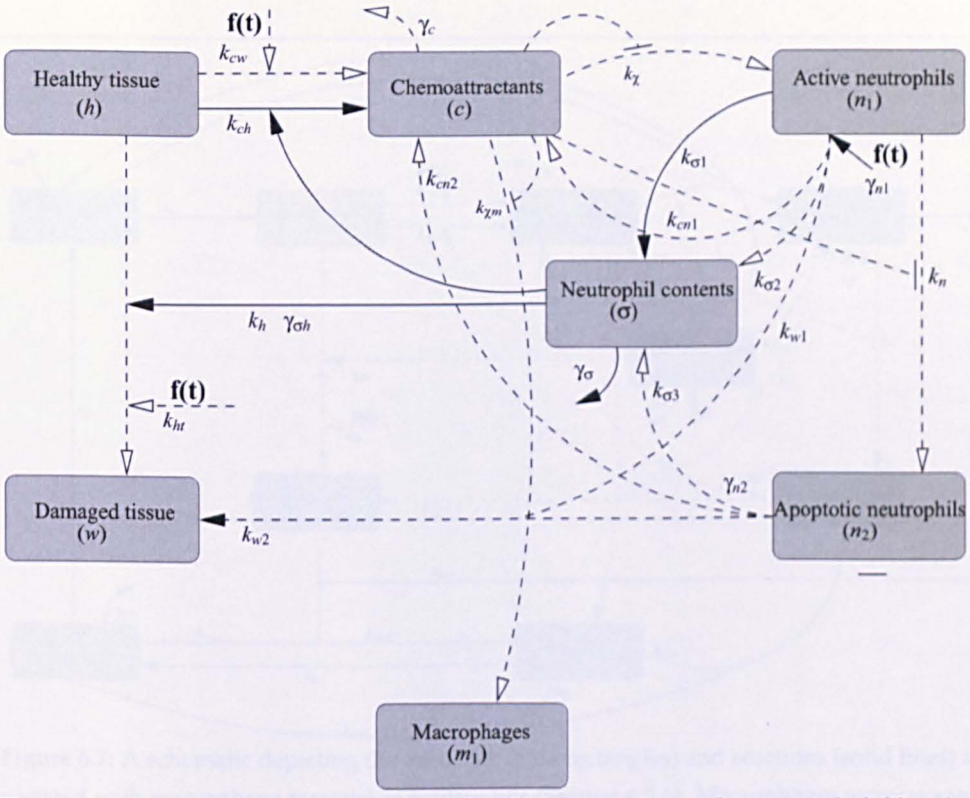

Figure 6.6: A schematic depicting the variables (blue rectangles) and reactions (solid lines) associated with neutrophil toxicity (Section 6.2.5). Active neutrophils release neutrophil contents in an attempt kill any bacteria present ($k_{\sigma 1}$). Neutrophil contents causes damage to healthy tissue (k_h) and the subsequent release of chemoattractants (k_{ch}). The variables (grey rectangles) and reactions (dashed lines) introduced in previous Figures (6.1, 6.3, 6.4) are included for clarity. See Table 6.2 for a definition of the parameters.

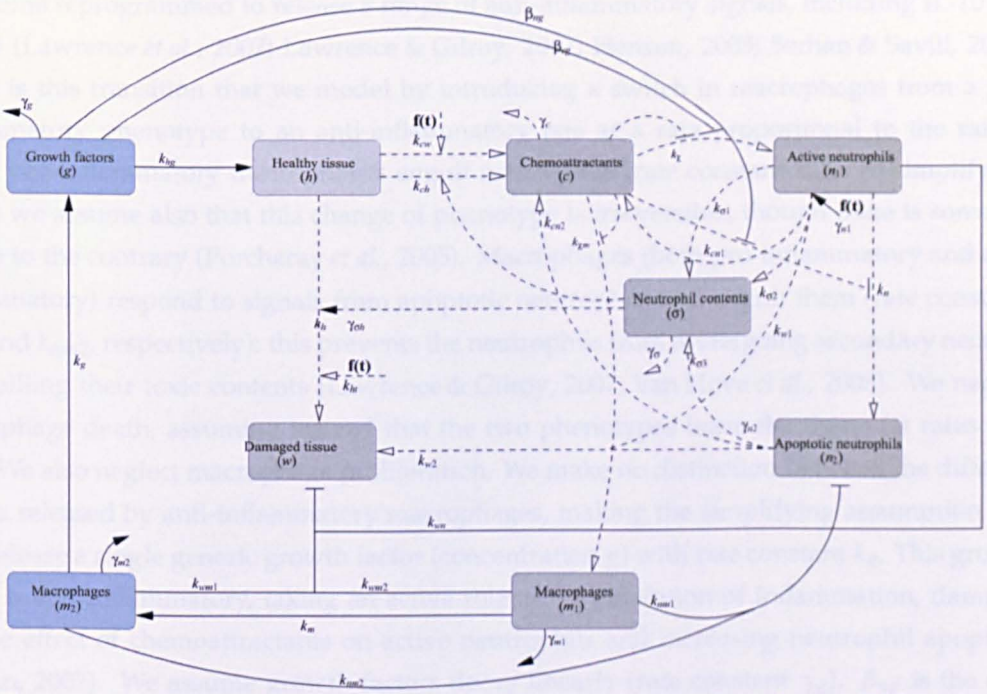

Figure 6.7: A schematic depicting the variables (blue rectangles) and reactions (solid lines) associated with macrophage removal of neutrophils (Section 6.2.6). Macrophages remove apoptotic neutrophils and switch phenotype to an anti-inflammatory form releasing growth factors. Growth factors dampen neutrophil influx and increase neutrophil apoptosis. The variables (grey rectangles) and reactions (dashed lines) introduced in previous Figures (6.1, 6.3, 6.4) are included for clarity. See Table 6.2 for a definition of the parameters.

6.2.6 Process 5: Macrophages remove neutrophils

Macrophages are known to be heterogeneous in their response to various mediators and to exhibit a range of activated states. Several researchers have proposed that, in an inflammatory environment, macrophages sequentially exhibit pro- and anti-inflammatory properties (Stout *et al.*, 2005; Porcheray *et al.*, 2005; Gordon & Taylor, 2005). We introduce a population of anti-inflammatory macrophages (m_2) in addition to the previously described pro-inflammatory phenotype; both types of macrophages (pro-inflammatory and anti-inflammatory) and active neutrophils are phagocytes and remove damaged tissue at rates k_{wm1}, k_{wm2} and k_{wn} respectively. Recognition of apoptotic neutrophils by macrophages is thought to cause macrophages to become reprogrammed to release a range of anti-inflammatory signals, including IL-10 and TGF-β (Lawrence *et al.*, 2007; Lawrence & Gilroy, 2007; Henson, 2005; Serhan & Savill, 2005), and it is this transition that we model by introducing a switch in macrophages from a pro-inflammatory phenotype to an anti-inflammatory one at a rate proportional to the rate at which pro-inflammatory macrophages engulf neutrophils (rate constant k_m). To simplify the model we assume also that this change of phenotype is irreversible, though there is some evidence to the contrary (Porcheray *et al.*, 2005). Macrophages (both pro-inflammatory and anti-inflammatory) respond to signals from apoptotic neutrophils and engulf them (rate constants k_{nm1} and k_{nm2}, respectively): this prevents the neutrophils from undergoing secondary necrosis and spilling their toxic contents (Lawrence & Gilroy, 2007; Van Hove *et al.*, 2008). We neglect macrophage death, assuming instead that the two phenotypes leave the tissue (at rates γ_{m1}, γ_{m2}). We also neglect macrophage proliferation. We make no distinction between the different signals released by anti-inflammatory macrophages, making the simplifying assumption that they release a single generic growth factor (concentration g) with rate constant k_g. This growth factor is anti-inflammatory, taking an active role in the resolution of inflammation, dampening the effect of chemoattractants on active neutrophils and increasing neutrophil apoptosis (Serhan, 2007). We assume growth factors decay linearly (rate constant γ_g). β_{ng} is the concentration of g over which the effect of g, on the rate of apoptosis, is half-maximal. β_{cg} is the concentration of g over which the effect, on the rate of influx of neutrophils, is half-maximal. Healthy tissue is replaced in the downstream proliferative stage in which growth factors initiate tissue repair (rate constant k_{hg}). All of these events are depicted in Figure 6.7 and the ODEs, with the newly introduced terms described above (depicted in red), are:

$$\frac{dn_1}{dt} = \frac{k_\chi c}{(\beta_\chi + c)\left(1 + \frac{g}{\beta_{cg}}\right)} - \gamma_{n1} f(t) n_1 - \frac{k_n n_1 \left(1 + \frac{g}{\beta_{ng}}\right)}{\left(1 + \frac{c}{\beta_c}\right)}, \tag{6.2.5a}$$

$$\frac{dn_2}{dt} = \frac{k_n n_1 \left(1 + \frac{g}{\beta_{ng}}\right)}{\left(1 + \frac{c}{\beta_c}\right)} - \gamma_{n2} n_2 - \underbrace{\left(k_{nm1} m_1 + k_{nm2} m_2\right) n_2}_{\text{phagocytosis}}, \tag{6.2.5b}$$

$$\frac{dm_1}{dt} = \frac{k_{\chi m} c}{\beta_{\chi m} + c} - \underbrace{k_m k_{nm1} m_1 n_2}_{\text{switch}} - \underbrace{\gamma_{m1} m_1}_{\text{removal}}, \tag{6.2.5c}$$

$$\frac{dm_2}{dt} = k_m k_{nm1} m_1 n_2 - \gamma_{m2} m_2, \tag{6.2.5d}$$

$$\frac{dh}{dt} = \underbrace{k_{hg} g h (1-h-w)}_{\text{downstream repair}} - k_{ht} f(t) h - k_h h \left(\frac{\sigma^2}{\beta_\sigma^2 + \sigma^2} \right) \sigma, \tag{6.2.5e}$$

$$\frac{dw}{dt} = k_{ht} f(t) h + k_h h \left(\frac{\sigma^2}{\beta_\sigma^2 + \sigma^2} \right) \sigma + k_{w1} \gamma_{n1} f(t) n_1 + k_{w2} \gamma_{n2} n_2 - \underbrace{k_{wm1} m_1 w - k_{wm2} m_2 w - k_{wn} n_1 w}_{\text{phagocytosis}}, \tag{6.2.5f}$$

$$\frac{d\sigma}{dt} = k_{\sigma 1} n_1 + k_{\sigma 2} \gamma_{n1} f(t) n_1 + k_{\sigma 3} \gamma_{n2} n_2 - \gamma_{\sigma h} h \left(\frac{\sigma^2}{\beta_\sigma^2 + \sigma^2} \right) - \gamma_\sigma \sigma, \tag{6.2.5g}$$

$$\frac{dc}{dt} = k_{cw} f(t) h + k_{ch} h \left(\frac{\sigma^2}{\beta_\sigma^2 + \sigma^2} \right) + k_{cn1} \gamma_{n1} f(t) n_1 + k_{cn2} \gamma_{n2} n_2 - (\gamma_{cn} n_1 + \gamma_{cm} m_1) c - \gamma_c c, \tag{6.2.5h}$$

$$\frac{dg}{dt} = \underbrace{k_g m_2}_{\text{production}} - \underbrace{\gamma_{gn} n_1 g}_{\text{uptake}} - \underbrace{\gamma_g g}_{\text{decay}}. \tag{6.2.5i}$$

6.2.7 Model summary

The complete network diagram is shown in Figure 6.8 and, for clarity, we restate the corresponding system of equations:

$$\frac{dn_1}{dt} = \frac{k_\chi c}{(\beta_\chi + c)\left(1 + \frac{g}{\beta_{cg}}\right)} - \gamma_{n1} f(t) n_1 - \frac{k_n n_1 \left(1 + \frac{g}{\beta_{ng}}\right)}{\left(1 + \frac{c}{\beta_c}\right)}, \tag{6.2.6a}$$

$$\frac{dn_2}{dt} = \frac{k_n n_1 \left(1 + \frac{g}{\beta_{ng}}\right)}{\left(1 + \frac{c}{\beta_c}\right)} - \gamma_{n2} n_2 - (k_{nm1} m_1 - k_{nm2} m_2) n_2, \tag{6.2.6b}$$

$$\frac{dm_1}{dt} = \frac{k_\chi m c}{\beta_\chi m + c} - k_m k_{nm1} m_1 n_2 - \gamma_{m1} m_1, \tag{6.2.6c}$$

$$\frac{dm_2}{dt} = k_m k_{nm1} m_1 n_2 - \gamma_{m2} m_2, \tag{6.2.6d}$$

$$\frac{dh}{dt} = k_{hg} g h (1-h-w) - k_{ht} f(t) h - k_h h \left(\frac{\sigma^2}{\beta_\sigma^2 + \sigma^2} \right) \sigma, \tag{6.2.6e}$$

$$\frac{dw}{dt} = k_{ht} f(t) h + k_h h \left(\frac{\sigma^2}{\beta_\sigma^2 + \sigma^2} \right) \sigma + k_{w1} \gamma_{n1} f(t) n_1 + k_{w2} \gamma_{n2} n_2 - k_{wm1} m_1 w - k_{wm2} m_2 w - k_{wn} n_1 w, \tag{6.2.6f}$$

$$\frac{d\sigma}{dt} = k_{\sigma 1} n_1 + k_{\sigma 2} \gamma_{n1} f(t) n_1 + k_{\sigma 3} \gamma_{n2} n_2 - \gamma_{\sigma h} h \left(\frac{\sigma^2}{\beta_\sigma^2 + \sigma^2} \right) - \gamma_\sigma \sigma, \tag{6.2.6g}$$

$$\frac{dc}{dt} = k_{cw} f(t) h + k_{ch} h \left(\frac{\sigma^2}{\beta_\sigma^2 + \sigma^2} \right) + k_{cn1} \gamma_{n1} f(t) n_1 + k_{cn2} \gamma_{n2} n_2 - (\gamma_{cn} n_1 + \gamma_{cm} m_1) c - \gamma_c c, \tag{6.2.6h}$$

$$\frac{dg}{dt} = k_g m_2 - \gamma_{gn} n_1 g - \gamma_g g. \tag{6.2.6i}$$

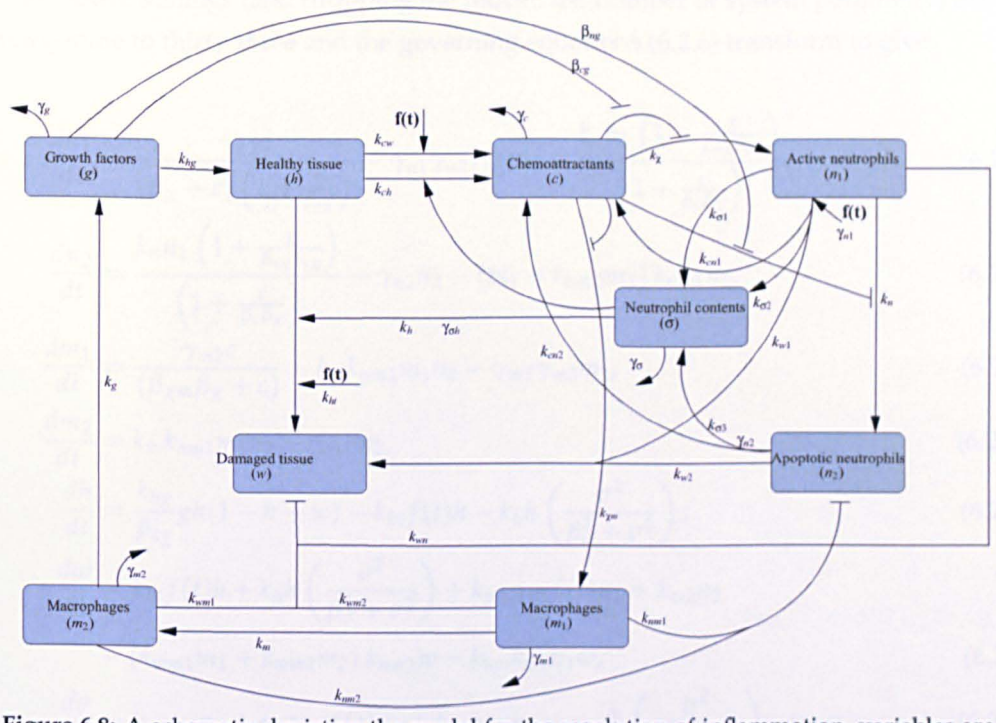

Figure 6.8: A schematic depicting the model for the resolution of inflammation, variables are denoted by blue rectangles and reactions by solid lines. See Table 6.2 for a definition of the parameters.

6.2.8 Nondimensionalisation

We nondimensionalise equations (6.2.6), using tildes to represent dimensionless quantities. We scale time with the timescale for the decay rate of the chemoattractant concentration, so that $\tilde{t} = \gamma_c t$. The chemoattractant is rescaled with the typical initial concentration of chemoattractants released in response to tissue damage, such that

$$c = \frac{k_{cw}}{\gamma_c}\tilde{c}.$$

We rescale neutrophils, n_1 and n_2 such that

$$n_1 = \frac{k_\chi}{\gamma_{n2}}\tilde{n}_1, \qquad n_2 = \frac{k_\chi}{\gamma_{n2}}\tilde{n}_2$$

a ratio of a typical population of neutrophils per unit volume in response to the initial concentration of chemoattractants released upon damage. We proceed in a similar manner for the macrophages with m_1 and m_2 being rescaled such that

$$m_1 = \frac{k_{\chi m}}{\gamma_{m2}}\tilde{m}_1, \qquad m_2 = \frac{k_{\chi m}}{\gamma_{m2}}\tilde{m}_2.$$

Neutrophil contents (σ) and growth factors (g) are rescaled, to balance production with decay in response to initial concentrations of neutrophils and macrophages respectively

$$\sigma = \frac{k_{\sigma 2}\gamma_{n2}}{\gamma_\sigma}\frac{k_\chi}{\gamma_{n2}}\tilde{\sigma}, \qquad g = \frac{k_g}{\gamma_g}\frac{k_{\chi m}}{\gamma_{m2}}\tilde{g}.$$

Under the above scalings (and dropping the tildes), the number of system parameters reduces from thirty-nine to thirty-three and the governing equations (6.2.6) transform to give:

$$\frac{dn_1}{dt} = \frac{\gamma_{n2}c}{(\beta_\chi + c)\left(1 + \frac{g}{\beta_{cg}}\right)} - \gamma_{n1}\gamma_{n2}f(t)n_1 - \frac{k_n n_1 \left(1 + \frac{g}{\beta_{ng}\beta_{cg}}\right)}{\left(1 + \frac{c}{\beta_c \beta_\chi}\right)}, \tag{6.2.7a}$$

$$\frac{dn_2}{dt} = \frac{k_n n_1 \left(1 + \frac{g}{\beta_{ng}\beta_{cg}}\right)}{\left(1 + \frac{c}{\beta_c \beta_\chi}\right)} - \gamma_{n2}n_2 - (m_1 - k_{nm2}m_2)\, k_{nm1}n_2, \tag{6.2.7b}$$

$$\frac{dm_1}{dt} = \frac{\gamma_{m2}c}{(\beta_{\chi m}\beta_\chi + c)} - k_m k_{nm1} m_1 n_2 - \gamma_{m1}\gamma_{m2}m_1, \tag{6.2.7c}$$

$$\frac{dm_2}{dt} = k_m k_{nm1} m_1 n_2 - \gamma_{m2}m_2, \tag{6.2.7d}$$

$$\frac{dh}{dt} = \frac{k_{hg}}{\beta_{cg}} gh(1 - h - w) - k_{ht}f(t)h - k_h h\left(\frac{\sigma^2}{\beta_\sigma^2 + \sigma^2}\right), \tag{6.2.7e}$$

$$\frac{dw}{dt} = k_{ht}f(t)h + k_h h\left(\frac{\sigma^2}{\beta_\sigma^2 + \sigma^2}\right) + k_{w1}\gamma_{n1}f(t)n_1 + k_{w2}n_2$$
$$- (k_{wm1}m_1 + k_{wm2}m_2)\, k_{nm1}w - k_{wn}k_{w1}n_1 w, \tag{6.2.7f}$$

$$\frac{d\sigma}{dt} = k_{\sigma 1}\gamma_\sigma n_1 + \gamma_\sigma \gamma_{n1} f(t)n_1 + k_{\sigma 3}\gamma_{n2}n_2 - \gamma_{\sigma h} h\left(\frac{\sigma^2}{\beta_\sigma^2 + \sigma^2}\right) - \gamma_\sigma \sigma, \tag{6.2.7g}$$

$$\frac{dc}{dt} = f(t)h + k_{ch}h\left(\frac{\sigma^2}{\beta_\sigma^2 + \sigma^2}\right) + k_{cn1}\gamma_{n1}f(t)n_1 + k_{cn2}\gamma_{n2}n_2$$
$$- (\gamma_{cn}n_1 + \gamma_{cm}m_1)\, c - c, \tag{6.2.7h}$$

$$\frac{dg}{dt} = \gamma_g m_2 - \gamma_{gn}k_{w1}n_1 g - \gamma_g g. \tag{6.2.7i}$$

In equations (6.2.7) we have introduced the following dimensionless parameter groupings:

$$\tilde{k}_{ch} = \frac{k_{ch}}{k_{cw}}, \quad \tilde{k}_{cn1} = \frac{k_{cn1}k_\chi}{\gamma_c}, \quad \tilde{k}_{cn2} = \frac{k_{cn2}k_\chi}{\gamma_{n2}}, \quad \tilde{k}_h = \frac{k_h}{\gamma_c},$$
$$\tilde{k}_{hg} = \frac{k_{hg}\beta_{cg}}{\gamma_c}, \quad \tilde{k}_{ht} = \frac{k_{ht}}{\gamma_c}, \quad \tilde{k}_n = \frac{k_n}{\gamma_c}, \quad \tilde{k}_{nm1} = \frac{k_{nm1}k_{\chi m}}{\gamma_c \gamma_{m2}},$$
$$\tilde{k}_{nm2} = \frac{k_{nm2}}{k_{nm1}}, \quad \tilde{k}_m = \frac{k_m \gamma_{m2} k_\chi}{\gamma_{n2}k_{\chi m}}, \quad \tilde{k}_{w1} = \frac{k_{w1}k_\chi}{\gamma_c}, \quad \tilde{k}_{w2} = \frac{k_{w2}\gamma_c}{k_{w1}\gamma_{n2}},$$
$$\tilde{k}_{wm1} = \frac{k_{wm1}}{k_{nm1}}, \quad \tilde{k}_{wm2} = \frac{k_{wm2}}{k_{nm1}}, \quad \tilde{k}_{wn} = \frac{k_{wn}}{k_{w1}\gamma_{n2}}, \quad \tilde{k}_{\sigma 1} = \frac{k_{\sigma 1}}{k_{\sigma 2}\gamma_{n2}},$$
$$\tilde{k}_{\sigma 3} = \frac{k_{\sigma 3}\gamma_\sigma}{k_{\sigma 2}\gamma_{n2}}, \quad \tilde{\beta}_c = \frac{\beta_c}{\beta_\chi}, \quad \tilde{\beta}_{cg} = \frac{\beta_{cg}\gamma_g\gamma_{m2}}{k_g k_{\chi m}}, \quad \tilde{\beta}_{ng} = \frac{\beta_{ng}}{\beta_{cg}},$$
$$\tilde{\beta}_\chi = \frac{\beta_\chi \gamma_c}{k_{cw}}, \quad \tilde{\beta}_{\chi m} = \frac{\beta_{\chi m}}{\beta_\chi}, \quad \tilde{\beta}_\sigma = \frac{\beta_\sigma \gamma_c}{k_{cw}} \frac{\gamma_\sigma}{k_{\sigma 2}k_\chi}, \quad \tilde{\gamma}_{cn} = \frac{\gamma_{cn}k_\chi}{\gamma_{n2}k_{cw}},$$
$$\tilde{\gamma}_{cm} = \frac{\gamma_{cm}k_{\chi m}}{\gamma_{m2}k_{cw}}, \quad \tilde{\gamma}_g = \frac{\gamma_g}{\gamma_c}, \quad \tilde{\gamma}_{gn} = \frac{\gamma_{gn}}{k_{w1}\gamma_{n2}}, \quad \tilde{\gamma}_{n1} = \frac{\gamma_{n1}}{\gamma_{n2}},$$
$$\tilde{\gamma}_{n2} = \frac{\gamma_{n2}}{\gamma_c}, \quad \tilde{\gamma}_{m2} = \frac{\gamma_{m2}}{\gamma_c}, \quad \tilde{\gamma}_{m1} = \frac{\gamma_{m1}}{\gamma_{m2}}, \quad \tilde{\gamma}_\sigma = \frac{\gamma_\sigma}{\gamma_c},$$
$$\tilde{\gamma}_{\sigma h} = \frac{\gamma_{\sigma h}\gamma_\sigma}{k_\chi k_{cw} k_{\sigma 2}}.$$

We assume that at $t = 0$ all tissue is healthy ($h = 1, w = 0$) and that there are no white blood cells ($n_1 = 0, n_2 = 0, m_1 = 0, m_2 = 0$) or mediators present ($\sigma = 0, c = 0, g = 0$). See Table 6.2

	Param.	Definition	Unit	Value	Sources
production.	k_{ch}	c from σ	pg mm^{-3} day^{-1}	10	estimated
	k_{cn1}	c from necrosis of n_1	pg cell^{-1}	1×10^{-3}	estimated
	k_{cn2}	c from necrosis	pg cell^{-1}	1×10^{-3}	estimated
	k_{cw}	c from damage to tissue	pg mm^{-3} day^{-1}	7×10^{-3}	estimated
	k_g	g from m_2	pg cell^{-1} day^{-1}	0.07	Waugh & Sherratt (2007)
	$k_{\sigma 1}$	σ from n_1	pg cell^{-1} day^{-1}	1×10^{-2}	estimated
	$k_{\sigma 2}$	σ from damage to n_1	pg cell^{-1}	1×10^{-2}	estimated
	$k_{\sigma 3}$	σ from necrosis	pg cell^{-1}	1×10^{-2}	estimated
	k_χ	max. n_1 influx	cell mm^{-3} day^{-1}	650	Butterfield *et al.* (2006)
	$k_{\chi m}$	max. m_1 influx	cell mm^{-3} day^{-1}	150	Warrender *et al.* (2006)
phagocytosis	k_{nm1}	n_2 by m_1	cell^{-1} mm^3 day^{-1}	1×10^{-3}	Marée *et al.* (2005), Wigginton & Kirschner (2001)
	k_{nm2}	n_2 by m_2	cell^{-1} mm^3 day^{-1}	1×10^{-4}	Marée *et al.* (2005), Wigginton & Kirschner (2001)
	k_{wm1}	tissue by m_1	cell^{-1} mm^3 day^{-1}	0.01	estimated
	k_{wm2}	tissue by m_2	cell^{-1} mm^3 day^{-1}	0.01	estimated
	k_{wn}	tissue by n_1	cell^{-1} mm^3 day^{-1}	0.01	estimated
tissue	k_h	damage to tissue by σ	day^{-1}	0.1	estimated
	k_{hg}	repair of tissue	pg^{-1} mm^3 day^{-1}	1.0	estimated
	k_{ht}	external damage to tissue	day^{-1}	3×10^{-3}	estimated
	k_{w1}	necrotic debris from n_1	cell^{-1} mm^3	4×10^{-3}	estimated
	k_{w2}	necrotic debris from n_2	cell^{-1} mm^3	4×10^{-4}	estimated
sat. constants	β_c	c damping n_1 apoptosis	pg mm^{-3}	3×10^{-1}	estimated
	β_{cg}	g damping n_1 migration	pg mm^{-3}	5×10^{-1}	estimated
	β_{ng}	g enhancing n_1 apoptosis	pg mm^{-3}	0.8	estimated
	β_σ	σ damage to tissue	pg mm^{-3}	0.1	estimated
	β_χ	half max neutrophil influx	pg mm^{-3}	0.6	estimated
	$\beta_{\chi m}$	half max macrophage influx	pg mm^{-3}	0.6	estimated
uptake of	γ_{cm}	c by m_1	cell^{-1} mm^3 day^{-1}	1×10^{-3}	estimated
	γ_{cn}	c by n_1	cell^{-1} mm^3 day^{-1}	1×10^{-3}	estimated
	γ_{gn}	g by n_1	cell^{-1} mm^3 day^{-1}	1×10^{-3}	estimated
	$\gamma_{\sigma h}$	σ by h	pg mm^{-3} day^{-1}	1×10^{-3}	estimated

Continued on next page

	Param.	Definition	Unit	Value	Sources
decay\removal\switch	k_m	switch from m_1 to m_2	nondimensional	10	estimated
	k_n	n_1 apoptosis	day^{-1}	2.77	Summers *et al.* (2010)
	γ_c	decay of c	day^{-1}	4	Schugart *et al.* (2008)
	γ_g	decay of g	day^{-1}	9	Waugh & Sherratt (2007)
	γ_{m1}	removal of m_1	day^{-1}	0.0495	Waugh & Sherratt (2006) Owen & Sherratt (1997), Wigginton & Kirschner (2001), Warrender *et al.* (2006)
	γ_{m2}	removal of m_2	day^{-1}	0.0495	Waugh & Sherratt (2006), Owen & Sherratt (1997), Wigginton & Kirschner (2001), Warrender *et al.* (2006)
	γ_{n1}	n_1 necrosis	day^{-1}	1	estimated
	γ_{n2}	secondary necrosis	day^{-1}	2.77	Haslett (1999)
	γ_σ	decay of σ	day^{-1}	4	estimated

Table 6.2: Definitions, units and values of the parameters. We remark that, in the absence of suitable data, many of these parameters are estimated (as marked). Explanations for other values are presented in Section 6.2.9. Limited parameter sensitivity has been performed and the model was robust to changes within reasonable changes.

for the parameter values used and Table 6.3 for the corresponding nondimensional parameter values. Tissue damage ($f(t)$) takes the form shown in Figure 6.9 and the steady states are dependent on the termination of this damage ($f(t) = 0$).

6.2.9 Parameter estimates

For several reasons it is difficult to determine precise values for all the parameters: some biological mechanisms remain unclear; there is a lack of published data; and, the values of parameters can vary between tissue types, individuals and over time. Where no specific data are available, estimates are taken from the cited literature, and extra weight attached to data from humans or human cells and soft-tissue-specific data relative to data from other sources. If no data are available then order of magnitude estimates that give biologically realistic results are employed. We will investigate these values and their effect on the outcome of the inflammatory response. A brief description of the parameter values employed and the sources considered is included below, while Table 6.2 contains a summary of the values used.

Neutrophils. Neutrophils are the first white blood cells to arrive in areas of damaged tissue, responding faster than macrophages so that $k_\chi > k_{\chi m}$ (Butterfield *et al.*, 2006; Majno & Joris, 2004). They are known to have a short lifespan of 6-12 hours (Summers *et al.*, 2010) , although, within inflamed tissue, the rate of neutrophil apoptosis can decrease. This leads us to set $k_n = 2.77\ \text{day}^{-1}$. Many different stimuli, including mechanical trauma, can cause damage and death (necrosis) to healthy tissue and cells. We account for this in our model via the term $f(t)$ which represents an external stimulus that causes damage to both healthy tissue (h) and to neutrophils (n_1) (we neglect damage to macrophages as we could find no evidence that they contribute to damage in an inflammatory setting). γ_{n1} is a parameter specific to neutrophil necrosis and is included to reflect this process in all the relevant terms, the resultant release of neutrophil contents (in product with $k_{\sigma 2}$) and chemoattractants (k_{cn1}), and the addition of necrotic neutrophils to damaged tissue (k_{w1}). All three of these parameter will need to be estimated based on producing qualatively realistic simulations as no data are available. Different functional forms of $f(t)$ will be employed and the parameter γ_{n1} fitted to reflect the damage to active neutrophils. The mechanisms of secondary necrosis of neutrophils are still unclear: following (Haslett, 1999) we set $\gamma_{n2} = 2.77\,\text{day}^{-1}$.

Macrophages. Warrender *et al.* (2006) assume a maximal recruitment rate for macrophages of 100 cells $\text{ml}^{-1}\ \text{s}^{-1}$. Accordingly we fix $k_{\chi m} = 150$ cell $\text{mm}^{-3}\ \text{day}^{-1}$. Macrophages are known to live within tissue for days, weeks or months (Owen & Sherratt, 1997) with most leaving via the lymphatics. Previous models involving macrophages assume half lives in the range $3 - 63$ days (Waugh & Sherratt, 2006; Owen & Sherratt, 1997; Wigginton & Kirschner, 2001; Warrender *et al.*, 2006). We assume macrophages of both phenotypes are removed at the same rate $0.0495\ \text{day}^{-1}$ (γ_{m1}, γ_{m2}), equating to a half life of fourteen days.

We assume that recognition and engulfment of apoptotic cells or debris are fast processes. While the rate of this process is likely to vary with environmental factors, such as tissue type and health, as well as the type of particle being removed, we assume that it occurs at a constant rate. The rate at which macrophages engulf apoptotic thymoctes (cells present in the thymus) *in-vitro* has been estimated for mice by Marée *et al.* (2005) to be $10^{-7} - 10^{-6}$ mL $\text{cell}^{-1}\ \text{h}^{-1}$ whereas Wigginton & Kirschner (2001) use values of macrophage phagocytosis of $1.25 \times 10^{-9} - 1.25 \times 10^{-7}$ mL $\text{cells}^{-1}\ \text{day}^{-1}$ in a model of mycobacterium tuberculosis. While we realise that these rates may not correlate with our model, we use them to obtain an initial estimate of $1 \times 10^{-3}\ \text{mm}^3\ \text{cell}^{-1}\ \text{day}^{-1}$ for k_{nm1}, the rate at which pro-inflammatory macrophages remove apoptotic neutrophils and assume that the rate at which pro-resolution macrophages remove neutrophils (k_{mn2}) is reduced due to them being partially sated. The rates at which macrophages, and active neutrophils, consume generic damaged tissue (k_{wm1}, k_{wm2}, k_{wn}) are unknown and will be estimated below. The nondimensional parameter k_m, included in the the switch of active neutrophils to apoptotic will be adjusted to produce the most realistic simmulations.

Nondimensional parameter	Value	Nondimensional parameter	Value
$\tilde{k}_{ch}$	1.4×10^3	$\tilde{\beta}_c$	0.50
$\tilde{k}_{cn1}$	0.16	$\tilde{\beta}_{cg}$	0.02
$\tilde{k}_{cn2}$	0.23	$\tilde{\beta}_{ng}$	1
$\tilde{k}_h$	2.5×10^{-2}	$\tilde{\beta}_\chi$	342.86
$\tilde{k}_{hg}$	0.13	$\tilde{\beta}_{\chi m}$	1
$\tilde{k}_{ht}$	7.5×10^{-4}	$\tilde{\beta}_\sigma$	35.16
$\tilde{k}_n$	0.69	$\tilde{\gamma}_{cn}$	33.52
$\tilde{k}_{nm1}$	0.76	$\tilde{\gamma}_{cm}$	432.90
$\tilde{k}_{nm2}$	0.10	$\tilde{\gamma}_g$	2.25
$\tilde{k}_m$	0.77	$\tilde{\gamma}_{gn}$	0.09
$\tilde{k}_{w1}$	0.65	$\tilde{\gamma}_{n1}$	0.36
$\tilde{k}_{w2}$	0.14	$\tilde{\gamma}_{n2}$	0.69
$\tilde{k}_{wm1}$	10	$\tilde{\gamma}_{m1}$	0.01
$\tilde{k}_{wm2}$	10	$\tilde{\gamma}_{m2}$	1
$\tilde{k}_{wn}$	0.90	$\tilde{\gamma}_\sigma$	1
$\tilde{k}_{\sigma 1}$	0.36	$\tilde{\gamma}_{\sigma h}$	0.09
$\tilde{k}_{\sigma 3}$	1.44		

Table 6.3: Nondimensional parameter values. See Table 6.2 for a definition of the dimensional parameters.

Tissue and external damage. In the absence of suitable data, parameters relating to tissue in its healthy and unhealthy states (k_h, k_{hg}, k_{ht}, k_{w2}) must be estimated to give the best biologically expected results.

Chemoattractant. In the context of this model there are no available data for the rates of production of generic chemoattractants (k_{cn2}, k_{cw}, k_{ch}) or for their uptake (γ_{cn}, γ_{cm}). Therefore these values will be estimated. We expect mediators to have half lives that are at least an order of magnitude smaller than those of cells. Accordingly we follow Schugart *et al.* (2008) and use a value of $\gamma_c = 4$ day^{-1} for chemoattractant decay. With no data available we estimate β_χ, $\beta_{\chi m}$ β_c.

Neutrophil contents. Parameter estimates for the production, uptake and decay rates of neutrophil contents ($k_{\sigma 1}$, $k_{\sigma 3}$, $\gamma_{\sigma h}$, β_σ) are not available. We assume that they are similar in magnitude to the corresponding values for the growth factors and chemoattractants. We assume that, as neutrophils would only release a small amount of granule contents in response to bacteria, $k_{\sigma 1} < k_{\sigma 3}$.

Growth factors. Following, Waugh & Sherratt (2007) who estimated the rate of production of TGF-β by macrophages we fix $k_g = 0.07$ pg cell^{-1} day^{-1}. We also adopt their estimate of 9 day^{-1} for the linear decay rate of the growth factors (γ_g). In the absence of suitable data we estimate the rate of uptake of growth factors by neutrophils (γ_{cn}). Growth factors are assumed to increase rates of neutrophil apoptosis. Since there is a lack of data for the concentration of growth factor (β_{ng}) required for this to occur, it will be estimated assuming it is of a similar order of magnitude to (β_χ).

6.3 Model outcome and steady states

Inflammation has two possible outcomes: resolution and chronic inflammation. Resolution is successful if neutrophils and macrophages leave the tissue, inflammatory mediators subside and the subsequent healing phases are achieved. By contrast, self-perpetuating (or chronic) inflammation is initiated if white blood cells remain within the tissue, causing further tissue damage. While it is thought that chronic inflammation can resolve successfully it more often progresses to poor healing and an inferior tissue prone to injury (Barr, 2004). We argue that a realistic model of inflammation should exhibit bistability, the two steady states corresponding to resolution and chronic inflammation. A bistable system typically exhibits hysteresis and key parameters must exceed a threshold value to effect a switch between the two stable steady states. If the stimulus is gradually removed, the system may remain in the state. We would expect a low level of damage to result in our model returning to a steady state where all cell, mediator and damaged tissue levels are zero (resolution). If a threshold level of damage is passed, then the model would settle to a second steady state where cell, mediator and damaged tissue levels settle to some positive value (chronic response).

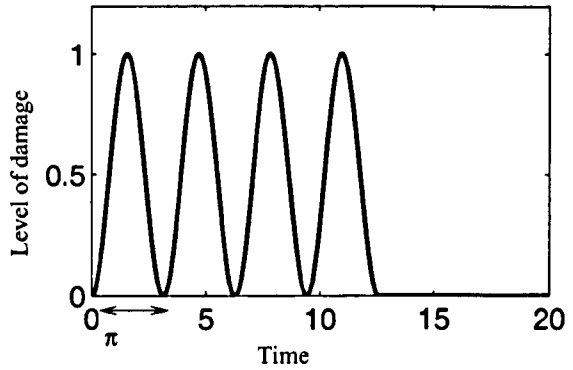

Figure 6.9: An example of external damage $f(t)$.

Due to the complexity of our system it is not possible to derive explicit analytical expressions for the steady state solutions for the general case. However by integrating the ODEs numerically (using ode15s, a stiff ODE solver within MATLAB) it is possible to identify two distinct stable steady states. To obtain these steady states we use the parameter values described above. These are summarised in Table 6.2. The following simulations use the healthy steady state for initial conditions of the variables with all cells, mediators and damaged tissue set to zero and healthy tissue set to one.

In Figure 6.10 we present simulation results of the nondimensional model (equations (6.2.7)), scaled back to dimensional form, showing the response to one cycle of periodic damage ($A = 1$) with $f(t) = H(A\pi - t)\sin^2(t)$ where

$$H(A\pi - t) = \begin{cases} 1 & \text{if } t < A\pi \\ 0 & \text{if } t > A\pi \end{cases}$$

(see Figure 6.9 for a sketch of $f(t)$ which is dimensionless). This causes damage to tissue and the release of chemoattractants. In response, neutrophils and macrophages are recruited (see Panels A and B). Neutrophils undergo apoptosis, but can also undergo necrosis, releasing their toxic contents (Panel D). Macrophages remove apoptotic neutrophils, and this triggers a switch in macrophage phenotype where they release growth factors. All inflammatory cells and their mediators subside and the system returns to a normal steady state which we term steady state I (SSI), evidence that the model can simulate resolution of inflammation. In this figure (6.10) and subsequent time-dependent solutions we provide a conversion from cells (neutrophils and macrophages) to volume fractions. Macrophages are know to have a variable volume, changing in response to stimulus, we use a constant volume of $10^{-6}mm^3$ to convert macrophages per mm^3 to a volume fraction (Poulter & Turk, 1975). Neutrophils are smaller than macrophages and less variable in volume. We use a volume of $10^{-7}mm^3$ to convert neutrophils per mm^3 to a volume fraction (Ting-Beall *et al.*, 1993).

Keeping the same form of $f(t)$ (see Figure 6.9), but increasing the number of cycles of damage from one to four, with the same initial conditions and parameter values, we find that a second stable steady state exists. Simulations of this are shown in Figure 6.11.

In contrast to SSI, we observe a significant amount of tissue damage (Figure 6.11 C). Levels of

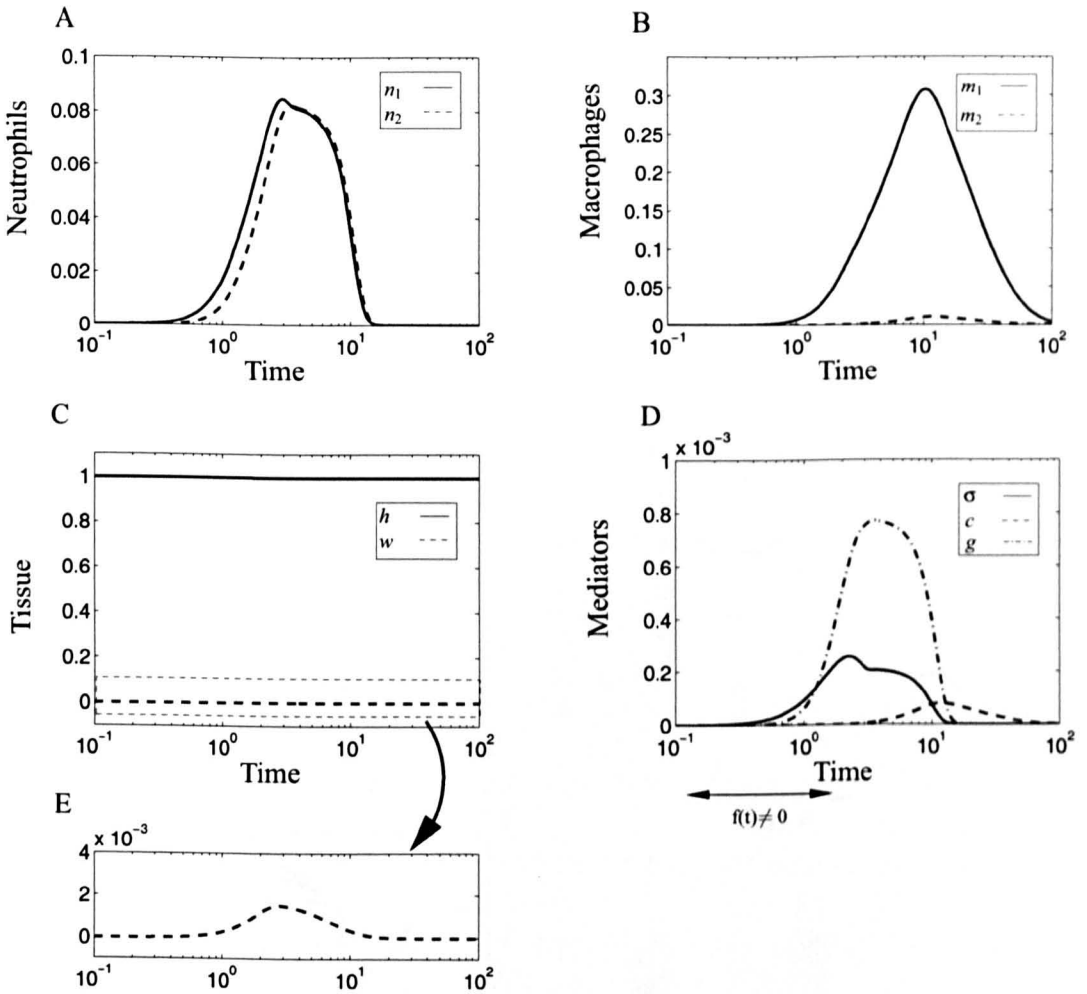

Figure 6.10: Numerical simulations of equations (6.2.7) illustrating how the system evolves to steady state I. Inflammation subsides with all cells and mediators settling to zero. It is $f(t)$ that causes the inflammatory response, its duration being shown in panel D. One cycle of damage results in an increase in chemoattractants, neutrophils and their contents: it is not enough to sustain damage (Panel C) and upon cessation of damage all cells and mediators subside. Panel E shows a zoomed in region of C demonstrating that some damage does accumulate. Parameter values are taken from Table 6.2. In Figure 6.11 we present results from a simulation in which all system parameters and initial conditions are identical to those here, apart from $f(t)$ which is the same functional form but increased from one to four cycles of damage. Assuming a macrophage volume of 10^{-6} mm^3 (Poulter & Turk, 1975), 0.1 macrophages per mm^3 equates to a volume fraction of 10^{-7}. Similarly, assuming a typical neutrophil volume of 10^{-7} mm^3 (Ting-Beall *et al.*, 1993), 0.1 neutrophils per mm^3 converts to a volume fraction of 10^{-8}.

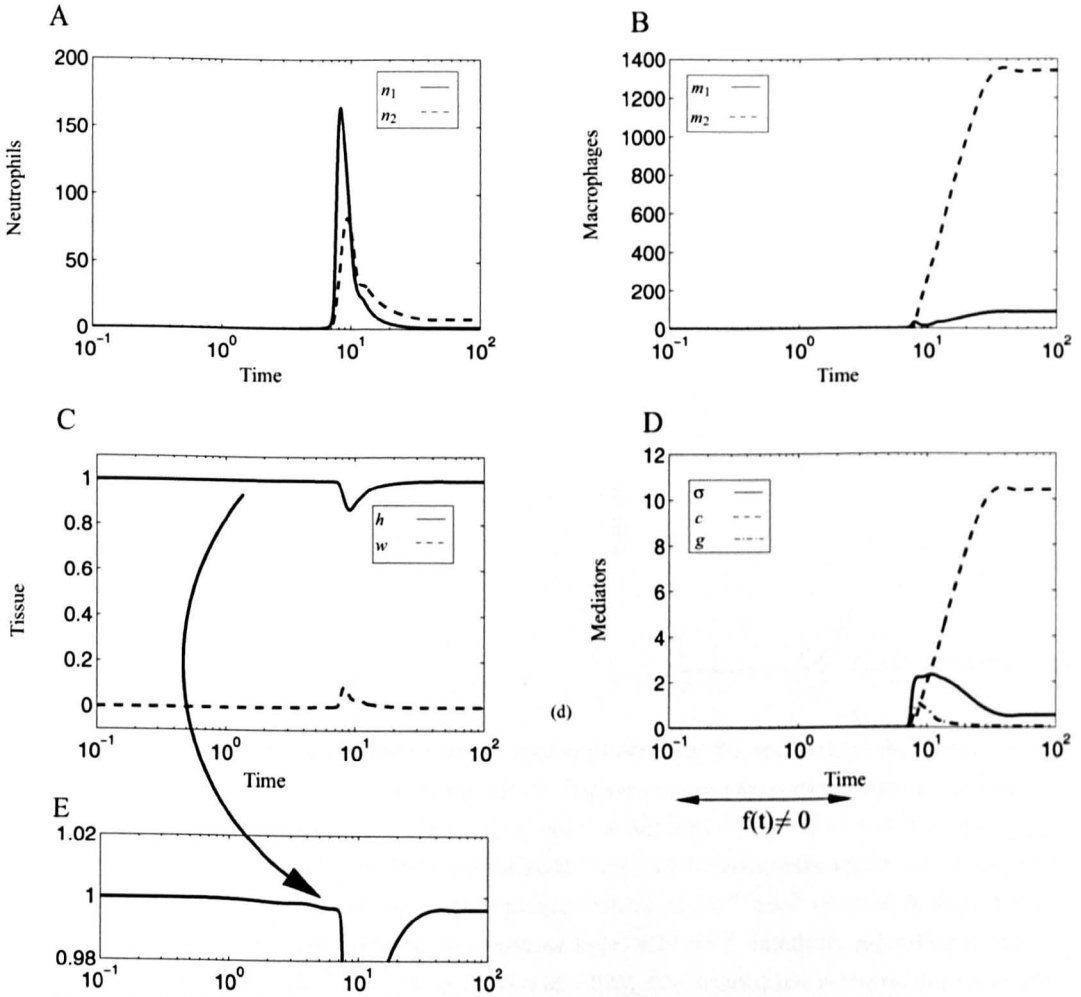

Figure 6.11: Numerical simulations of equations (6.2.7) illustrating how the system evolves to steady state II. This is an unhealthy response to injury where positive values persist for all cells and mediators. The majority of macrophages have switched to an anti-inflammatory phenotype (B), releasing growth factors (D) that reduce the level of neutrophils but some neutrophils persist. Physiologically we relate this to chronic inflammation. Damage occurs to tissue (Panel C) and Panel E shows a zoomed in region of C demonstrating that at SSII $h \neq 1$. Note that the model is not designed to account explicitly for volume fractions such that $h + w \neq 1$. Parameter values are shown in Table 6.2. It is $f(t)$ that causes the inflammatory response, its duration being shown in panel D. In Figure 6.10 we presented results from a simulation in which all system parameters and initial conditions are identical, apart from $f(t)$. Assuming a macrophage volume of 10^{-6} mm^3 (Poulter & Turk, 1975), 1000 macrophages per mm^3 equates to a volume fraction of 10^{-3}. Similarly, assuming a typical neutrophil volume of 10^{-7} mm^3 (Ting-Beall *et al.*, 1993), 100 neutrophils per mm^3 converts to a volume fraction of 10^{-5}.

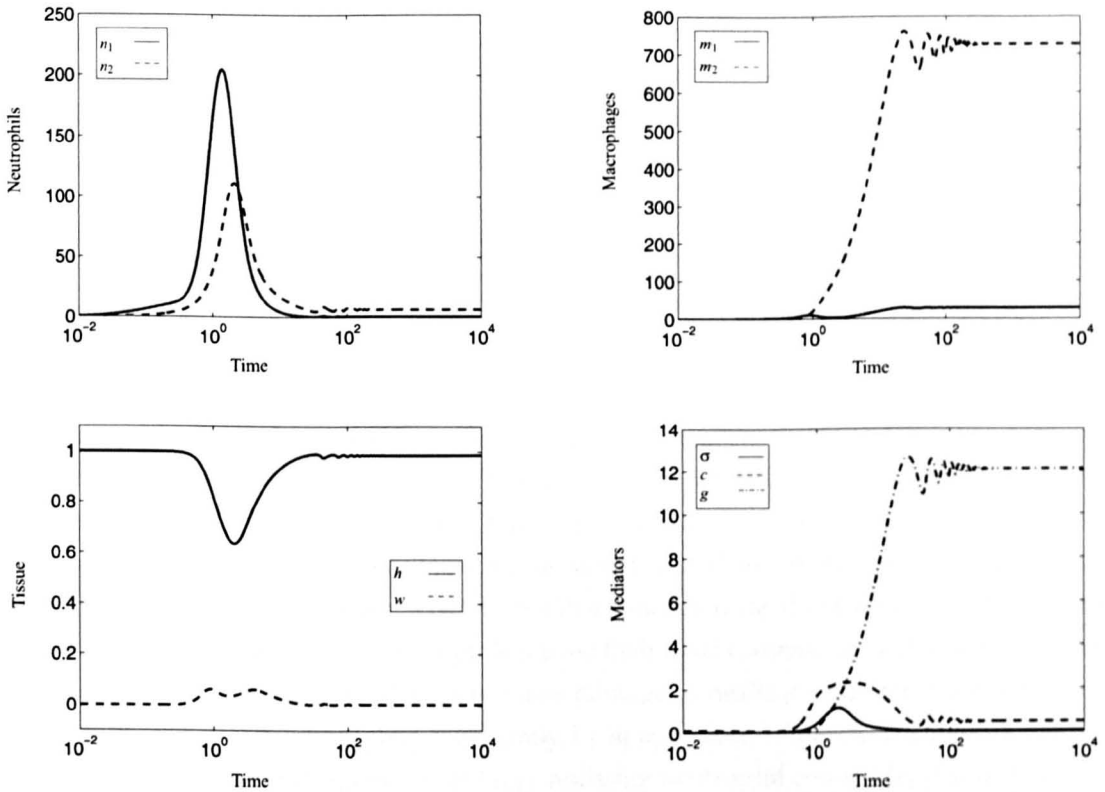

Figure 6.12: Numerical simulations of our model illustrating the oscillations that result when $k_g = 1$ pg cell^{-1} day^{-1}, $k_{cn2} = 0.01$ pg cell^{-1}. The remaining parameter values are shown in Table 6.2. Initial conditions $n_1 = n_2 = m_1 = m_2 = 0$ cell mm^{-3}, $h = 1$, $w = 0$, $\sigma = g = 0$ pg mm^{-3} , $c = 0.1$ pg mm^{-1}. It is the positive initial value of the chemoattractant that drives the inflammatory process. Assuming a macrophage volume of 10^{-6} mm^3 (Poulter & Turk, 1975), 1000 macrophages per mm^3 equates to a volume fraction of 10^{-3}. Similarly, assuming a typical neutrophil volume of 10^{-7} mm^3 (Ting-Beall *et al.*, 1993), 100 neutrophils per mm^3 converts to a volume fraction of 10^{-5}.

all cells and mediators are significantly greater than in Figure 6.10. As levels of anti-inflammatory macrophages and growth factors rise there is a drop in the levels of neutrophils, chemoattractants and neutrophil contents (all pro-inflammatory). However this is not sufficient to ensure a return to SSI. Instead the cells and their mediators settle to positive steady values and we term the resulting solution steady state II (SSII). Physiologically we can relate SSII to chronic inflammation where successful healing is not achieved because the inflammatory response is not resolved.

The model is also found to display damped oscillatory behaviour. This is dependent on modifications to the parameter values representing the production of growth factors (k_g) and the production of chemoattractants in response to secondary necrosis (k_{cn2}). Figure 6.12 shows

simulations exhibiting such behaviour. This oscillatory behaviour may be unphysiological but could be seen as repeated attempts to heal alternating with enhanced inflammation gradually subsiding and ending up at the non-trivial steady state.

As discussed above many of the parameter values had to be estimated or modified from the literature. Therefore, in the next section, we perform bifurcation analysis to understand better the system dynamics, investigating the influence of parameter variations on the outcome of the system (varying one parameter at a time, holding all others fixed). We will also discuss our intuitions about the effect of the positive and negative feedback mechanisms through the bifurcation diagrams. As the parameter space is vast we focus on a small subset comprising what we believe to be the key control parameters.

6.4 Feedback loops

The system (6.2.7) displays bistability. The positive and negative feedback loops incorporated in our model are shown schematically in Figures 6.13 and 6.14 respectively, and are intimately associated with the system's bistability. Only those feedback loops that are independent of external damage ($f(t) \neq 0$) are shown as it is assumed that all externally derived damage has been removed at the steady state. Positive feedback mechanisms (independent of $f(t)$) occur via two main pathways. Active neutrophils release their toxic contents ($k_{\sigma 1}$), in defence against suspected bacteria infiltration. These can cause damage to healthy tissue releasing, chemoattractants (k_{ch}). Active neutrophils die, naturally, by apoptosis (k_n). If apoptotic neutrophils are not removed they can undergo necrosis (γ_{n2}), releasing neutrophil content ($k_{\sigma 3}$) and chemoattractants (k_{cn2}). These positive feedback loops drive inflammation.

All negative feedbacks operate through macrophages, which increase within the system in response to chemoattractants. Macrophages remove apoptotic neutrophils (rate constants k_{nm1}, k_{nm2}) having a negative effect by preventing them undergoing secondary necrosis (γ_{n2}) the latter being a positive feedback mechanism. Macrophage engulfment of apoptotic neutrophils results in a switch in macrophage phenotype to an anti-inflammatory form whereby macrophages release various mediators (rate constant k_g). Growth factors have a complicated interaction with positive feedback loops. They dampen neutrophil influx and increase the rate of neutrophil apoptosis. Decreasing the population of active neutrophils is clearly anti-inflammatory as active neutrophils release toxic neutrophil contents ($k_{\sigma 1}$). An increase in the population of apoptotic neutrophils can be pro-inflammatory (if they undergo secondary necrosis (rate γ_{n2})) but, if macrophages safely remove apoptotic neutrophils then the pathway has an anti-inflammatory effect. Negative feedback loops can push the inflammatory response towards resolution and a healthy outcome.

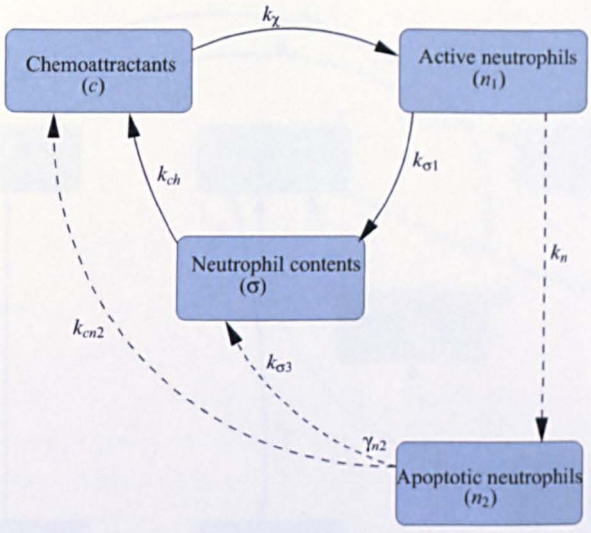

Figure 6.13: Network diagram showing the positive, pro-inflammatory feedback loops. Positive feedbacks that effect the stability of the steady states operate through two pathways. The first through the release of neutrophil contents from active neutrophils ($k_{\sigma 1}$) that can cause damage to healthy tissue (not shown to simplify the diagram) and the subsequent release of chemoattractants (k_{ch}). The second pathway operates via neutrophil apoptosis (k_n) which can then turn necrotic releasing neutrophil contents ($k_{\sigma 3}$) and chemoattractants (k_{cn2}). Negative feedback loops are showin in Figure 6.14.

6.5 Key control parameters

We focus on three key parameters: the production rate of anti-inflammatory growth factor (k_g), which forms part of the negative feedback loop that operates through dampening neutrophil influx enhancing neutrophil apoptosis; the rate of neutrophil apoptosis (k_n); and the rate at which neutrophils undergo secondary necrosis (γ_{n2}), a positive feedback mechanism. The rate of neutrophil apoptosis (k_n) is of particular interest as a therapeutic target it being believed that increasing this rate will enhance the resolution of inflammation (Hallett *et al.*, 2008; Rossi *et al.*, 2007). All bifurcation diagrams are produced with AUTO with the resulting data plotted with MATLAB. They all show the steady state of the chemoattactant as a function of the parameter being varied. We choose this variable as the chemoattractant is central to the system, driving inflammation.

6.5.1 Anti-inflammatory growth factor (rate constant k_g)

A generic growth factor or anti-inflammatory mediator (g) is included in the model. It has two anti-inflammatory effects: it enhances the rate of neutrophil apoptosis and dampens neutrophil influx (see Figure 6.14). It should be noted that while dampening neutrophil influx is clearly anti-inflammatory, increasing neutrophil apoptosis plays a more complicated role. For the growth factor to have an anti-inflammatory effect the increased levels of apoptotic neutrophils need to be removed before they progress to secondary necrosis.

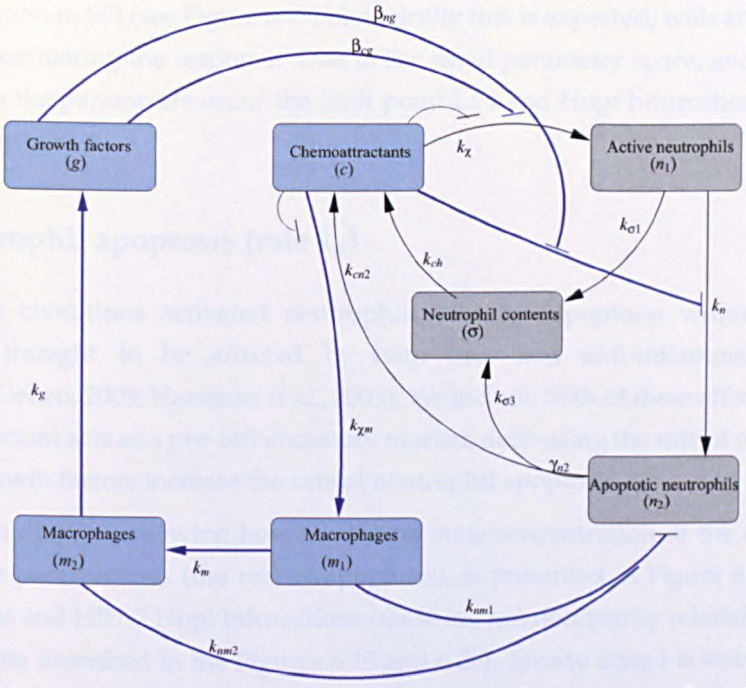

Figure 6.14: Network diagram showing the negative, anti-inflammatory feedback loops (blue). Positive feedback loops are shown (black) for completeness. Macrophages are central to negative feedback loops acting through the removal of apoptotic neutrophils (k_{nm1}, k_{nm2}) and through the release of growth factors (rate k_g), which dampen neutrophil influx and increase the rate of neutrophil apoptosis.

Figure 6.15 illustrates the bifurcation behaviour of the system (6.2.6) in terms of the concentration of the chemoattractant as k_g varies. LP1-4 indicate limit points and HB1-2 indicate Hopf bifurcations. There is an interval of bistability (LP1 $< k_g <$ HB1) where both steady states are stable. For values of $k_g <$ LP1 the system is monostable with SSI stable. This is unexpected: biologically we would expect the system to resolve to SSII (an unhealthy state) if levels of the anti-inflammatory growth factor are low. Time-dependent solutions of the system with values of k_g in this range (Figure 6.16) illustrate that levels of healthy tissue decline to zero, which is of course unphysical. With $h = 0$ the positive feedback loops (functioning through neutrophil contents (σ)) that normally drive inflammation are turned off. The system then settles to SSI, a healthy response.

Steady state II gains stability at LP1, and loses stability via a subcritical Hopf bifurcation at HB1. A Hopf bifurcation involves the loss of stability of a steady state and the emergence of a periodic solution and as we can see time-dependent solutions of the system with k_g set to just before the Hopf bifurcation display damped oscillations (see Figure 6.17).

For values to the right of HB1 only the lower steady state is stable, while the upper and the middle are unstable. Tissue damage now results in excitable behaviour, in the sense that there is a large build up of cells and mediators before the system ultimately relaxes to steady state I (see Figure 6.18). The unstable steady state that folds under from steady state II remains positive for its entire length. Time-dependent solutions with values of k_g to the right of LP2

result in resolution to SSI (see Figure 6.19) biologically this is expected, with anti-inflammatory mechanisms dominating the response. Due to the small parameter space, and the unphysical range in which the parameters occur the limit point LP4 and Hopf bifurcation at HB2 are not investigated further.

6.5.2 Neutrophil apoptosis (rate k_n)

Under normal conditions activated neutrophils undergo apoptosis within a few hours. This rate is thought to be affected by both pro- and anti-inflammatory mediators (Kobayashi & DeLeo, 2009; Heasman *et al.*, 2003). We include both of these effects in our model; the chemoattractant acts as a pro-inflammatory marker, decreasing the rate of neutrophil apoptosis, while growth factors increase the rate of neutrophil apoptosis.

The bifurcation diagram showing how the steady state concentration of the chemoattractant varies with the parameter k_n (the rate of apoptosis), is presented in Figure 6.21. LP1-2 indicate limit points and HB1-2 Hopf bifurcations (these are not necessarily related to the similarly numbered points described in the Figures 6.15 and 6.26). Steady state I is stable for all values of k_n. For very low values of neutrophil apoptosis ($k_n <$ LP1 (see Figure 6.15)) there is a unique stable steady state which corresponds to SS1 (values of k_n in this range are unlikely to be physical, neutrophils would die very slowly). There is a fold bifurcation at $k_n =$ LP1 and for LP1 $< k_n <$ HB1 we have a small area of parameter space where the system has one stable steady state and two unstable. At the subcrisitical Hopf bifurcation (HB1) we have a second branch of stable solutions which correspond to SSII. In fact, we have bistability for all $k_n >$ HB1.

It could be expected that a high level of neutrophil apoptosis would have an anti-inflammatory effect with the system always settling to steady state I. The bifurcation diagram (Figure 6.21) does not display this behaviour. From time-dependent simulations (Figure 6.23) with a high rate of neutrophil apoptosis ($k_n = 10\ \text{day}^{-1}$) we can see that though there is a large number of macrophages present neutrophils, though declining significantly, are not being fully removed. By increasing the rate of macrophage phagocytosis of neutrophils (k_{nm1}) we can modify the structure of the bifurcation diagram (see Figure 6.22). Now, even with a high level of stimulus, time-dependent solutions with a high value of neutrophil apoptosis ($k_n = 10$) result in the model resolving to steady state I (see Figure 6.24). Due to the upper two steady states being unstable this takes a large excursion through parameter space before all mediators and cells settle to zero. .

6.5.3 Secondary necrosis (rate γ_{n2})

Apoptotic neutrophils eventually break down, losing membrane integrity so that their granules release their toxic content and chemoattractants into the surrounding tissue. This has a pro-inflammatory effect, termed secondary necrosis, that is incorporated in our model via the parameters γ_{n2}, $k_{\sigma 3}$ and k_{cn2}.

In Figure 6.26 we present a bifurcation diagram showing the concentration of the chemoattrac-

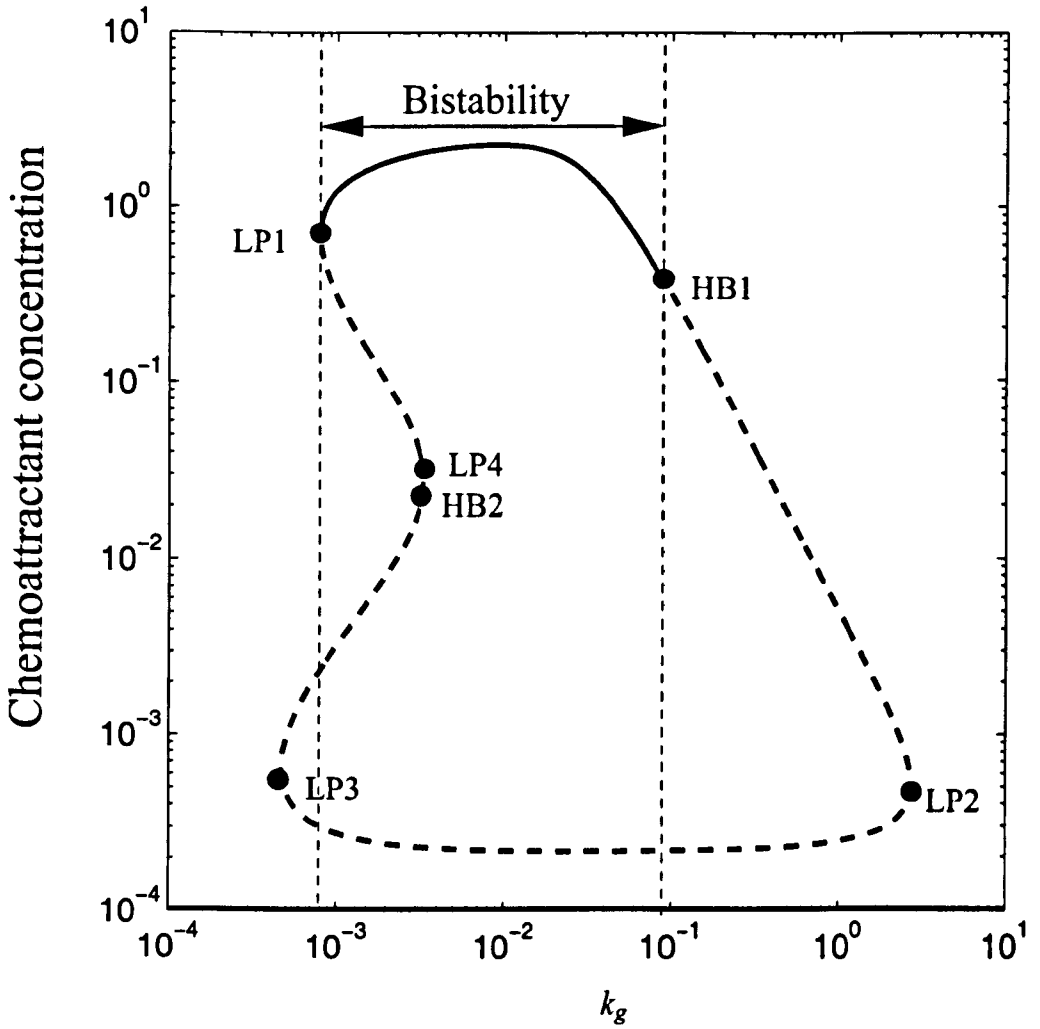

Figure 6.15: Bifurcation diagram showing how the existence and stability of the steady state solutions change as k_g (the rate that macrophages produce growth factor) varies, other parameter values held fixed (see Table 6.2). SSI is represented by the green line and SSII by the blue. Stable steady states are shown as solid lines and unstable ones by dotted lines. The system is bistable for an intermediate range of k_g (LP1< k_g <HB1). SSII gains stability at LP1 and loses stability via a subcritical Hopf bifurcation (HB1). To the right of HB1 there is an area where the upper two steady states are unstable and the lower stable (see Figure 6.18 for time-dependent solutions in this range). At k_g > LP2 there is only one steady state (SSI) (see Figure 6.19 for time-dependent solutions in this range). (LP1, $k_g = 7.88 \times 10^{-4}, c = 6.91 \times 10^{-1}$; LP2, $k_g = 2.73, c = 5.15 \times 10^{-4}$; LP3, $k_g = 4.66 \times 10^{-4}, c = 6.44 \times 10^{-4}$; LP4, $k_g = 3.26 \times 10^{-3}, c = 6.2.77 \times 10^{-2}$; HB1, $k_g = 8.29 \times 10^{-2}, c = 4.21 \times 10^{-1}$; HB2, $k_g = 3.26 \times 10^{-3}, c = 6.272 \times 10^{-2}$.)

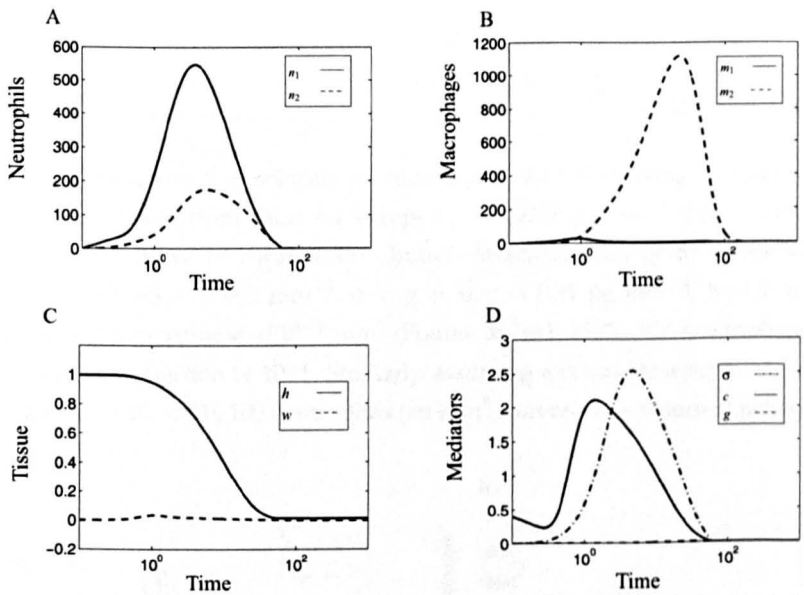

Figure 6.16: Time-dependent solution of equations (6.2.6) illustrating resolution to SSI for very low values the parameter k_g. Healthy tissue being depleted (panel C). Parameter values taken from Table 6.2 except $k_g = 0.0001$ pg cell^{-1} day^{-1}. Initial conditions are slightly perturbed from SSI ($n_1 = n_2 = m_1 = m_2 = 0$ cell mm^{-3}, $\sigma = g = 0$ pg mm^{-3}, $c = 0.4$ pg mm^{-3} $h = 1$, $w = 0$). Assuming a macrophage volume of 10^{-6} mm^3 (Poulter & Turk, 1975), 1000 macrophages per mm^3 equates to a volume fraction of 10^{-3}. Similarly, assuming a typical neutrophil volume of 10^{-7} mm^3 (Ting-Beall *et al.*, 1993), 100 neutrophils per mm^3 converts to a volume fraction of 10^{-5}.

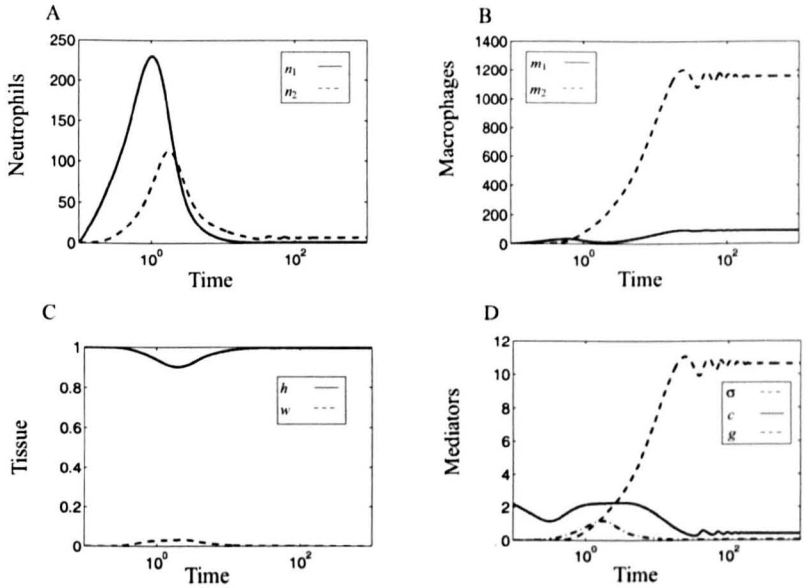

Figure 6.17: Time-dependent solution of equations (6.2.6) illustrating damped oscillations. Parameter values taken from Table 6.2 except $k_g = 0.083$ pg cell^{-1} day^{-1} (HB1 in the bifurcation diagram shown in Figure 6.15). Initial conditions are slightly perturbed from SSI ($n_1 = n_2 = m_1 = m_2 = 0$ cell mm^{-3}, $\sigma = g = 0$, $c = 0.42$ pg mm^{-3}, $h = 1$, $w = 0$). Assuming a macrophage volume of 10^{-6} mm^3 (Poulter & Turk, 1975), 100 macrophages per mm^3 equates to a volume fraction of 10^{-4}. Similarly, assuming a typical neutrophil volume of 10^{-7} mm^3 (Ting-Beall *et al.*, 1993), 100 neutrophils per mm^3 converts to a volume fraction of 10^{-5}.

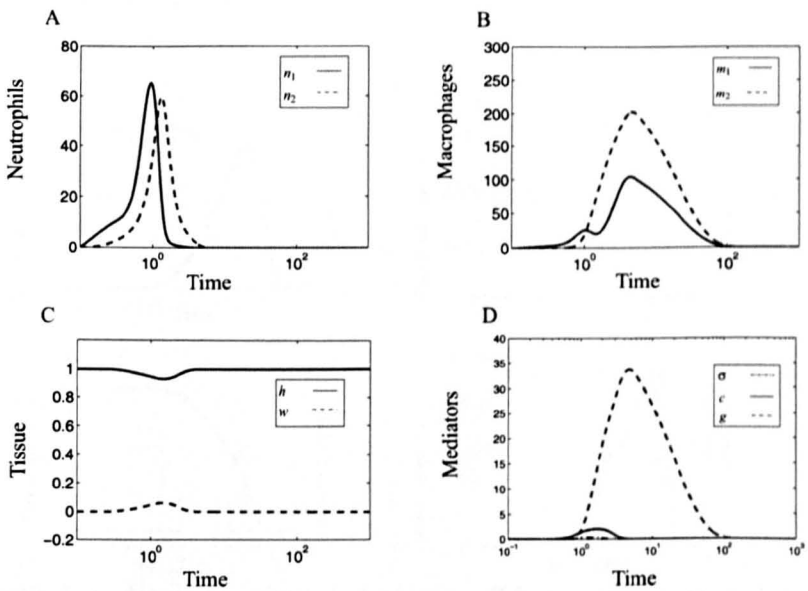

Figure 6.18: Time-dependent solutions of equations (6.2.6) illustrating excitable behaviour. Parameter values taken from Table 6.2 except $k_g = 1.55$ pg cell$^-$ day^{-1} (a point between HB1 and LP1 in the bifurcation diagram shown in Figure 6.15). Initial conditions are slightly perturbed from SSI ($n_1 = n_2 = m_1 = m_2 = 0$ cell mm^{-3}, $\sigma = g = 0$, $c = 0.001$ pg mm^{-3}, $h = 1$, $w = 0$). Assuming a macrophage volume of 10^{-6} mm^3 (Poulter & Turk, 1975), 100 macrophages per mm^3 equates to a volume fraction of 10^{-4}. Similarly, assuming a typical neutrophil volume of 10^{-7} mm^3 (Ting-Beall *et al.*, 1993), 100 neutrophils per mm^3 converts to a volume fraction of 10^{-5}.

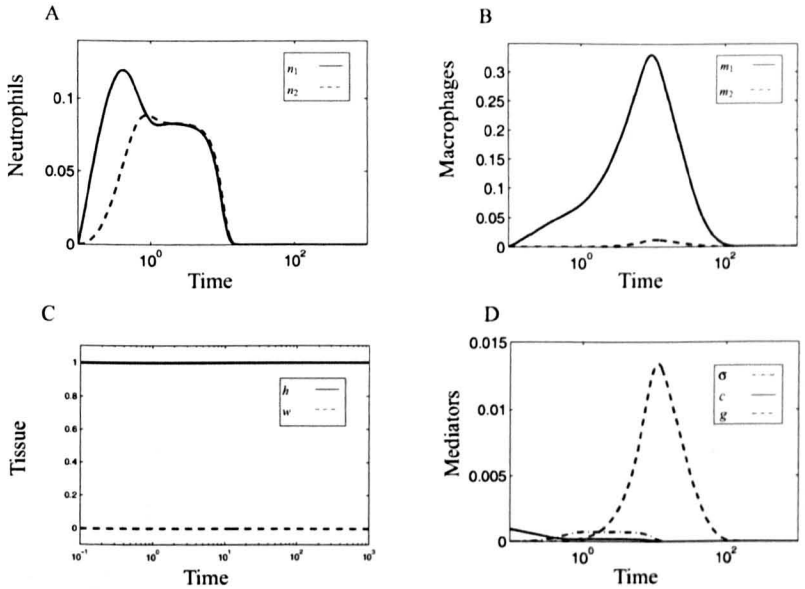

Figure 6.19: Time-dependent solutions of equations (6.2.6) illustrating resolution to SSI for large values of k_g. Parameter values taken from Table 6.2 except $k_g = 20$ pg cell^{-} day^{-1} (a point between HB1 and LP2 in the bifurcation diagram shown in Figure 6.15). Initial conditions are slightly perturbed from SSI ($n_1 = n_2 = m_1 = m_2 = 0$ cell mm^{-3}, $\sigma = g = 0$, $c = 0.001$ pg mm^{-3}, $h = 1$, $w = 0$).Assuming a macrophage volume of 10^{-6} mm^3 (Poulter & Turk, 1975), 0.1 macrophages per mm^3 equates to a volume fraction of 10^{-7}. Similarly, assuming a typical neutrophil volume of 10^{-7} mm^3 (Ting-Beall *et al.*, 1993), 0.1 neutrophils per mm^3 converts to a volume fraction of 10^{-8}.

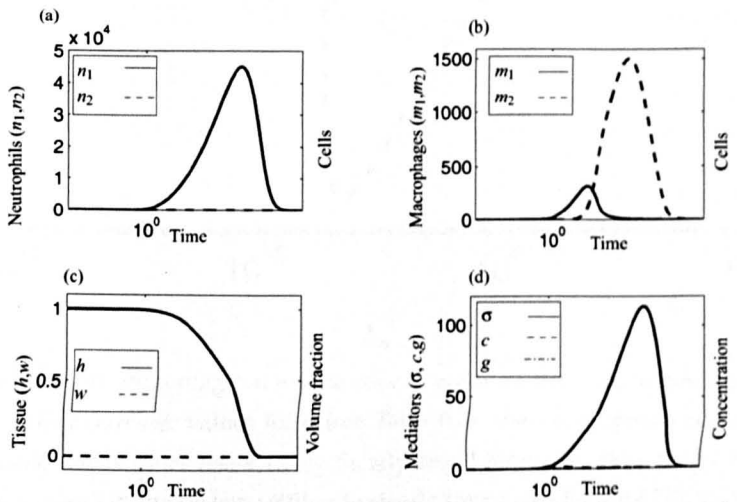

Figure 6.20: Time-dependent solutions of equations (6.2.6) illustrating resolution to SSI with very low values of neutrophil apoptosis. Parameter values taken from Table 6.2 except $k_n = 0.0003$ day^{-1}. Initial conditions where such that the system was slightly perturbed from SSI ($n_1 = n_2 = m_1 = m_2 = 0$ cell mm^{-3}, $\sigma = g = 0$, $c = 0.1$ pg mm^{-3}, $h = 1$, $w = 0$). Assuming a macrophage volume of 10^{-6} mm^3 (Poulter & Turk, 1975), 1000 macrophages per mm^3 equates to a volume fraction of 10^{-3}. Similarly, assuming a typical neutrophil volume of 10^{-7} mm^3 (Ting-Beall *et al.*, 1993), 10000 neutrophils per mm^3 converts to a volume fraction of 10^{-3}.

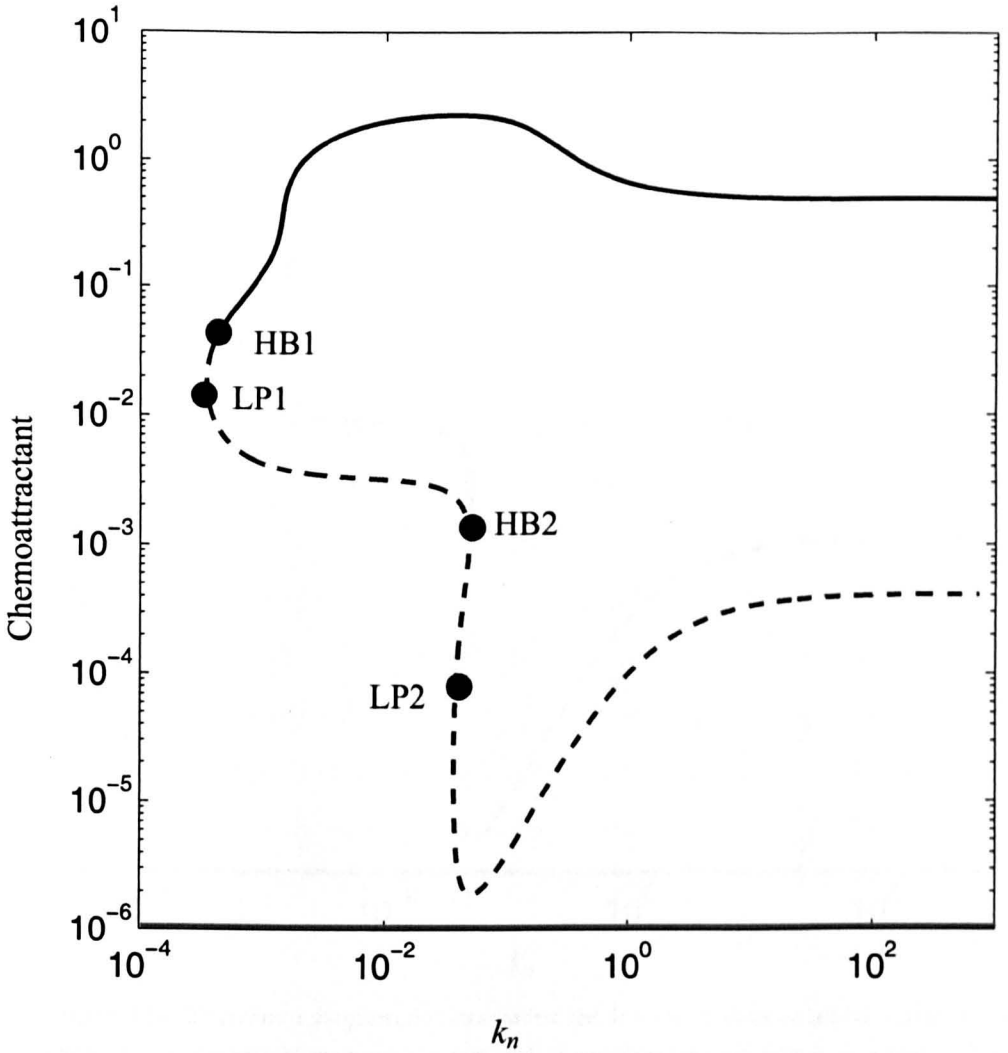

Figure 6.21: Bifurcation diagram for the concentration of the chemoattractant as a function of k_n with other parameter values fixed (see Table 6.2). Full and broken curves indicate stable and unstable steady states respectively. Steady state I (green) is stable for all values of k_n. Low values of k_n result in the system settling to steady state I (see Figure 6.20); values of k_n this low are likely to be non-physical. Bistability occurs for HB1 $< k_n$ where steady state II (blue) is stable. (LP1, $k_n = 3.44 \times 10^{-4}$, $c = 8.19 \times 10^{-2}$; LP2, $k_n = 3.66 \times 10^{-2}$, $c = 1.8 \times 10^{-5}$; HB1, $k_n = 5.02 \times 10^{-4}$, $c = 5.41 \times 10^{-2}$; HB2, $k_n = 4.83 \times 10^{-2}$, $c = 1.07 \times 10^{-3}$.)

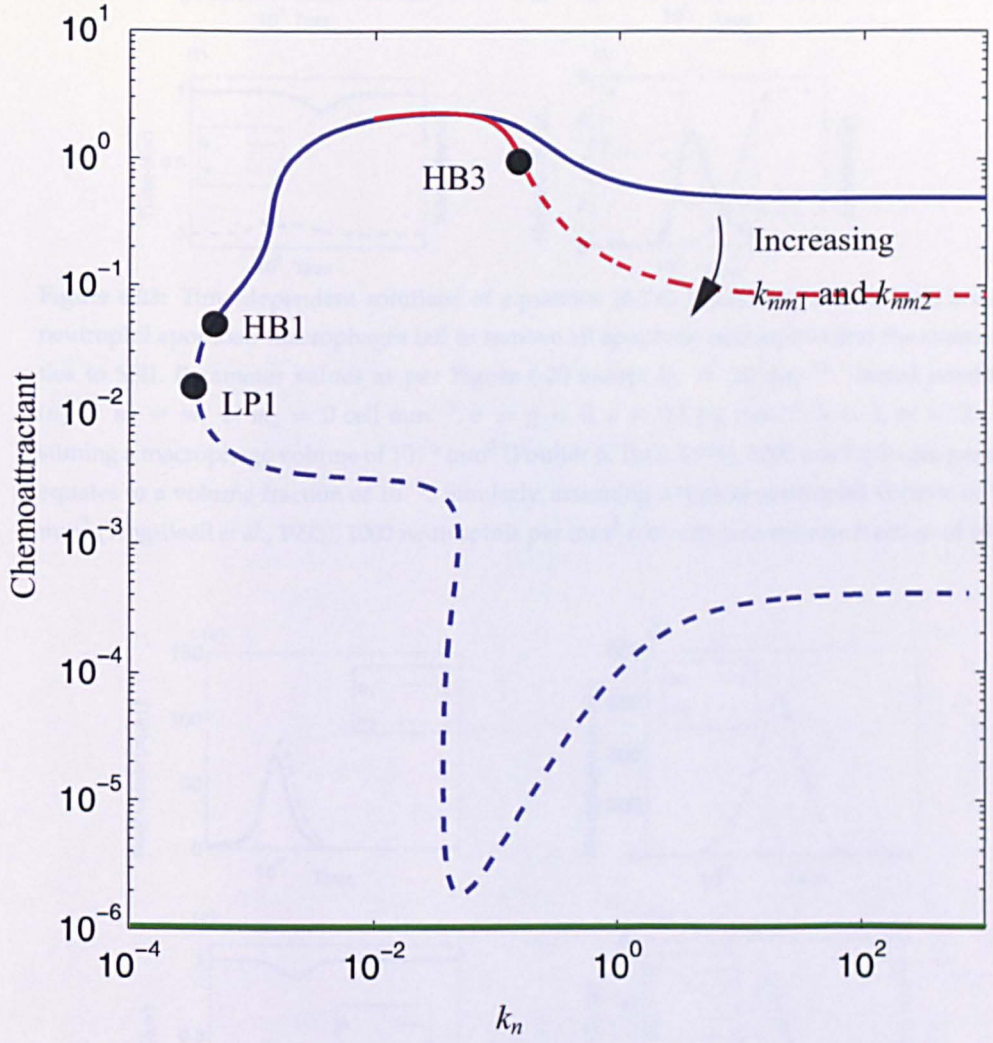

Figure 6.22: Bifurcation diagram demonstrating the introduction of an additional Hopf bifurcation when the rate of macrophage removal of apoptotic neutrophils is increased. The diagram is for the concentration of the chemoattractant as a function of k_n. All other parameter values are fixed (see Table 6.2) apart from k_n (neutrophil apoptosis), k_{nm1} and k_{nm2} (the rates of macrophage phagocytosis of apoptotic neutrophils) which is different for each bifurcation curve. The original bifurcation curve (Figure 6.21 ($k_{nm} = 0.0001$)) is shown in blue and where the new curve departs from this in red. The new curve has k_n increased by two orders of magnitude ($k_{nm1} = 0.01$, $k_{nm2} = 0.001$). Full and broken curves indicate stable and unstable steady states respectively. The introduction of HB3 ($k_n \approx 0.15$ day^{-1}) changes the stability of SSII meaning that at high rates of neutrophil apoptosis the system now resolves to SS1.

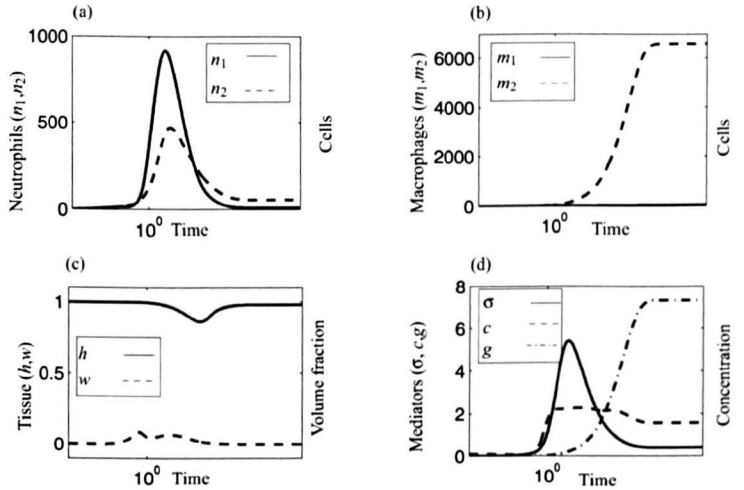

Figure 6.23: Time-dependent solutions of equations (6.2.6) illustrating that at high levels of neutrophil apoptosis macrophages fail to remove all apoptotic neutrophils and the system settles to SSII. Parameter values as per Figure 6.20 except $k_n = 10$ day^{-1}. Initial conditions ($n_1 = n_2 = m_1 = m_2 = 0$ cell mm^{-3}, $\sigma = g = 0$, $c = 0.1$ pg mm^{-3}, $h = 1$, $w = 0$,). Assuming a macrophage volume of 10^{-6} mm^3 (Poulter & Turk, 1975), 1000 macrophages per mm^3 equates to a volume fraction of 10^{-3}. Similarly, assuming a typical neutrophil volume of 10^{-7} mm^3 (Ting-Beall *et al.*, 1993), 1000 neutrophils per mm^3 converts to a volume fraction of 10^{-4}.

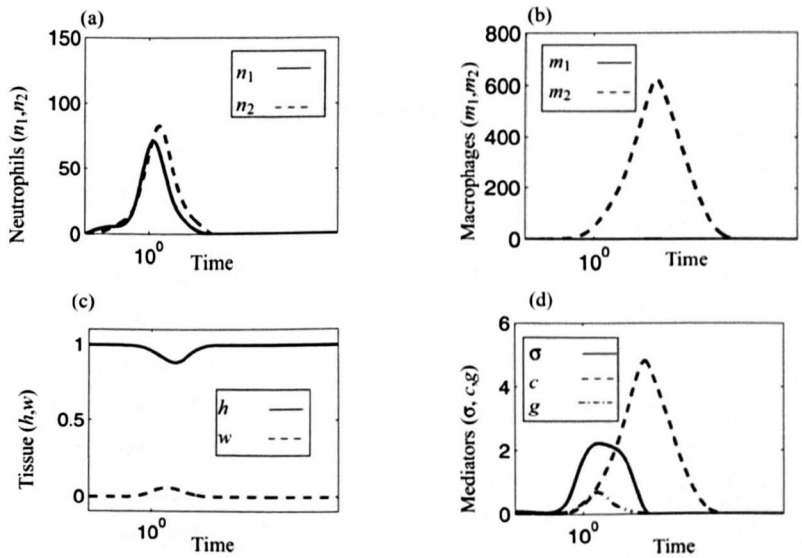

Figure 6.24: Time-dependent solutions of equations (6.2.6) illustrating that at high levels of neutrophil apoptosis the system resolves to SSI. This is dependent on the increase on the rate that macrophages remove neutrophils (k_{nm1}, k_{nm2}), which we have increased. Parameter values taken from Table 6.2 except $k_n = 10$ day^{-1}, $k_{nm1} = 0.01$, $k_{nm2} = 0.001$ cell^{-1} mm^3 day^{-1}. Initial conditions where such that the system was perturbed from SSI ($n_1 = n_2 = m_1 = m_2 = 0$ cell mm^{-3}, $\sigma = g = 0$, $c = 0.1$ pg mm^{-3}, $h = 1$, $w = 0$). Assuming a macrophage volume of 10^{-6} mm^3 (Poulter & Turk, 1975), 1000 macrophages per mm^3 equates to a volume fraction of 10^{-3}. Similarly, assuming a typical neutrophil volume of 10^{-7} mm^3 (Ting-Beall *et al.*, 1993), 100 neutrophils per mm^3 converts to a volume fraction of 10^{-5}.

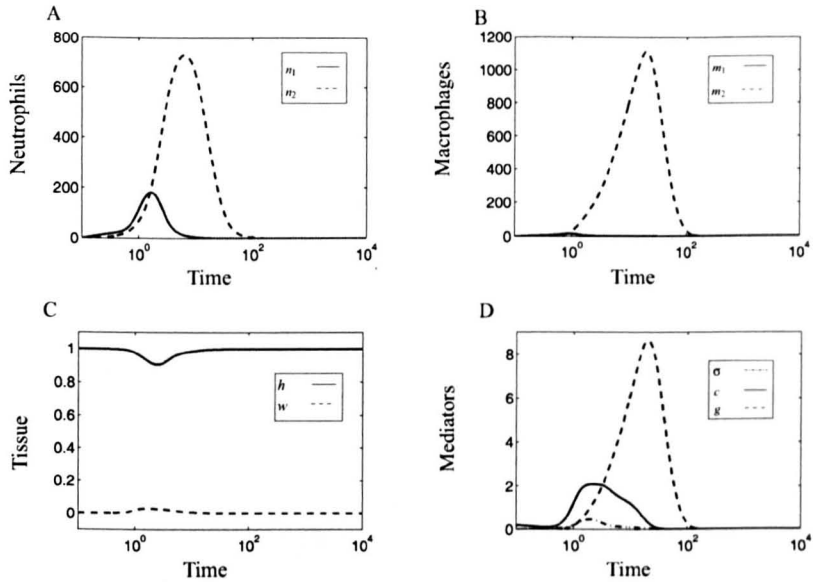

Figure 6.25: Time-dependent solutions of equations (6.2.6) illustrating resolution to SSI with $HB1 < \gamma_{n2} < HB2$ (Figure 6.26). Parameter values taken from Table 6.2 except $\gamma_{n2} = 0.035$ day^{-1}. Initial conditions are slightly perturbed from SSI ($n_1 = n_2 = m_1 = m_2 = 0$ cell mm^{-3}, $\sigma = g = 0$, $c = 0.1$ pg mm^{-3}, $h = 1$, $w = 0$,). The simulations show that a small perturbation from SSI results in all species returning to SSI after a large excursion in parameter space. Assuming a macrophage volume of 10^{-6} mm^3 (Poulter & Turk, 1975), 1000 macrophages per mm^3 equates to a volume fraction of 10^{-3}. Similarly, assuming a typical neutrophil volume of 10^{-7} mm^3 (Ting-Beall *et al.*, 1993), 100 neutrophils per mm^3 converts to a volume fraction of 10^{-5}.

tant as a function of γ_{n2}, the rate of secondary necrosis. Once again Steady state I is stable for all values of γ_{n2}. Very low values of secondary necrosis ($\gamma_{n2} <$ LP1) result in macrophages being able to remove all apoptotic neutrophils before they can undergo necrosis. There are two areas of bistability, steady state II gains stability at LP1 and loses stability via a Hopf bifurcation HB1 for a small area of parameter space. SSII then gains stability at a further Hopf bifurcation and retains this until very high values of secondary necrosis (LP2). Figure 6.25 shows time-dependent simulations for a rate of secondary necrosis in the middle region between the two Hopf bifurcations ($\gamma_{n2} = 0.01$ day^{-1}). In this region steady state I is stable and both branches of steady state II are unstable, a small perturbation from steady state I results in all species returning to steady state I through a large excursion. Time-dependent simulations with γ_{n2} close to HB1 or HB2 display damped oscillations (see Figures 6.27 and 6.28 respectively). Large values of secondary necrosis (γ_{n2}>LP2 result in the system settling to SSI, while values of secondary necrosis this large are entirely unphysical this is slightly unexpected.

6.6 Discussion and further work

In this chapter we have presented a model of the inflammatory response to tissue damage. Inflammation is not only of interest as a response to skeletal tissue damage but persistent inflammation is recognised as a central process in the pathogenesis of many diverse diseases

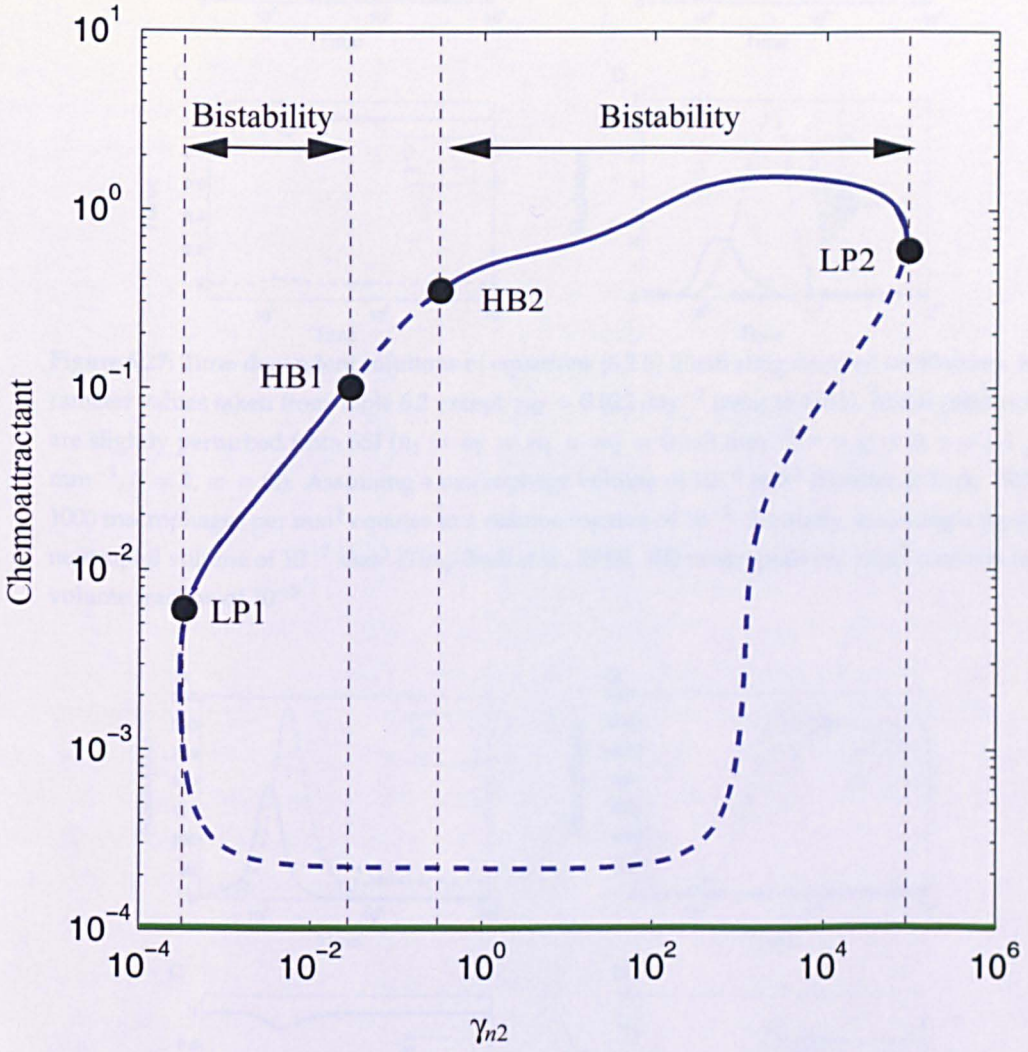

Figure 6.26: Bifurcation diagram showing how the existence and stability of the steady state solutions change as γ_{n2} (the rate of secondary necrosis) varies, other parameter values held fixed (see Table 6.2). SSI is represented by the red line and SSII by the blue. Stable steady states are shown as solid lines and unstable ones by dotted lines. Steady state I (green) is stable for all values of γ_{n2}. Low values of secondary necrosis ($\gamma_{n2} <$ LP1) result in the system settling to steady state I. There are two intervals of bistability LP1 $< \gamma_{n2} <$ HB1 and HB2 $< \gamma_{n2} <$ LP2. High values of γ_{n2} result in SSI being acheived. (LP1, $\gamma_{n2} = 2.96 \times 10^{-4}$, $c = 2.61 \times 10^{-3}$; LP2, $\gamma_{n2} = 8.48 \times 10^{4}$, $c = 6.38 \times 10^{-1}$; HB1, $\gamma_{n2} = 2.61 \times 10^{-2}$, $c = 1.03 \times 10^{-1}$; HB2, $\gamma_{n2} = 4.59 \times 10^{-2}$, $c = 3.97 \times 10^{-1}$

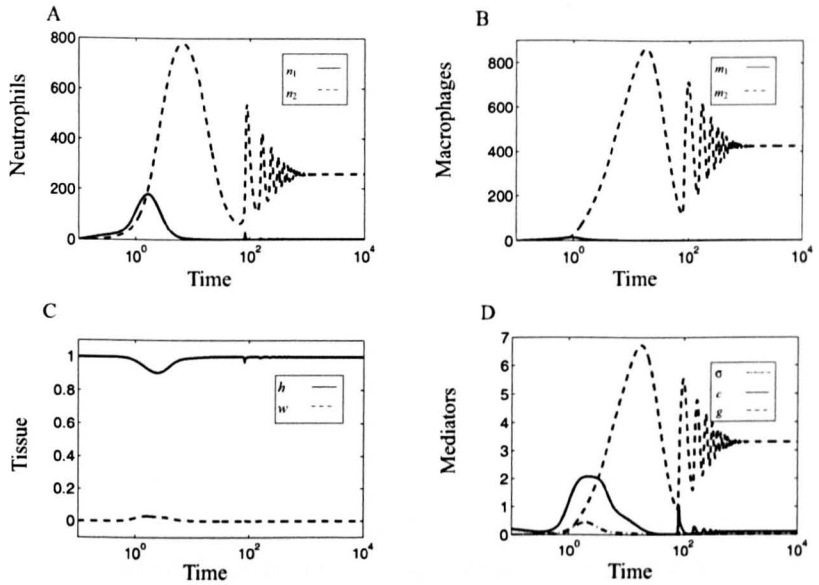

Figure 6.27: Time-dependent solutions of equations (6.2.6) illustrating damped oscillations. Parameter values taken from Table 6.2 except $\gamma_{n2} = 0.022$ day^{-1} (near to HB1). Initial conditions are slightly perturbed from SSI ($n_1 = n_2 = m_1 = m_2 = 0$ cell mm^{-3}, $\sigma = g = 0$, $c = 0.1$ pg mm^{-3}, $h = 1$, $w = 0$,). Assuming a macrophage volume of 10^{-6} mm^3 (Poulter & Turk, 1975), 1000 macrophages per mm^3 equates to a volume fraction of 10^{-3}. Similarly, assuming a typical neutrophil volume of 10^{-7} mm^3 (Ting-Beall *et al.*, 1993), 100 neutrophils per mm^3 converts to a volume fraction of 10^{-5}.

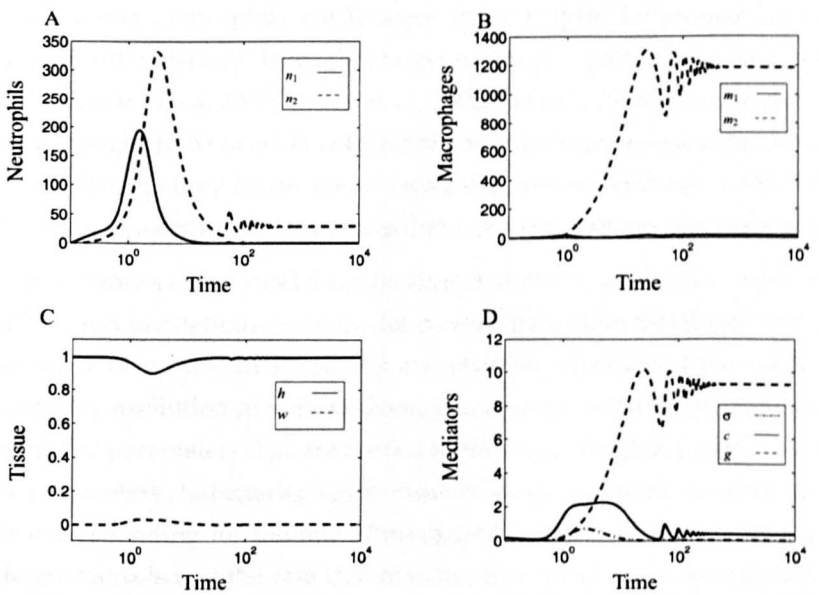

Figure 6.28: Time-dependent solutions of equations (6.2.6) illustrating damped oscillations. Parameter values taken from Table 6.2 except $\gamma_{n2} = 0.05$ day^{-1} (near to HB2). Initial conditions are slightly perturbed from SSI ($n_1 = n_2 = m_1 = m_2 = 0$ cell mm^{-3}, $\sigma = g = 0$, $c = 0.1$ pg mm^{-3}, $h = 1$, $w = 0$,). Assuming a macrophage volume of 10^{-6} mm^3 (Poulter & Turk, 1975), 1000 macrophages per mm^3 equates to a volume fraction of 10^{-3}. Similarly, assuming a typical neutrophil volume of 10^{-7} mm^3 (Ting-Beall *et al.*, 1993), 100 neutrophils per mm^3 converts to a volume fraction of 10^{-5}.

including bronchial asthma, Alzeihemer's, cystic fibrosis and chronic obstructive pulmonary disease (Maderna & Godson, 2003; Haslett, 1999). The resolution of inflammation is crucial if tissue is to be repaired and was thought to be a passive process but is now recognised as an active process with dysregulation of key features of resolution contributing to inflammatory diseases (Rossi *et al.*, 2007). Previous mathematical models concentrate on single populations of white blood cells and the mechanisms that drive inflammation (Lauffenburger & Keller, 1979; Lauffenburger & Kennedy, 1981, 1983; Alt & Lauffenburger, 1985). We incorporate recent biological evidence that the resolution of inflammation is dependent on active anti-inflammatory processes centering around the interaction between separate populations of white blood cells (namely neutrophils and macrophages) and the interactions between them. Our model incorporates damage being caused in the functional form $f(t)$ and this can be modified to model different disease scenarios.

Neutrophils can play a dual role in inflammation, being essential, in a dirty environment, for the removal and killing of bacteria but, via the same mechanisms, they can cause damage to healthy tissue (Whyte *et al.*, 2008). They have a short life dying naturally via apoptosis. Apoptotic neutrophils can further break down (a process called secondary necrosis) spilling their toxic content and causing further damage to tissue (Serhan *et al.*, 2008). Macrophages are thought to be central to anti-inflammatory pathways safely removing apoptotic neutrophils and releasing anti-inflammatory mediators that actively dampen pro-inflammatory processes (Sampson, 2000; Gordon & Taylor, 2005). In sterile environments , such as tendon ruptures or wounds inflicted during surgery, the role of neutrophils is controversial. Within the context of muscle loading neutrophils are thought to be helpful for muscle hypertrophy with non-steroidal anti-inflammatory drugs that target neutrophil pathways being shown to impair muscle growth (Koh & Pizza, 2009; Toumi *et al.*, 2006; Tidball, 2005). In a surgical environment neutrophils are thought to be at odds with rapid healing (Szpaderska & DiPietro, 2005). Neutrophils, and the damage they cause, are of increasing interest and our model tries to capture some of their characteristics by incorporating them as a seperate species from macrophages.

We find that its dynamics of our model can be classified into four regimes: monostability, bistability, excitability and oscillations. Our model demonstrates that bistability and hysteresis exists in a wide range of parameter space and we relate the outcome of the stable steady states to either the healthy resolution of inflammation or a chronic, self-perpetuating state. We focus on a small subset of parameters that are central to the many feedback mechanisms within our model. These parameters characterise key features of the interactions between neutrophils and macrophages corresponding to: the rate of neutrophil apoptosis, the rate that apoptotic neutrophils undergo necrosis and the rate that macrophages produce growth factors. We explore the effects of perturbing these parameters via bifurcation diagrams and use the model to identify how these parameters govern the behaviour of the system toward the different outcomes. While we believe that we have identified the key large time outcomes we have not attempted to capture all the unstable branches or dependence on all of the parameters.

There is much interest in finding new therapeutic drugs to limit inflammation with the hope that, where the persistence of inflammation has become divorced from the inciting agent, tar-

geting pro-resolution pathways will offer some success (Serhan *et al.*, 2007; Pizza *et al.*, 2005). Particular targets under investigation are the rate that neutrophils undergo apoptosis and the ability of macrophages to remove them, both processes thought to be controllable by mediators (Rossi *et al.*, 2007; Henson, 2005; Maderna & Godson, 2003; Haslett, 1999). We have investigated the effect of perturbing the rate that neutrophils undergo necrosis in our model. We found that incresing neutrophil apoptosis is not necessarily anti-inflammatory, its effects being dependent on the ability of macrophages to remove neutrophils before they can cause further damage.

The model helps us to represent current knowledge about the mechanisms of inflammation, particularly its resolution and how neutrophils and macrophages might effect this. It has limitations imposed by the incomplete knowledge of the biology and a more sophisticated model may be possible as the parameter values and biological mechanisms are better described. Our model provides a good starting place in the modelling of inflammation that can be modified to incorporate further biological mechanisms as they are better understood. It demonstrates the damage that neutrophils can cause to healthy tissue leading to progression to a self-perpetuating inflammatory condition that is no longer reliant on the initial stimulus. The model demonstrates that therapeutic mechanisms that target the rate of neutrophil apoptosis, accelerating it with the aim of dampening inflammation may need to up-regulate the removal of apoptotic neutrophils.

CHAPTER 7

A spatial model of inflammation

7.1 Introduction

In the previous chapters we treated the problem as spatially homogeneous, with populations of cells and mediators in a well-mixed environment. While this provides useful insight, it is desirable to extend the model to investigate damage to tissue in a spatial form and, in particular, how the diffusion of mediators affect the outcome of the inflammatory phase. First, however, it is desirable to simplify the existing model, since adding this extra dimension will compound further its already uninviting complexity. We wish to retain the bistable outcome of the model, allowing us to relate the two stable steady states to subsidence of the inflammatory response or to progression to a self-perpetuating condition that is no longer reliant on the initial stimulus. We will concentrate on the central biological mechanisms of neutrophil apoptosis, necrosis and the removal of apoptotic neutrophils by macrophages allowing the bifurcation analysis of the previous chapter to guide us. As will become clear in what follows, the results here are preliminary ones and numerous other directions would be interesting to explore.

7.2 Simplifying the existing model

Let us remind ourselves of the system of dimensional ODEs

$$\frac{dn_1}{dt} = \frac{k_\chi c}{(\beta_\chi + c)\left(1+\frac{g}{\beta_{cg}}\right)} - \gamma_{n1} f(t) n_1 - \frac{k_n n_1 \left(1+\frac{g}{\beta_{ng}}\right)}{\left(1+\frac{c}{\beta_c}\right)}, \tag{7.2.1a}$$

$$\frac{dn_2}{dt} = \frac{k_n n_1 \left(1+\frac{g}{\beta_{ng}}\right)}{\left(1+\frac{c}{\beta_c}\right)} - \gamma_{n2} n_2 - \left(k_{nm1} m_1 - k_{nm2} m_2\right) n_2, \tag{7.2.1b}$$

$$\frac{dm_1}{dt} = \frac{k_{\chi m} c}{\beta_{\chi m} + c} - k_m k_{nm1} m_1 n_2 - \gamma_{m1} m_1, \tag{7.2.1c}$$

$$\frac{dm_2}{dt} = k_m k_{nm1} m_1 n_2 - \gamma_{m2} m_2, \tag{7.2.1d}$$

$$\frac{dh}{dt} = k_{hg}gh(1-h-w) - k_{ht}f(t)h - k_h h\left(\frac{\sigma^2}{\beta_\sigma^2+\sigma^2}\right)\sigma, \tag{7.2.1e}$$

$$\frac{dw}{dt} = k_{ht}f(t)h + k_h h\left(\frac{\sigma^2}{\beta_\sigma^2+\sigma^2}\right)\sigma + k_{w1}\gamma_{n1}f(t)n_1 + k_{w2}\gamma_{n2}n_2 - k_{wm1}m_1 w - k_{wm2}m_2 w - k_{wn}n_1 w, \tag{7.2.1f}$$

$$\frac{d\sigma}{dt} = k_{\sigma 1}n_1 + k_{\sigma 2}\gamma_{n1}f(t)n_1 + k_{\sigma 3}\gamma_{n2}n_2 - \gamma_{\sigma h}h\left(\frac{\sigma^2}{\beta_\sigma^2+\sigma^2}\right) - \gamma_\sigma\sigma, \tag{7.2.1g}$$

$$\frac{dc}{dt} = k_{cw}f(t)h + k_{ch}h\left(\frac{\sigma^2}{\beta_\sigma^2+\sigma^2}\right) + k_{cn1}\gamma_{n1}f(t)n_1 + k_{cn2}\gamma_{n2}n_2 - (\gamma_{cn}n_1 + \gamma_{cm}m_1)c - \gamma_c c, \tag{7.2.1h}$$

$$\frac{dg}{dt} = k_g m_2 - \gamma_{gn}n_1 g - \gamma_g g. \tag{7.2.1i}$$

We simplify these by adopting the following assumptions. We shall assume that (almost) all the tissue is healthy ($h = 1$) and in so doing remove the equation for its evolution and the downstream equation for damaged tissue (equations (7.2.1e), (7.2.1f)). We then combine both macrophage phenotypes (m_1 and m_2) into one equation. We assume that macrophage removal of apoptotic neutrophils occurs at a constant rate (k_{nm1}), removing k_{nm2} from the third term in equation (7.2.1b) and that macrophage production of growth factors occurs upon macrophage engulfment of apoptotic neutrophils introducing the new parameter k_{gm}: this allows us to remove equation (7.2.1d). We assume the uptake of all mediators is negligible (removing terms from equations (7.2.1g), (7.2.1h), (7.2.1i)). We then simplify the positive feedback loops by concentrating on the release of necrotic contents by apoptotic neutrophils when they undergo secondary necrosis. Assuming that $k_{\sigma 1} << 1$ allows us to remove the first term in equation (7.2.1g) representing the release of toxic contents by active neutrophils. We then assume that necrosis of apoptotic neutrophils causes a stronger chemotactic response through damage to tissue ($k_{\sigma 3}$, k_{ch}), rather than as a direct release of chemoattractants (k_{cn2}) allowing us to neglect the second (removing the fourth term in equation (7.2.1h)). We simplify the terms for the influx of neutrophils and macrophages by removing saturable kinetics (equations (7.2.1a), (7.2.1c)). We remove the terms associated with neutrophil necrosis in response to external damage (γ_{n1}, $k_{\sigma 1}$, k_{cn1}) instead focusing solely on the release of chemoattractants from general damaged tissue (k_{cw}). Under these assumptions we arrive at the following simplified model which comprises six ODEs and, as we show below, retains much of the behaviour of equations (7.2.1):

$$\frac{dn_1}{dt} = k_\chi c - \frac{k_n n_1(\beta_{ng}+g)}{(\beta_c+c)}, \tag{7.2.2a}$$

$$\frac{dn_2}{dt} = \frac{k_n n_1(\beta_{ng}+g)}{(\beta_c+c)} - \gamma_{n2}n_2 - k_{nm1}m_1 n_2, \tag{7.2.2b}$$

$$\frac{dm_1}{dt} = k_{\chi m}c - \gamma_{m1}m_1, \tag{7.2.2c}$$

$$\frac{d\sigma}{dt} = k_{\sigma 3}\gamma_{n2}n_2 - \gamma_\sigma\sigma, \tag{7.2.2d}$$

$$\frac{dc}{dt} = k_{cw}f(t) + k_{ch}\left(\frac{\sigma^2}{\beta_\sigma^2+\sigma^2}\right) - \gamma_c c, \tag{7.2.2e}$$

$$\frac{dg}{dt} = k_g k_{gm} m_1 n_2 - \gamma_g g. \tag{7.2.2f}$$

Equations (7.2.2) define our simplified model (Figure 7.1 is a schematic of the model). It has sixteen parameters in common with the model presented in Chapter 6 (equations 6.2.6) and one newly introduced parameter (k_{gm}). The parameter values used are identical to Chapter 6 except k_{gm}, k_χ, $k_{\chi m}$ and k_{cw} (see Table 7.1 for values of these and the other parameters included in this model). We obtain the value for the parameter k_{gm} based on the values of macrophage and apoptotic neutrophil populations at SSII for the model of the previous chapter ($m_2 = k_{gm} m_1 n_2$ on the basis of quasi-equilibrium) and therefore set $k_{gm} = 1$. The rates of influx of white blood cells (k_χ and $k_{\chi m}$) have different units to those of Chapter 6 and are modified accordingly to incorporate β_χ and $\beta_{\chi m}$ respectively. The rate that the function $f(t)$ produces chemoattractants is estimated to produce sufficient chemoattractants to initiate damage.

7.2.1 Nondimensionalisation

We begin by nondimensionalising (7.2.2) in a manner similar to that used in Chapter 6. Time is scaled with the decay rate of the chemoattractant so that $\tilde{t} = \gamma_c t$. The chemoattractant is then rescaled balancing production of the chemoattractant (from σ) with its decay such that

$$c = \tilde{c}\frac{k_{ch}}{\gamma_c}, \tag{7.2.3a}$$

On comparison of equations (7.2.2a), (7.2.2c) to (7.2.1a), (7.2.1c) we observe that the influx of neutrophils and macrophages due to chemotaxis has been simplified to remove saturable kinetics such that

$$\text{active neutrophils:} \qquad n_1 = \tilde{n}_1 \frac{k_\chi}{\gamma_{n2}}\frac{k_{ch}}{\gamma_c}, \tag{7.2.3b}$$

$$\text{apoptotic neutrophils:} \qquad n_2 = \tilde{n}_2 \frac{k_\chi}{\gamma_{n2}}\frac{k_{ch}}{\gamma_c}, \tag{7.2.3c}$$

$$\text{macrophages:} \qquad m_1 = \tilde{m}_1 \frac{k_{\chi m} k_{ch}}{\gamma_{m1}\gamma_c}, \tag{7.2.3d}$$

For the remaining variables we follow Chapter 6, balancing production and decay, so that

$$\text{neutrophil contents:} \qquad \sigma = \tilde{\sigma}\frac{k_{\sigma 3}\gamma_c}{\gamma_\sigma}\left(\frac{k_\chi k_{ch}}{\gamma_{n2}\gamma_c}\right), \tag{7.2.3e}$$

$$\text{growth factors:} \qquad g = \tilde{g}\frac{k_g k_{gm}}{\gamma_g}\left(\frac{k_{\chi m} k_{ch}}{\gamma_{m1}\gamma_c}\right)\left(\frac{k_\chi k_{ch}}{\gamma_{n1}\gamma_c}\right), \tag{7.2.3f}$$

where tildes denote nondimensionless variables. When we use the above scalings in equations (7.2.2) the following dimensionless groups emerge (listed in order of equation):

$$\tilde{k}_n = \frac{k_n}{\gamma_c}, \quad \tilde{\beta}_{ng} = \frac{\beta_{ng}\gamma_g}{k_g k_{gm}}\frac{\gamma_{m1}}{k_{\chi m}}\frac{\gamma_c}{k_{ch}}\frac{\gamma_{n1}}{k_\chi}\frac{\gamma_c}{k_{ch}}, \tag{7.2.4a}$$

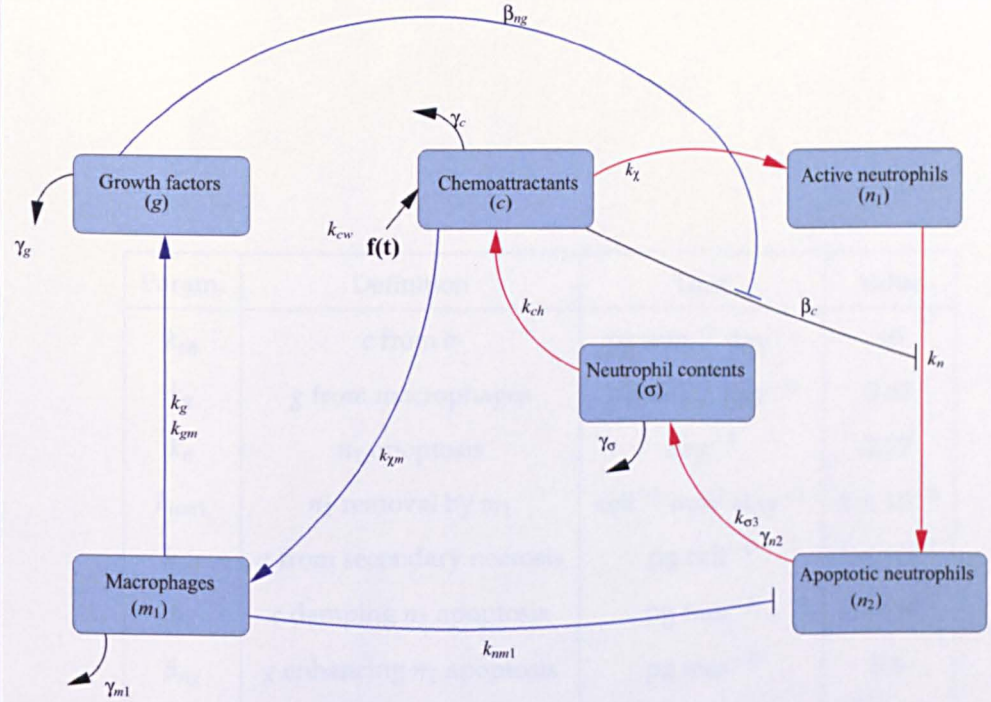

Figure 7.1: A schematic depicting the variables (blue) and reactions (solid lines) that define our simplified model of the inflammatory response. When compared to the schematic presented in the previous chapter (Figure 6.8) we can see that the model has been significantly simplified. The positive feedback loops present in the full model (see Figure 6.13) have been simplified to the release of neutrophil contents by apoptotic neutrophils undergoing secondary necrosis (red lines). Negative feedback loops (blue lines) centre around the macrophages, their consumption of apoptotic neutrophils and subsequent release of growth factors that enhance neutrophil apoptosis.

$$\tilde{\beta}_c = \frac{\beta_c \gamma_c}{k_{ch}}, \quad \tilde{\gamma}_{n2} = \frac{\gamma_{n2}}{\gamma_c}, \quad \tilde{k}_{nm1} = \frac{k_{nm1} k_{\chi m} k_{ch}}{\gamma_{m1} \gamma_c^2}, \quad \tilde{\gamma}_{m1} = \frac{\gamma_{m1}}{\gamma_c}, \tag{7.2.4b}$$

$$\tilde{\beta}_\sigma = \beta_\sigma \frac{\gamma_\sigma}{k_{\sigma 3} \gamma_c} \frac{\gamma_{n2}}{k_\chi} \frac{\gamma_c}{k_{ch}}, \quad \tilde{\gamma}_\sigma = \frac{\gamma_\sigma}{\gamma_c}, \tag{7.2.4c}$$

$$\tilde{k}_{cw} = \frac{k_{cw}}{k_{ch}}, \quad \tilde{\gamma}_g = \frac{\gamma_g}{\gamma_c}. \tag{7.2.4d}$$

Under the above rescalings and dropping the tildes equations (7.2.2) transform to give the following dimensionless system of six ordinary differential equations with eleven dimensionless parameters:

$$\frac{dn_1}{dt} = \gamma_{n2} c - \frac{k_n n_1 \left(1 + \frac{g}{\beta_{ng}}\right)}{\left(1 + \frac{c}{\beta_c}\right)}, \tag{7.2.5a}$$

$$\frac{dn_2}{dt} = \frac{k_n n_1 \left(1 + \frac{g}{\beta_{ng}}\right)}{\left(1 + \frac{c}{\beta_c}\right)} - \gamma_{n2} n_2 - k_{nm1} m_1 n_2, \tag{7.2.5b}$$

$$\frac{dm_1}{dt} = \gamma_{m1} c - \gamma_{m1} m_1, \tag{7.2.5c}$$

Param.	Definition	Unit	Value
k_{ch}	c from σ	pg mm^{-3} day^{-1}	10
k_g	g from macrophages	pg cell^{-1} day^{-1}	0.07
k_n	n_1 apoptosis	day^{-1}	2.77
k_{nm1}	n_2 removal by m_1	cell^{-1} mm^3 day^{-1}	1×10^{-3}
$k_{\sigma 3}$	σ from secondary necrosis	pg cell^{-1}	1×10^{-2}
β_c	c damping n_1 apoptosis	pg mm^{-3}	3×10^{-1}
β_{ng}	g enhancing n_1 apoptosis	pg mm^{-3}	0.8
β_σ	σ damage	pg mm^{-3}	0.1
γ_c	natural decay of c	day^{-1}	4
γ_g	natural decay of g	day^{-1}	9
γ_{m1}	rate of removal of m_1	day^{-1}	0.0495
γ_{n2}	secondary necrosis	day^{-1}	2.77
γ_σ	natural decay of σ	day^{-1}	4
k_{cw}	c from damage to tissue	pg mm^{-3} day^{-1}	7×10^{-3}
k_χ	neutrophil influx	cell pg^{-1} day^{-1}	1083
$k_{\chi m}$	macrophage influx	cell pg^{-1} day^{-1}	250
k_{gm}	g from macrophages	cell^{-1} mm^3	1

Table 7.1: Definitions, units and values of the parameters that appear in equations (7.2.2). Parameters that appear in the model presented in Chapter 6 are shown in the top sixteen rows. Note that k_χ and $k_{\chi m}$ have different units to the parameters for neutrophil and macrophage influx defined in Chapter 6 due to the removal of saturable kinetics. The parameters k_χ, $k_{\chi m}$ and k_{cw} appear in the ODE model defined by equations (7.2.2) but not in the related spatial model (see equations (7.3.2)). The last parameter k_{gm} is new to this model.

$$\frac{d\sigma}{dt} = \gamma_\sigma \gamma_{n2} n_2 - \gamma_\sigma \sigma, \tag{7.2.5d}$$

$$\frac{dc}{dt} = k_{cw} f(t) + \left(\frac{\sigma^2}{\beta_\sigma^2 + \sigma^2} \right) - c, \tag{7.2.5e}$$

$$\frac{dg}{dt} = \gamma_g m_1 n_2 - \gamma_g g. \tag{7.2.5f}$$

As in Chapter 6 we assume that at $t = 0$ there are no white blood cells ($n_1 = 0$, $n_2 = 0$, $m_1 = 0$) or mediators ($\sigma = 0$, $c = 0$, $g = 0$) present. Tissue damage takes the same form with $f(t) = H(A\pi - t)\sin^2(t)$ where

$$H(A\pi - t) = \begin{cases} 1 & \text{if } t < A\pi \\ 0 & \text{if } t > A\pi \end{cases}$$

(see Figure 6.9 in the previous chapter for a sketch of $f(t)$ which is dimensionless). The steady states are dependent on the termination of this damage ($f(t) = 0$). See Table 7.1 for the parameter values used.

7.2.2 Model outcome and steady states

In Figure 7.2 we present numerical simulations of the nondimensional model (equations (7.2.5)) showing the response to one cycle of periodic damage. We obtain a similar outcome to simulations presented in the previous chapter, with all inflammatory cells and their mediators subsiding and the system returning to a normal steady state which we term steady state I (SSI), evidence that the model can simulate resolution of inflammation.

Keeping the same form of $f(t)$, but increasing the number of cycles of damage from one to four, with the same initial conditions and parameter values, we find that a second stable steady state exists (see Figure 7.3). As in Chapter 6 this steady state is characterised by all cells and mediators settling to positive values. We term this solution steady state II (SSII).

The above results demonstrate that the simplified system exhibits bistability. We now investigate this further by studying the effect of varying three key parameters, γ_{n2}, k_g and k_{nm1} (γ_{n2} represents the rate that neutrophils undergo secondary necrosis (participating in the positive feedback loop), k_g represents the rate of production of growth factors (participates and in a negative feedback loop) and k_{nm1} represents the rate that macrophages consume apoptotic neutrophils (which participates in a further negative feedback loop)). See Figure 7.1 for a schema depicting the various feedback loops.

In Figure 7.4 we present a bifurcation diagram showing how the steady state concentration of the chemoattractant c varies with γ_{n2}, the rate of secondary necrosis. The bifurcation structure is similar to that obtained in Chapter 6 (see Figure 6.26). There are two areas of bistability, steady state II gains stability at LP and loses stability at a Hopf bifurcation HB1 for a small area of parameter space. SSII then gains stability at a further Hopf bifurcation and this is retained (in the simplified model) for $\gamma_{n2} >$ HB2. This in contrast to the unexpected bifurcation behaviour presented in the previous chapter where, for large values of secondary necrosis, the system was

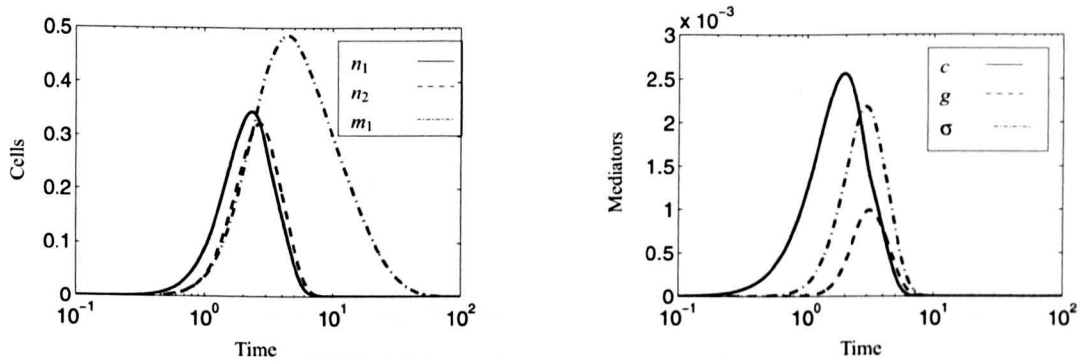

Figure 7.2: Numerical simulations of equations (7.2.5) illustrating how the system evolves to steady state I. Inflammation subsides, with all cells and mediators settling to zero. As in Chapter 6 it is $f(t)$ that causes the inflammatory response. One cycle of damage results in an increase in chemoattractants, neutrophils and their contents: each cycle is not enough to sustain damage so that upon cessation of damage all cells and mediators subside. Parameter values are taken from Table 7.1.

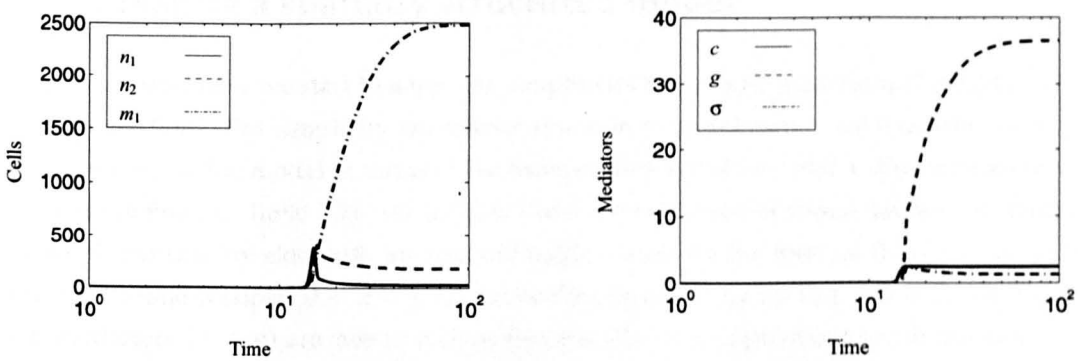

Figure 7.3: In this case the system evolves to steady state II. This is an unhealthy response to injury which is consistent to chronic inflammation in which all cells and mediators evolve to positive values. The macrophages release significant levels of growth factors which reduce the number of neutrophils but not enough to prevent ongoing damage. Parameter values are stated in Table 7.1. In Figure 7.2 we presented results from a simulation in which all system parameters and initial conditions are identical, apart from the functional form of $f(t)$. Here we present results from a simulation in which all system parameters and initial conditions are identical to used to generate the results presented in Figure 7.3, apart from the functional form of $f(t)$ which is increased from one to four cycles of damage.

monostable resolving to SSI. In the middle region between the two Hopf bifurcations again, SSI is stable but both branches of SSII are unstable resulting in excitable behaviour.

Figure 7.5 illustrates the bifurcation behaviour of the system (7.2.2) in terms of the steady state concentration of the chemoattractant as we vary k_g, a key parameter in a negative feedback loop. The system is bistable for $0 < k_g <$ HB. Steady state II loses stability via a Hopf bifurcation when $k_g =$ HB. For HB $< k_g <$ LP there are three steady states, but only the lower branch is stable and simulations in this range exhibit excitable dynamics. For $k_g >$ LP, the system settles to SSI. We remark, that in contrast to the behaviour reported in Chapter 6, where the system settled to SSI for small values of k_g (see Figure 6.15), for the present model the system settles to SSII when k_g is small.

Figure 7.6 illustrates the bifurcation behaviour of the system (7.2.2) in terms of the steady state concentration of the chemoattractant as we vary k_{nm1}, a key parameter in another negative feedback loop. As we vary k_{nm1} the system displays similar dynamics to varying k_g. It is bistable for $0 < k_{nm1} <$ HB. Steady state II loses stability via a Hopf bifurcation when $k_{nm1} =$ HB. Yet again simulations in the range (HB $< k_{nm1} <$ LP) exhibit excitable dynamics and for $k_{nm1} >$ LP, the system settles to SSI.

We have taken our original model of inflammation, presented in the previous chapter, and derived a legitimate reduced model to simplify its complexity before we apply it in a more complicated spatial context.

7.3 Creating a spatially structured model

We now explain how we start to adapt the simplified ODE model (equations (7.2.5)) to include spatial variations. For simplicity we restrict attention to one-dimensional Cartesian geometry and hence frame the model in terms of the independent variables t and x (the dependent variables are defined in Table 7.2). We assume there are two areas of tissue, an area of damaged tissue placed side by side with an area of healthy tissue on the interval $0 < x < L$, so that damaged tissue occupies $0 < x < L/2$ and healthy tissue occupies $L/2 < x < L$. We suppose that mediators (σ, c, g) are free to diffuse between the two populations (with constant diffusion coefficients D_σ, D_c, D_g) while white blood cells (n_1, n_2, m_1) remain still in comparison. Cells move much slower than mediators (being larger) so this is a useful initial assumption. Thus only the differential equations representing the mediators require spatial derivatives. The damage term $f(t)$ from the ODE model above is now replaced by a positive initial perturbation to the chemoattractant concentration.

We scale displacements all with the interval length L and employ the following nondimensionalisations for the diffusion coefficients (for all other parameters and mediators the nondimensionalisations from (7.2.3)-(7.2.4) remain).

$$\tilde{D}_c = \frac{D_c}{\gamma_c L^2}, \quad \tilde{D}_c = \frac{D_\sigma}{\gamma_\sigma L^2}, \quad \tilde{D}_g = \frac{D_g}{\gamma_c L^2}. \tag{7.3.1}$$

When we incorporate the modifications outlined above into equations (7.2.5), dropping the

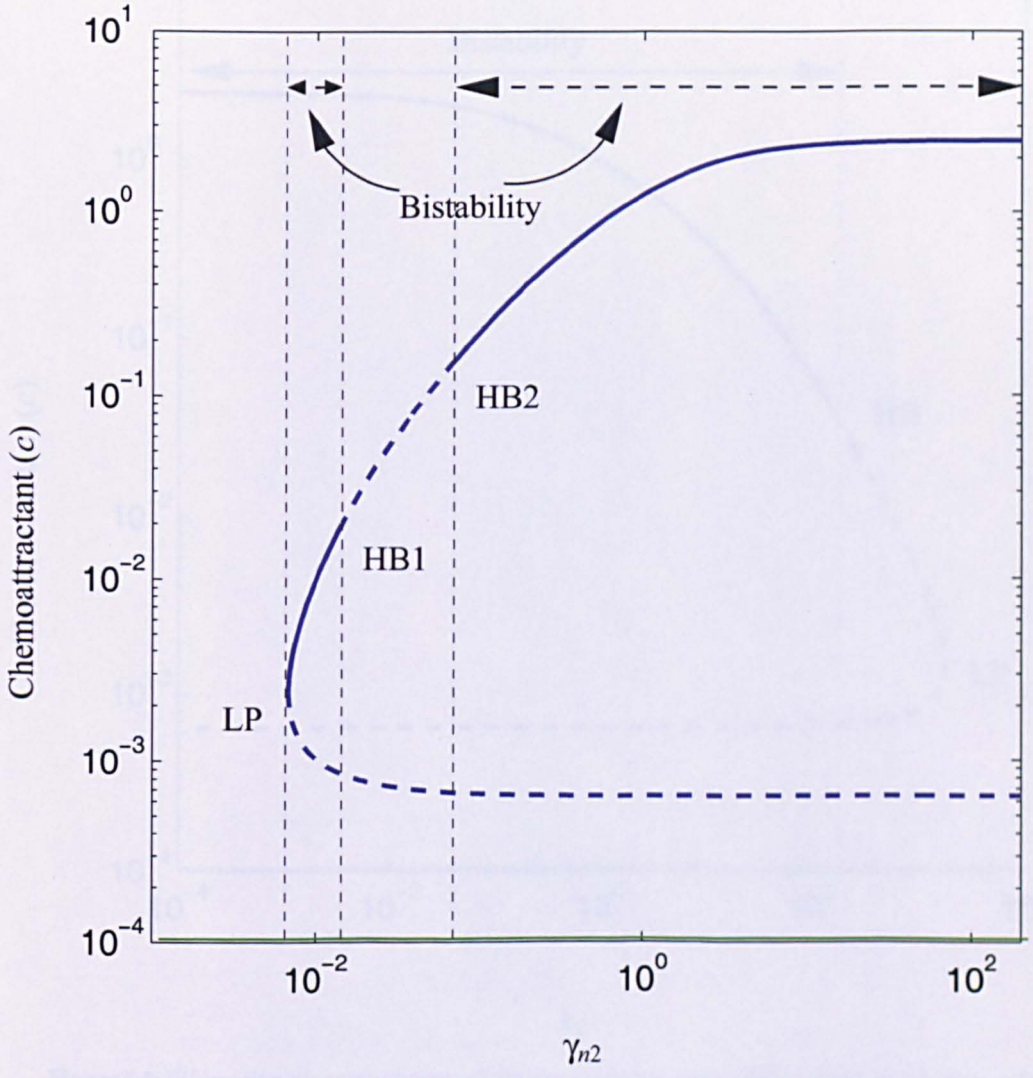

Figure 7.4: Bifurcation diagram showing how the existence and stability of the steady state solutions change as we vary γ_{n2}, the rate at which apoptotic neutrophils undergo secondary necrosis (other parameter values held fixed at values stated in Table 7.1). SSI is presented by the green line and SSII by the blue. Stable steady states are shown as solid lines and unstable ones by broken lines. As in Chapter 6, there are two intervals of bistability, LP $< \gamma_{n2} <$ HB2 and HB1 $< \gamma_{n2}$ but SSII now retains stability for high values of γ_{n2}.

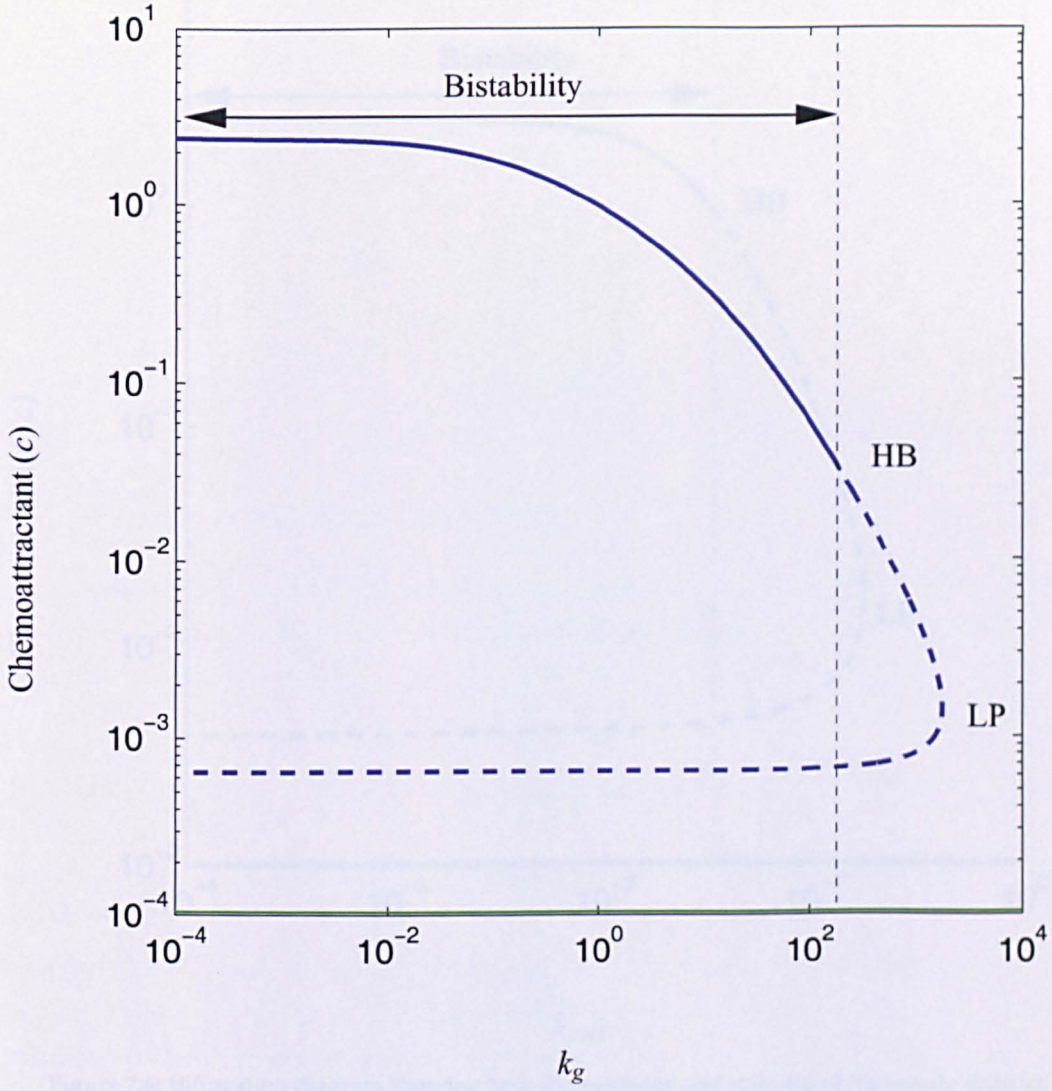

Figure 7.5: Bifurcation diagram showing how the existence and stability of the steady state solutions change as we vary k_g, the rate that macrophages produce growth factors (other parameter values are held fixed at values stated in Table 7.1). SSI is presented by the green line and SSII by the blue. Stable steady states are shown as solid lines and unstable ones by broken lines. The system is bistable for $k_g <$ HB. SSII loses stability via a subcritical Hopf bifurcation (when $k_g =$ HB). For HB $< k_g <$ LP there is an area where the lower steady state is stable and the upper two unstable. The two unstable steady states coalesce at $k_g =$ LP so that at $k_g >$ LP there is only one stable steady state (SSI).

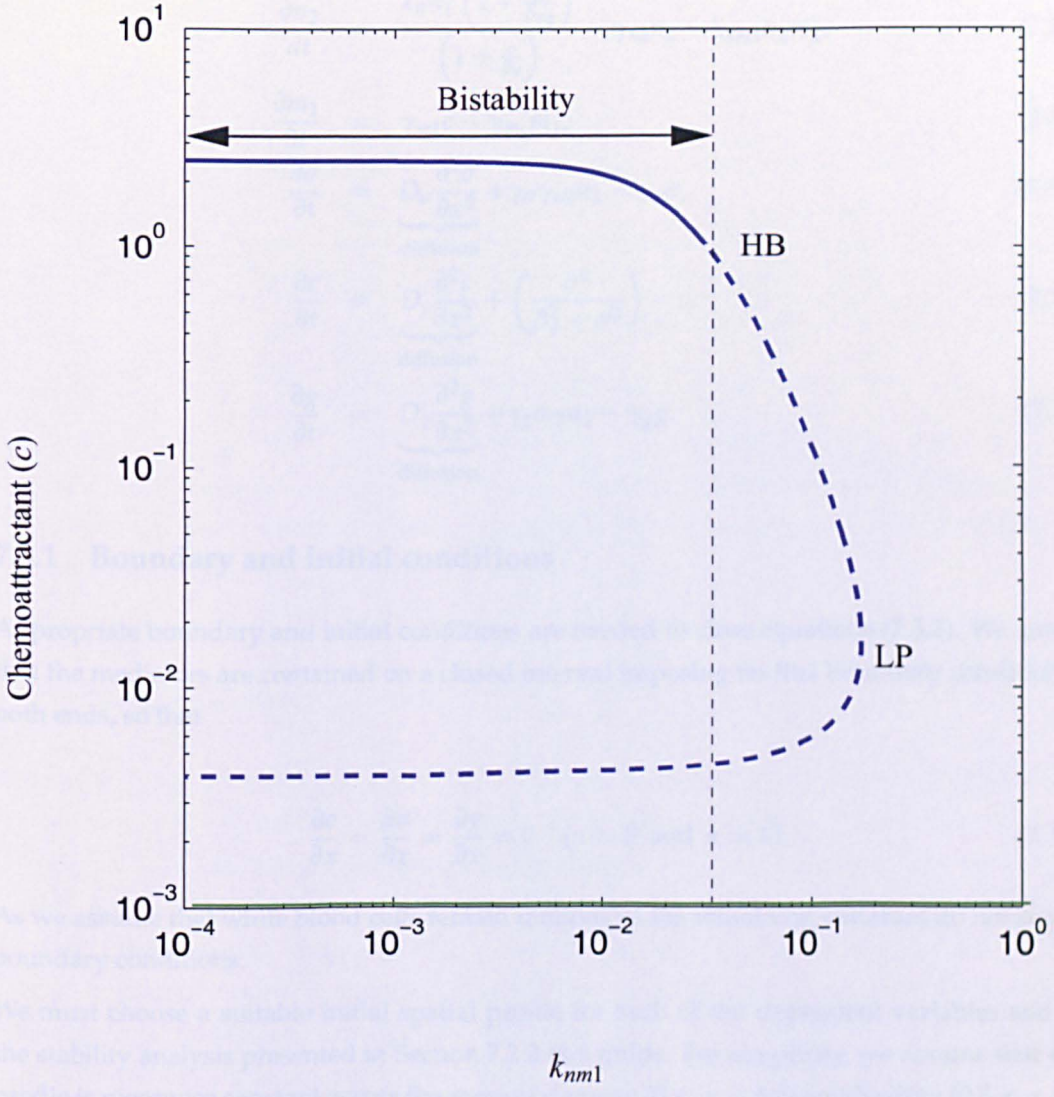

Figure 7.6: Bifurcation diagram showing how the existence and stability of the steady state solutions change as we vary k_{nm1}, the rate that macrophages remove apoptotic neutrophils (other parameter values are held fixed at values stated in Table 7.1). SSI is presented by the green line and SSII by the blue. Stable steady states are shown as solid lines and unstable ones by broken lines. The system displays similar dynamics to Figure 7.5, a bifurcation diagram for k_g. Both k_g and k_{nm1} participate in negative feedback loops. The system is bistable for $k_{nm1} <$ HB and SSII loses stability via a subcritical Hopf bifurcation (when $k_{nm1} =$ HB). For HB $< k_{nm1} <$ LP there is an area where the lower steady state is stable and the upper two unstable. The two unstable steady states coalesce at $k_{nm1} =$ LP so that at $k_{nm1} >$ LP there is only one stable steady state (SSI).

tildes, we obtain the following system of partial differential equations:

$$\frac{\partial n_1}{\partial t} = \gamma_{n2}c - \frac{k_n n_1\left(1+\frac{g}{\beta_{ng}}\right)}{\left(1+\frac{c}{\beta_c}\right)}, \tag{7.3.2a}$$

$$\frac{\partial n_2}{dt} = \frac{k_n n_1\left(1+\frac{g}{\beta_{ng}}\right)}{\left(1+\frac{c}{\beta_c}\right)} - \gamma_{n2}n_2 - k_{nm1}n_2 m_1, \tag{7.3.2b}$$

$$\frac{\partial m_1}{\partial t} = \gamma_{m1}c - \gamma_{m_1}m_1, \tag{7.3.2c}$$

$$\frac{\partial \sigma}{\partial t} = \underbrace{D_\sigma \frac{\partial^2 \sigma}{\partial x^2}}_{\text{diffusion}} + \gamma_\sigma \gamma_{n2} n_2 - \gamma_\sigma \sigma, \tag{7.3.2d}$$

$$\frac{\partial c}{\partial t} = \underbrace{D_c \frac{\partial^2 c}{\partial x^2}}_{\text{diffusion}} + \left(\frac{\sigma^2}{\beta_\sigma^2+\sigma^2}\right) - c, \tag{7.3.2e}$$

$$\frac{\partial g}{\partial t} = \underbrace{D_g \frac{\partial^2 g}{\partial x^2}}_{\text{diffusion}} + \gamma_g m_2 n_2 - \gamma_g g. \tag{7.3.2f}$$

7.3.1 Boundary and initial conditions

Appropriate boundary and initial conditions are needed to close equations (7.3.2). We assume that the mediators are contained on a closed interval imposing no flux boundary conditions at both ends, so that

$$\frac{\partial c}{\partial x} = \frac{\partial \sigma}{\partial x} = \frac{\partial g}{\partial x} = 0 \quad (x = 0 \text{ and } x = 1). \tag{7.3.3a}$$

As we assume that white blood cells remain motionless the remaining variables do not require boundary conditions.

We must choose a suitable initial spatial profile for each of the dependent variables and use the stability analysis presented in Section 7.2.2 as a guide. For simplicity, we assume that each profile is piecewise constant across the areas of damage ($0 < x < 0.5$) and healthy ($0.5 < x < 1$) tissue.

To initialise the model we choose the steady state obtained for simulations of the simplified ODE model above with $k_{nm1} = 0.26$ (to place us just to the left of the Hopf bifurcation HB in Figure 7.6). For a healthy response we use an initial perturbation of $n_1 = n_2 = m_1 = \sigma = g = 0$ and $c = 0.001$, for which the ODE system settled to SSI with $n_1 = n_2 = m_1 = s = g = c = 0$. In contrast, for an unhealthy response use an initial perturbation of $n_1 = n_2 = m_1 = \sigma = g = 0$ and $c = 0.1$. For which the ODE system settled to SSII with $n_1 \approx 1{,}7$, $n_2 \approx 168$, $m_1 \approx 1777$, $s \approx 0.17$, $g \approx 3.1$, $c \approx 1.7$.) The composite initial condition for each of the variables are shown as thick black lines in Figures 7.7, 7.8 and 7.9.

Variable	Description	Unit
n_1	active neutrophils	cells mm^{-3}
n_2	apoptotic neutrophils	cells mm^{-3}
m_1	pro-inflammatory macrophages	cells mm^{-3}
σ	neutrophil toxic contents	pg mm^{-3}
c	chemoattractants	pg mm^{-3}
g	growth factors	pg mm^{-3}

Table 7.2: Definitions of the model dependent variables and their units.

Param.	Definition	Unit
D_c	Chemoattractant diffusivity	$mm^2\ day^{-1}$
D_g	Growth factor diffusivity	$mm^2\ day^{-1}$
D_σ	σ diffusivity	$mm^2\ day^{-1}$

Table 7.3: Definitions, units and values of the parameters newly introduced to the spatial model. Parameters for the nonspatial terms are common to the ODE model presented in this chapter are shown in Table 7.1.

7.4 Numerical solutions

To integrate the system (equations 7.3.2, 7.3.3) numerically we use the method of lines. Firstly we uniformly discretise the spatial domain using N grid points, so that $x_j = j/(N-1)$ $(j = 0 \ldots N-1)$. We then semi-discretise the governing equations in space using second-order centred finite differences; this reduces the PDE model to a system of $6N$ ODEs coupling the spatially discretised variables c_j ($c_j = c(x_j)$), σ_j and g_j, $n_{1,j}$, $m_{1,j}$ and $m_{2,j}$ $(j = 0 \ldots N-1)$. The no-flux boundary conditions at each end of the domain are implemented using ghost points in a straightforward manner. The resulting system is solved numerically using the `ode15` solver in *MATLAB*. Simulations were typically conducted using $N = 100$ grid points, but the results have been checked by varying N to ensure they are insensitive to the spatial resolution.

We use the parameter values from the ODE model (Table 7.1) but we have three new parameters (D_c, D_σ and D_g) which we assume are equal since the mediators are likely to be of a similar size and move in a similar manner. In simulations we set $D_c = D_\sigma = D_g = 0.1\ mm^2\ day^{-1}$ and use the initial conditions constructed in Section 7.3.1 above.

In Figure 7.7 we illustrate the temporal evolution of the system with $k_{nm1} = 0.268$ where a damaged region (SSII) is completely healed (SSI) with all mediators and cells settling to zero.

However, when $k_{nm1} = 0.26$ (all other parameters and initial conditions as before) a damaged region overwhelms a healthy region (Figure 7.8) with all mediators and cells settling to SSII

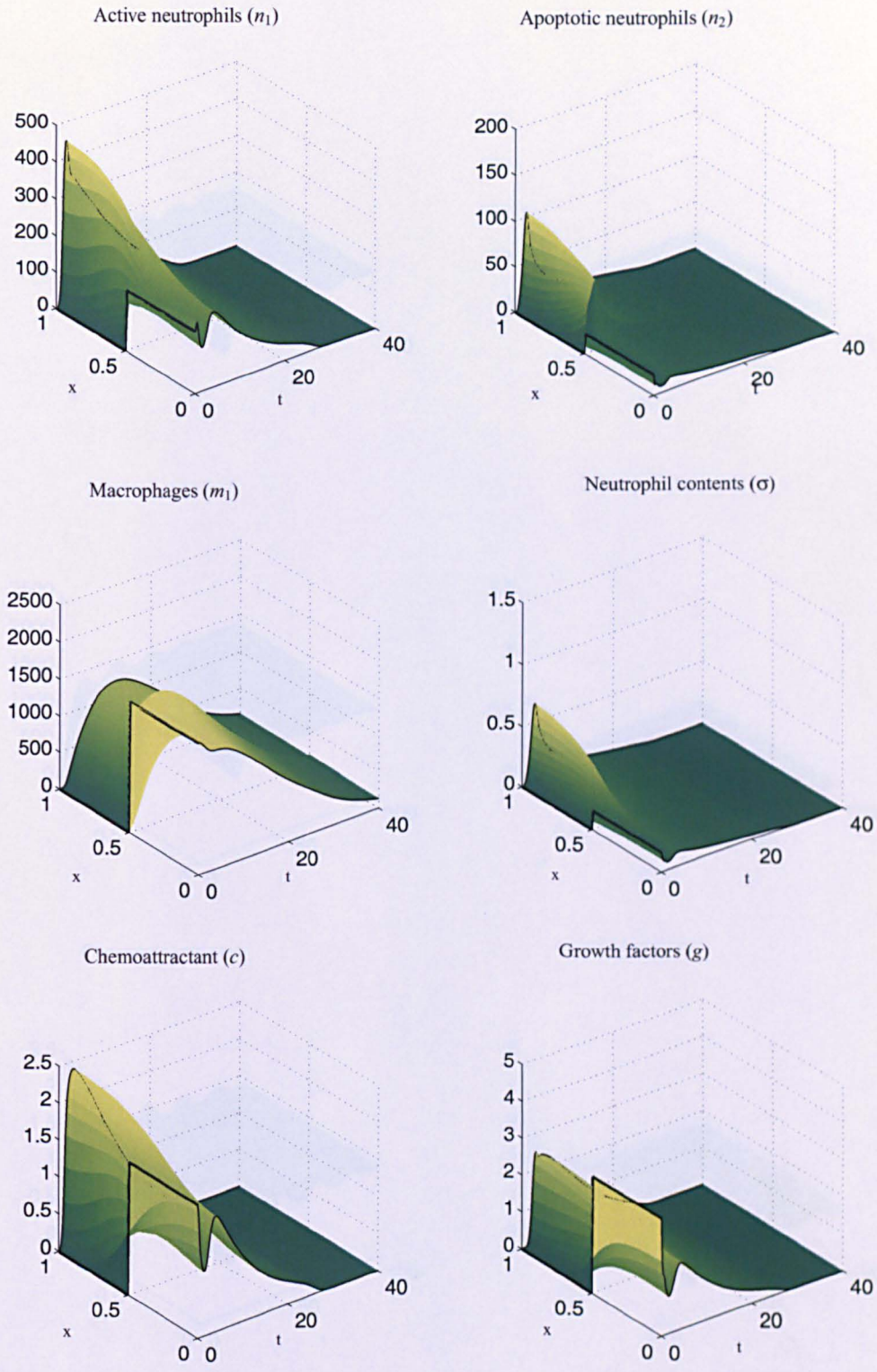

Figure 7.7: When $k_{nm1} = 0.268$ the system resolves to SSI. Solutions of are of the system (7.3.2), (7.3.3) with initial conditions of SSII imposed on $0 < x < 1/2$ and SSI imposed on $1/2 < x < 1$. Parameter values are taken from Table 7.1 except $D_c = D_\sigma = D_g = 0.1$ and $k_{nm1} = 0.268$.

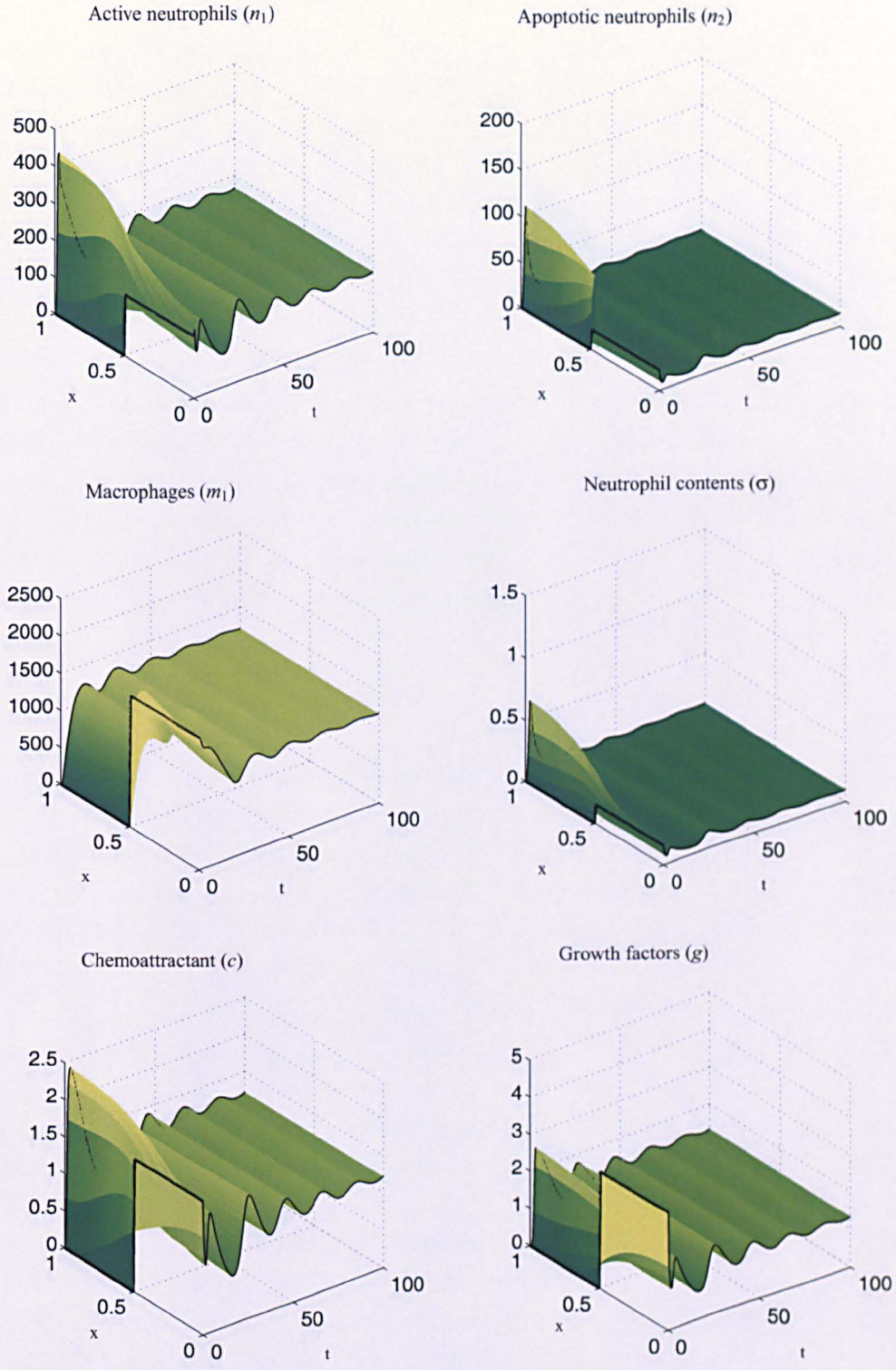

Figure 7.8: When $k_{nm1} = 0.26$ the system resolves, through a series of damped oscillations to SSII. Solutions of are of the system (7.3.2), (7.3.3) with initial conditions of SSII imposed on $0 < x < 1/2$ and SSI imposed on $1/2 < x < 1$. Parameter values are taken from Table 7.1 except $D_c = D_\sigma = D_g = 0.1$ and $k_{nm1} = 0.26$.

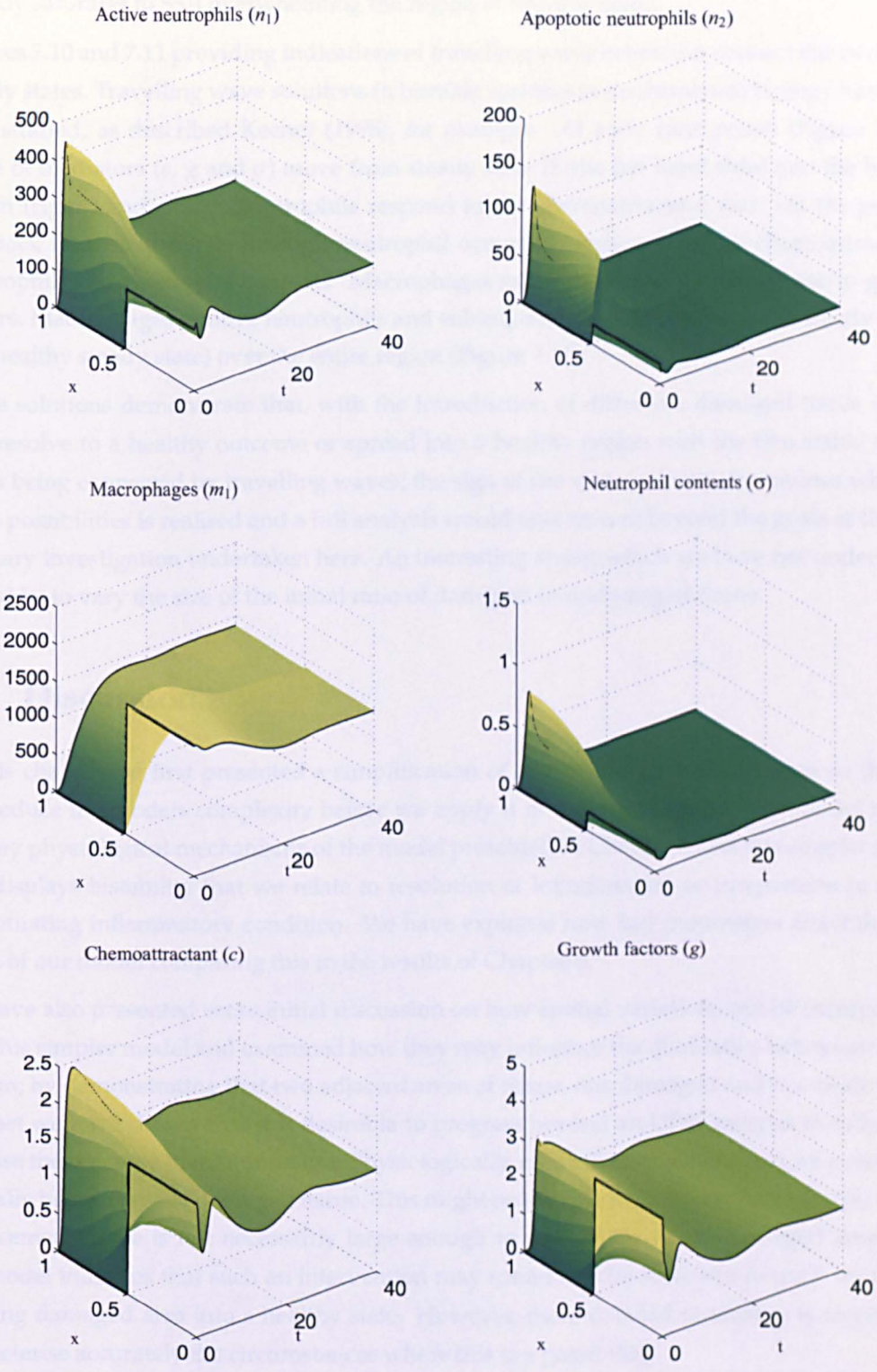

Figure 7.9: When $k_{nm1} = 0.23$ the system resolves to SSII. Solutions of are of the system (7.3.2), (7.3.3) with initial conditions of SSII imposed on $0 < x < 1/2$ and SSI imposed on $1/2 < x < 1$. Parameter values are taken from Table 7.1 except $D_c = D_\sigma = D_g = 0.1$ and $k_{nm1} = 0.23$.

with an intermediary period of damped oscillation.

Finally, Figure 7.9 shows the temporal evolution for $k_{nm1} = 0.23$ (all other parameters and initial conditions as before), where we are now further from the Hopf bifurcation and the system quickly saturates to SSII overwhelming the region of healthy tissue.

Figures 7.10 and 7.11 providing indications of travelling wave behaviour connect the two stable steady states. Travelling wave solutions in bistable systems in mathematical biology have been well studied, as described Keener (1998), for example. At early time points (Figure 7.10) a wave of mediators (c, g and σ) move from steady state II (the left hand side) into the healthy region (right hand side). Neutrophils respond to the chemoattractant and, via the positive feedback from neutrophils through neutrophil necrosis, produce a rise in chemoattractants, neutrophils and neutrophil contents. Macrophages follow later and produce a rise in growth factors. Macrophages remove neutrophils and subsequently the system settles to steady state I (the healthy steady state) over the entire region (Figure 7.11).

These solutions demonstrate that, with the introduction of diffusion, damaged tissue can either resolve to a healthy outcome or spread into a healthy region with the two stable steady states being connected by travelling waves; the sign of the wave velocity determines which of these possibilities is realised and a full analysis would take us well beyond the goals of the preliminary investigation undertaken here. An interesting study, which we have not undertaken, would be to vary the size of the initial ratio of damaged to undamaged tissue.

7.5 Discussion

In this chapter we first presented a simplification of our model for inflammation so that we can reduce the models complexity before we apply it in a spatial context. The model retains the key physiological mechanisms of the model presented in Chapter 6 and this simpler model still displays bistability that we relate to resolution of inflammation or progression to a self-perpetuating inflammatory condition. We have explored how key parameters affect the outcome of our model comparing this to the results of Chapter 6.

We have also presented some initial discussion on how spatial variations can be incorporated into this simpler model and examined how they may influence the qualitative behaviour of the system; by demonstrating that two adjacent areas of tissue, one damaged and one healthy, can interact we have shown that it is desirable to progress beyond an ODE analysis to fully characterise the outcome of inflammation. Physiologically, medical intervention may be possible to partially heal an area of damaged tissue. This might be the case in cartilage, for example, where replacement tissue is not necessarily large enough to replace the whole damaged area. Our toy model indicates that such an intervention may sometimes be sufficient to push the neighbouring damaged area into a healthy state. However, more detailed modelling is required to characterise accurately the circumstances where this is a possibility.

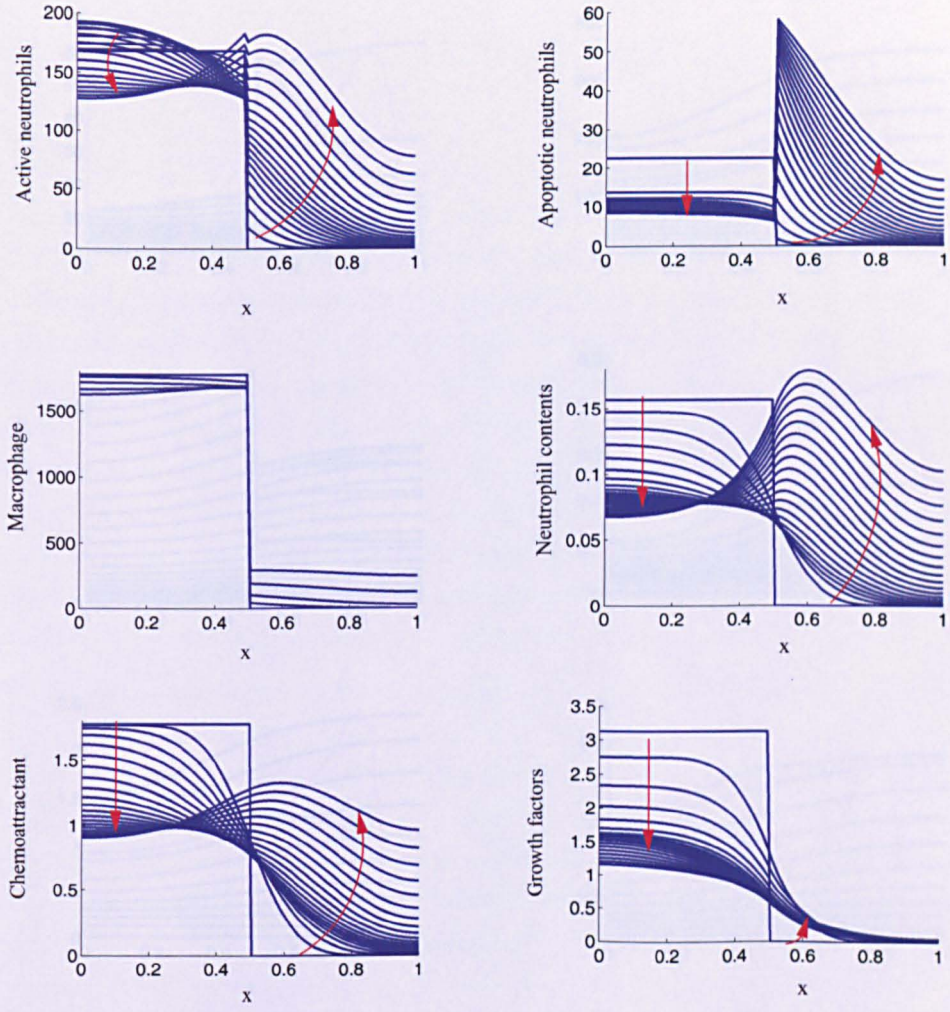

Figure 7.10: Evolution of the system (7.3.2), (7.3.3) at early time points. We plot the variables as a function of length x at equally spaced times. Red arrows indicate the way in which the cells and mediators change as t increases. Initial conditions of SSII are imposed on $0 < x < 1/2$ and SSI imposed on $1/2 < x < 1$. Parameter values are taken from Table 7.1 except $D_c = D_\sigma = D_g = 0.1$ and $k_{nm1} = 0.268$. At early time points chemoattractants, growth factors and neutrophil contents diffuse into the healthy region. Neutrophils respond and we can see that chemoattractants and neutrophil contents subsequently are produced as a result.

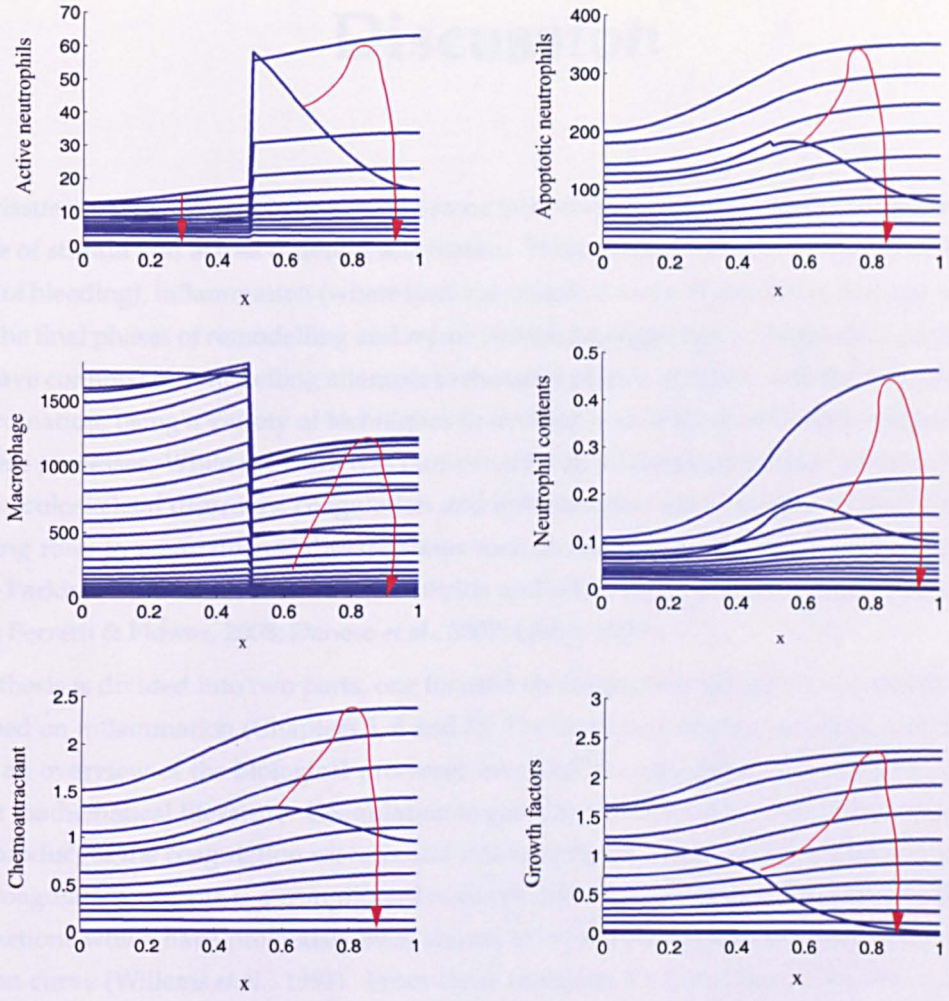

Figure 7.11: Evolution of the system (7.3.2), (7.3.3) at later time points. We plot the variables as a function of length x at equally spaced times. Red arrows indicate the way in which the cells and mediators change as t increases. Initial conditions of SSII are imposed on $0 < x < 1/2$ and SSI imposed on $1/2 < x < 1$. Parameter values are taken from Table 7.1 except $D_c = D_\sigma = D_g = 0.1$ and $k_{nm1} = 0.268$. At later time points macrophages arrive in the healthy region (right hand side) following the evolution of the chemoattractant which, along with all cells and mediators, rise before they settle to SSI. The whole region resolving to a healthy steady state.

CHAPTER 8

Discussion

Soft tissue repair is thought to involve the same inter-related and overlapping phases for a wide range of stimuli and across different soft tissues. These phases include: coagulation (the stopping of bleeding), inflammation (where bacteria are killed and cell and tissue damage removed) and the final phases of remodelling and repair (where damaged tissue is replaced). In this thesis we have confined our modelling attempts to the early phases of repair, namely coagulation and inflammation, using a variety of techniques to develop and analyse new mathematical models of these processes. While the work was motivated by an interest in soft tissue repair in response to musculoskeletal disorders, coagulation and inflammation are of interest in their own right, playing roles in many diverse disease states such as Alzheimer's disease, cardiovascular disease, Parkinson's disease, rheumatoid arthritis and inflammatory bowel disease (Serhan *et al.*, 2008; Perretti & Flower, 2008; Danese *et al.*, 2007; Libby, 2008).

This thesis is divided into two parts, one focused on coagulation (Chapters 2, 3 and 4) and one focused on inflammation (Chapters 5, 6 and 7). The work on coagulation began (in Chapter 2) with an overview of the biological processes involved in coagulation and a review of the relevant mathematical literature. Coagulation is governed by the enzyme thrombin which is the end product of the coagulation cascade and it is here that we focused our modelling attempts. The coagulation cascade is a complicated network and we began by considering a reduced set of reactions which have previously been shown to reproduce the characteristic thrombin generation curve (Willems *et al.*, 1991). From these reactions we formulated a model comprising fourteen ordinary differential equations which we analysed using asymptotic techniques in order to elucidate its underlying mechanisms. Having identified a small parameter ϵ (the ratio of the rate of activation of the slowly acting protein C inhibitory system to the fast acting rate at which antithrombin III inhibits thrombin) we rescaled the system parameters and dependent variables in order to bring the appropriate reactions into leading-order balance. To determine the variable scalings required for each subsequent timescale we manipulated the long term behaviour of the leading-order system on the preceding timescale. The resulting analysis exhibits seven distinct timescales, each covering an individual step required for the formation of the enzyme thrombin. This type of asymptotic analysis is particularly useful for complex biological networks such as this. It enables us to distinguish the timescales on which such a network

operates and also provides means to derive simplified models. We have demonstrated this by providing a series of network diagrams that highlight the dominant reactions on each timescale and identify two of the reduced models that capture the major interactions in thrombin's explosive growth and subsequent inhibition. We were able to identify the physiological mechanisms, such as the initial concentrations of factor V and prothrombin, responsible for the rate of thrombin growth. We obtained an equation that approximates the characteristic time-lag for thrombin that occurs before explosive growth. Two possible bifurcation points exist within the asymptotic analysis and these require a more detailed biological investigation before it is possible to determine if they are physiological.

In chapter 4 we extended the model presented in chapter 3 to include the extrinsic and intrinsic pathways associated with the coagulation cascade, generating a model that encompasses (if in a somewhat simplified form) the complete coagulation cascade relevant to haemostasis. Where possible the parameter values were taken from literature and we solved the resulting system of twenty-nine ordinary equations numerically. By performing a series of simulations of subsystems of this model we were able to highlight the contribution of the extrinsic and intrinsic pathway to coagulation. Subsystem one comprises the reactions of the extrinsic and common pathways and simulations with a low level of tissue factor revealed a peak thrombin concentration of 4 nM after 25 minutes. Subsystem two extends subsystem one by incorporating factors associated with the intrinsic pathway but neglects thrombin activation of factor XI. We found that the inclusion of the intrinsic pathway substantially increases the peak thrombin concentration (from 4 to 750 nM) and reduces the time taken to reach the peak from 25 to 21 minutes. We conclude that the contribution of the intrinsic pathway makes a significant contribution to thrombin formation. By running successive simulations of subsystem two with decreasing initial concentration of the procoagulants VIII and IX, we were able to compare our model to experiments of thrombin formation in plasma deficient in factor VIII and IX which can be related to haemophilia A and B respectively. Haemophilia A and B are characterised by a prolonged time to clot and a reduction in peak thrombin concentrations (Salvagno *et al.*, 2009; Dargaud *et al.*, 2005). Simulations of haemophilia A were in close agreement to experimental results (Salvagno *et al.*, 2009) and once the model presented was modified to remove competition for the various factors simulation results for haemophilia B also showed close correlation to experimental data (Dargaud *et al.*, 2005). The mechanisms of competition and how these are captured are an area for further investigation.

The motivation for Chapter 4 was recently published experimental data which indicate that thrombin can activate factor XI (Kravtsov *et al.*, 2009). There is interest in factor XI as a therapeutic target since it is thought to play a key role in thrombosis but a lesser role in haemostasis (Gailani & Renne, 2007*b*). Simulations of the full model, under activation by factor XIa, are qualitatively similar to experiments designed to assess the sensitivity of thrombin production to factor XIa activation (Kravtsov *et al.*, 2009). They do, however, show a marked increase in peak thrombin formation. Simulations of the full model and of subsystem two assessed against data from experiments in which levels of thrombin formation in plasma deficient in factor XI were compared with those performed in plasma containing factor XI (Kravtsov *et al.*, 2009).

These showed good qualitative agreement, with detection of thrombin activation of factor XI possible at low levels of tissue factor activation although there were discrepancies in the total amount of thrombin formed. There are several possible explanations for these discrepancies. We have had to rely on established estimates for the parameters representing the rate of intrinsic tenase formation and the rates at which protein C and ATIII degrade intrinsic tenase. There could also be missing some biological complexity such as the interaction of cell surfaces and an extended model may produce better results. To date the only mathematical model to specifically assess the contribution of thrombin activation of factor XI to thrombin generation (Kramoroff & Nigretto, 2001) failed to detect any such contribution. Their model was based on a reduced subset of the coagulation cascade reflecting the APPT screening test which uses high levels of activation via FXIIa which our results suggest would mask the effects of thrombin's activation of factor XI.

The asymptotic analysis presented in Chapter 3 is based on a subset of reactions. An extension of this to the whole cascade would be interesting particularly in determining the parameters and initial conditions from the full cascade that contribute to thrombin's time lag and explosive growth. Before this could be achieved the parameters related to protein C activation and its role in factors V and VIII would need better data as there are at present deficiencies in their values and the asymptotic analysis of the reduced pathway leads us to suspect that these would be important.

There is evidence to suggest that there are very strong interactions between platelets, other cell types and the formation of thrombin (Hoffman, 2004) and investigation of these interactions represents an interesting extension to our models on coagulation. The cellular processes regulating thrombin formation occur on different length and timescales, indicating that a spatially structured model of clot formation could provide useful new insight into the ways in which these processes interact.

In part I we used mathematical methods to investigate an area of biology (coagulation) which has been well-studied and tested in-vitro for which a comprehensive and reliable set of parameter values is available. In part two we focused on the less well understood process of coagulation which now is attracting increasing interest, as it has been implicated in many diverse diseases (Serhan *et al.*, 2008; Perretti & Flower, 2008). We began in Chapter 5, with a biological description of inflammation and a review of the relevant mathematical literature. Whereas most existing mathematical models concentrate on the processes that drive inflammation (Lauffenburger & Kennedy, 1981, 1983; Alt & Lauffenburger, 1985; Kumar *et al.*, 2004), we focused on the mechanisms that promote its resolution (Lawrence & Gilroy, 2007; Haslett, 1999; Nathan, 2002; Maderna & Godson, 2003).

In chapter 6 we presented our model of inflammation. Where previous mathematical models have tended to concentrate on a generic white blood cell (Lauffenburger & Keller, 1979; Lauffenburger & Kennedy, 1981, 1983; Alt & Lauffenburger, 1985; Reynolds *et al.*, 2006) we accounted for two distinct cell types (namely neutrophils and macrophages) their interactions and their involvement in promoting and resolving inflammation. Neutrophils, while being essential for the removal of pathogens, can cause damage to healthy tissue by releasing of their toxic

factors while macrophages promote resolution of inflammation by removing neutrophils before they can cause damage and by releasing anti-inflammatory growth factors (Lawrence & Gilroy, 2007; Giles & Lawrence, 2008; Haslett, 1999; Ward *et al.*, 1999). Using numerical simulations and bifurcation analysis we found that our model exhibits bistability and hysteresis over a wide range of parameter space. We related the outcome of the stable steady states to either the healthy resolution of inflammation or a chronic, self-perpetuating state. We performed a limited parameter sensitivity analysis in which we focused on parameters associated with the many feedback mechanisms within our model. These correspond to: the rate of neutrophil apoptosis, the rate that apoptotic neutrophils undergo necrosis and the rate that macrophages produce growth factors. We explored the effects of perturbing these parameters via bifurcation diagrams and discussed how these parameters govern the behaviour of the system towards the different outcomes.

In Chapter 7 we simplified our model of inflammation concentrating on the key biological interactions of neutrophils and macrophages retaining neutrophils ability to cause damage to healthy tissue. We demonstrated that this simplified model retains the key outcomes of the model presented in Chapter 6. We had, thus far, only considered the model under the assumption that the cells and mediators could be treated as representing a spatially homogeneous environment. While this is a useful assumption we presented some preliminary work on extending our model spatially.

There is much interest in finding new therapeutic drugs to limit inflammation. It is hoped that where the persistence of inflammation has become divorced from the inciting agent targeting pro-resolution pathways will offer some success (Serhan *et al.*, 2007; Pizza *et al.*, 2005). Particular targets under investigation are the rate at which neutrophils undergo apoptosis and the ability of macrophages to remove them, both processes thought to be controllable by mediators (Rossi *et al.*, 2007; Henson, 2005; Maderna & Godson, 2003; Haslett, 1999). We used our model, via a bifurcation analysis, to investigate the effects of perturbing these parameters on the outcome of the system. We found that increasing the rate of neutrophil apoptosis alone may not be sufficient to obtain a healthy outcome. It is essential that macrophages are capable of removing apoptotic neutrophils safely preventing the spilling of toxic contents and the perpetuation of inflammation. The model helps us to represent current knowledge about the mechanisms of inflammation, particularly its resolution and how neutrophils and macrophages might effect this. It has limitations imposed by the incomplete knowledge of the biology and a more sophisticated model may be possible as the parameter values and biological mechanisms are better described. We hope the model does, however, provide a good starting place in the modelling of inflammation, and can be modified to incorporate further biological mechanisms as they become understood.

If therapeutic targets are to be identified for inflammation and coagulation it is crucial that the mechanisms controlling the resolution of inflammation and the formation of thrombin are understood as fully as possible. As we have stated, inflammation and coagulation participate in many disease conditions and so the importance of understanding has relevance not only to musculoskeletal disorders but many other diseases. In this work we have developed and anal-

ysed models which, when combined with experimental results, provide new insight into the physical mechanisms regulating inflammation and its resolution, coagulation and the formation of thrombin.

APPENDIX A

Supplementary Material for Chapter Three

A.1 Calculation of λ and β for the third timescale

Substituting the solution for factor Xa ($\check{F}_x^a = k_{1a}\gamma_{1a}\check{T}$) into equations (3.5.9a)-(3.5.9b) we have the system

$$\frac{d\check{F}_v^a}{d\check{T}} = \frac{f_{v0}}{f_{v0}+k_{2am}}\check{F}_{ii}^a + \frac{k_{2b}k_{1a}\gamma_{1a}f_{v0}}{f_{v0}+1+f_{ii0}}\check{T} - k_{1a}\gamma_{1a}\check{T}\check{F}_v^a, \tag{A.1.1a}$$

$$\frac{d\check{B}_{va}^{xa}}{d\check{T}} = q_{3a}k_{1a}\gamma_{1a}\check{T}\check{F}_v^a, \tag{A.1.1b}$$

$$\frac{d\check{F}_{ii}^a}{d\check{T}} = \frac{k_{4a}q_{4b}f_{ii0}}{q_{4a}(f_{ii0}+k_{4bm})}\check{B}_{va}^{xa}. \tag{A.1.1c}$$

Sequentially differentiating for F_v^a results in

$$\frac{d^2\check{F}_v^a}{d\check{T}^2} = \frac{f_{v0}}{(f_{v0}+k_{2am})}\frac{k_{4a}q_{4b}f_{ii0}}{q_{4a}(f_{ii0}+k_{4bm})}\check{B}_{va}^{xa} + \frac{k_{2b}k_{1a}\gamma_{1a}f_{v0}}{f_{v0}+1+f_{ii0}} \tag{A.1.2a}$$

$$-k_{1a}\gamma_{1a}\check{F}_v^a - k_{1a}\gamma_{1a}\check{T}\frac{d\check{F}_v^a}{d\check{T}}, \tag{A.1.2b}$$

$$\frac{d^3\check{F}_v^a}{d\check{T}^3} = \frac{f_{v0}}{(f_{v0}+k_{2am})}\frac{k_{4a}q_{4b}f_{ii0}}{q_{4a}(f_{ii0}+k_{4bm})}q_{3a}k_{1a}\gamma_{1a}\check{T}\check{F}_v^a \tag{A.1.2c}$$

$$-2k_{1a}\gamma_{1a}\frac{d\check{F}_v^a}{d\check{T}} - k_{1a}\gamma_{1a}\check{T}\frac{d^2\check{F}_v^a}{d\check{T}^2}. \tag{A.1.2d}$$

We then assume Va to be of the form $\check{F}_v^a \sim \eta f_v e^{\lambda\check{T}}$ where $f_v = \check{T}^\beta$ where f_v is to be determined and the constant η, β and λ need to be calculated. This differentiates to

$$\begin{aligned}
\frac{d\check{F}_v^a}{d\check{T}} &\sim \eta e^{\lambda\check{T}}\left(\frac{df_v}{d\check{T}}e^{\lambda\check{T}} + \eta\lambda f_v\right),\\
\frac{d^2\check{F}_v^a}{d\check{T}^2} &\sim \eta e^{\lambda\check{T}}\left(\frac{d^2f_v}{d\check{T}^2} + 2\lambda\frac{df_v}{d\check{T}} + \lambda^2 f_v\right),\\
\frac{d^3\check{F}_v^a}{d\check{T}^3} &\sim \eta e^{\lambda\check{T}}\left(\frac{d^3f_v}{d\check{T}^3} + 3\lambda\frac{d^2f_v}{d\check{T}^2} + 3\lambda^2\frac{df_v}{d\check{T}} + \lambda^3 f_v\right),
\end{aligned} \tag{A.1.3}$$

which, when substituted into A.1.2d results in

$$\frac{d^3 f_v}{d\tilde{T}^3} + 3\lambda \frac{d^2 f_v}{d\tilde{T}^2} + 3\lambda^2 \frac{df_v}{d\tilde{T}} + \lambda^3 f_v =$$
$$\frac{f_{v0}}{(f_{v0}+k_{2am})} \frac{k_{4a}\, a_{4b}\, f_{ii0}}{q_{4a}\,(f_{ii0}+k_{4bm})} q_{3a}\, k_{1a}\, \gamma_{1a} \tilde{T} f_v - 2\, k_{1a}\, \gamma_{1a} \left(\frac{df_v}{d\tilde{T}} + \lambda f_v \right)$$
$$-k_{1a}\, \gamma_{1a} \tilde{T} \left(\frac{d^2 f_v}{d\tilde{T}^2} + 2\lambda \frac{df_v}{d\tilde{T}} + \lambda^2 f_v \right) \qquad \text{(A.1.4a)}$$

Balancing terms we can see that

$$\frac{f_{v0}}{(f_{v0}+k_{2am})} \frac{k_{4a}\, q_{4b} f_{ii0}}{q_{4a}\,(f_{ii0}+k_{4bm})} q_{3a}\, k_{1a}\, \gamma_{1a} \tilde{T} f_v - k_{1a}\, \gamma_{1a} \tilde{T} \lambda^2 f_v = 0$$

and therefore

$$\lambda = \sqrt{\frac{f_{v0}\, f_{ii0}\, q_{3a}\, k_{4a}\, q_{4b}}{q_{4a}(f_{v0}+k_{2am})(f_{ii0}+k_{4bm})}}. \qquad \text{(A.1.5)}$$

Also

$$\lambda^3 f_v = -2\, k_{1a}\, \gamma_{1a} \lambda f_v - 2\, k_{1a}\, \gamma_{1a} \tilde{T} \lambda \frac{df_v}{d\tilde{T}},$$

and therefore

$$f_v = \eta \tilde{T}^{-\left(\frac{\lambda^2 + 2k_{1a}\gamma_{1a}}{2k_{1a}\gamma_{1a}}\right)}.$$

Since this is equivalent to $f_v = \eta \tilde{T}^{\beta}$, we can see that

$$\beta = -\left(\frac{\lambda^2 + 2k_{1a}\, \gamma_{1a}}{2k_{1a}\, \gamma_{1a}} \right). \qquad \text{(A.1.6)}$$

If we now assume $\tilde{B}_{va}^{xa} \sim A \tilde{T}^{\beta+1} e^{\lambda \tilde{T}}$ then

$$\frac{d\tilde{B}_{va}^{xa}}{d\tilde{T}} \sim A(\beta+1)\tilde{T}^{\beta} e^{\lambda \tilde{T}} + A\lambda \tilde{T}^{\beta+1} e^{\lambda \tilde{T}},$$

substituting this into equation A.1.1b results in

$$A(\beta+1)\tilde{T}^{\beta} e^{\lambda \tilde{T}} + A\lambda \tilde{T}^{\beta+1} e^{\lambda \tilde{T}} = \eta k_{1a}\, \gamma_{1a}\, q_{3a} \tilde{T}^{\beta+1} e^{\lambda \tilde{T}} \qquad \text{(A.1.7)}$$

from which, at leading order, we can see that

$$A\lambda \tilde{T}^{\beta+1} e^{\lambda \tilde{T}} = \eta k_{1a}\, \gamma_{1a}\, q_{3a} \tilde{T}^{\beta+1} e^{\lambda \tilde{T}}$$

and therefore

$$A = \frac{\eta\, k_{1a}\, \gamma_{1a}\, q_{3a}}{\lambda}$$

resulting in

$$\tilde{B}_{va}^{xa} \sim \frac{\eta k_{1a}\, \gamma_{1a}\, q_{3a}}{\lambda} T^{\beta+1} e^{\lambda \tilde{T}}.$$

We now assume $\tilde{F}_{ii}^{a} \sim B\tilde{T}^{\beta+1}e^{\lambda\tilde{T}}$ then

$$\frac{d\tilde{F}_{ii}^{a}}{d\tilde{T}} \sim B(\beta+1)\tilde{T}^{\beta}e^{\lambda\tilde{T}} + B\lambda\tilde{T}^{\beta+1}e^{\lambda\tilde{T}}$$

which, when substituted into equation A.1.1c, results in

$$B(\beta+1)\tilde{T}^{\beta}e^{\lambda\tilde{T}} + B\lambda\tilde{T}^{\beta+1}e^{\lambda\tilde{T}} = \frac{\eta\, k_{1a}\,\gamma_{1a}\,k_{4a}\,q_{4b}\,q_{3a}\,f_{ii0}}{q_{4a}\,(f_{ii0}+k_{4bm})\,\lambda}\tilde{T}^{\beta+1}e^{\lambda\tilde{T}}.$$

At leading order this implies

$$B\eta\lambda\tilde{T}^{\beta+1}e^{\lambda\tilde{T}} = \frac{\eta\, k_{1a}\,\gamma_{1a}\,k_{4a}\,q_{4b}\,q_{3a}\,f_{ii0}}{q_{4a}\,(f_{ii0}+k_{4bm})\,\lambda}\tilde{T}^{\beta+1}e^{\lambda\tilde{T}}$$

resulting in

$$B = \frac{\eta k_{1a}\,\gamma_{1a}\,k_{4a}\,q_{4b}\,q_{3a}\,f_{ii0}}{q_{4a}\,(f_{ii0}+k_{4bm})\,\lambda^{2}}. \tag{A.1.8}$$

APPENDIX B

Summary of figures from Chapter Four

Table B.1 summarises the figures from Chapter 4 providing a reference to the various simulations presented in the chapter and the systems of equations used to produce them. Subsystem one (One) comprises the reactions of the extrinsic and common pathway. Subsystem two (Two) additionally includes the reactions of the intrinsic pathway. Simulations of the full model (Full) include thrombin activation of factor XI. Modifications of the model remove competition for thrombin (between fibrinogen and factors V, VIII and XI) for the intrinsic tenase (between factor IX and X) and for factor Xa (between factor V and prothrombin). Simulation of this full modified model are run (Modified full) and for subsystem two (Modified two).

Figure	Model	Desciption
4.1	-	Model schema illustrating the procoagulants, activated factors and inactivated factors position within the cascade.
4.2	-	Model schema illustrating which factors comprise the intrinsic, extrinsic and common pathway.
4.3	-	TF:VIIa profile, from Orfeo *et al.* (2005).
4.5	-	Schema of TFPI inhibition.
4.4	One	Profiles of the major component factors of subsystem one.
4.6	One	Simulations illustrating activation levels that cause complete prothrombin conversion to thrombin.
4.7, 4.8	Two	Profiles of the major component factors of subsystem two.
4.9	One, Two	Simulations illustrating the contribution of the intrinsic pathway to thrombin generation.
4.10	Two	Simulations with various levels of the procoagulant VIII

Continued on next page

Figure	Model	Desciption
		relevant to the clinical condition Haemophilia A.
4.11	Two	Simulations with various levels of the procoagulant IX relevant to the clinical condition Haemophilia B.
4.12	Full	A series of profiles showing how factor IXa influences thrombin generation in factor XI deficient plasma.
4.13	Two, Full	Simulations demonstrating the contribution of thrombin activation of factor XI to thrombin formation.
4.14	Modified Full Modified Two	Simulations illustrating the contribution of thrombin activation of factor XI to the generation of thrombin.
4.15	Modified two	Simulations with various levels of the procoagulant IX relevant to the clinical condition Haemophilia B.

Table B.1: Summary of Figures from Chapter 4.

References

ADAMS, D. H. & LLOYD, A.R. 1997 Chemokines: leucocyte recruitment and activation cytokines. *Lancet* **349**, 490–495.

AKGUL, C., MOULDING, D. A. & EDWARDS, S. W. 2001 Molecular control of neutrophil apoptosis. *FEBS Letters* **487**, 318–322.

ALT, W. & LAUFFENBURGER, D. 1985 Transient behaviour of a chemotaxis system modelling certain types of tissue inflammation. *J. Math. Biol.* **24**, 691–722.

ANAND, M., RAJAGOPAL, K. & RAJAGOPAL, K.R. 2005 A model for the formation and lysis of blood clots. *Pathophysiol. Haemost. Thromb.* **34**, 109–120.

ANAND, M., RAJAGOPAL, K. & RAJAGOPAL, K.R. 2008 A model for the formation, growth, and lysis of clots in quiescent plasma. a comparison between the effects of antithrombin iii deficiency and protein c deficiency. *J. Thromb. Biol.* **253**, 725–738.

ANAND, M., RAJAGOPAL, K. & RAJAGOPAL, K. R. 2003 A model incorporating some of the mechanical and biochemical factors underlying clot formation and dissolution in flowing blood. *J. Theor. Med.* **5**, 183–218.

ARNOLD, L., HENRY, A, PORON, F., BABA-AMER, Y., VAN ROOIJEN, N., PLONQUET, A., GHERARDI, R.K. & B., CHAZAUD 2007 Inflammatory monocytes recruited after skeletal muscle injury switch into antiinflammatory macrophages to support myogenesis. *J. Exp. Med.* **204**, 1057–1069.

ASSELTA, R., TENCHINI, M. L. & DUGA, S. 2006 Inherited defects of coagulation factor v: the hemorrhagic side. *J. Thromb. Haemost* **4**, 26–34.

ATAULLAKHANOV, F. & PANTELEEV, M. 2005 Mathematical modelling and computer simulation in blood coagulation. *Pathophysiol. Haemost. Thromb.* **34**, 60–70.

BAGLIA, F. A. & WALSH, P. N. 1998 Prothrombin is a cofactor for the binding of factor xi to the platelet surface and for platelet-mediated factor xi activation by thrombin. *Biochemistry* **37**, 2271–2281.

BAGLIN, T. 2005 The measurement and application of thrombin generation. *Br J. Haematol.* **130**, 653–661.

BARR, A. E. BARBE, M.F. 2004 Inflammation reduces physiological tissue tolerance in the development of work-related musculoskeletal disorders. *J. of Electromyogr. Kinesiol.* **14**, 77–85.

BELTRAMI, E. & JESTY, J. 1995 Mathematical analysis of activation thresholds in enzyme-catalyzed positive feedbacks: Application to the feedbacks of coagulation. *Proc. Natl. Acad. Sci.* **92**, 8744–8748.

BROZE, G. 1995 Tissue factor pathway inhibitor and the revised theory of coagulation. *Annu. Rev. Med.* **46**, 103–112.

BUNGAY, S. D. 2008 Modelling the effect of amplification pathway factors on thrombin generation: a comparison of hemophilias. *Transfus. Apher. Sci.* **38**, 41–7.

BUNGAY, S. D., GENTRY, P. A. & D., GENTRY R. 2003 A mathematical model of lipid-mediated thrombin generation. *Math. Med. Biol.* **20**, 105–129.

BUNGAY, S. D., GENTRY, P. A. & GENTRY, R. D. 2006 Modelling thrombin generation in human ovarian follicular fluid. *Bull. Math. Biol.* **68**, 2283–2302.

BURKE, B. & LEWIS, C., ed. 2002 *The macrophage*. Oxford University Press.

BUTENAS, S., VAN'T VEER, C. & MANN, K. G. 1999 'normal' thrombin generation. *Blood* **94**, 2169–2178.

BUTTERFIELD, A., BEST, T. & MERRICK, M. 2006 The dual roles of neutrophils and macrophages in inflammation: A critical balance between tissue damage and repair. *Journal of Athletic Training* **41** (4), 457–465.

CHOW, C. C., CLERMONT, G., KUMAR, R., LAGOA, C., TAWADROUS, Z., GALLO, D., B., BETTEN, BARTELS, J., CONSTANTINE, G., FINK, M. P., BILLIAR, T. R. & VODOVOTZ, Y. 2005 The acute inflammatory response in diverse shock states. *Shock* **24**, 74–84.

COLMAN, R. W. 2006 Are hemostasis and thrombosis two sides of the same coin? *J. Exp. Med.* **203**, 493–495.

COLMAN, R. W., HIRSH, J., MARDER, V. J., CLOWES, A. W. & GEORGE, J. N., ed. 2000 *Hemostasis and thrombosis*. Lippincott Williams & Wilkins.

CRAWLEY, J. T. B., ZANARDELLI, S., CHION, C. K. N. K. & LANE, D. A. 2007 The central role of thrombin in hemostasis. *J. Thromb. Haemost.* **5**, 95–101.

DAHLBÄCK, B. & VILLOUTREIX, B. 2005 Regulation of blood coagulation by the protein c anticoagulant pathway. *Arterioscler. Thromb. Vasc. Biol.* **25**, 1311–1320.

DANESE, S., PAPA, A., SAIBENI, S., REPICI, A. & MATESCI, A. MAURIZIO, V. 2007 Inflammation and coagulation in inflammatory bowl disease:the clot thickens. *Am. J. Gastroenterol.* **102**, 174–186.

DARGAUD, Y., BÉGUIN, S., LIENHART, A., TRZECIAK, C., BORDET, J.C., HEMKER, H.C. & NEGRIER, C. 2005 Evaluation of thrombin generating capacity in plasma from patients with haemophilia a and b. *Thromb. Haemost.* **93**, 475–480.

DAY, J., RUBIN, J., VODOVOTZ, Y., CHOW, C., REYNOLDS, A. & CLERMONT, G. 2006 A reduced mathematical model of the acute inflammatory response ii. capturing scenarios of repeated endotoxin administration. *J. Theor. Biol.* **242**, 237–256.

DE CRISTOFARO, R., & DE FILIPPIS, V. 2003 Interaction of the 268-282 region of glycoprotein ibalpha with the heparin-binding site of thrombin inhibits the enzyme activation of factor viii. *Biochem. J.* **373**, 593–601.

EMING, S., KREIG, T. & DAVIDSON, J. 2007 Inflammation in wound repair: molecular and cellular mechanisms. *J. Invest. Dermatol.* **127**, 514–525.

FOGELSON, A. 1992 Continuum models of platelet aggregation: formulation and mechanical properties. *SIAM J. Appl. Math.* **52**, 1089–1110.

FOGELSON, A. & GUY, R. 2004 Platelet-wall interactions in continuum models of platelet aggregation: formulation and numerical solution. *Math. Med. Biol.* **21**, 293–334.

FOGELSON, A. & KUHARSKY, A. 1998 Membrane binding-site density can modulate activation thresholds in enzyme systems. *J. Theor. Biol.* **193**, 1–18.

FORDE, M., PUNNETT, L. & WEGMAN, D. 2002 Pathomechanisms of work-related musculoskeletal disorders: conceptual issues. *Ergonomics* **45** (9), 619–630.

GAILANI, D. & BROZE, G. R. 1991 Factor xi activation in a revised model of coagulation. *Science* **253**, 909–912.

GAILANI, D. & RENNE, T. 2007*a* The intrinsic pathway of coagulation: a target for treating thromboembolic disease? *J. Thromb. Haemost.* **5**, 1106–1112.

GAILANI, D. & RENNE, T. 2007*b* Intrinsic pathway of coagulation and arterial thrombosis. *Arterioscler. Thromb. Vasc. Biol.* **27**, 2507–2513.

GAMMACK, D., DOERING, C. R. & KIRSCHNER, D. E. 2004 Macrophage response to mycobacteriom tuberculosis infection. *J. Math. Biol.* **48**, 218–242.

GAMMACK, D., GANGULI, S., MARINO, S., SEGOVIA-JUAREZ, J. & KIRSCHNER, D.E. 2005 Understanding the immune response in tuberculosis using different mathematical models and scales. *Multiscale Model. Simul.* **3**, 312–345.

GIANGRANDE, P.L.F. 2003 Six characters in search of an author: the history of the nomenclature of the coagulation factors. *Br. J. Haematol.* **121**, 703–712.

GIESEN, P.L.A., WILLEMS, G.M., HEMKER, H.C. & HERMENS, W.T. 1991 Membrane mediated assembly of the prothrombinase complex. *J. Biol. Chem.* **266**, 18720–18725.

GILES, K.M. & LAWRENCE, T. 2008 *The resolution of inflammation: A 'tipping point' in the development of chronic inflammatory diseases*, chap. 1, pp. 1–18. In Rossi & Sawatzky (2008).

GILROY, D. W., LAWRENCE, T., PERRETTI, M. & ROSSI, A. G. 2004 Inflammatory resolution: new opportunities for drug discovery. *Nature Reviews* **3**, 401–416.

GORDON, S. & TAYLOR, P.R. 2005 Monocyte and macrophage heterogeneity. *Immunology* **5**, 953–964.

GUO, Z. BUSSARD, K. M., CHATTERJEE, K., MILLER, R., VOGLER, E. A. & SIEDLECKI, C. A. 2006 Mathematical modeling of material-induced blood plasma coagulation. *Biomaterials* **27**, 796–806.

GURBEL, P.A., BECKER, R.C., MANN, K.G., STEINHUBL, S.R. & MICHELSON, A.D. 2007 Platelet function monitoring in patients with coronary artery disease. *J. Am. Coll. Cardiol.* **50**, 1822–1834.

GURTNER, G., WERNER, S., BARRANDON, Y. & LONGAKER, M. 2008 Wound repair and regeneration. *Nature* **453**, 314–320.

GUY, A. D., FOGELSON, A. L. & KEENER, J. P. 2007 Fibrin gel formation in a shear flow. *Math. Med. Biol.* **24**, 111–130.

GUYTON, A. 1992 *Human Physiology and Mechanisms of Disease.* W.B. Saunders.

HALLETT, J. M., LEITCH, A. E., RILEY, N. A., DUFFIN, R., HASLETT, C. & ROSSI, A. G. 2008 Novel pharmacological strategies for driving inflammatory cell apoptosis and enhancing resolution of inflammation. *Trends Pharmacol. Sci.* **29**, 250–257.

HASLETT, C. 1999 Granulocyte apoptosis and its role in the resolution and control of lung inflammation. *Am. J. Respir. Crit. Care Med.* **160**, 5–11.

HEASMAN, S.J., GILES, K.M., WARD, C., ROSSI, A.G., HASLETT, C. & DRANSFIELD, I. 2003 Mechanisms of steroid action and resistance in inflammation. glucocorticoid-mediated regulation of granulocyte apoptosis and macrophage phagocytosis of apoptotic cells: implication for the resolution of inflammation. *Journal of Endocrinology* **178**, 29–36.

HENSON, P. M. 2005 Dampening inflammation. *Nature Immunology* **6**, 1179–1181.

HIGGINS, D.L., LEWIS, S.D. & SHAFER, J.A. 1983 Steady state kinetic parameters for the thrombin-catalyzed conversion of human fibrinogen to fibrin. *J. Biol. Chem.* **258**, 9276–9282.

HOCKIN, M., JONES, K., EVERSE, J. & MANN, K. 2002 A model for the stoichiometric regulation of blood coagulation. *J. Biol. Chem.* **277** (21), 18322–18333.

HOFFMAN, M. 2003 A cell-based model of coagulation and the role of factor viia. *Blood Rev.* **17**, S1–S5.

HOFFMAN, M. 2004 Remodeling the blood coagulation cascade. *J. Thromb. Thrombolys.* **16**, 17–20.

H.S.E. 2002 *Upper limb disorders in the workplace.* H.S.E. Books.

H.S.E. 2003 *A pain in your workplace? Ergonomic problems and solutions.* H.S.E. Books.

HUANG, Z.F., WUN, T.C. & BROZE, G.J. 1993 Kinetics of factor xa inhibition by tissue factor pathway inhibitor. *J. Biol. Chem.* **268**, 26950–26955.

HULTIN, M. B. 1982 Role of human factor viii in factor x activation. *J. Clin. Invest.* **69**, 950–958.

JESTY, J., RODRIGUEZ, J. & BELTRAMI, E. 2005 Demonstration of a threshold response in a proteolytic feedback system: control of the autoactivation of factor xii. *Pathophysiol. Haemost. Thromb.* **34**, 71–79.

JESTY, J., WUN, T.C. & LORENZ, A. 1994 Kinetics of the inhibition of factor xa and the tissue factor-factor viia complex by the tissue factor pathway inhibitor in the presence and absence of herapin. *Biochemistry* **33**, 12686–12694.

JONES, K. & MANN, K. 1994 A model for the tissue factor pathway to thrombin ii. a mathematical simulation. *J. Biol. Chem.* **269**, 23367–23373.

KEENER, J. P. & SNEYD, J. 1998 *Mathematical Physiology*. Springer.

KEULARTS, I.M.L.W., ZIVELIN, A, SELIGSOHN, U., HEMKER, H.C. & BEGUIN, S. 2001 The role of factor xi in thrombin generation induced by low concentrations of tissue factor. *Thromb. Haemost.* **85**, 1060–1065.

KHANIN, M., LEYTIN, V. & POPOV, A. 1991 A mathematical model of the kinetics of platelets and plasma hemostasis system interaction. *Thromb. Res.* **64**, 659–666.

KHANIN, M., RAKOV, D. & KOGAN, A. 1998 Mathematical model for the blood coagulation prothrombin time test. *Thromb. Res.* **89**, 227–232.

KHANIN, M. & SEMENOV, V. 1989 A mathematical model of the kinetics of blood coagulation. *J. Theor. Biol.* **136**, 127–134.

KOBAYASH, S., VOYICH, J. & DELEO, F. 2003 Regulation of the neutrophil-mediated inflammatory response to infection. *Microbes and Infection* **5**, 1337–1344.

KOBAYASHI, S. D. & DELEO, F. R. 2009 Role of neutrophils in innate immunity: a systems biology-level approach. *Wiley Interdisciplinary Reviews: Systems Biology and Medicine* **?**, **?**

KOGAN, A. E., KARDAKOV, D. V. & KHANIN, M. A. 2001 Analysis of the activated partial thromboplastin time test using mathematical modeling. *Thrombosis research* **101**, 299–310.

KOH, T. J. & PIZZA, F. X. 2009 Do inflammatory cells influence skeletal muscle hypertrophy. *Frontiers in Bioscience* **E1**, 60–71.

KOMIYAMA, Y., PEDERSEN, A. H. & KISIEL, W. 1990 Proteolytic activation of human factors ix and x by recombinant human factor viia: effects of calcium, phospholipids and tissue factor. *Biochemistry* **29**, 9418–9425.

KRAMOROFF, A. & NIGRETTO, J. M. 2001 In vitro factor xi activation mechanism according to an optimized model of activated partial thromboplastin time test. *Blood Coagul. Fibrin* **12** (4), 289–299.

KRAVTSOV, D.V., MATAFONOV, A., TUCKER, E.I., SUN, M.F., WALSH, P.N., GRUBER, A. & GAILANI, D. 2009 Factor xi contributes to thrombin generation in the absence of factor xii. *Blood.* **114** (2), 452–458.

KRISHNASWAMY, S., CHURCH, W.R., NESHEIM, M.E. & MANN, K.G. 1987 Activation of human prothrombin by human prothrombinase. influence of factor va on the reaction mechanism. *J. Biol. Chem.* **262**, 3291.

KUHARSKY, A. & FOGELSON, A. 2001 Surface-mediated control of blood coagulation: the role of binding site densities and platelet deposition. *Biophys. J.* **80**, 1050–1074.

KUMAR, R., CHOW, C.C., BARTELS, J., CLERMONT, G. & VODOVOTZ, Y. 2008 A mathematical simulation of the inflammatory response to anthrax infection. *Shock* **29**, 104–111.

KUMAR, R., CLERMONT, G., VODOVOTZ, Y. & CHOW, C. 2004 The dynamics of acute inflammation. *J. Theor. Biol.* **230**, 145–155.

LAUFFENBURGER, D. & KELLER, K. 1979 Effects of leukocyte random motility and chemotaxis in tissue inflammatory response. *J. Theor. Biol.* **81**, 475–503.

LAUFFENBURGER, D. & KENNEDY, C. 1981 Analysis of a lumped model for tissue inflammation dynamics. *J. Math. Biosci.* **53**, 189–221.

LAUFFENBURGER, D. & KENNEDY, C. 1983 Localized bacterial infection in a distribute model for tissue inflammation. *J. Math. Biol.* **16**, 141–163.

LAWRENCE, T. & GILROY, D. W. 2007 Chronic inflammation: a failure of resolution? *Int. J. Exp. Path.* **88**, 85–94.

LAWRENCE, T., WILLOUGHBY, D. A. & GILROY, D. W. 2007 Anti-inflammatory lipid mediators and insights into the resolution of inflammation. *Annu. Rev. Immunol.* **25**, 101–37.

LAWSON, J., KALAFATIS, M., STRAM, S. & MANN, K. 1994 A model for the tissue factor pathway to thrombin i. an empirical study. *J. Biol. Chem.* **269** (37), 23357–23366.

LEE, A., WHYTE, M. K. & HASLETT, C. 1993 Inhibition of apoptosis and prolongation of neutrophil functional longevity by inflammatory mediators. *J. Leukoc. Biol.* **54**, 283–288.

LEVINE, S. 1966 Enzyme amplifier kinetics. *Science* **152**, 651–653.

LIBBY, P. 2008 Role of inflammation in atherosclerosis associated with rheumatoid arthritis. *Am. J. Med.* **121**, S21–31.

LU, G., BROZE, G. & KRISHNASWAMY, S. 2004 Formation of factors ixa and xa by the extrinsic pathway. *J. Biol. Chem.* **279**, 17241–17249.

LUSTER, A.D., ALON, R. & VON ANDRIAN, U.H. 2005 Immune cell migration in inflammation: present and future therapeutic targets. *Nat. Immunol.* **6**, 1182–1190.

MACKMAN, N. 2008 Triggers, targets and treatments for thrombosis. *Nature* **451**, 914–918.

MADERNA, P. & GODSON, C. 2003 Phagocytosis of apoptectic cells and the resolution of inflammation. *Biochimica et Biophysica Acta* **1639**, 141–151.

MAJNO, G. & JORIS, I. 2004 *Cells, Tissues, and Disease.* Oxford University Press.

MANN, K. 1987 The assembly of blood clotting complexes on membranes. *Trends in Biochemical Sciences* **12**, 229–233.

MANN, K. G. 2003 Thrombin formation. *CHEST* **124**, 4S–10S.

MANN, K. G., BUTENAS, S. & BRUMMEL, K. 2003 The dynamics of thrombin formation. *Arteriosclerosis Thromb. Vasc. Biol.* **23**, 17–25.

MARÉE, A.F.M., KOMBA, M., DYCK, C. ŁABECKI, M., FINEGOOD, D. T. & EDELSTEIN-KESHET, L. 2005 Quantifying macrophage defects in type 1 diabetes. *J. Theor. Biol.* **233**, 533–551.

MARÉE, A.F., KOMBA, M., FINEGOOD, D.T. & EDELSTEIN-KESHET, L. 2008 A quantitative comparison of rates of phagocytosis and digestion of apoptotic cells by macrophages from normal (balb/c) and diabetes-prone (nod) mice. *J. Appl. Physiol.* **104**, 157–169.

MARÉE, A.F.M., KUBLIK, R., FINEGOOD, D.T. & EDELSTEIN-KESHET, L. 2006 Modelling the onset of type 1 diabetes: can impaired macrophage phagocytosis make the difference between health and disease? *Philos. Transact. A.* **364**, 1267–1282.

MONKOVIC, D.D. & TRACY, P.B. 1990 Functional characterization of human platelet-released factor v and its activation by factor xa and thrombin. *J. Biol. Chem.* **265**, 17132–17140.

NAITO, K. & FUJIKAWA, K. 1991 Activation of human blood coagulation factor xi independent of factor xii. factor xi is activated by thrombin and factor xia in the presence of negatively charged surfaces. *J. Biol. Chem.* **266** (12), 7353–8.

NATHAN, C. 2002 Points of control in inflammation. *Nature* **420**, 846–852.

NESHEIM, M., TRACY, R. & MANN, K. 1984 "clotspeed," a mathematical simulation of the functional properties of prothrombinase. *J. Biol. Chem.* **259** (3), 1447–1453.

OLIVER, J.A., MONROE, D.M., ROBERTS, H.R. & HOFFMAN, M. 1999 Thrombin activates factor xi on activated platelets in the absence of factor xii. *Arterioscler. Thromb. Vasc. Biol.* **19**, 170–7.

ORFEO, T., BUTENAS, S., BRUMMEL-ZIEDINS, K.E. & MANN, K.G. 2005 The tissue factor requirement in blood coagulation. *J. Biol. Chem.* **280**, 42887–42896.

OSTERUD, B. & RAPAPORT, S. I. 1977 Activation of factor ix by the reaction product of tissue factor and factor vii: additional pathway for initiating blood coagulation. *Proc. Natl. Acad. Sci. U. S. A.* **74**, 5260–5264.

OWEN, M. R. & SHERRATT, J. A. 1997 Pattern formation and spatiotemporal irregularity in a model for macrophage-tumour interactions. *J. Theor. Biol.* **189**, 63–80.

PANTELEEV, M. A., OVANESOV, M. V., KIREEV, D. A., SHIBEKO, A. M., SINAURIDZE, E. I., ANANYEVA, N. M., BUTYLIN, A. A., SAENKO, E. L. & ATAULLAKHANOV, F. I. 2006 Spatial propagation and localization of blood coagulation are regulated by intrinsic and protein c pathways, respectively. *Biophys. J.* **90**, 1489–1500.

PANTELEEV, M. A., SAENKO, E. L., ANANYEVA, N. M. & ATAULLAKHANOV, F. I. 2004 Kinetics of factor x activation by the membrane-bound complex of factor ixa and factor viiia. *Biochem. J.* **381**, 779–794.

PEDICORD, D. L., SEIFFERT, D. & BLAT, Y. 2007 Feedback activation of factor xi by thrombin does not occur in plasma. *Proc. Natl. Acad. Sci. U. S. A.* **104**, 12855–12860.

PERRETTI, M. & FLOWER, R.J. 2008 *Anti-inflammatory glucocorticoids and annexin 1*, chap. 8, pp. 141–158. In Rossi & Sawatzky (2008).

PHEASANT, S. & HASLEGRAVE, C., ed. 1996 *Bodyspace anthropometry, ergonomics and the design of work*. Taylor and Francis.

PIETERS, J., LINDHOUT, T. & HEMKER, H. 1988 The limited importance of factor xa inhibition to the antigoagulant property of herapin in thromboplastin-activated plasma. *Blood* **72**, 2048–2052.

PIZZA, F. X., PETERSON, J.M., BAAS, J.H. & KOH, T. J. 2005 Neutrophils contribute to muscle injury and impair its resolution after lengthening contractions in mice. *J. Physiol.* **562**, 899–913.

PORCHERAY, F., VIAUD, S., RIMMANIOL, A. C., LEONE, C., SAMAH, B., DEREUDDRE-BOSQUET, N., DORMONT, D. & GRAS, G. 2005 Macrophage activation switching: an asset for the resolution of inflammation. *Clin. Exp. Immunol.* **142**, 481–489.

PORTH, C. 2005 *Pathophysiology: concepts of altered health states.*, 7th edn. Lippincott Williams & Wilkins.

POULTER, L.W. & TURK, J.L. 1975 Rapid quantification of changes in macrophage volume induced by lymphokine in vitro. *Clin. exp. Immunol.* **19**, 193–199.

PUNNETT, L. & WEGMAN, D. 2004 Work-related musculoskeletal disorders: the epidemiologic evidence and the debate. *J. Electromyogr. and Kinesiol.* **14**, 13–23.

QIAO, Y., XU, C., ZENG, Y., XU, X., ZHAO, H. & XU, H. 2004 The kinetic model and simulation of blood coagulation - the kinetic influence of activated protein c. *Med. Eng. Phys.* **26**, 341–347.

RAWALA-SHEIKH, R., AHMAD, S.S., ASHBY, B. & WALSH, P.N. 1990 Kinetics of coagulation factor x activation by platelet-bound factor ixa. *Biochemistry* **29**, 2606–2611.

REID, C., RUSHE, M., JARPE, M., VAN VLIJMEN, H., DOLINSKI, B., QIAN, F., CACHERO, T., CUERVO, H., YANACHKOVA, M., NWANKWO, C., WANG, X. ETIENNE, N. GARBER E., V., BAILLY, DE FOUGEROLLES, A. & BORIACK-SJODIN, P. 2006 Structure activity relationships of monocyte chemoattractant proteins in complex with a blocking antibody. *Protein Eng. Des. Sel. 2006* **19**, 317–324.

RENNE, T., NIESWANDT, B. & GAILANI, D. 2006 The intrinsic pathway of coagulation is essential for thrombus stability in mice. *Blood Cells Mol. Dis.* **36**, 158–151.

RENNÉ, T., POZGAJOVÁ, M., GRÜNER, S., SCHUH, K., PAUER, H.U., BURFEIND, P., GAILANI, D. & NIESWANDT, B. 2006 Defective thrombus formation in mice lacking coagulation factor xii. *J. Exp. Med.* **203**, 493–5.

REYNOLDS, A., RUBIN, J., CLERMONT, G., DAY, J., VODOVOTZ, Y. & ERMENTROUT, G. 2006 A reduced mathematical model of the acute inflammatory response i. derivation of model and analysis of anti-inflammation. *J. Theor. Biol.* **242**, 220–236.

REZAIE, A. R. & ESMON, C. T. 1993 Conversion of glutamic acid 192 to glutamine in activated protein changes the substrate specificity and increases reactivity toward macromolecular inhibitors. *J. Biol. Chem.* **268**, 19943–19948.

RIEWALD, M. & RUF, W. 2003 Science review: role of coagulation protease cascades in sepsis. *Crit. Care* **7** (2), 123–129.

ROSING, J., TANS, G., GOVERS-RIEMSLAG, J.W., ZWAAL, R.F. & HEMKER, H.C. 1980 The role of phospholipids and factor va in the prothrombinase complex. *J. Biol. Chem.* **255**, 274–83.

ROSSI, A. & SAWATZKY, D., ed. 2008 *The resolution of inflammation (Progress in inflammation research)*.. Birkhauser Verlag AG.

ROSSI, A. G., HALLETT, J.M., SAWATZKY, D.A., TEIXEIRA, M.M. & HASLETT, C. 2007 Modulation of granulocyte apoptosis can influence the resolution of inflammation. *Biochem Soc. Trans.* **35**, 288–291.

SALVAGNO, G.L., ASTERMARK, J. & LIPPI, G. 2009 Thrombin generation assay: a useful routine check-up tool in the management of patients with haemophilia. *Haemophilia* **15**, 290–6.

SAMPSON, A. P. 2000 The role of eosinophils and neutrophils in inflammation. *Clin. Exp. Allergy* **30**, 22–27.

SCHOEN, P., LINDHOUT, T., WILLEMS, G. & HEMKER, H. C. 1989 Antithrombin iii dependent anti-prothrombinase activity of heparin and heparin fragments. *J. Biol. Chem.* **264**, 10002–10007.

SCHUGART, R. C., FRIEDMAN, A., ZHAO, R. & SEN, C. K. 2008 Wound angiogenesis as a function of tissue oxygen tension: a mathematical model. *Proc. Natl Acad. Sci. USA* **105**, 2628–33.

SCOTT, A., KHAM, K.M., ROBERTS, C. R. & COOK, J. L. DURONIO, V. 2004 What do we mean by the term "inflammation"? a contemporary basic science update for sports medicine. *Br. J. Sports. Med.* **38**, 372–380.

SEGERS, K., DAHLBACK, B. & NICOLAES, G.A.F. 2007 Coagulation factor v and thrombophilia: background and mechanisms. *Thromb. Haemost.* **98**, 530–542.

SERHAN, C. N. 2007 Resolution phase of inflammation: novel endogenous anti-inflammatory and proresolving lipid mediators and pathways. *Annu. Rev. Immunol.* **25**, 101–137.

SERHAN, C. N. 2008 *Novel liped mediators in resolution and their aspirin triggered epimers: lipoxins, resolvins, and protectins*, chap. 6, pp. 93–118. In Rossi & Sawatzky (2008).

SERHAN, C. N., BRAIN, S.D., BUCKLEY, C.D., GILROY, D. W., HASLETT, C., O'NEILL, L.A., PERRETTI, M., ROSSI, A. G. & WALLACE, J.L. 2007 Resolution of inflammation: state of the art, definistions and terms. *FASEB Journal* **21**, 325–330.

SERHAN, C. N., CHIANG, N. & VAN DYKE, T. E. 2008 Resolving inflammation: dual anti-inflammatory and pro-resolution lipid mediators. *Nature* **8**, 349–361.

SERHAN, C. N. & SAVILL, J. 2005 Resolution of inflammation: the beginning programs the end. *Nat. Immunol.* **6**, 1191–1197.

SINGER, P., SHAPIRO, H., THEILLA, M., ANBAR, R., SINGER, J. & COHEN, J. 2008 Anti-inflammatory properties of omega-3 fatty acids in critical illness: novel mechanisms and an integrative perspective. *Intensive Care Med.* **34**, 1580–1592.

SINHA, D., SEAMAN, F. S. & WALSH, P. N. 1987 Role of calcium ions and the heavy chain of factor xia in the activation of human coagulation factor ix. *Biochemistry* **26**, 3768–75.

SMITH, G.F. 1984 *The Thrombin,*, vol. 1. CRC Press Inc. Boca Raton.

SOLYMOSS, S., TUCKER, M.M. & TRACY, P.B. 1988 Kinetics of inactivation of membrane-bound factor va by activated protein c: protein s modulates factor xa protection. *J. Biol. Chem.* **263**, 14884–14890.

SOONS, H., JANSSEN-CLAESSEN, T., TANS, G. & HEMKER, H.C. 1987 Inhibition of factor xia by antithrombin iii. *Biochemistry* **26**, 4624–4629.

SPRONK, H., GOVERS-RIEMSLAG, J. & TEN CATE, H. 2003 The blood coagulation system as a molecular machine. *BioEssays* **25**, 1220–1228.

STOUT, R.D., JIANG, C., MATTA, B., TIETZEL, I. WATKINS, S. & SUTTLES, J. 2005 Macrophages sequentially change their functional phenotype in response to changes in microenvironmental influences. *J. Immunol.* **175**, 342–349.

SUMMERS, C., RANKIN, S. M., CONDLIFFE, A. M., SINGH, N, PETERS, A. M. & CHILVERS, E. R. 2010 Neutrophil kinetics in health and disease. *Trends in Immunology* **In Press**.

SUN, Y. & GAILANI, D. 1996 Identification of a factor ix binding site on the third apple domain of activated factor xi. *J. Biol. Chem.* **271**, 29023–29028.

SZPADERSKA, A. M. & DIPIETRO, L.A. 2005 Inflammation is surgical wound healing: friend or foe? *Surgery* **137**, 571–573.

TIDBALL, J.G. 2005 Inflammatory processes in muscle injury and repair. *Am. J. Physiol. Regul. Integr. Comp. Physiol.* **288**, 345–353.

TING-BEALL, H.P., NEEDHAM, D. & HOCHMUTH, R.M. 1993 Volume and osmotic properties of human neutrophils. *Bl* **81**, 2774–2780.

TOUMI, H., F'GUYER, S. & BEST, T. 2006 The role of neutrophils in injury and repair following muscle stretch. *J. Anat.* **208**, 459–470.

TRACY, P.B., EIDE, L.L. & MANN, K.G. 1985 Human prothrombinase complex assembly and function on isolated peripheral blood cell populations. *J. Biol. Chem.* **260**, 2119.

TRAN, C., JONES, A.D. & DONALDSON, K. 1995 Mathematical model of phagocytosis and inflammation after the inhalation of quartz at different concentrations. *Scand. J. Work. Environ. Health* **21**, 50–54.

TSIANG, M., PABORSKY, L. R., LI, W. X., JAIN, A. K., MAO, C. T., DUNN, K. E., LEE, D. W., MATSUMURA, S. Y., MATTEUCCI, M. D., COUTRE, S. E., LEUNG, L. L., & GIBBS, C. S. 1996 Protein enhgineering thrombin for optimal specificity and potency of anticoagulant acticity i vivo. *Biochemistry* **35**, 16449–16457.

TUCKER, E. I., MARZEC, U. M., WHITE, T. C., HURST, S., RUGONYI, S., MCCARTY, O. J., GAILANI, D., BRUBER, A. & HANSON, S. R. 2009 Prevention of vascular graft occlusion and thrombus-associated thrombin generation by inhibition of factor xi. *Blood* **113**, 936–944.

VAN HOVE, C. L., MAES, T., JOOS, G. F. & TOURNOY, K. G. 2008 Chronic resolution in asthma: a contest of persistence vs resolution. *Allergy* **63**, 1095–1109.

VASSILEVA, V. & PIQUETTE-MILLER, M. 2010 Inflammation: extinguishing the fires within. *Clin. Pharmacol. Ther.* **87**, 375–379.

VAN VEEN, J. J., GATT, A. & MAKRIS, M. 2008 Thrombin generation testing in routine clinical practice: are we there yet? *Br. J. Haematol.* **142**, 889–903.

VAN'T VEER, C. & MANN, K. G. 1997 Regulation of tissue factor initiated thrombin generation by the stoichiometric inhibitors tissue factor pathway inhibitor, antithrombin-iii, and heparin cofactor-ii. *J. Biol. Chem.* **272**, 4367–4377.

WALSH, P. N., BRADFORD, H. SINHA, D., PIPERNO, J. R. & TUSZYNSKI, G. P. 1984 Kinetics of the factor xia catalyzed activation of human blood coagulation factor ix. *J. Clin. Invest.* **73**, 1392–1399.

WARD, C., DRANSFIELD, I., CHILVERS, E.R., HASLETT, C. & ROSSI, A.G. 1999 Pharmacological manipulation of granulocyte apoptosis: potential therapeutic targets. *Trends Pharmacol. Sci.* **20**, 503–509.

WARN-CRAMER, B. J. & BAJAJ, S. P. 1986 intrinsic versus extrinsic coagulation. kinetic considerations. *Biochem. J.* **239**, 757–762.

WARRENDER, C., FORREST, S. & KOSTER, F. 2006 Modeling intercellular interactions in early mycobacterium infection. *Bull. Math. Biol.* **68**, 223–2261.

WAUGH, H. V. & SHERRATT, J. A. 2006 Macrophage dynamics in diabetic wound healing. *Bull. Math. Biol.* **68**, 197–207.

WAUGH, H. V. & SHERRATT, J. A. 2007 Modeling the effects of treating diabetic wounds with engineered skin substitutes. *Wound Rep. Reg.* **15**, 556–565.

WHYTE, M.K., HASLETT, C. & CHILVERS, E.R. 2008 *Granulocyte apoptosis*, chap. 2, pp. 19–37. In Rossi & Sawatzky (2008).

WIEBE, E.M., STAFFORD, A.R., FREDENBURGH, J.C. & WEITZ, J.I. 2003 Mechanism of catalysis of inhibition of factor ixa by antithrombin in the presence of heparin or pentasaccharide. *J. Biol. Chem.* **278**, 35767–35774.

WIELDERS, S.J., BÉGUIN, S., HEMKER, H.C. & LINDHOUT, T. 2004 Factor xi-dependent reciprocal thrombin generation consolidates blood coagulation when tissue factor is not available. *Arterioscler. Thromb. Vasc. Biol.* **24** (6), 1138–42.

WIGGINTON, J. E. & KIRSCHNER, D. 2001 A model to predict cell-mediated immune regulatory mechanisms during human infection with mycobacterium tuberculosis. *J. Immunol.* **166**, 1951–1967.

WILLEMS, G., LINDHOUT, T., HERMENS, W. & HEMKER, H. 1991 Simulation model for thrombin generation in plasma. *Haemostasis* **21**, 197–207.

XU, Z., CHEN, N., KAMOCKA, M. N., ROSEN, E. D. & ALBER, M. 2008 A multiscale model of thrombus development. *J. R. Soc. Interface* **5** (24), 705–722.

XU, Z, CHEN, N., SHADDEN, S.C., MARSDEN, J.E., KAMOCKA, M.M., ROSEN, E. D. & ALBER, M. 2009 Study of blood flow impact on growth of thrombi using a multiscale model. *Soft Matter* **5**, 769–779.

XU, Z., LIOI, J., MU, J., KAMOCKA, M.M., LIU, X., CHEN, D.Z., E.D., ROSEN & ALBER, M. 2010 A multiscale model of venous thrombus formation with surface-mediated control of blood coagulation cascade. *Biophys. J.* **98**, 1723–1732.

ZARNISTA, V. I. & ATAULLAKHANOV, F. I. 2001 Dynamics of spatially nonuniform patterning in the model of blood coagulation. *Chaos* **11**, 57–70.

ZARNITSINA, V., POKHILKO, A. & ATAULLAKHANOV, F. 1996*a* A mathematical model for the spatio-temporal dynamics of intrinsic pathway of blood coagulation. i. the model description. *Thromb. Res.* **84** (4), 225–236.

ZARNITSINA, V., POKHILKO, A. & ATAULLAKHANOV, F. 1996*b* A mathematical model for the spatio-temporal dynamics of intrinsic pathway of blood coagulation. ii. results. *Thromb. Res.* **84** (5), 333–344.

ZHUO, R., MILLER, R., BUSSARD, K. M., SIEDLECKI, C.A. & VOGLER, E.A. 2005 Procoagulant stimulus processing by the intrinsic pathway of blood plasma coagulation. *Biomaterials* **26**, 2967–73.